AD-A037 102 ROCKWELL INTERNATIONAL MCGREGOR TEX ROCKETDYNE DIV F/G 21/9.2
AIR LAUNCH INSTRUMENTED VEHICLES EVALUATION (ALIVE).(U)
FEB 77 J D BURTON F04611-74-C-0009
UNCLASSIFIED R-4939 AFRPL-TR-76-101 NL

1 OF 3
AD A037102

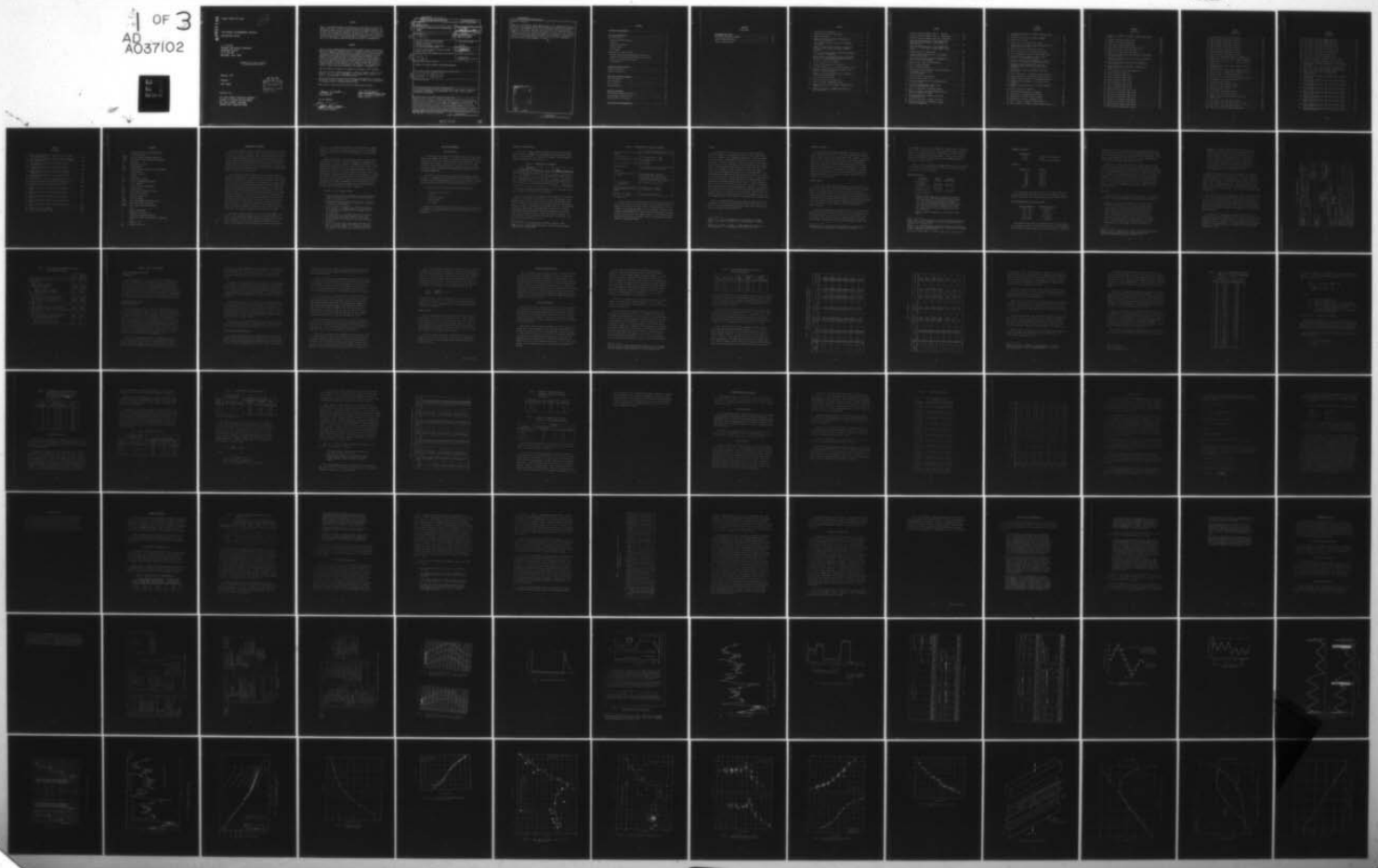

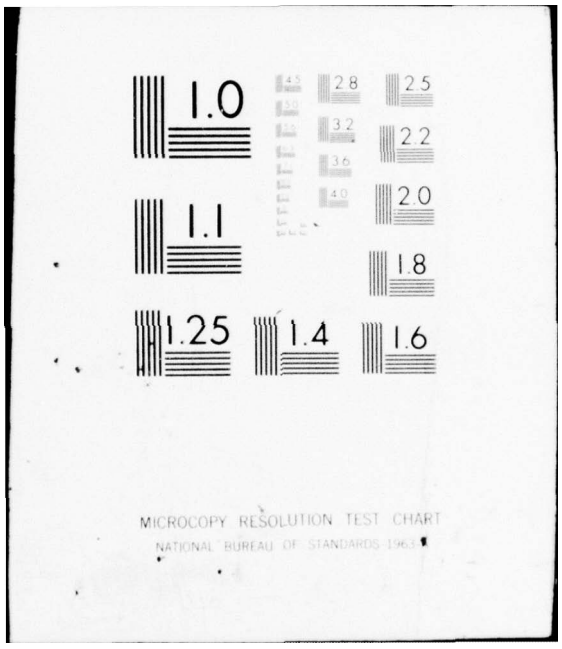
1.0
1.1
1.25
1.4
1.6
1.8
2.0
2.2
2.5
2.8
3.2
3.6
4.0
MICROCOPY RESOLUTION TEST CHART
NATIONAL BUREAU OF STANDARDS 1963

Report AFRPL-TR-76-101

(12)

AIR-LAUNCH INSTRUMENTED VEHICLES EVALUATION (ALIVE)

J. D. Burton
Rockwell International Corporation
Rocketdyne Division
P. O. Box 548
McGregor, Texas 76657

APPROVED FOR PUBLIC RELEASE
DISTRIBUTION UNLIMITED

February 1977

Program I

Final Report

PREPARED FOR:

Air Force Rocket Propulsion Laboratory
Director of Science and Technology
Air Force Systems Command
Edwards AFB, California 93523

NOTICES

When U.S. Government drawings, specifications, or other data are used for any purpose other than a definitely related government procurement operation, the Government thereby incurs no responsibility nor any obligation whatsoever, and the fact that the Government may have formulated, furnished, or in any way supplied the said drawings, specifications or other data, is not to be regarded by implication or otherwise, or in any manner licensing the holder or any other person or corporation, or conveying any rights or permission to manufacture, use or sell any patented invention that may in any way be related thereto.

FOREWORD

The Air Launch Instrumented Vehicles Evaluation (ALIVE) Program, under Contract F04611-74-C-0009, JON 314812WK consists of: Program I, under which GFE propellant and two SRBDM instrumented structural prototype motors are being evaluated; and Program II, starting 14 months after go-ahead, which comprises a similar evaluation of GFE propellant and three Modular Weapon Instrumented Vehicle (MWIV) structural prototype motors. The primary objective of the program is to evaluate the effects of an air-launch environment on the aging characteristics of two advanced HTPB propellant formulations developed under Contract F04611-72-C-0069; a second objective is to evaluate several motor designs in a representative 5-year air-launch service environment. The program was initiated in January 1974 and is scheduled to be completed in December 1977.

This Final Report for Program I is submitted in response to Data Item B004.

The Air Force Rocket Propulsion Laboratory, Edwards, CA 93523 is sponsor of the contract. Dr. J. L. Trout, AFRPL/MKPB, is the Program Monitor and Mr. W. H. Miller is Program Manager at Rocketdyne-McGregor.

This report has been reviewed by the Information Office/DOZ and is releasable to the National Technical Information Service (NTIS). At NTIS it will be available to the general public, including foreign nations.

This report is unclassified and suitable for general public release.

James L Trout

J. L. TROUT, GS-13
Project Engineer

Robert K Middleton

ROBERT R. MIDDLETON, Captain, USAF
Chief, Surveillance & Mechanical Behavior Section

FOR THE COMMANDER

Charles R Cooke

CHARLES R. COOKE, Director
Solid Rocket Division

UNCLASSIFIED
SECURITY CLASSIFICATION OF THIS PAGE (When Data Entered)

REPORT DOCUMENTATION PAGE

READ INSTRUCTIONS BEFORE COMPLETING FORM

1. REPORT NUMBER: AFRPL-TR-76-101	2. GOVT ACCESSION NO.
3. RECIPIENT'S CATALOG NUMBER	
4. TITLE (and Subtitle): AIR LAUNCH INSTRUMENTED VEHICLES EVALUATION (ALIVE).	5. TYPE OF REPORT & PERIOD COVERED: Final Report January 1974 — December 76
6. PERFORMING ORG. REPORT NUMBER: R-4939	
7. AUTHOR(s): J. D. Burton	8. CONTRACT OR GRANT NUMBER(s): F04611-74-C-0009
9. PERFORMING ORGANIZATION NAME AND ADDRESS: Rockwell International Corporation, Rocketdyne Division, P.O. Box 548, McGregor, Texas 76657	10. PROGRAM ELEMENT, PROJECT, TASK AREA & WORK UNIT NUMBERS: 3148 12WK
11. CONTROLLING OFFICE NAME AND ADDRESS: Air Force Rocket Propulsion Laboratory/MKPB, Edwards AFB, CA 93523	12. REPORT DATE: February 1977 13. NUMBER OF PAGES: 238
14. MONITORING AGENCY NAME & ADDRESS (if different from Controlling Office): 229p.	15. SECURITY CLASS. (of this report): UNCLASSIFIED 15a. DECLASSIFICATION/DOWNGRADING SCHEDULE: n/a

16. DISTRIBUTION STATEMENT (of this Report)

APPROVED FOR PUBLIC RELEASE; DISTRIBUTION UNLIMITED

17. DISTRIBUTION STATEMENT (of the abstract entered in Block 20, if different from Report)

18. SUPPLEMENTARY NOTES

19. KEY WORDS (Continue on reverse side if necessary and identify by block number)

SOLID PROPELLANT ROCKET ENGINES; INSTRUMENTATION; FLIGHT TESTING; SIMULATION; STORAGE; HIGH TEMPERATURE; LOW TEMPERATURE; CYCLIC LOADS; AGING; HYDROXYL TERMINATED POLYBUTADIENE

20. ABSTRACT (Continue on reverse side if necessary and identify by block number)

Report presents results of a program conducted to evaluate the effects of air-launch missile environments on the aging characteristics of advanced HTPB propellants and representative motor designs incorporating these propellants. The study addressed aging of two 12-inch-diameter, SRBDM-type motors cast with moderate-burning-rate propellant. The propellant was characterized, service-life loads were evaluated, and the motors were analyzed and subjected to accelerated storage and simulated captive-flight environmental testing. Carton propellant from the same batch from which the motors were cast was aged in the

DD FORM 1 JAN 73 1473 EDITION OF 1 NOV 65 IS OBSOLETE

UNCLASSIFIED
SECURITY CLASSIFICATION OF THIS PAGE (When Data Entered)

Block 20. Continued

laboratory. Subsequently, aging characteristics of the propellant were determined from motor response and the motor design and test methods were evaluated. The motors, instrumentation, and tests are described; and test results are presented. Test results indicate: Characteristics of the propellant tested change very slowly over a period from 6 months to 5 years after cast; the grain configuration tested is structurally adequate to withstand at least 5 years of use in the tactical air-launch environment; current analytical techniques are adequate; and the ALIVE approach to accelerated service-life simulation is feasible and can be made reasonably accurate.

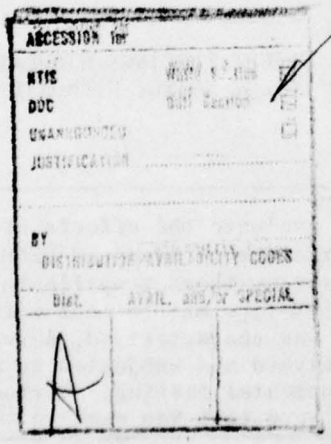

CONTENTS

CONTENTS
(Continued)

TABLES

FIGURES

FIGURES

(Continued)

FIGURES

(Continued)

FIGURES

(Continued)

FIGURES

(Continued)

FIGURES

(Continued)

GLOSSARY

a	Inside grain radius, half crack length
$\dot{a}$	Crack tip velocity
AFRPL	Air Force Rocket Propulsion Laboratory
ALIVE	Air-Launch Instrumented Vehicle Evaluation
A_n	Amplitude
b	Outside grain radius
BDU	Bomb Dummy Unit
DAME	Determination of Aircraft Missile Environment
E	Young's modulus
F	Farenheit (degrees)
f_n	Frequency
g	Gravitational constant
HTPB	Hydroxy-Terminated Polybutadiene
K	Kelvin (degrees)
K_I	Stress intensity-crack opening
K_l	Stiffness factor
MWIV	Modular Weapon Instrumented Vehicle
PSD	Power spectral density
psi	Pounds per square inch
rms	Root mean square
SEALS	Severe Environment Air-Launched System
SFPI	SEALS Fighter Point Intercept
SRBDM	Short Range Bomber Defense Missile
t	Time
T	Absolute temperature
u	Change in core radius, in.
α	Coefficient of thermal expansion
ΔT	Temperature change from strain-free temperature
ε	Strain
ν	Poisson's ratio
σ_m^T	Maximum true stress

INTRODUCTION AND SUMMARY

As with most ordnance items, solid propellant rocket motors tend to be time-limited in their serviceability. This time-limited nature is said to be the result of aging of the rocket motor. The characteristics that quantitatively define aging are essential to assessing the useful life of a rocket. Therefore, the aging characteristics of a given motor system have been defined in surveillance studies of that system after it has been deployed in the field for a period of time. This approach is lacking in that it would be clearly advantageous to have a reliable service-life evaluation before a system is placed in production.

The Air-launch Instrumented Vehicles Evaluation (ALIVE) program is addressed to this problem. The program has three objectives, two of which are specific, and the third, general. The specific objectives are: (1) To evaluate the effect of air-launch missile environments on the aging characteristics of Air Force advanced HTPB propellants and (2) To evaluate representative motor designs incorporating these formulations. In particular, there are two propellant formulations and two sizes of motors. The first program, designated Program I - Short Range Bomber Defense Missile (SRBDM) addressed the aging of two 12-inch diameter motors cast with a moderate-burning-rate propellant. The second program, Program II - Modular Weapon Instrumented Vehicle (MWIV), concerns the study of three 18-inch-diameter motors cast with a low-burning-rate propellant. The third, or general, objective of ALIVE is to provide the Air Force Systems Project Offices (SPO's) with a basic approach to testing new weapon systems prior to their production. This objective encompasses both programs of the ALIVE.

This report describes activities of the first program, SRBDM. Under Air Force Contract F04611-72-C-0069, Thiokol Corporation, Huntsville, Alabama, formulated a number of HTPB propellants for tactical air-launch motors. Thiokol used one of these formulations, TP-H8214, in fabricating two 12-inch-diameter motors, instrumented with grain stress/strain

sensors, in a configuration representative of that required for SRBDM propulsion. These motors, along with several cartons of cured propellant cast with them, were delivered to Rocketdyne for use on the ALIVE program.

ALIVE Program I effort was divided into three distinct but interrelated phases of activity. In Phase I, Planning, the propellant was characterized, service-life loads for the SRBDM were evaluated, the motor design was analyzed, and a 2-year test plan to simulate 5 years of motor deployment was formulated. The second phase, Experimental, involved subjecting the motors to accelerated storage and simulated captive-flight environmental testing and laboratory aging of carton propellant. In Phase III, Assessment, the aging characteristics of the propellant determined from motor response, adequacy of the motor design, and evaluation of the test method were studied. Recommendations for the disposition of the two motors were also developed. Detailed efforts involved in each of the three phases are depicted in Figures 1 through 3.

In summary, results obtained indicate:

1. Characteristics of moderate-burning-rate Propellant TP-H8214 change very slowly over a period from 6 months to approximately 5 years after cast.
2. The grain configuration tested is adequate from a structural standpoint to withstand at least 5 years of use in the tactical air-launch environment.
3. Current analytical techniques, e.g., THVINC viscoelastic stress analysis, are adequate insofar as can be determined in the instance of a design that is not marginal in its test environment.
4. The ALIVE approach to accelerated service-life simulation is feasible and can be made reasonably accurate. The present program required some qualitative assessments, which can be made on a quantitative basis with sufficient information.
5. Because a distinct, albeit slight, aging trend was noted and since the motors appear quite adequate to withstand the air-launch environment, it is recommended that service-life simulation testing be extended with increased load severity.

TEST PLAN DEVELOPMENT

LOADS DEFINITION

An investigation was conducted to determine realistic loading environments for the SRBDM. This effort, in the form of literature reviews and interviews with cognizant personnel on other systems, culminated with the information that follows. As will be noted in the section on the Motor Test Plan, planned loading conditions were based on this input, with adjustments as warranted by additional information that became available as the program progressed.

To establish a basis for the test program the following assumptions were made: (1) SRBDM will be deployed world wide, (2) the missile will be externally carried (although internal carry on the B-1 aircraft is probable), and (3) standard transportation and handling procedures will be used.

Loading conditions are discussed under the following headings:

Handling and Transportation
Storage
Operational Readiness
Captive Flight
Free Flight

Load levels and durations are discussed under each of these subsections, with emphasis on environments relating to structural integrity of the propellant grain.

HANDLING AND TRANSPORTATION

Since it was assumed standard transportation and handling procedures will be used for the SRBDM motors, background information generally applicable to solid rocket motors is quoted. Environments typically applicable during transportation are shown in Table 1.

TABLE 1.[1] TRANSPORTATION ENVIRONMENTS

	Temperature		Shock	Drop, No Damage	Vibration
	Max/Time	Min/Time			
Truck	125 F/2 hr to 90 F/24 hr	-20 F/36 hr	3.5 g 25--50 msec	1 ft to bed or dock	± 1 g at 1--60 Hz
Rail	125 F/2 hr to 90 F/24 hr	-20 F/36 hr	25 g 11--18 msec	1 ft to bed or dock	± 2 g at 10--60 Hz
Air	110 F/4 hr	-30 F/4 hr	negligible	1 ft to floor	3 g at 20--500 Hz

Further work by Wagner[2] delves more deeply into the vibrational requirements. Results of this study are shown in Table 2.

Duration of the vibration environment is not estimated in either Table 1 or Table 2. Actual durations, of course, will vary with each rocket motor. Regarding current practice, however, one may refer to MIL-STD-810B, Table 514.1-VII, where it is noted test levels and durations may be determined depending on the mode of transportation, the weight of the unit, and the number of resonances the unit has. By assuming four resonances for the system weighing approximately 500 pounds, the combined duration for land and air carry is about 23 minutes dwell at each of the resonance frequencies (in each axis) with 46 minutes frequency cycling between 5 and 500 Hertz. The specified input acceleration is ± 1.5 g.

---

[1] JANNAF Bulletin of the Working Group on Mechanical Behavior, 1969.

[2] Wagner, F. R.: Solid Load Definition Study: The Vibration Environment, AFRPL TR-68-100, January 1969.

TABLE 2. TRANSPORTATION* VIBRATION ENVIRONMENT

	Measured Vibration Levels
Truck	
a. paved road	0.35 g (peak) (max at 4 Hz)
b. rough roads (20--25 mph)	1.7 g (peak) (max at 10 Hz) 2.1 g (peak)
c. cross-country (1--10 mph)	5.0 g (peak)
Tractor-Trailer	3.7 g (peak) (max in 240--350 Hz region) (occurred less than 1% of time)
Railroad	
a. over the road (50--70 mph)	0.8 g (peak) (max at 1000 Hz) 2.2 g (peak) (max value noted 93% of vibration was less than 0.75 g) 2.0 g (peak) (predominant frequencies in 2.5 to 7.5 and 50 to 62 Hz regions
b. switching shock (transient)	35 g (peak) with 8 mph impact
Aircraft, propeller-driven with reciprocating or turbo engine	5.0 g (rms) (max at 400 Hz) 5.0 g (peak) (1 to 250 Hz)
Aircraft, jet engine	2.8 g (rms) (max at 800 Hz)

*By common carrier

It was difficult to resolve which of the referenced vibration environments is the more realistic since features such as shipping containers, number of resonances the unit has in such a shipping container, spectral content of the loading environment, etc., were unknown. Therefore, the procedure from MIL-STD-810 was used, realizing this probably represented an overtest of the units. Two support points were used between the units, and the vibration test jig, and dual control accelerometers were placed adjacent to both attach points.

STORAGE

Air-launched tactical solid rocket motors are usually stored in magazines or bunkers. The geographic location of these storage bunkers, of course, determines the environmental temperatures to which the rocket motors are exposed. Measurements have been made of tactical motor skin temperatures at various locations. A statistical analysis of all measured data indicates that on a world-wide basis the maximum motor skin temperature of a 12-inch-diameter rocket motor would be less than 130 F for 97% of the time.[1] Further, diurnal cycling in the desert shows approximately sinusoidal temperature variations with a double amplitude of 70 F maximum during the summer and 60 F minimum during the winter, Ref. Figure 4. In the arctic not only is the baseline temperature lower, but the sinusoidal variations are less with a double amplitude of 40 F maximum during the summer and 30 F minimum during the winter, Figure 5. Igloo-stored motors get as cold as -9 F in the arctic, but for only a few hours. Arctic-dump-stored motors may reach -40 F for approximately 8 hours.[2] It is doubtful that a rocket motor ever reaches an equilibrium temperature (throughout the propellant grain) at either the hot or cold extremes. The majority of the propellant (and at the perforation surface) is more probably at about 90 F in the summer and -25 F in the winter in the somewhat protected dump storage.

While it is highly unlikely that any single motor would be exposed to a composite load history approximating both tropical desert and arctic conditions, such a history might be more realistic than that to which rocket motors are currently tested and qualified.

---

[1] Schafer, H. C.: Measured Temperatures of Solid Rocket Motors Dump Stored in the Tropics and Desert, Part 1, NWC TP-5039-Pt 1, November 1972.

[2] Kurotori, I. S. and H. C. Schafer: Storage Temperature of Explosive Hazard Magazines, P. 4, Cold Extremes, NWC TP-4143, May 1968.

OPERATIONAL READINESS

Due to personnel and equipment limitations, operations are closed down at temperatures below -65 F. Thus, rocket motors may be subjected to this extreme cold for only short periods of time. However, it has been found from the literature that a more realistic equilibrium temperature (soak) is -53 F.[1] Further, when testing motors for low-temperature operational capability, the motor should be conditioned to -53 F then subjected to the expected worst air-carriage temperature for its determined duration and tested. For externally carried missiles, the worst conditions are considered to be the combined vibrations and high aerodynamic heating from the cold operation readiness extreme. These environments are discussed below.

CAPTIVE FLIGHT

During captive flight significant thermal and vibration loads may be imposed on a rocket motor. There are many combinations of these loadings. However, the general consensus is that the most severe combination of loads will be a high-altitude loiter in which the grain is significantly cooled (but vibration levels are low), followed by a high-speed dash that contributes both to a high thermal gradient (due to the aerodynamic heating) and to high vibration levels. From this combination high stresses and strains are developed in the propellant grain from both thermal and dynamic loadings.

The most severe temperature environment, relative to propellant/liner bond stresses and bore strains is the -53 F cold soak (operational readiness) followed by Mach 0.6 loiter at 35,000 feet for 5 hours where the case reaches -75 F, thence followed by a high-speed dash, e.g., Mach 2 at 30,000 feet. Data measured on a modified Bomb Dummy Unit (BDU) from

---

[1] Lewandowski, W. J.: Extreme Cold Ground Temperature Demonstrated for Air-Launched Solid Rocket Motors, AFRPL-TR-71-68, July 1971.

Project DAME[1] show the case skin temperature (without external insulation) rose to 170 F in about 10 minutes. This temperature history is plotted in Figure 6. The SEALS Fighter Point Intercept Mission (SFPI)[2] would be a more severe aerodynamic heating environment. However, neither of these would be a representative mission profile for the SRBDM when carried internally in the B-1 aircraft.

Discussions with personnel at the Rockwell International B-1 Division[3] revealed that stores carried by the B-1 aircraft are expected to be subjected to the following environments:

Temperature Extremes

Environmental Parameters	Internal Carry*	External Carry (Pylon)
Ground, deg F		
Non-operating	-60 to 160	-65 to 125
Operating	-60 to 160	-65 to 125
Ground Alert, deg F	-30 to 160	
In-Flight, deg F	-65 to 160	-65 to 307**
Transient, deg F/sec	6	6

*Apparently these temperature extremes are experienced during the short times during which bomb-bay doors are open (approximately 10 seconds per shot). Bay temperatures are controlled during operation. During the basic subsonic high-altitude cruise mission (an extreme cold condition) the minimum temperature in the bay at the coolest location is -32 F. The air flow is such that natural convection can be assumed for heat transfer calculations.

**Maximum stagnation temperature on all exposed leading edges

[1] Jones, W. B.: Simulation Testing of a Modified Bomb Dummy Unit (Project DAME), AFRPL-TR-72-107, Rockwell International, Rocketdyne Division, McGregor, Texas, December 1972.

[2] Thomas, B. L.: High Burning Rate Extended Environment Solid Propellant Program, Final Report, AFRPL-TR-73-40, Rockwell International, Rocketdyne Division, McGregor, Texas, April 1973.

[3] Personnel included Messrs. H. J. McNeil, Roger Tyler, and Phil Cloud.

Mechanical Vibrations

Frequency, Hz	
5--15	0.34-in. double amplitude
15--63	4.0 g
63--100	0.020 in. double amplitude

Acoustics

Frequency, Hz	Decibels
53	139 ± 10
100	150 ± 9
212	157 ± 3
425	157 ± 3
850	157 ± 3
1700	156 ± 4
3400	147 ± 6
6800	138 ± 10
Overall	164^{+4}_{-2}

For the extreme conditions of acoustic cavity response (bay doors open at maximum turbulence conditions) the bay attachment fittings are expected to experience the following multidirectional random vibration:

Expected Random Response to Acoustic Inputs

Frequency Range, Hz	Vibration Power Level
20 to 80	+ 3 db/octave
80 to 200	0.3 g^2/Hz
200 to 250	-6 db/octave
250 to 600	0.12 g^2/Hz
600 to 2000	-6 db/octave

The boundary condition for estimating the expected random response was investigated in detail. From this investigation it was concluded that the operational extremes assumed are sufficiently nonrealistic that these

vibration levels will not be experienced by an internally carried store. Thus, these random vibration levels were considered indicative of trends only, and absolute levels were not used in the motor test program. In the absence of more appropriate data, the vibration levels measured during Project DAME were used for preparing the test plan.

Referring to vibration data available from other aircraft, a wide disparity between measured vibration levels and those specified for qualification testing was found.[1] A random spectrum that has been recommended for use in qualifying externally carried stores is shown in Figure 7. This is as compared with a measured spectrum on the Air Force Project DAME (Figure 7), all of which is below 0.01 g^2/Hz. These measured DAME data are considered more realistic and indicate that levels shown in Figure 7 are too severe for qualifying solid rocket motors. Random spectra do, however, represent the environment more accurately than dwells at resonance frequencies.

FREE FLIGHT

Launch eject loads initiate the free-flight condition for the missile. Two methods of separating the SRBDM from the aircraft were considered:

Method 1 -- Use modified MAU-12B/A ejector rack that has two sway braces (two legs each) 20 inches apart with the missile center-of-gravity Station 93.42 centered between them and two mounting lugs--one at Station 54.95, the other at Station 146.75. The ejection load of 20,600 lbf (10,300 lbf each pad) is transmitted to the motor case by two pads located at the center of the two legs of each sway brace (i.e., 20 inches apart - cg Station 93.42 centered between them). The 10,300 lbf is applied in 0.079 second. The size of each pad is 1 sq in.

[1] Dreher, J. F., E. D. Lakin, and E. A. Tolle: "Vibracoustic Environment and Test Criteria for Aircraft Stores during Captive Flight," Shock and Vibration Bulletin No. 39, Supplement, 1969.

Method 2 -- Use modified MAU-12B/A ejector rack that has two sway braces (two legs each) located at Stations 59 and 143 (motor case dome attachments) and two mounting lugs; one at Station 54.95, the other at Station 146.75. The ejection load is transmitted to the motor case by two pads located at the center of the legs of each sway brace. The force at Station 59 is 8500 lbf and is applied in 0.066 second; at station 143 the force is 6300 lbf and is applied in 0.049 second. The size of each pad is 1 sq in.

Ignition pressurization is next in the sequence. The chamber is pressurized to 2500 psi (nominal pressure at 70 F) in less than 0.060 second. Longitudinal accelerations of 40 g occur early in flight and 80 g near motor burnout. Lateral maneuvering accelerations may be as high as 50 g. Aerodynamic heating will occur during flight; but due to case external insulation the case wall will not be heated during the duration of the rocket motor firing. Vibration levels during free flight are not known.

Environmental loads data are summarized in Table 3 (Ref. also Figure 8). These data represent the best estimate to date and are subject to revision as new data become available. Combinations and sequence of application of these loads will be dependent on typical mission profiles and on deployment procedures for the rocket motors (at present unknown). However, it is felt that a reasonable test program has been planned from the available data.

A representative training mission schedule of a modern aircraft weapons system and typical loading histories for a new air-launched rocket motor are included for information purposes in Figure 9 and Table 4 and in Figure 10 and 11, respectively. This type information could be equally applicable to the SRBDM and hence was considered in scoping the SRBDM-ALIVE Motor Test Plan.

TABLE 3. SRHDM LOADS SUMMARY

Load	Acceleration	Temperature
Handling and Transportation, Land and Air	Shock: 100 g for 6 msec, 6 directions (MIL-STD-810B) Vibration: 1.5 g, 5 to 500 Hz (MIL-STD-810B) Est: 23 minutes at each of 4 resonances in each axis 46-minute frequency cycling (MIL-STD-810B)	Maximum: 125 F/2 hr[1] 90 F/24 hr Minimum: -30 F/4 hr[1]
Storage	1 g, transverse, 5 years	Dump Maximum: 130 F[2] Magazine Minimum: -9 F[3] Bunker Minimum: -40 F[4]
Operational Readiness		-53 F soak[5]
Captive Flight	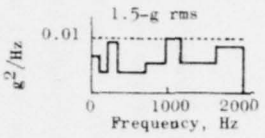 Power spectral density from Project DAME[6] (Ref. Figure 8 for spectral density)	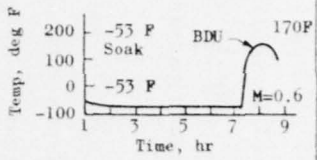
Free Flight Launch Pressurization Maneuvering	Shock: 100 g for 6 msec, transverse (MIL-STD-810B)[2] Acceleration, g Axial / Lateral Near Launch 40 / 50 Near Burnout 80 / 50	

[1] JANNAF Bulletin of the Working Group on Mechanical Behavior, 1969.

[2] Schafer, H. C.: Measured Temperatures of Solid Rocket Motors Dump Stored in the Tropics and Desert, Part I, NWC TP-5039-Pt 1, November 1972.

[3] Kurotori, I. S. and H. C. Schafer: Storage Temperature of Explosive Hazard Magazines, P. 4, Cold Extremes, NWC TP-4143, May 1968.

[4] Turner, S. W. and L. I. Fox: An Analysis of Subterranean Storage Bunkers Subject to Adverse Arctic Temperature Cycles, AFRPL-TR-71-38, March 1971.

[5] Lewandowski, W. J.: Extreme Cold Ground Temperature Demonstrated for Air-Launched Solid Rocket Motors, AFRPL-TR-71-68, July 1971.

[6] Jones, W. B.: Simulation Testing of a Modified Bomb Dummy Unit (Project DAME), AFRPL-TR-72-107, Rockwell International, Rocketdyne Division, McGregor, Texas, December 1972.

TABLE 4. LOADING HISTORY OF TWO RECENTLY DEVELOPED AIR-LAUNCHED ROCKET MOTORS

	Motor No. 1	Motor No. 2
Total Number Days at Base	495	332
Flight History		
Number Flights-Launcher/hr	11/98.9	3/24
Number Flights-Pylon/hr	16/137.4	20.185
Total Number Flights/hr	27/236.3	23/209
Number hr Flown at < 15,000 ft	84.7	49.6
Number hr Flown at > 15,000 ft	151.6	159.4
Installation History		
Days without Ejector/% Total Base Time	110/22	166/50
Days with Ejector/% Total Base Time	385/78	166/50
Days on Launcher or Pylon/% Total Base Time	305/62	144/43
Days on Aircarft/% Total Base Time	143/29	115/35
Storage History		
Days in Shop (IMF) at 70 F/% Total Base Time	100/20	46/14
Days in Bunker at 50 F/% Total Base Time	252/51	171/51
Days Outside (including Flight)/% Total Base Time	143/29	115/35
Temperature History		
Days of Outside Time < 32 F/% Outside Time	41/29	20/17
Days of Outside Time > 80 F/% Outside Time	23/16	9/8
Days of Outside Time with > 0.1 in. Precipitation/% Outside Time	35/24	27/23
Coldest Day Outside Time, deg F	-20	-20
Hottest Day Outside Time, deg F	90	89

LOADINGS, TESTS, AND INSPECTION

INITIAL INSTRUMENTATION RESPONSE AND CORRELATION

Before entering the 5-year service life cycle each motor was subjected to a representative seasonal thermal cycle with conditioning at each step for ≈ 24 hours (until equilibrium temperature was achieved across the web), Ref. Figure 12. Gage readings were taken at each step and after the grain had equalized thermally a 5 to 65 psia pressure correlation check was made. These tests verified instrumentation functionality and ranges of readouts and provided an initial comparison point from which the influence of extended aging and service-life loadings was assessed.

SLOW-RATE SEASONALLY INDUCED THERMAL CYCLIC LOADING

Both instrumented motors were stored in a thermally controlled conditioning box throughout the 5-year life cycle. Each was removed periodically for X-ray inspection. Motor 7 was also removed twice and subjected to loadings equivalent to 5 years of cumulative captive flight time. During seasonal cycling, data from all transducer circuits were recorded daily, using automatic paper tape printing multiplexers. Each motor was subjected to five seasonal cycles during the 24-month period, the first 2.5 years with temperature extremes representative of storage in a tropical desert climate and the last 2.5 years representative of storage in an arctic winter. Thermal amplitudes were derived from data collected during the Loads Definition Study of the SRBDM missions.

Figures 4 and 5 present the extremes of temperatures actually observed in dumps used for the storage of solid propellant air-launched rockets. The desert storage history was chosen for the first part of the seasonally induced thermal cycling test (the first 2.5 years) as it

was believed the higher temperatures would be more apt to lead to propellant degradation than would the colder arctic history. For the last 2.5 years it was supposed that the motors were moved to an arctic storage dump and the lower excursions of an arctic winter were imposed on the motors.

In Figure 13 these annual temperature excursions are redrawn showing the simulation test temperature for the tropic desert year and the arctic winter. During the time of year when the mean temperature is above 70 F, i.e., 6 months, the effects of strain-inducing cumulative damage are considered negligible but chemically induced changes are important mechanisms of degradation. When the temperature is below 70 F exactly the opposite is true.

The testing sequence was to have the effect of compressing a real-time 5-year service life into a 2-year test program. To accomplish this the actual mean temperatures above 70 F were increased slightly as required to accelerate the chemical aging and those below 70 F were lowered to magnify the effects of the strain-induced cumulative damage. Even so, as shown in Figure 13, these exaggerated temperatures remained within the envelope formed by the daily excursions.

These tests were actually performed by placing the motors in a manually controlled conditioning box. Temperatures were stepped 14 degrees each week for the tropical cycle and 10 degrees for the arctic cycle.

CAPTIVE FLIGHT AND OTHER LOADINGS

As shown in Figure 14 Motor 7 was removed from the seasonal cycling sequence twice during the 24-month period and received a series of vibratory and thermal excursions considered representative of near-continuous service as a weapon on flight status for 5 years. These two interruptions

lasted about 45 days each; 15 days for set up and 30 days for the actual tests. The first test was conducted during the Spring of the start of the third simulated year.

Figure 15 shows the thermal environments associated with these tests. These excursions were greater than those associated with storage: the -60 F is representative of the lower operational temperatures in the arctic, 170 F is typical of aeroheat (on an insulated motor case) or of reflected heat from a desert runway in the sun. In addition, thermal steps or shocks of the magnitude expected of maximum daily excursions were imposed.

Vibratory loads were also imposed on the motor during these tests. The sine sweeps were primarily to facilitate a comparison of the analyses with the gage outputs, but the amplitudes (3 g) were chosen to reflect those imposed on motors during vehicular transportation. Random vibration levels imposed evolved from those observed during the Air Force Rocket Propulsion Laboratory's DAME program. They were increased, as discussed below, to account for the fact that only 120 hours of actual vibration time were used to simulate the 1000 hours of actual flight time expected during 5 years of full-time flying-status service.

Based on observations made during service-life studies of deployed missiles it was assumed that a typical motor on training-flight status may make as many as 25 flights with a total flight time of 200 hours per year (Ref. Table 4). It was further assumed that in a 5-year life cycle an SRBDM might endure as many as 1000 hours of captive flight.

Vibration levels imposed on the Bomb Dummy Unit during captive flight are shown in Figure 16. These data provided the basis for the design of the random vibration intensities applied to Motor 7 during the simulation of captive flight. The envelope, shown by the broken horizontal line in the figure, was conservatively taken to be the random vibration density the SRBDM will experience continuously during the 1000 hours of flight time.

Since it is prohibitively expensive to subject the motor to 1000 hours of vibration testing it became necessary to establish a relationship between test amplitude and the test duration. This was done by assuming the slope of such a curve would be the same as the stress-vs-time to failure curve that is usually considered the same as the log-log slope of the constant-load-to-failure curve. For this propellant it was -0.22. So the amplitude is proportional to the test time raised to the -0.22 power. This means that the amplitude of a test lasting 120 hours must be

$$\frac{A_{200}}{A_{1000}} = \frac{1000^{+0.22}}{120^{+0.22}} = 1.59$$

This amplitude ratio, squared, is indicated by the topmost heavy solid horizontal line in Figure 16. It specifies the power spectral density (PSD) input to the motor during the 20 days of simulated captive-flight testing shown in Figure 15.

GRAIN INSPECTION

Points of radiographic and visual inspection are indicated on the loading figures. Typically, X-ray inspections were performed cold to permit better flaw detection. Borescopic inspections, while indicated at cold temperatures, were conducted at ambient conditions. Gage response monitored 7 days a week throughout the 2-year test program provided insight into the aging of the propellant grain. The other inspections provided for more complete flaw detection.

Low-rate pressurization tests were conducted at intervals to serve as gage correlation checks and provide simple analytical/experimental comparison to assess propellant aging characteristics and response to cumulative loadings.

Page 18 is blank

PROPELLANT CHARACTERIZATION

The solid propellant grain performs structural, thermal, and ballistic roles in the rocket motor. Techniques to assess its capability to perform these roles have been developed over the past decades. The majority of these techniques are adaptations of tests devised for characterizing materials such as rubber or metals. Without developing all the reasons, it should be restated that solid propellant is a structurally and chemically complex material that escapes accurate definition by overly simple means. The state of the art of propellant characterization has generally stayed ahead of analytical capabilities though the two are not independent. The characterization of Propellant TP-H8214 for ALIVE was based on state-of-the-art tests.

BASELINE PROPERTIES

The characterization of freshly cured propellant serves two purposes: (1) to provide data for motor response analysis and (2) to establish a baseline from which propellant aging effects can be evaluated. The basic test specimen for structural response characterization is the uniaxial tensile test specimen or "dogbone." Data obtained from these specimens include relaxation (constant strain) modulus, constant strain rate modulus, and failure properties.

The uniaxial relaxation modulus determined at a strain level of about 0.03 in./in. is shown in Figure 17. The time-temperature equivalence, obtained by empirical shift of the relaxation data, is plotted in Figure 18. The constant strain rate test was used by the propellant manufacturer to characterize the propellant shortly after motor cast and again at Rocketdyne when the propellant was received about 4 months after cast to compare baseline data in the different laboratories. Initial (low strain) modulus, tensile strength, and strain at maximum tensile strength were measured.

Modulus data from both Thiokol[1] and Rocketdyne are compared in Figure 19. Tensile failure data are shown as Smith plots (tensile strength vs strain at maximum strength) in Figures 20 and 21. For comparison, 2.0 in./min crosshead data obtained at Rocketdyne are also plotted in Figure 20. These same tensile data are also plotted as functions of reduced strain rate in Figures 22 and 23. The only difference in data generated at Thiokol and those generated at Rocketdyne appears to be in the magnitude and location of the peak in the strain at maximum stress, Figure 22. Because of the scatter in the data it is not possible to determine whether this difference is real, e.g., due to difference in propellant age, test technique, etc.

Another type of uniaxial failure characterization test was also performed. The constant-load-to-failure characteristic is an essential element of a damage analysis, as discussed later. Results of this test are plotted in Figure 24.

The crack opening stress intensity factor, KI, was measured using pre-cracked biaxial strips. The 6.5- x 1- x 0.25-inch test specimens were bonded to aluminum end bars as shown in Figure 25, using Rocketdyne's A-122 bond system. The test specimens, which were milled on a Van Norm milling machine especially modified for remote operations, were tested as indicated in Table 5. Testing was conducted on a Universal Instron test machine equipped with a temperature conditioning box. The specimens were pulled in tension at a crosshead rate of 0.02 in./min at four different test temperatures, 110, 20, -40, and -80 F. The 0.5-inch precracks (0.25-inch half-crack length) were cut at the center of each specimen using an X-Acto knife blade. Crack tip growth was measured to the nearest 1/32 inch by placing a machinist's scale below the expected

[1] Roys, G. P., et al: Development of HTPB Propellants for Air-Launched Missiles, Quarterly Report, November 1973 through January 1974, AFRPL-TR-74-03, Thiokol Corporation, Huntsville, AL, 15 February 1974.

TABLE 5. CRACK PROPAGATION BIAXIAL STRIP TESTS
(TP-H8214 PROPELLANT)

Test No.	Carton No.	Slab No.	Test Temp, deg F	Crosshead Speed, in./min	Length of Initial Pre-crack, in.
158	118	1	110	0.02	0.5
159	118	2	20	0.02	0.5
170	118	3	-40	0.02	0.5
171	118	6	-80	0.02	0.5

line of crack propagation. The test specimens were pulled at the constant crosshead rate with the pull continuing uninterrupted to complete separation of the specimens. Scale readings were taken off the crack tip positions at random points and recorded at the corresponding points in time on the Instron load time chart.

The reduced data were taken from the Instron force-time chart, which provided a record of crack length, load, and time. Figures 26 and 27 are typical replots obtained from Instron charts. Crack tip velocities ($\dot{a}$), were calculated using graphical methods for each test at uniform time intervals using the half crack length vs time replot, such as that shown in Figure 27. Table 6 summarizes reduced crack tip velocity data.

Stress intensity factors (K_I) were determined from the relationship established using a finite element program. In this analysis biaxial strip load was related to crack and sheet dimensions, assuming a Young's modulus of 1000 psi, a Poisson's ratio of 0.49, and sheet size 6.5 x 1 x 0.25 inch. Figure 28 shows the theoretical relationship between load and half crack length obtained from the finite element analysys. Figure 29 compares the theoretical stress intensity factors obtained using the finite element analysis with Mueller's infinitely long biaxial

TABLE 6. SUMMARY OF REDUCED DATA FROM BIAXIAL TEST STRIPS WITH HALF INCH PRE-CRACKS AT CENTER, TP-H8214 PROPELLANT

Time, min	Test Temp, deg F	Strain ϵ, in./in.	Crack Tip Velocity, $\dot{a}$, in./min	Stress Intensity Factor, K_I	log $\dot{a}$	log K_I	log $\left[K_I(1+\epsilon)\right]$
4	110	0.08	0.0266	37.2	-1.575	1.434	1.467
	20	0.08					
	-40	0.08	0.0083	157	2.08	2.19	2.229
	-80	0.08	0.047	742	-1.327	2.870	2.903
5	110	0.10	0.033	36.8	-1.474	1.565	1.607
	20	0.10	0.0147	54.0	-1.832	1.73	1.773
	-40	0.10	0.0142	185	-1.84	2.26	2.308
	-80	0.10	0.090	788	-1.045	2.896	2.937
6	110	0.12	0.0476	46.8	-1.322	1.670	1.719
	20	0.12	0.0192	68.0	-1.716	1.83	1.881
	-40	0.12	0.0166	206	-1.778	2.31	2.36
	-80	0.12	0.104	780	-0.982	2.892	2.94
7	110	0.14	0.0588	56.2	-1.230	1.749	1.806
	20	0.14	0.028	81.0	-1.552	1.90	1.96
	-40	0.14	0.02	221	-1.698	2.34	2.40
	-80	0.14	0.104	760	-0.982	2.88	2.937
8	110	0.16	0.066	64.3	-1.176	1.808	1.872
	20	0.16	0.0388	94.0	-1.411	1.97	2.037
	-40	0.16	0.035	230	-1.45	2.36	2.42
	-80	0.16	0.0106	730	-0.974	2.86	2.92
9	110	0.18	0.0769	71.5	-1.114	1.854	1.926
	20	0.18	0.0583	105.0	-1.234	2.02	2.093
	-40	0.18	0.040	235	-1.397	2.37	2.44
	-80	0.18					
10	110	0.20	0.100	76.8	-1.0	1.885	1.96
	20	0.20	0.0586	115.0	-1.232	2.06	2.139
	-40	0.20	0.0464	237	-1.33	2.374	2.45
	-80	0.20					

TABLE 6. CONTINUED

Time, min	Test Temp, deg F	Strain ϵ, in./in.	Crack Tip Velocity, $\dot{a}$, in./min	Stress Intensity Factor, K_I	log $\dot{a}$	log K_I	log $\left[K_I(1+\epsilon)\right]$
11	110	0.22	0.117	81.6	-0.931	1.911	1.99
	20	0.22	0.0607	124.0	-1.216	2.09	2.179
	-40	0.22	0.0482	237	-1.31	2.37	2.46
	-80	0.22					
12	110	0.24	0.160	82.0	-0.795	1.91	2.007
	20	0.24	0.0627	128.0	-1.202	2.107	2.20
	-40	0.24	0.0615	234	-1.211	2.369	2.46
	-80	0.24					
13	110	0.26	0.208	80.5	-0.681	1.905	2.006
	20	0.26	0.0754	127.0	-1.122	2.103	2.304
	-40	0.26	0.0694	229	-1.158	2.35	2.46
	-80	0.26					
14	110	0.28	0.285	79.2	-0.545	1.898	2.005
	20	0.28	0.0833	124.0	-1.079	2.09	2.20
	-40	0.28	0.075	222	-1.12	2.34	2.45
	-80	0.28					
15	110	0.30					
	20	0.30	0.1029	120.0	-0.987	2.07	2.193
	-40	0.30	0.0764	214	-1.116	2.33	2.44
	-80	0.30					
16	110	0.32					
	20	0.32	0.125	115.0	-0.903	2.06	2.18
	-40	0.32	0.0833	204	-1.079	2.30	2.43
	-80	0.32					
17	110	0.34					
	20	0.34	0.20	109.0	-0.698	2.03	2.16
	-40	0.34					
	-80						

strip analysis.[1] Figure 30 was obtained by ratioing K_I in Figure 29 to load P in Figure 28; the resulting ratio is independent of the particular modulus (1000 psi) and strain (1.0) used in the calculations. Using the relationship shown in Figure 30, stress intensity factors were obtained for the various crack lengths and corresponding loads. Reduced stress intensity factors are summarized in Table 6.

Figure 31 is a plot of the log of stress intensity factor K_I vs log of the crack tip velocity, $\dot{a}$. In this case data are shown from the initial point where the pre-crack started to grow to the time when the stress intensity factor had reached a maximum value.

Figure 32 is a plot of the log of the stress intensity factor adjusted for change in sheet thickness, i.e., log $\left[K_I(1+\epsilon)\right]$, vs log of the crack tip velocity, $\dot{a}$. Data in this case are plotted over the entire test period, i.e., not terminated at the point where the stress intensity factor reached a maximum value.

Other measurements made on the propellant at Rocketdyne included hardness, density, burn rate, and specific heat. Rex hardness measurements showed a value of 60 throughout the carton bulk except for points near the edges (< 1/8 inch) where the hardness increased slightly (less than 65). Average density, measured by fluid displacement, was 0.0661 lb/cu in.

Burn rate data were obtained over a pressure range of 600 to 1600 psia, using a strand bomb. The rate was 0.78 in./sec at 1000 psia and 70 F with a pressure exponent of about 0.6.

---

[1] Mueller, H. K. and W. G. Knauss: "Crack Propagation in a Linearly Viscoelastic Strip," Journal of Applied Mechanics, 38, Series E, 1971, pp 843--848.

A differential scanning calorimeter was used to heat and cool a small propellant specimen at a constant rate and monitor the resulting specimen temperature. The rate of the temperature change was then used to deduce the energy in Btu's required to change a unit mass (in pounds) of propellant 1 degree (Fahrenheit), i.e., the specific heat. This was completed for a range of temperatures from 180 to 375 K as shown in Table 7.

Finally, strain evaluation cylinder data from Thiokol[1] were used to evaluate the bulk properties of the TP-H8214 propellant. Nine 2-inch diameter cylinders, designated TX-318, were cast, three each with three different core diameters: 0.218, 0.435, and 0.75 inch. The motors were subjected to quasi-equilibrium cooldown and conditioning as outlined in the ICRPG Solid Propellant Mechanical Behavior Manual. The resulting inner bore strains as reported are shown in Figure 33.

Using the cure dilatation data reported subsequently[2] the strain-free temperature for the strain evaluation cylinders was calculated. The "net effective volume change" taken from the data plotted in Figure 34 was reported as -0.59% (shrinkage). Using this number with a volumetric coefficient of thermal expansion of 3 x $\left(0.000055 \frac{\text{cu in./cu in.}}{\text{deg F}}\right)$ = 0.000165/deg F the calculated strain-free temperature is 180 F, approximately 35 degrees (F) above the cure temperature of 145 F.

The strains and the temperature changes measured from 180 F for two sets of strain evaluation cylinders, those with web fractions of 0.625

---

[1] Roys, et al; op cit

[2] Mueller and Knauss; op cit

TABLE 7. VALUES OF THE SPECIFIC HEAT FOR TP-H8214 PROPELLANT AS A FUNCTION OF TEMPERATURE

Temperature		Specific Heat
deg K	deg F	C, Btu/lb-deg F
375	215.6	0.281
370	206.6	0.282
365	197.6	0.282
360	188.6	0.278
355	179.6	0.278
350	170.6	0.278
345	161.6	0.275
340	152.6	0.273
335	143.6	0.271
330	134.6	0.272
325	125.6	0.270
320	116.6	0.268
315	107.6	0.254
310	98.6	0.252
305	89.6	0.250
300	80.6	0.246
295	71.6	0.244
290	62.6	0.235
285	53.6	0.234
280	44.6	0.235
275	35.6	0.230
270	26.6	0.226
265	17.6	0.223
260	8.6	0.219
255	- 0.4	0.215
250	- 9.4	0.211
245	- 18.4	0.208
240	- 27.4	0.202
235	- 36.4	0.201
230	- 45.4	--
225	- 54.4	0.193
220	- 63.4	0.186
215	- 72.4	0.180
210	- 81.4	--
205	- 90.6	0.180
200	- 99.6	0.171
195	-108.6	--
190	-117.6	--
185	-126.6	--
180	-135.6	0.120

and 0.7825 corresponding to core diameters of 0.1250 and 1.565 inch, respectively, were used with simultaneous equations to find α and ν. Each equation was of the form

$$2\left[\frac{u}{a} - (1 + \nu_c)\,\alpha_c\,\Delta T\right]\nu + \Delta T\left[\left(\frac{a}{b}\right)^2 - 1\right]\xi =$$
$$\frac{u}{a}\left[\left(\frac{a}{b}\right)^2 + 1\right] - 2\,(1 + \nu_c)\,\alpha_c\,\Delta T$$

where

- u - change in core radius (in.)
- a,b - inside and outside grain radii, respectively (in.)
- ΔT - temperature change from strain free temperature (deg F)
- ξ - $(1 + \nu)\,\alpha$, a variable change (in./in./deg F)
- α,ν - coefficient of thermal expansion (in./in./deg F) and Poisson's ratio, respectively

and the subscript c indicates a case property.

The simultaneous equations were solved at each temperature where the strains were measured and reported. The results of these calculations are shown in Table 8. Both the effective coefficient of thermal expansion and Poisson's ratio remained surprisingly constant for all temperatures.

As a result of these calculations the values of these properties used for thermal analyses were:

$$\alpha = 5.5 \times 10^{-5} \text{ in./in./deg F}$$
$$\nu = 0.490$$

TABLE 8. BULK PROPERTIES CALCULATED FROM CENTER PORT STRAINS MEASURED IN STRAIN EVALUATION CYLINDERS WITH WEB FRACTIONS OF 0.625 AND 0.7825

SEC Temperature, deg F	Coefficient of Thermal Expansion, α, in./in./deg F	Poisson's Ratio, ν
77	5.1×10^{-5}	0.486
50	5.7×10^{-5}	0.488
35	5.4×10^{-5}	0.489
20	5.9×10^{-5}	0.484
5	5.8×10^{-5}	0.485
-10	5.5×10^{-5}	0.488
-35	5.5×10^{-5}	0.488
-50	5.4×10^{-5}	0.490
-65	5.2×10^{-5}	0.492

LABORATORY AGING TESTS

Twelve cartons of propellant were subjected to aging at 77, 110, 140, and 170 F (3 cartons at each temperature). Additional unopened cartons were stored at 77 F in the thermal conditioning box with the motors undergoing 2-year aging tests.

Subsequent to the aging tests on the laboratory cartons, a surface aging effect on the propellant was noted. One of the cartons stored for 72 weeks at 170 F was tested to determine propellant properties as functions of distance from the surface. These data are plotted in Figures 35 and 36. This carton, like the others in the laboratory aging tests, had been opened, sampled, resealed, and stored in a container purged with dry nitrogen. It is apparent that oxidation at the surface had nontheless occurred. Since the same procedure had been followed for all cartons,

the aging effects noted were primarily attributed to surface response. Data from the stored cartons are presented in Figures 47 through 39.

Aging data for elevated-temperature storage are obviously biased by the initial 18 weeks of storage at ambient (elapsed time from propellant cure to start of aging program). The plots, Figures 37 through 39, are based on time at temperature.

Mean aging rates for the three storage temperatures and three characteristics are listed in Table 9 along with the extrapolated initial values. These rates are replotted as functions of temperature in Figure 40. Only a limited amount of bulk aging data were available—that from the 170 F carton discussed above and data from unopened cartons stored for 2 years at 77 F. Data from these tests, with an admitted bit of interpolation, would indicate bulk aging characteristics as tabulated in Table 10 and plotted in Figure 41.

TABLE 9. SURFACE AGING RATES FOR TP-H8214

Storage Temp, deg F	Extrapolated 1-Week (Initial) Values			Logarithmic Rate of Aging		
	$E_{rel(10)}$, psi	σ_m^T, psi	ε_m, in./in.	$\frac{d \log E_{rel(10)}}{d \log t}$, psi/wk	$\frac{d \log \sigma_m^T}{d \log t}$, psi/wk	$\frac{d \varepsilon_m}{dt}$, in./in./wk
170				0.696	0.356	-0.1605
140	45	84	0.50	0.416	0.256	-0.130
110				0.262	0.151	-0.103
77				0.136	0.097	-0.0735

TABLE 10. ESTIMATED BULK AGING RATE FOR TP-H8214

Storage Temp, deg F	Extrapolated 1-Week (Initial) Values			Logarithmic Rate of Aging		
	$E_{rel}(10)$, psi	σ_m^T, psi	ϵ_m, in./in.	$\frac{d \log E_{rel}(10)}{d \log t}$, psi/wk	$\frac{d \log \sigma_m^T}{d \log t}$, psi/wk	$\frac{d \epsilon_m}{dt}$, in./in./wk
170				0.441	0.225*	-0.078*
140	45	84	0.50	0.318	0.165	-0.070
110				0.215	0.117	-0.056
77				0.123*	0.072*	-0.050*

*Based on bulk propellant tests

The object of this study was to develop the ability to estimate the amount of change occurring in a motor in the field. As a test of the validity of the aging estimates, carton propellant stored with the motors for 2 years was sampled. Regarding prediction, to calculate how much change will occur in ~ 1 week of storage at a temperature, T, one must first determine the cumulative change preceding the start of that week's storage. Dividing the cumulative change by the aging rate, R, for the storage temperature, T, yields an equivalent age, A', on which to base the computation. In equation form:

$$C_1 (T) = \left(\frac{C_o}{R (T)} + t\right) R (T)$$

where

C_o - total change at start of test
$R (T)$ - aging rate at temperature, T
$C_1 (T)$ - total change after t weeks of storage at T

Table 11 lists the storage temperatures, equivalent age, and cumulative change for each of the three test characteristics for the 2-year motor test cycle. Since the effective rate of change was nearly zero for temperatures below 63 F, they have been condensed in the table. The resultant predicted and measured properties are given in Table 12.

These results are within the accuracy of the uniaxial response. These aging effects are small compared with values obtained after 2-year storage at 77 F. The question now to be answered is: How will they compare with values obtained after 5 years of actual storage in the environment that was being simulated? This environment, discussed previously, is shown in Figure 14. Tropic storage is the most significant for the chemically induced aging effect. For the ALIVE program, the motor is assumed to be subjected to 2.5 years of this storage (reaching the summer maximum three times). A similar analysis of this environment, assuming the aging rates shown in Figure 41, yields the comparison between simulation and actual environment shown in Table 13. The result is based on assuming the mean daily temperature for the motor and assuming the motor is stored for 40 weeks at 77 F before deployment. Results shown in Table 13 show that changes in modulus and tensile strength are slightly severe (simulation vs actual), while strain remains the same.

Thus, based on characterization data and the environment to which the motors were subjected, we expected:

1. Only slight changes in material properties during the 2-year test of 5-year service life
2. Aging resulting from the 2-year storage environment should adequately simulate 5 years of service life storage of which 2.5 years are spent in a tropical climate

Surface aging phenomena appear to be more severe than bulk aging. The effect this has on a sealed motor and the potential for reversibility through bore treatment are not explored here.

TABLE 11. CALCULATED AGING EFFECTS OF TWO-YEAR STORAGE CYCLING

Week	Temp, deg F	Equivalent Age at Temp, wk	Cumulative Change in Log E_{rel}	Equivalent Age at Temp, wk	Cumulative Change in Log σ_m	Equivalent Age at Temp, wk	Cumulative Change in ϵ_m, in./in.
1	77	40.0 + 1	0.198	40.0 + 1	0.116	40.0 + 1	-0.0645
2	90	17.6 + 1	0.202	21.6 + 1	0.118	26.2 + 1	-0.0653
3	104	10.2 + 1	0.210	12.9 + 1	0.121	18.0 + 1	-0.0665
4	118	7.3 + 1	0.223	8.9 + 1	0.127	13.6 + 1	-0.0683
5--6	130	6.2 + 2	0.257	7.3 + 2	0.142	11.7 + 2	-0.0706
7	118	11.4 + 1	0.266	13.0 + 1	0.146	17.4 + 1	-0.0741
8	104	21.4 + 1	0.270	23.9 + 1	0.148	26.6 + 1	-0.0749
9	90	49.9 + 1	0.271	50.2 + 1	0.149	44.3 + 1	-0.0754
10	77	159.7 + 1	0.271	116.4 + 1	0.149	76.6 + 1	-0.0756
11--20	≤ 63	--	0.271	--	0.149	--	-0.0758
21	77	160.7 + 1	0.271	117.6 + 1	0.149	78.5 + 1	-0.0760
22	90	50.6 + 1	0.272	52.1 + 1	0.150	46.8 + 1	-0.0764
23	104	22.9 + 1	0.276	26.0 + 1	0.152	29.5 + 1	-0.0772
24	118	13.6 + 1	0.283	15.5 + 1	0.155	20.7 + 1	-0.0784
25--26	130	10.1 + 2	0.305	11.4 + 2	0.166	16.8 + 2	-0.0815
27	118	18.0 + 1	0.311	19.9 + 1	0.168	24.6 + 1	-0.0825
28	104	35.8 + 1	0.313	38.7 + 1	0.169	38.6 + 1	-0.0831
29	90	93.2 + 1	0.314	87.6 + 1	0.169	67.0 + 1	-0.0834
30	77	356.0 + 1	0.314	225.5 + 1	0.170	121.5 + 1	-0.0835
31--40	≤ 63	--	0.314	--	0.170	--	-0.0836
41	77	357.0 + 1	0.314	226.7 + 1	0.170	123.2 + 1	-0.0838
42	90	94.6 + 1	0.315	89.3 + 1	0.170	69.4 + 1	-0.0841
43	104	35.5 + 1	0.317	40.3 + 1	0.171	41.3 + 1	-0.0846
44	118	20.2 + 1	0.322	22.0 + 1	0.174	27.8 + 1	-0.0855
45--46	130	13.9 + 2	0.339	15.2 + 2	0.182	21.7 + 2	-0.0879
47	118	24.8 + 1	0.343	26.6 + 1	0.184	31.7 + 1	-0.0887
48	104	51.8 + 1	0.345	54.0 + 1	0.185	50.9 + 1	-0.0892
49	90	141.0 + 1	0.345	132.1 + 1	0.185	91.2 + 1	-0.0894
50	77	643.7 + 1	0.346	369.0 + 1	0.185	171.7 + 1	-0.0895
51--104	≤ 63	--	0.346	--	0.185	--	-0.0896

TABLE 12. PREDICTED VS MEASURED PROPELLANT PROPERTIES AFTER TWO-YEAR STORAGE WITH MOTORS

Characteristics	Predicted	Actual
E_{rel} (10), psi	100	84
σ_m^T, psi	129	125
ϵ_m, in./in.	0.41	0.37

TABLE 13. COMPARISON OF PREDICTED AGING EFFECT, SIMULATED VS ACTUAL STORAGE ENVIRONMENT

Predicted Characteristics	Storage	
	Simulated (Accelerated) Environment	2.5 Years in Tropics
E_{rel} (10), psi	100	91
σ_m^T, psi	129	124
ϵ_m, in./in.	0.41	0.41

Data obtained from propellant stored 2 years at 77 F and from propellant stored with the motors are shown in Figures 42 through 45. The consistent, if small, changes are apparent.

In lieu of direct vibration measurement of the dynamic modulus of this propellant, the in-situ dynamic gage was used to monitor propellant dynamic modulus as a function of age. These gages were removed at the end of the 16-week aging program. The gages themselves were exhibiting aging problems, which raised questions as to the validity of the data obtained. Because of the gage dynamics, data at frequencies above 10 Hertz were discarded. Figures 46 and 47 illustrate the results as mean values (of three samples) of the "real" component of the modulus, E', and

the loss tangent, tan φ, vs frequency and sample storage time. The general trends of the data--increase in modulus with frequency and aging time with decrease in loss tangent with aging time--indicate postcuring. Scatter of the data and inconsistencies in the test technique combined with the aging behavior of the gages themselves restrict use of these data for quantitative purposes.

MOTOR DESCRIPTION AND ANALYSIS

The experimental effort on the motors was based on the loads definition studies and on an analysis of the motors. This section describes the motors, the embedded instrumentation, and the stress analysis leading to the actual testing.

MOTOR DESCRIPTION

Two 12-inch-diameter motors, Figures 48 and 49, were cast in December 1973 and delivered to Rocketdyne at McGregor, Texas, in March 1974. The propellant grains are 69 inches long and are floated at the forward end of each motor. The grain configuration is an axisymmetric cylinder of 67% web fraction in the forward half tapering to a 27% web fraction at the aft termination plane.

The motors were instrumented before they were shipped with stress and strain gages and temperature sensors as indicated in Figures 48 and 49. Figure 50 illustrates the inner bore clip gage installation.

GAGE CALIBRATION

As discussed in the Test Plan Description, the motors were thermally cycled from 77 to 160 to -20 to 77 F with grain pressurization for normal grain response calibration. They were conditioned at 30-degree (F) intervals for about 20 hours (well beyond the time required to attain thermal equilibrium as indicated by thermocouple rakes) then subjected to a pressurization cycle in 10-psi increments from -10 to 50 psig. Pressures were held 15 minutes at each step to permit grain creep to stabilize. The holding time was slightly short at -20 F resulting in a hysterisis of about 0.8 millivolts in the ambient pressure normal gage reading. Gage load and no-load data are plotted in Figures 51 through 82.

Figure 51 shows a typical normal gage pressure response for the gages on Motor 7. Gage sensitivity factors as determined in these tests are summarized in Figures 52 and 53. Gage no-load data as determined by Thiokol-Huntsville are shown in Figures 54 and 55. The data scatter and limited number of temperatures resulted in a high degree of uncertainty, which, in turn, affected the interpretation of motor stress state as the program continued. There was an apparent malfunction in the thermal compensation circuit on Normal Gage N4-60.

Shear gage calibration data were available from pre-installation data obtained from Thiokol-Huntsville. Pre-cast no-load data for these gages are shown in Figures 56 and 57. Sensitivity data are shown in Figures 58 through 71.

Thermistors for the shear gages had been calibrated but those for the normal gages were calibrated during the thermal cycle. These calibrations are shown in Figures 72 through 81. Thermistor N4-58 was not connected, and Thermistor N4-62 did not function.

A plot of cooling during a step in the thermal cycle is shown in Figure 82. Clip gage calibrations are given in Table 14.

Quick-look normal gage data are summarized in Table 15. The disparity in gage-indicated bond stresses at the end of propellant cure indicated a distinct possiblity of a non-uniform stress state induced during cure by partial adhesion of the curing grain to the mandrel. Because reduced stresses are so strongly influenced by gage no-load data, the data scatter must be primarily attributed to this no-load uncertainty.

TABLE 14. CLIP GAGE CALIBRATION DATA

Gage	Temperature, deg F			
	150	70	0	-65
C7-36				
Φ, mv/in.	537.8	491.3	496.5	463.6
E_o, mv	-0.2	0.8	2.6	3.6
C4-37				
Φ, mv/in.	596.3	564.2	558.0	539.8
E_o, mv	-1.2	-1.5	-1.3	-1.7
C7-38				
Φ, mv/in.	546.8	498.2	481.2	450.6
E_o, mv	-0.4	-0.1	0.4	0.8
C4-39				
Φ, mv/in.	542.4	505.2	479.0	446.5
E_o, mv	1.7	1.2	0.5	0.4
C4-40				
Φ, mv/in.	543.0	482.7	458.6	446.1
E_o, mv	5.2	6.9	8.9	10.3
C4-41				
Φ, mv/in.	520.3	497.2	492.6	480.3
E_o, mv	-3.1	-4.3	-5.9	-7.4
C4-42				
Φ, mv/in.	582.4	551.7	532.7	490.8
E_o, mv	-2.7	-2.5	-2.2	-2.1
C4-43				
Φ, mv/in.	558.1	534.7	535.4	503.3
E_o, mv	3.8	4.4	4.8	5.4
C7-45				
Φ, mv/in.	571.3	544.8	535.5	506.2
E_o, mv	-1.6	-0.8	0.0	0.5
C7-46				
Φ, mv/in.	552.6	552.8	515.4	483.9
E_o, mv	9.4	9.9	10.5	11.4
C7-47				
Φ, mv/in.	522.9	530.7	502.4	473.0
E_o, mv	-0.8	0.0	0.8	1.5
C7-48				
Φ, mv/in.	534.2	510.6	495.9	469.6
E_o, mv	-2.3	-1.8	-1.2	-0.7

TABLE 15. QUICK-LOOK NORMAL STRESS GAGE DATA

Gage	Stress, psi								
	158 F	145 F (End of Cure)	127 F	100 F	89 F	66 F	58 F	10 F	-17 F
N4-58									
Absolute	4.6	17.7	3.9	4.8	5.1	7.7	11.5	11.1	7.3
Delta	0.0	--	-0.7	0.2	0.5	3.1	6.9	6.5	2.7
N4-62									
Absolute	9.6	30.0	15.5	19.7	20.2	27.0	35.0	50.4	64.8
Delta	0.0	--	5.9	10.1	10.6	17.4	25.4	40.8	55.2
N4-64									
Absolute	2.3	24.7	6.3	9.0	9.5	12.3	14.3	16.3	18.5
Delta	0.0	--	4.0	6.7	7.2	10.0	12.0	14.0	16.2
N7-57									
Absolute	22.8	34.8	24.5	26.6	27.9	29.4	33.2	36.9	42.7
Delta	0.0	--	1.7	3.8	5.1	6.6	10.4	14.1	19.9
N7-59									
Absolute	6.5	19.3	6.7	6.6	4.6	5.8	7.2	7.2	5.7
Delta	0.0	--	0.2	0.1	-1.9	-0.7	0.7	0.7	-0.8
N7-61									
Absolute	-11.0	-0.6	-10.8	-10.7	-9.5	-10.0	-6.3	-2.6	4.7
Delta	0.0	--	0.2	0.3	1.5	1.0	4.7	8.4	15.7
N7-63									
Absolute	9.9	17.9	9.3	10.6	10.3	10.8	13.8	15.6	20.1
Delta	0.0	--	-0.6	0.7	0.4	0.9	3.9	5.7	10.2

STRESS ANALYSIS

The circular-port geometry of the SRBDM makes the motor design amenable to analysis using an axisymmetric finite element model. The primary analytical tool used was the Air Force-developed viscoelastic computer code THVINC. The basic material properties—uniaxial relaxation modulus, conductivity, and coefficient of thermal expansion—used in the analysis are discussed in the Propellant Section.

For analyzing thermal results, an example case of cooling the motor from 160 to -20 F for 48 hours is discussed. The temperature-vs-time plot shown in Figure 83 describes the through-the-web thermal response near the motor mid-plane. Equilibrium temperature is virtually obtained in about 22 hours. Inner bore hoop strains at the mid-plane and near the forward end of the grain (where the grain is floated) are plotted as functions of time in Figure 84. Very little creep is predicted for this propellant (i.e., the strain changes very little after equilibrium temperature conditions are reached).

Finally, bond-line normal stresses at each of the three instrumented planes are plotted in Figure 85. The highest stress level occurs, of course, at the motor mid-plane. The relative softness of this propellant and the low web fraction of the motor design are reflected in the predicted bond stress of less than 3 psi.

Extending this analysis to the 2-year thermal history for each of the motors yields the bond stress-vs-time profiles plotted in Figures 86 and 87. The effects of bulk aging as described in the Propellant Section have been incorporated into these results, which essentially reflect the aging process.

The other loading of significance is that of transverse vibration. An analysis of the dynamic response was conducted using the CXL-450 computer code, which admits viscoelastic parameters in a plane strain solution.

A y displacement at each of the circumferential case nodes was input to obtain frequency response solutions. For sinusoidal vibration the displacement is expressed

$$y = y_{max} \sin 2\pi ct$$

where

c - forcing frequency in Hertz

t - time in seconds

Differentiating twice gives the acceleration

$$\ddot{y} = -(2\pi c)^2 y_{max} \sin 2\pi ct$$

which yields

$$\left| y_{max} \right| = \frac{\ddot{y}}{(2\pi c)^2}$$

as an expression for the input displacement as a function of forcing frequency.

The frequency response solution for a viscoelastic structure was obtained by substitution of viscoelastic coefficients, expressed as frequency-dependent complex numbers, for the elastic material property coefficients in the corresponding elastic solution:

$$E^* (i\omega) = E' (\omega) + i E'' (\omega) \longrightarrow E$$

$$\nu^* (i\omega) = \nu' (\omega) + i \nu'' (\omega) \longrightarrow \nu$$

Lame's relations hold for the complex moduli, thus,

$$\nu^* (i\omega) = 1/2 - \frac{E^* (i\omega)}{6 B^* (i\omega)}$$

Material properties used for the propellant are those measured for TP-H8214. Frequency-dependent values for E* (iω) are plotted in Figure 88. Propellant density was 0.066 lbm/cu in.; bulk modulus was assumed to be 3.5×10^5 psi.

The case was assumed to be elastic with the following properties:

Modulus	3.2×10^7 psi
Thickness	0.12 in.
Poisson's Ratio	0.3
Density	0.283 lbm/cu in.

The actual motor has a thin rubber liner between the propellant grain and the case. The liner was not included in this analysis because its viscoelastic properties were not available and its effect on the overall results was expected to be minor due to the small amount present.

A number of steady-state solutions were calculated for frequencies ranging between 50 and 3000 Hertz. Calculations made between 50 and 1200 Hertz indicated a first resonance at approximately 1000 Hertz. Subsequent computations at 1500, 2000, and 3000 Hertz indicate a second resonance near 2000 Hertz. The ratio of calculated normal stress to stress for a unit load application in the outer propellant element in the direction of load input was used to determine resonant frequencies. The results are shown in Figure 89. The ratio of calculated displacement at the inner bore node 90 degrees from the direction of motion to the input displacement is also plotted in Figure 89 and verifies the resonant frequencies indicated by the stress amplitude ratio. The displacement configuration for the nodal points located on the radial line perpendicular to the direction of motion is shown in Figure 90 for frequencies ranging from 100 to 1000 Hertz. For the SRBDM propellant web, we expect a non-resonance bond stress of about 0.3 psi/g. For a 3-g input then, a 1-psi dynamic stress is predicted at the lower frequencies.

STRENGTH ANALYSIS

The low stresses and strains that result from the low motor web fraction are not expected to cause motor failure even after extended aging when the motors are tested within the regime of service-environments. Referring to the constant-load-to-failure characterization, Figure 24, a stress of less than 10 psi is insufficient to cause perceptible damage. Therefore, one would not expect motor failure in the 2-year testing of these motors.

MOTOR TEST RESPONSE

Motor response to the various environmental loadings is interpreted in terms of the response of the embedded gages. The data are examined in three areas: (1) response to the pressurization calibration cycles conducted before and after the 2-year service-life simulation, (2) response of the gages in SRBDM 7 during captive-flight simulation, and (3) response to the slow thermal variation of the accelerated storage cycling.

Reduction of gage output to engineering units is based on the no-load calibration and sensitivity data supplied with the motors. As a practical matter, motor aging is as readily monitored by comparing raw gage outputs.

PRESSURIZATION CALIBRATION CYCLES

Pressurization calibration, described previously, was conducted over the range of 158 to -17 F in September 1975 and over the range of 153 to -45 F in September 1976. Raw gage outputs are plotted in Figures 91 through 96. From these data, we note slight changes in gage outputs with relatively little change in thermal stress or strain responses.

Changes in level of output are tabulated in Table 16, wherein we see no consistent pattern to indicate a difference between the two motors. Changes in stress/strain at each motor site are compared in Table 17.

TABLE 16. EFFECTS OF AGING ON SRBDM MOTOR GAGES

Motor No.	Average Change in Clip Gage Response, mv	Average Change in Normal Stress Gage Response, mv	Average Change in Shear Stress Gage Response, mv
4	-1.4	-2.0	-0.1
7	-3.5	-0.6	-1.0

TABLE 17. COMPARATIVE STRESS/STRAIN RESPONSE COOL-DOWN FROM 150 TO -10 F

Motor	Location	September 1975			September 1976		
		Bond Stress, psi	Bore Strain, %	Shear Stress, psi	Bond Stress, psi	Bore Strain, %	Shear Stress, psi
4	Fwd	-	3.9	8.4	-	4.0	7.1
	Center	14.2 15.2	5.8	1.6	13.4 15.9	5.9	2.7
	Aft	4.2	-	-	6.6	-	-
7	Fwd	9.1	4.4	9.6	7.2	-	7.2
	Center	16.2	5.4	3.4	15.9	5.5	3.9
	Aft	0.2	-	-	5.4	-	-

The shift in clip gage output (Table 16) is perhaps indicative of a tightening cure (and corresponding volumetric shrinkage of the grain). The change is on the order of 1% strain on Motor 4, which was temperature cycled only, and 2% strain on Motor 7, which was temperature cycled and subjected to captive-flight simulation. Stress changes are much less significant. The smaller change in Motor 7 resulted from a large positive change (less stress) in the gage at the forward end of the motor. The stresses may have changed less from the initial readings than would have been expected due to the age of the motors and their exposure to the environment before the start of testing. In addition, normal stress gages have a tendency to drift somewhat with time. Nonetheless, laboratory tests of aged cartons and the motor gage data indicate that TP-H8214 propellant is susceptible to aging at a very low rate.

For comparison with analysis, a replot of average stresses and strains for the 1975 cycle is presented in Figure 97 along with the temperature environment in that cycle. Although the strains compare favorably, measured stresses are higher than predicted by almost four times. Three sources of error are identifiable:

1. A limited study in the laboratory of uniaxial vs multiaxial behavior indicated higher multiaxial stiffness (modulus) than normally expected. Typically, the uniaxial/biaxial/triaxial modulus ratio is 6/8/9. For TP-H8214, however, the observed ratio was on the order of 5/8/10. Thus, the triaxial stiffness (representative of propellant bulk) is ~ 50% higher than expected. This could indicate a 50% higher stress than calculated.

2. The gage calibration and long-term behavior result in a significant uncertainty in the stress gage measured stresses.

3. The motors were aged ~ 9 months before the conduct of the first test. The effects of the aging are somewhat indeterminate because early aging on the carton propellant was not obtained and subsequent aging was marked by surface effects.

Actually, the fact that measured stress exceeds the analytic prediction by a factor of four indicates the overall uncertainty in both analysis and measurement. In any event, stress levels are still below that required to induce significant damage as measured by the constant-load-to-failure method.

CAPTIVE-FLIGHT SIMULATION TESTS

Motor 7 was subjected to two series of handling and captive-flight simulation tests as indicated in Figure 15. Characterization 3-g sine surveys were conducted over the temperature range 170 to -60 F in one transverse axis. Gage and motor response are illustrated in Figures 98 through 109. The 3-g control input, plotted in Figure 98, represents the average input to two rings located approximately 14 inches forward and aft of the center of gravity of the motor. Figure 99 shows the response at the motor center of gravity. Response peaks at 115 and 240 Hertz are noted. Figures 100 and 101 provide response at the floated forward end of the grain and the adjacent case. Response peaks at 115 and 185 Hertz and minor peaks at 265, 330, and 550 Hertz were recorded.

The major responses were characterized by a grain amplification of less than 2:1. Plots of internal gage outputs are shown in Figure 109. Gage N7-57 output was so noisy in this test that analysis was precluded. Cables for this gage were subsequently repaired, and it was monitored during the dynamic tests. Gage N7-59, located under the thin aft propellant web showed virtually no response due to the high noise level. Subsequent testing yielded peak outputs of nearly 1 millivolt (~ 1 psi) at this site. Normal Gage N7-61, at the motor center plane, responded in the 110 and 260 Hertz bands. Gage N7-63, located near the root of the forward floater, responded to forward end resonances with peaks up to 5 millivolts (~ 5 psi) at 115 and 185 Hertz and a 2.5-millivolt peak at 260 Hertz. Shear Gage S7-135, at the motor mid-plane, responded at only one frequency, 120 Hertz. Gage S7-137, also at the mid-plane, responded at 115 Hertz and with a small significant response at 175 Hertz. The forward head shear gage, S7-140, peaked, like Normal Gage N7-63, at 115 and 185 Hertz with smaller peaks at 260 and 320 Hertz. The clip gages, responses from two of which are shown, did not exhibit any significant dynamic response.

From these data we can characterize dynamic response of the SRBSM motor as follows:

1. The motor exhibits bending-type motion at about 115 and 250 Hertz.

2. The forward end has additional response, probably due to the floated forward head in the grain, at 185, 330, and 550 Hertz.

3. None of these resonances excite the inner bore as a true grain resonance (predicted to occur at about 1000 Hertz).

4. The small web fraction and cylindrical geometry of the motor design and the increasing stiffness of propellant with frequency do not produce serious grain response under dynamic conditions.

The effect of temperature on dynamic response is small. At 165 F, no distinct forward head resonances were noted. Three frequencies produced dynamic peaks, 170 and 230 Hertz and a band from 420 to 480 Hertz. At 0 F, the forward end had a distinct resonance at 100 Hertz, the entire motor at 115 Hertz and again at 200 Hertz. At -65 F, the forward head showed a small peak at about 100 Hertz and the entire motor at about 200 Hertz. Oscilloscope display of the forward head accelerometers and gages gave no indication of banging between the floated end of the grain and the case wall.

Responses of the gages to the 3-g sine sweeps conducted as a part of each series of captive-flight simulations are tabulated for comparison in Table 18. No discernible trend in the response was noted between the first and second series of tests. The actual installation of the motor in the vibration fixture was probably more significant in terms of change in response than were the effects of aging and cumulative damage.

The simultaneous application of random vibration and aeroheating was the principal part of the captive-flight simulation. Each series of simulation tests consisted of 10 cycles of aeroheating/vibration. The thermal cycle of -30 to 170 F for 130 minutes and back to -30 F constituted the most significant load on the motor. This thermal response is exemplified by data plotted in Figures 110 and 111, which show the temperature profile and stress/strain gage outputs over one aeroheat cycle. Figures 112 through 115 show the cycle-to-cycle response of each gage for the 10-cycle series conducted in 1975. The uncertainty of the data during aeroheat (rapid rate of temperature change) is large because of the thermal gradient near the gages. Cycle-to-cycle repeatability of the gages is demonstrated.

The random vibration imposed on the motor was adapted from flight data recorded during F-111 captive flight of a Bomb Dummy Unit (BDU)

TABLE 18. COMPARATIVE RESPONSE OF SRBDM STRESS GAGES

3 g SINE SWEEP TESTS

Gage		165 F				75 F				-30 F				-60 F			
		f_1, Hz	A_1, mv	f_2, Hz	A_2, mv	f_1, Hz	A_1, mv	f_2, Hz	A_2, mv	f_1, Hz	A_1, mv	f_2, Hz	A_2, mv	f_1, Hz	A_1, mv	f_2, Hz	A_2, mv
N7-57	1975	230	1.15	430	2.50	250	1.60	320	0.86	70	0.48	110	1.05	75	0.44	110	0.64
	1976	215	1.35	400	1.20	260	1.20	380	1.50	70	1.20	95	1.15	75	0.25	110	0.25
N7-59	1975	165	1.62	350	0.55	150	1.70	260	0.48	-	-	160	0.70	100	0.24	-	-
	1976	160	1.05	360	0.33	165	1.12	335	0.87	95	0.36	180	0.28	-	-	-	-
N7-61	1975	180	1.80	430	5.25	120	1.80	260	2.80	100	2.0	210	2.05	100	1.15	215	1.21
	1976	190	1.90	400	3.40	175	1.20	380	4.20	-	-	205	1.85	100	0.70	220	0.83
N7-63	1975	180	2.60	215	2.80	170	5.4	265	4.3	100	3.10	185	1.46	100	0.94	190	0.45
	1976	160	2.60	200	2.75	160	5.1	210	4.5	95	2.45	190	1.05	95	0.31	180	0.19
S7-135	1975	180	1.35	-	-	120	0.53	-	-	-	-	-	-	-	-	-	-
	1976	1976	0.50	-	-	150	0.70	-	-	-	-	-	-	-	-	-	-

reported in AFRPL-TR-76-36. Because of the random input, rather than attempt a cycle-to-cycle comparison, the response at -30 F equilibrium temperature of the first 10 tests was averaged to obtain the results plotted in Figures 116 through 126. The input control, again the average at the rings, shown in Figure 116, had an rms g level of about 2 g. The peak gage response occurred on Gage N7-61, Figure 122, at about 260 Hertz and corresponds to a dynamic stress of about 0.4 psi.

Near the end of the 2-year test period, a second series of captive-flight simulation tests was run. The test conditions were altered according to updated results from the BDU captive-flight studies. The aeroheat thermal profile was made more severe in that the case wall (at the inlet air location) was controlled to about 180 F, whereas in the first test series the inlet air was controlled to 180 F. This resulted in case temperatures up to 55 degrees (F) higher during the second series. The random vibration input control was also modified to remove input emphasis at 900 and 1500 Hertz--"resonances" that were established to be a result of the data acquisition system on the BDU. The test results were essentially the same as those from the first test series. The case thermal profile through the 10-cycle test is shown in Figure 127. Representative gage responses are shown in Figures 128, 129, and 130. Cycle-to-cycle repeatability is demonstrated in Figure 128. The variation on the normal stress gages, Figures 129 and 130, was caused by cross-talk between the dc data recorder and the amplifiers used for dynamic (ac) signal recording. The average input control is plotted in Figure 131. A typical gage response, averaged over the 10 cycles, is shown in Figure 132. The peak rms dynamic stress of about 0.4 psi occurred at about 210 Hertz. There was no detectable response beyond about 650 Hertz. This is attributed to the modified input control without the overdriving at the higher frequencies and to the improvement in motor installation in the test fixture. A tighter fit between input rings, motor, and fixture was obtained (as a result of the learning process) for this test series.

In summary, the effects of the 20 cycles of simulated captive flight were not detected in the motor gage response to aeroheating or vibration. This is not to say there were no effects; but within the repeatability of the tests and the instrumentation response, no deleterious effects were observed.

SIMULATED FIVE-YEAR STORAGE

As described previously, both motors were subjected to 5 years of simulated storage in a 2-year test period. The test covered temperature extremes such as might be encountered in 2.5 years of desert storage (including three summers) and 2.5 years of arctic storage (including three winters). Gage outputs over the 2-year test are plotted chronologically in Figures 133 through 138. Data for Motor 4 were recorded on the Air Force Portable Data Acquisition System from Day 655 to Day 715. These data are indicated by a dashed line. Four of the six clip gages in Motor 4, Figure 133, show excellent repeatability over the test cycles. Gages C4-41 and C4-42 show drifts of 2 to 4 millivolts ($\sim$ 1% strain), especially during the tropical desert simulation. Note that the change in output over a given temperature cycle remains essentially constant. Since this shift occurs on two of the six gages, one would tend to attribute this to gage drift such as is often observed in stress gages over a period of time. Repeatability of the shear and stress gages in Motor 4 is less apparent but is equally present. No-load outputs of these gages vary considerably with temperature such that in some temperature regimes little change in output occurs. For observing time-related changes, however, a direct comparison of millivolt output is sufficient. Normal stress gage outputs are corrected for internal pressure in the sealed motors.

The same type of downward shift as noted on two clip gages in Motor 4 is seen on all clip gages in Motor 7, Figure 136. Similar comments for the normal and shear stress gages also apply.

Overall, a large amount of data was generated over the 2-year test period. In terms of the program objectives, if any significant aging of the SRBDM propellant occurred, it was of less significance than the uncertainty in the gage response. Although some shift changes in gage output are recorded, no major trends that would indicate significant change in grain response during a simulated 5-year storage are observed.

Page 52 is blank

CONCLUSIONS AND RECOMMENDATIONS

The effort conducted on this program was fairly extensive when compared with the typical aging assessment on a tactical solid rocket motor. An assessment of the techniques used on the program led to the following conclusions:

1. The use in internal instrumentation was of marginal value. On this system, at least, the detected aging effects are minimal. Uncertainty in interpretation of gage response and the rate of aging of the gages themselves, combined with the effort required to install, maintain, and monitor the gages and to interpret the data diminishes their effectiveness. In future applications of gages, one should evaluate the cost of sophisticated instrumentation against the cost of additional motors that can be destructively evaluated (overtested to failure and dissected) for aging effects. There are, however, applications in which gages would be especially useful, e.g., in large and very expensive motors.

2. Correlation between aging in the motor in simulated service and laboratory aging in cartons has been neither proven nor disproven. Carton aging remains a desirable feature of any aging study. To be fully effective, it should be initiated at the end of cure and continued over an extended period. It would be desirable to ensure chemical similitude (exposure to atmosphere, presence of liner, etc.) between the cartons and the motors. Rather complete characterization of the propellant is required since no one parameter is readily identified as the key to aging definition.

3. An accelerated service-life simulation test based on carton aging is feasible and potentially accurate. One major difficulty in its design is the determination of which parameters that show change with age are essential in defining motor aging rate. Such parameters as sol-gel ratio, relaxation modulus, and tensile failure properties do not show the same rates of change. Cumulative damage, which is of perhaps equal or greater importance, must be considered in designing a service-life simulation test.

4. A significant backlog of environmental data now exist so that a probable service environment for a given motor can be defined. A statistical analysis of the relative frequency of occurrence of the probable environment in the motor population would be desirable. Such an analysis might be accomplished on a system in the field. A new system would require considerable speculation.

In addition to observations concerning techniques, the following conclusions relative to the program objectives are made:

1. The moderate-burning-rate HTPB propellant, TP-H8214, shows slight aging tendencies, but no critical property degradation was observed in 70 weeks of elevated-temperature laboratory carton aging studies or in 2 years of simulated service-life testing. The possible exception to this conclusion is an apparent surface aging effect in the cartons. Steps taken to preclude exposure of carton propellant to the atmosphere were apparently insufficient. If the severity of this minimal exposure is indicative of the behavior of this propellant, it should be readily detected in a post-dissection test of propellant grain properties.
2. The SRBDM-type motor, using TP-H8214 propellant, is structurally adequate through 5 years of in-service use. The accelerated test program, based on laboratory aging data, is generally indicative of 5 years of rather hard field deployment—2.5 years tropic environment, 2.5 years arctic environment. Motor instrumentation indicates slight changes in propellant properties as a result of this simulated 5-year service life.

Evaluation of the comparatively different approaches taken on the two systems being studied under the ALIVE program is reserved until completion of the second part of the program.

Since the two SRBDM-type motors have not failed structurally and there is no indication that their ballistic performance has been degraded by the tests to date, the following recommendations for their future are made:

1. Instrumentation in these motors is functional and useful. Therefore, destructive testing should be delayed to permit obtaining a maximum of aging data.

2. Based on experience, whereas a 5-year service life is a desirable minimum, a 10-year or more service life is advantageous. Within this time frame, mission requirements tend to change and propellant state of the art tends to increase so that when a motor approaches the end of its useful life, regraining can incorporate these changes.

3. Data thus far obtained together with data collected during the AFRPL in-house aging study of TP-H8214 (Ref. AFRPL-TR-76-39) provide a basis for designing an improved service-life simulation to extend the simulation to 10 years with an additional 2 years of testing. A model of this program is presented in the following section.

Page 56 is blank

RECOMMENDED TEST PLAN

A model test plan to extend the simulation of 5 years of service life to 10 years is described below. Precise details, such as temperature limits and weeks at each temperature, are to be defined based on aging data from the ALIVE program and additional data that may be available from the AFRPL in-house aging study. Following the method already used, Motor 4 will continue in simulated storage and Motor 7 will be subjected to additional captive-flight simulation.

ACCELERATED STORAGE ENVIRONMENT

The same tropic/arctic environments are envisioned. A recommended change to the sequence of exposures is illustrated in Figure 139. The advantage of alternating arctic/tropic storage is in the expected progressive increase in grain stress response.

CAPTIVE-FLIGHT SIMULATION

An enhanced captive-flight-simulation profile--higher rates of heating, larger number of simulated flights, and higher magnitude of dynamic input--reflects recent conclusions regarding the captive-flight environment of tactical motors on high-performance aircraft. Figure 140 illustrates a typical flight aeroheat profile for 1 day. This would be repeated for 10 days with possible variation in the cold soak temperature.

OVERTEST AND DISSECTION

After the additional 2 years storage and flight simulation, an overtest, probably consisting of exposing the motors to the temperature extreme of -80 F would be made. Propellant strain capabilities and

expected induced strains should make exposure to a reasonably cold extreme a structural-flaw-inducing overtest. The presence of inner bore clip gages would be expected to accelerate failure. Following inducement of failure and an assessment of its occurrence in each of the two motors, both units would be dissected and the propellant thoroughly characterized.

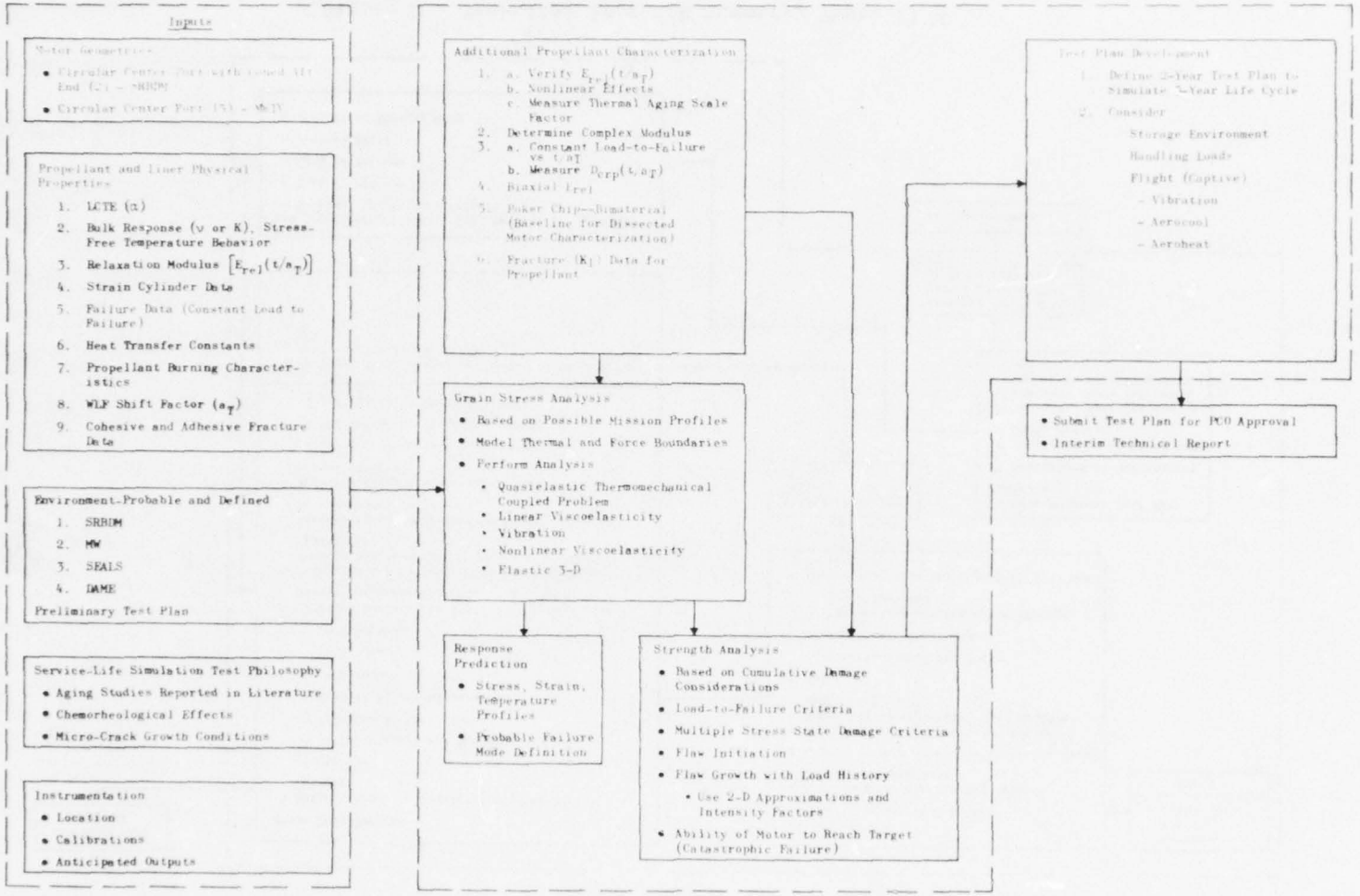

Figure 1. Technical Approach Summary, Phase I – Planning

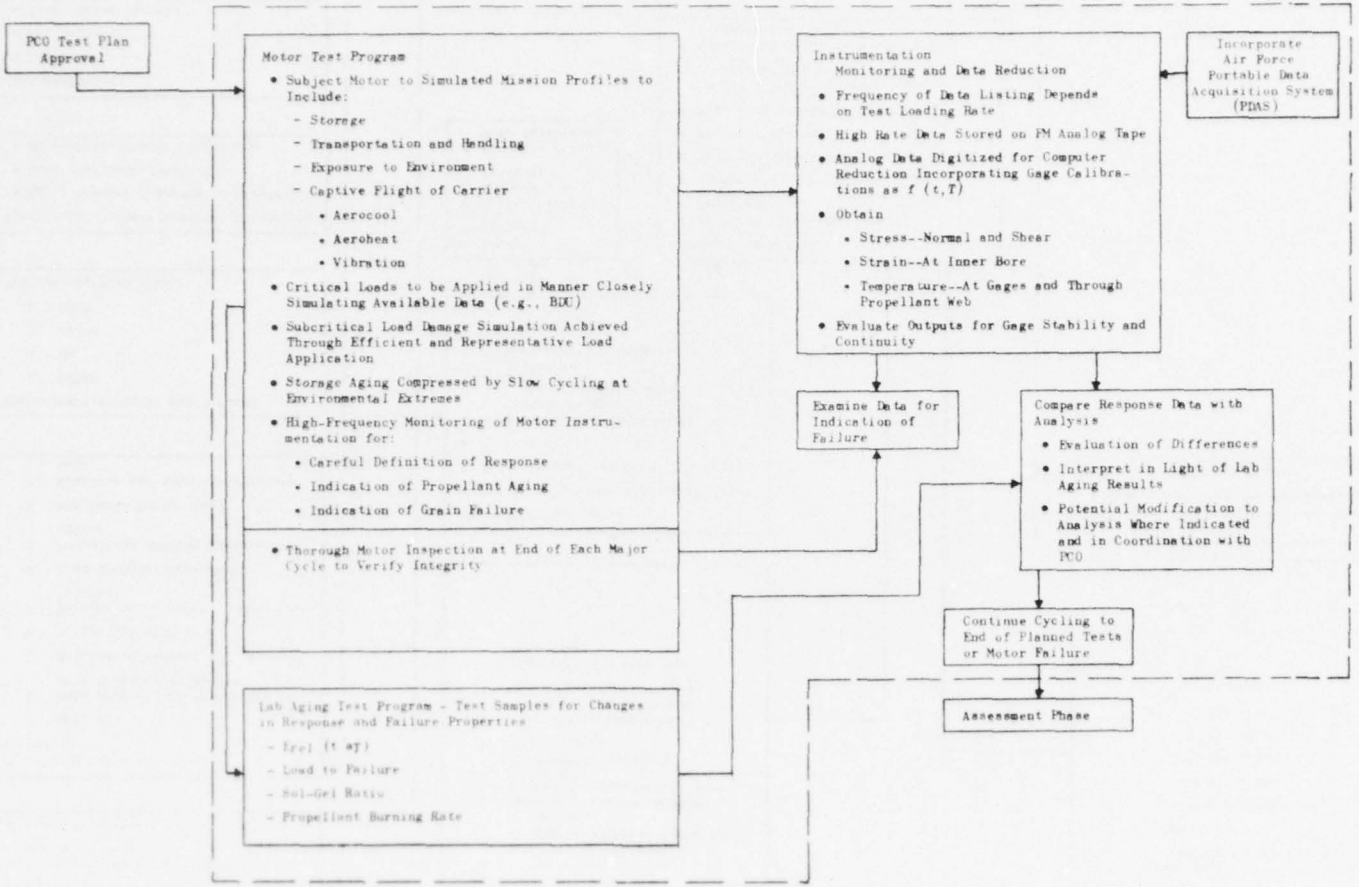

Figure 2. Technical Approach Summary, Phase II - Experimental

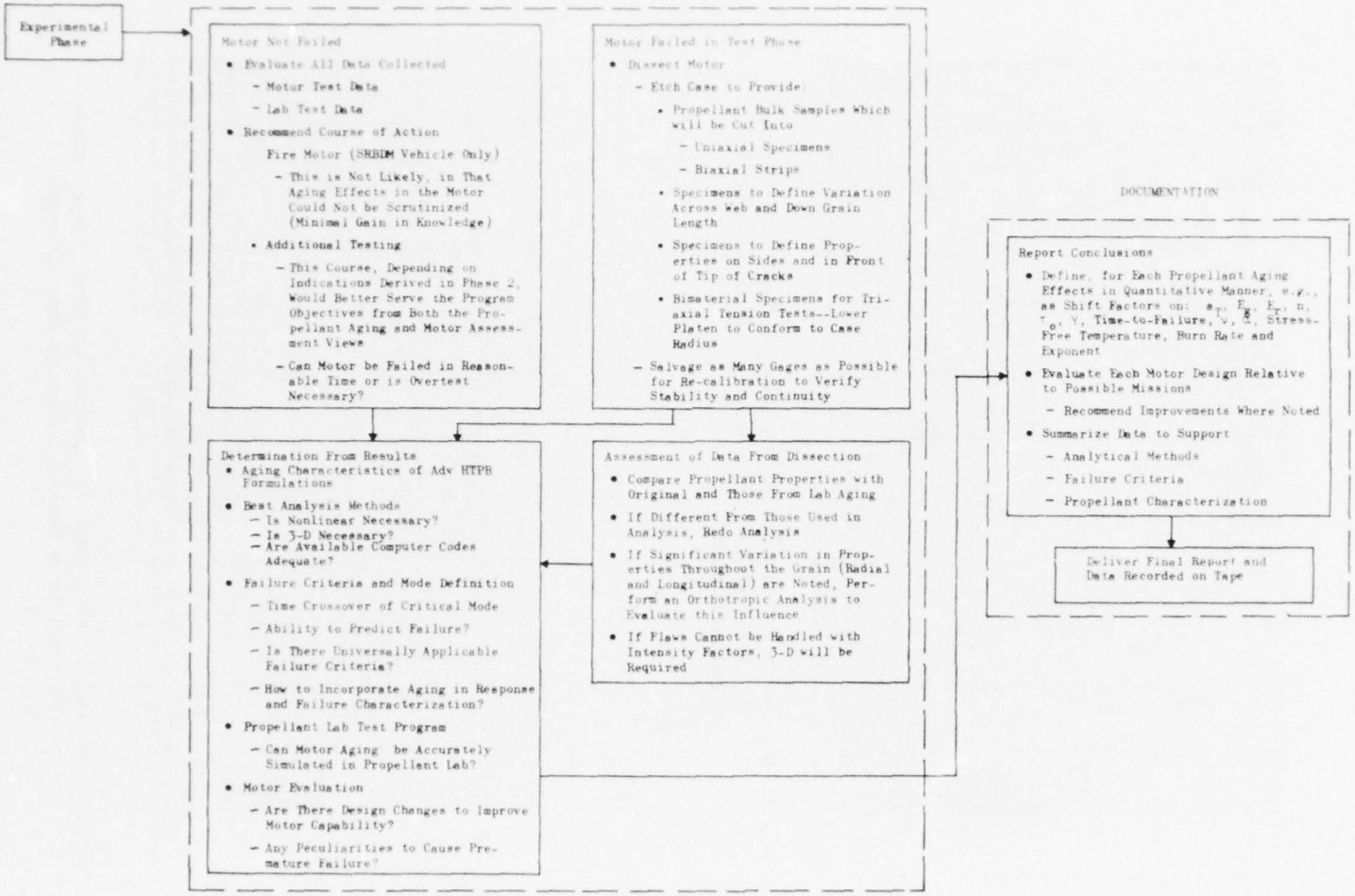

Figure 3. Technical Approach Summary, Phase III - Assessment

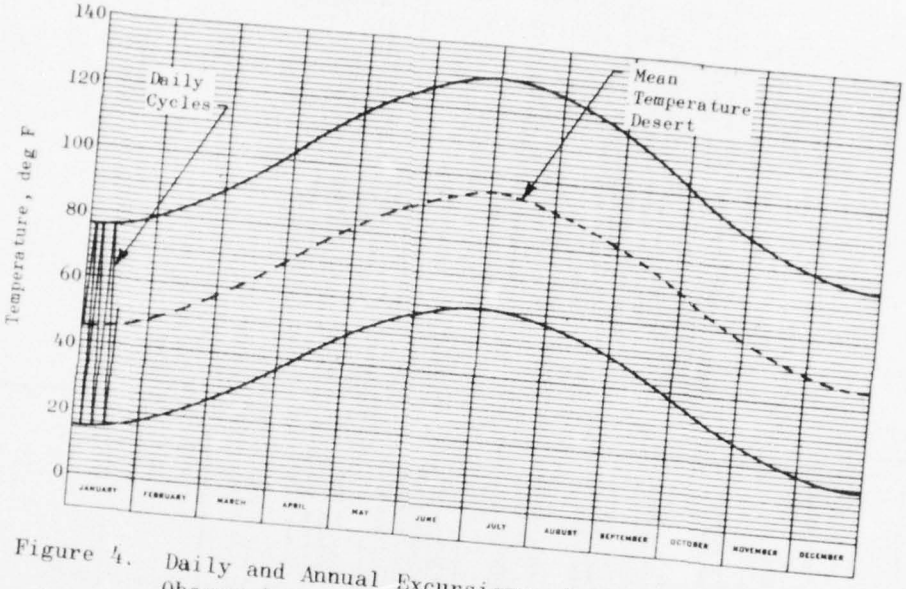

Figure 4. Daily and Annual Excursions of Case Temperatures Observed on a Rocket Motor in Dump Storage in a Tropical Desert

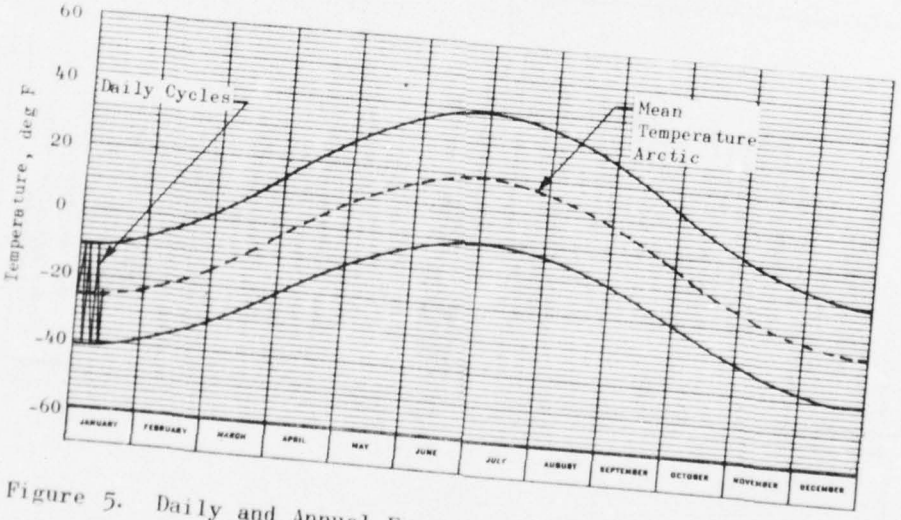

Figure 5. Daily and Annual Excursions of Case Temperatures Observed on a Rocket Motor in Dump Storage in the Arctic

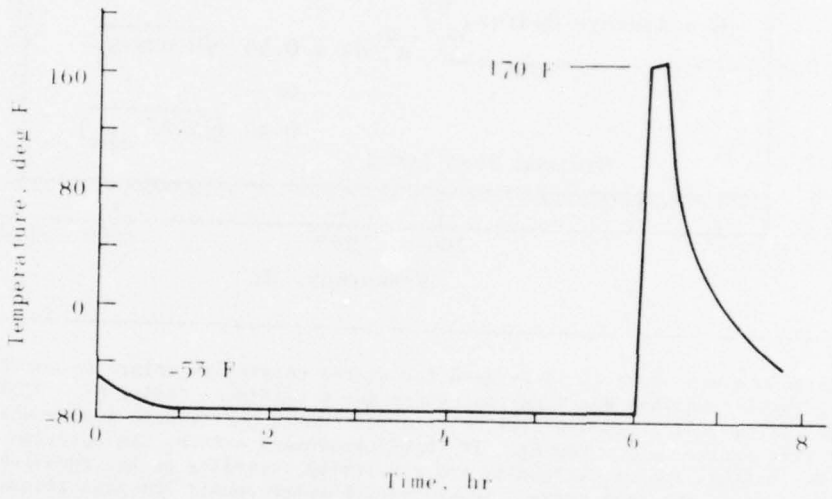

Figure 6. Estimated Motor Case Temperature

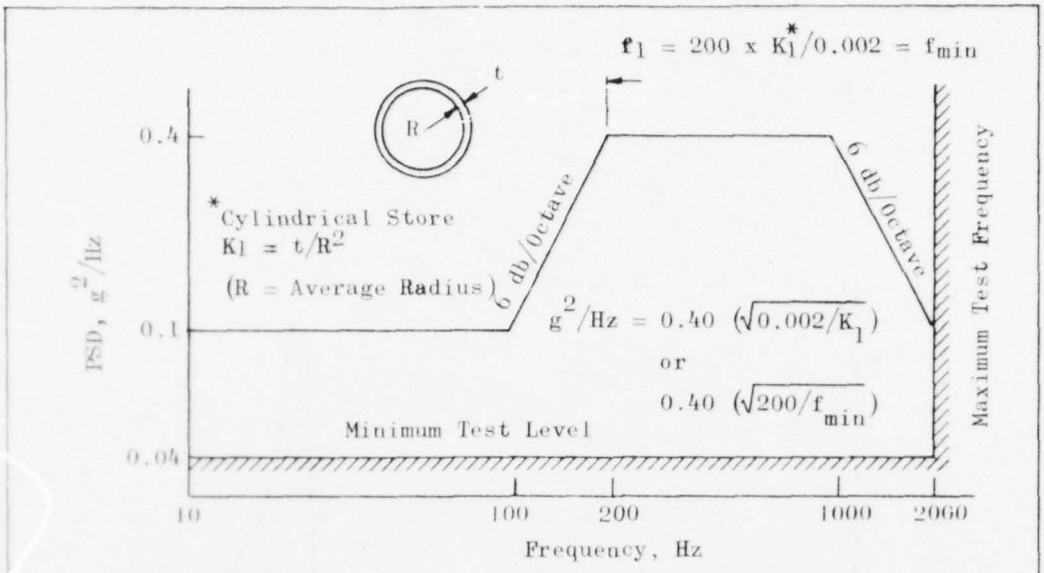

Test spectrum given above is to be used for stores carried on triple or multiple ejection racks such that a cylindrical store has a stiffness factor $K_1 = 0.002$ or a non-cylindrical store has flat or slightly curved panels with fundamental natural frequencies $f_{min} = 200$ Hz. If these parameters differ, the spectrum should be shifted, intact, laterally and vertically according to the equations given adjacent to the test curve. In no case, however, shall the test frequency continue beyond 2000 Hz or the test spectrum be lower than 0.04 g^2/Hz.

Functional and fatigue qualification test levels to be applied for a minimum of 1 hour on each of three mutually perpendicular axes. Levels and duration are established for stores carried at 0.9 Mach, 1000-foot altitude, $q \cong 1200$ psf and used for less than four missions. Stores carried longer or at different q should have the fatigue levels adjusted according to the relation

$$(g^2/Hz)_2 = (g^2/Hz)_1 \times \left[\frac{q_2}{1200}\right]^2 \times \left[\frac{M_2}{3}\right]^{0.25}$$

where the subscript 2 indicates the new test level, subscript 1 indicates the test level given on the curve above (after adjustment for K_1 or f_{min}), and M indicates the number of missions expected. This relation, without the $M_2/3$ term, should be used to adjust the functional test levels. Other test details should be in accord with MIL-STD-810.

Figure 7. Vibration Qualification Criteria for Externally Carried Aircraft Stores [1]

[1] Dreher, J. F., E. D. Lakin, and E. A. Tolle: "Vibracoustic Environment and Test Criteria for Aircraft Stores during Captive Flight," Shock and Vibration Bulletin No. 39, Supplement, 1969.

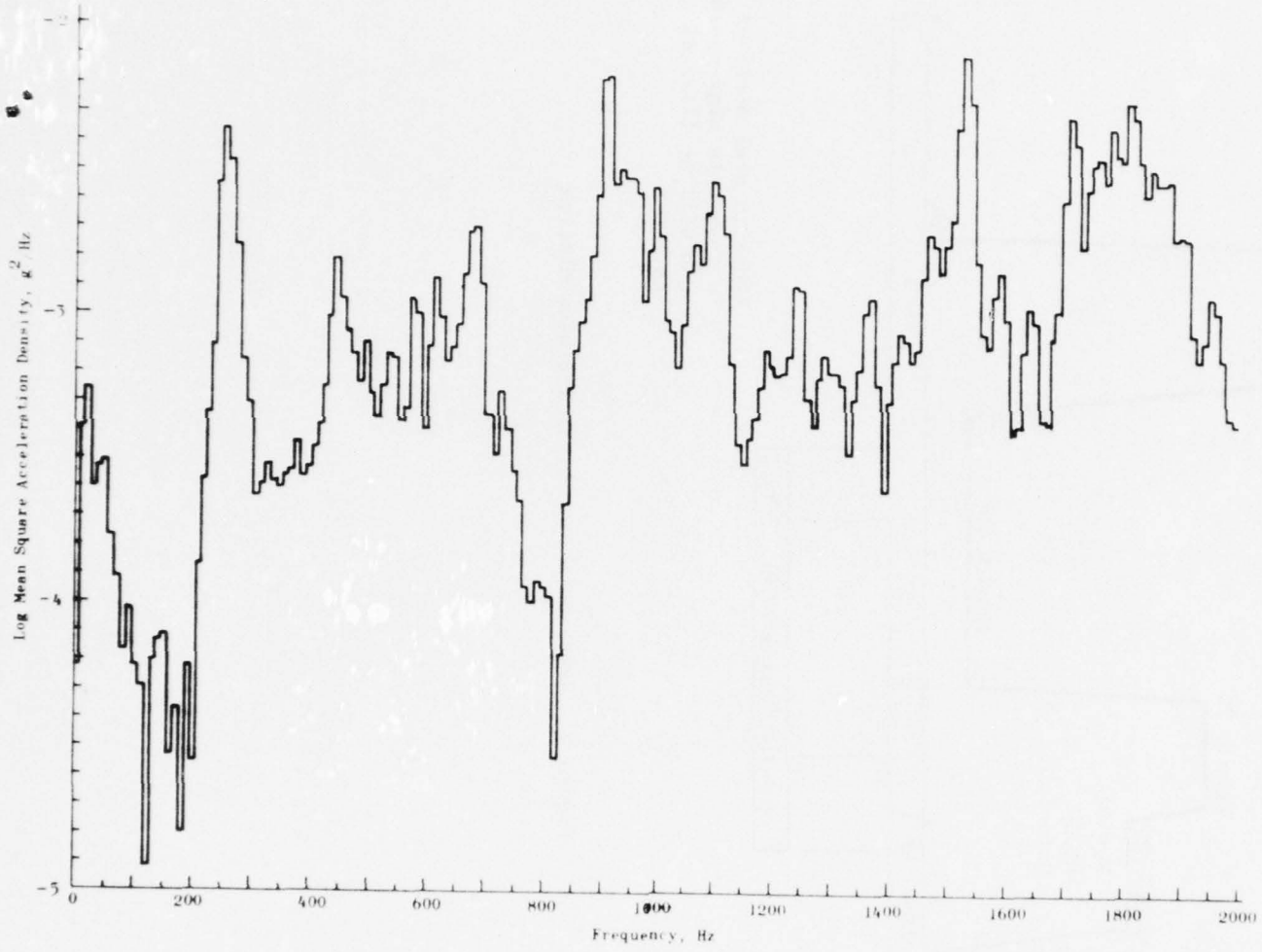

Figure 8. Power Spectral Densities on the Bomb Dummy Unit in Captive Flight, Project DAME

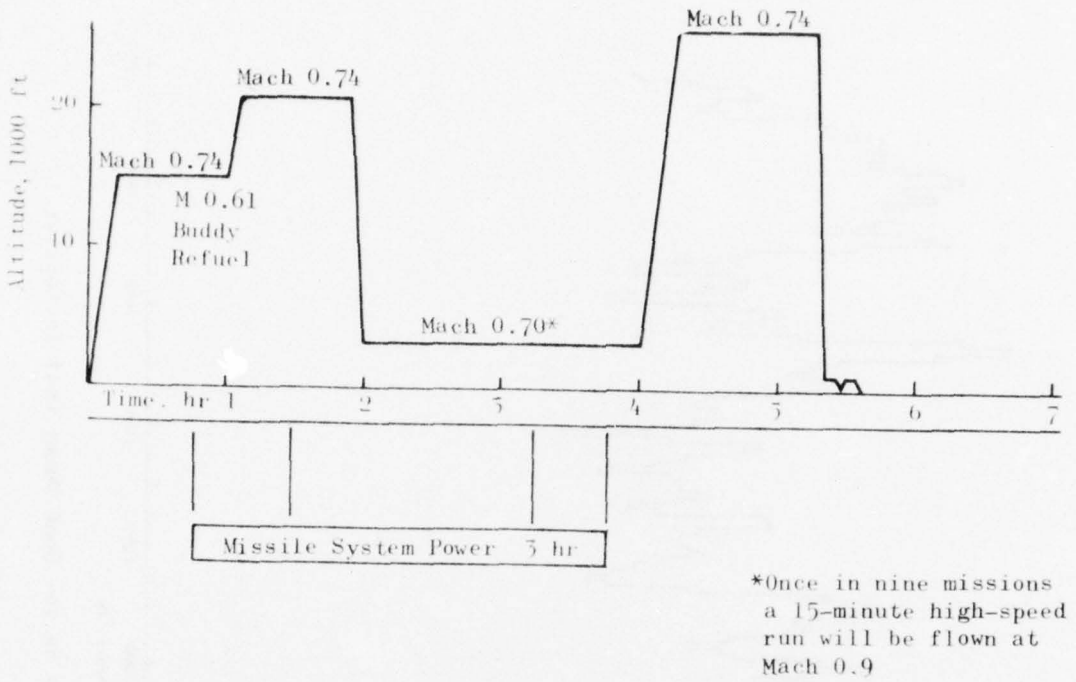

Figure 9. Representative Flight Training Mission

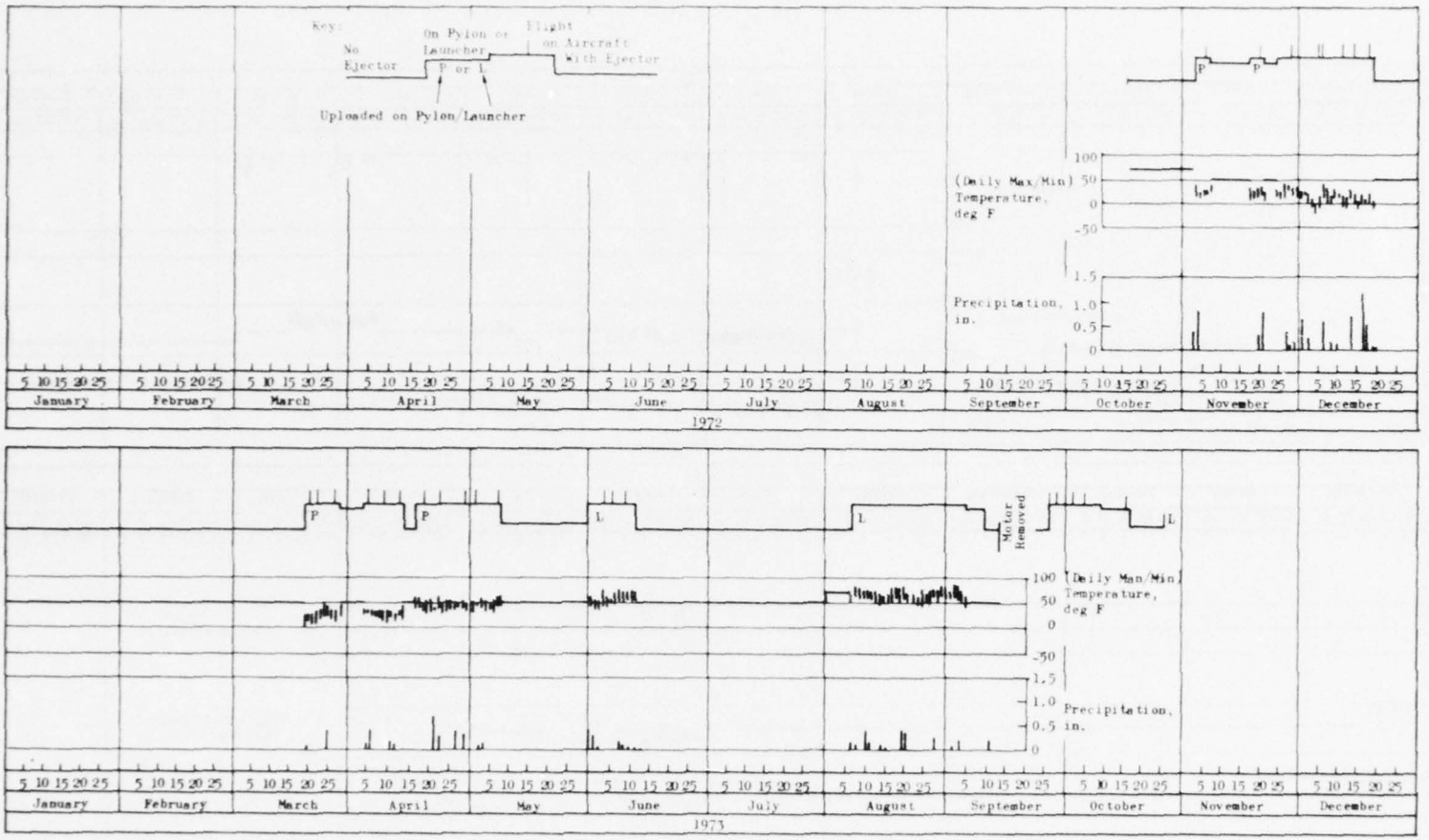

Figure 10. Motor 1 Loading Histogram

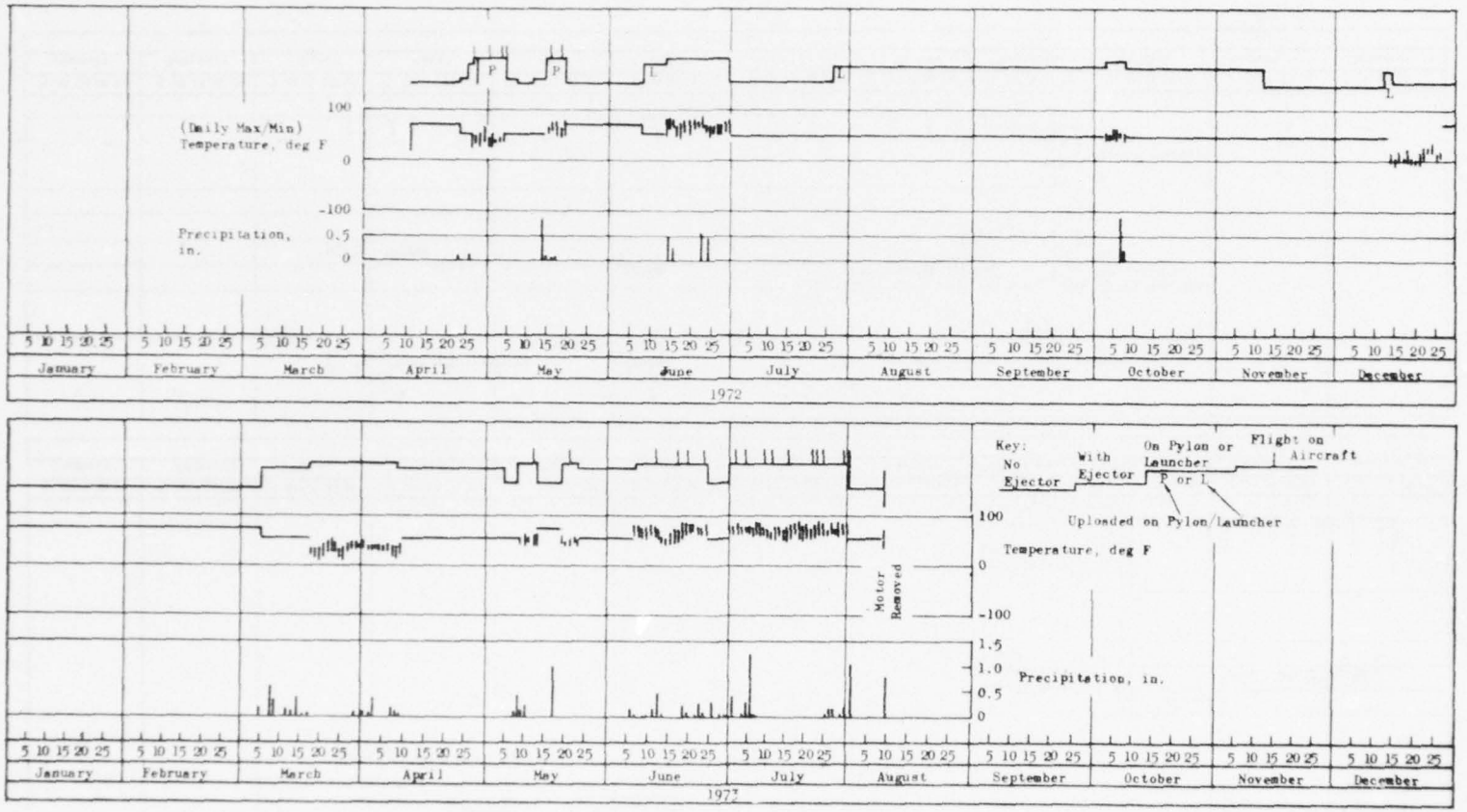

Figure 11. Motor 2 Loading Histogram

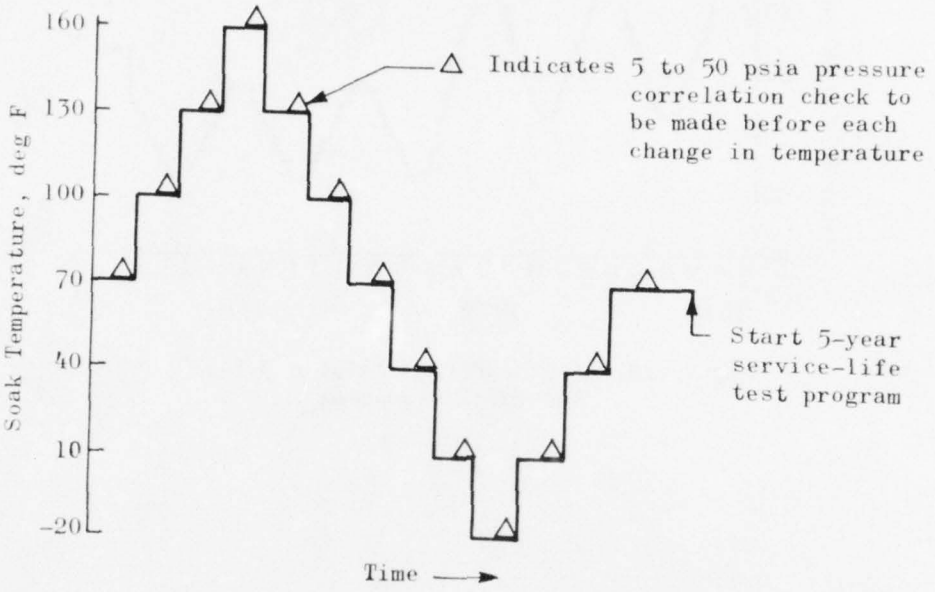

Figure 12. Thermal/Pressure Gage Response Initial Correlation

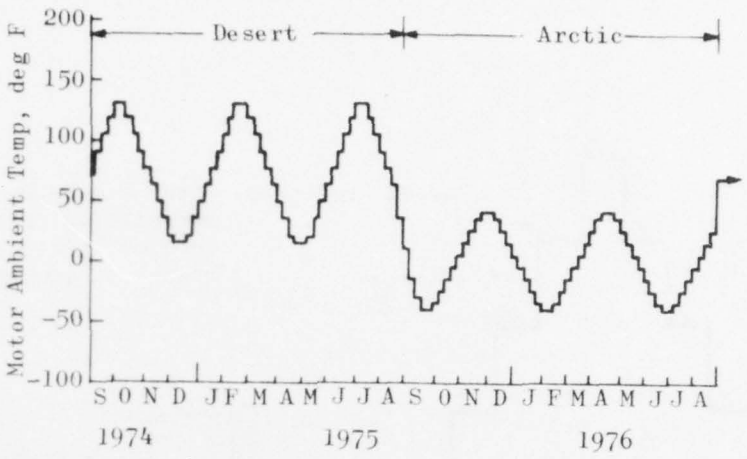

Figure 13. ALIVE SRBDM Simulated 5-Year Thermal Environment

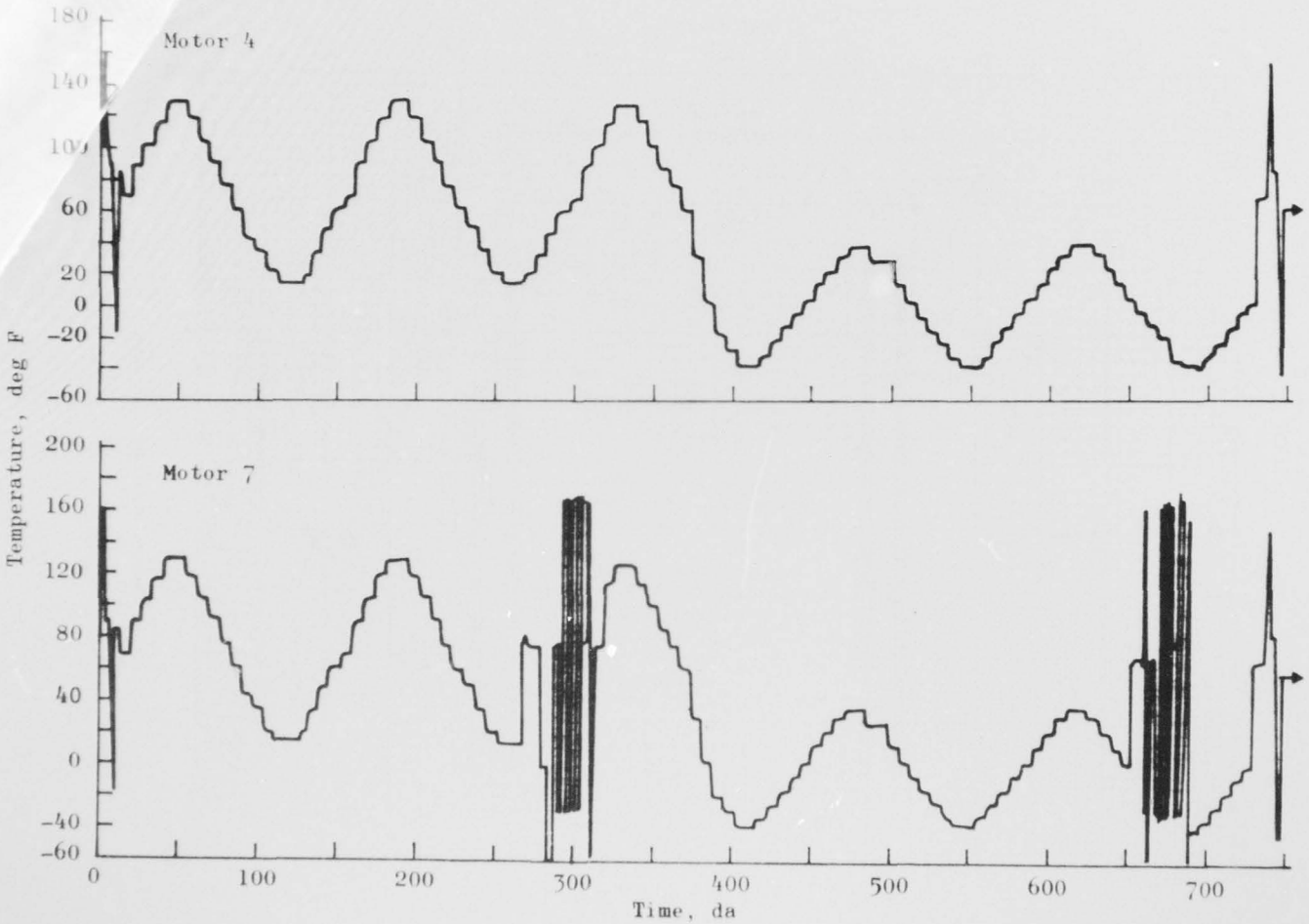

Figure 14. Seasonal Thermal Cycling Test History

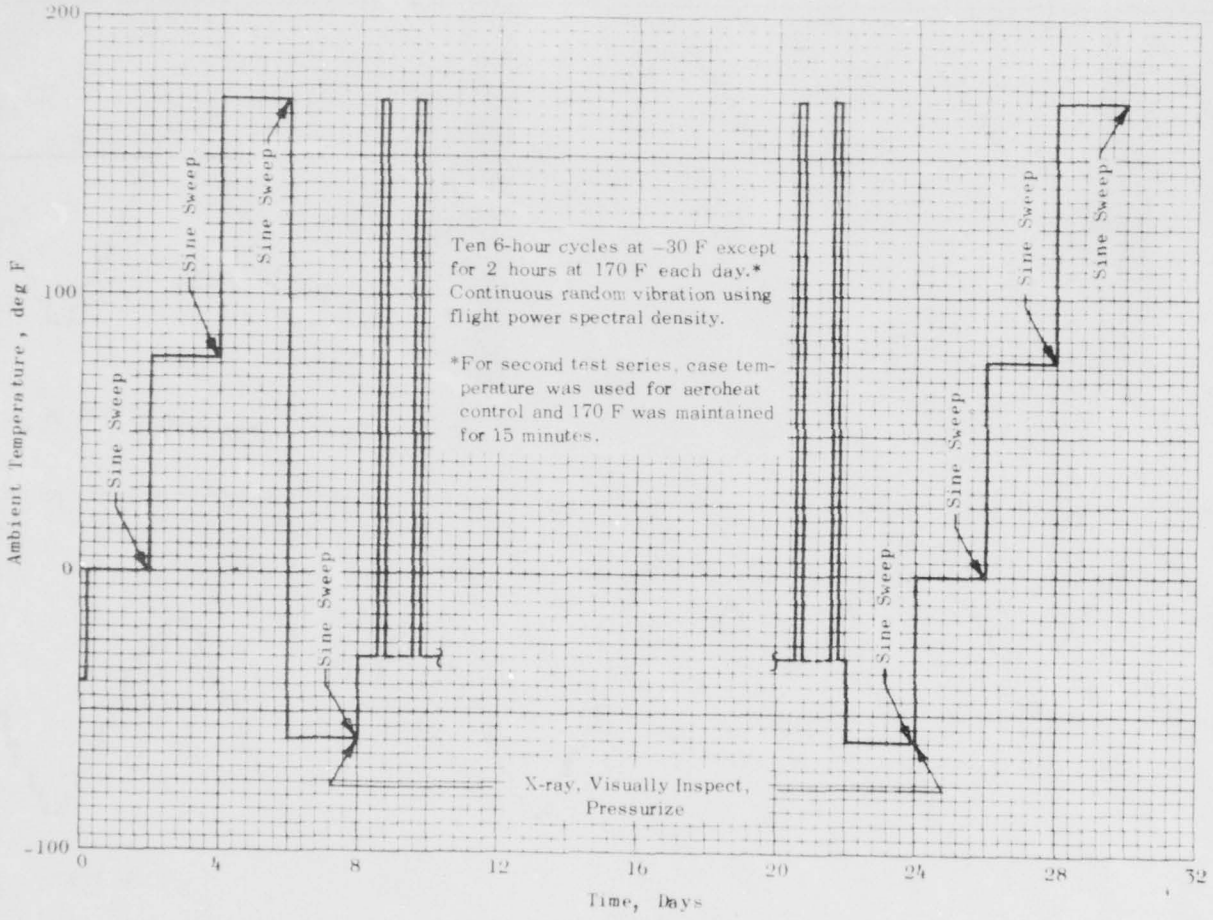

Figure 15. Simulated Flight Loads, Motor 7

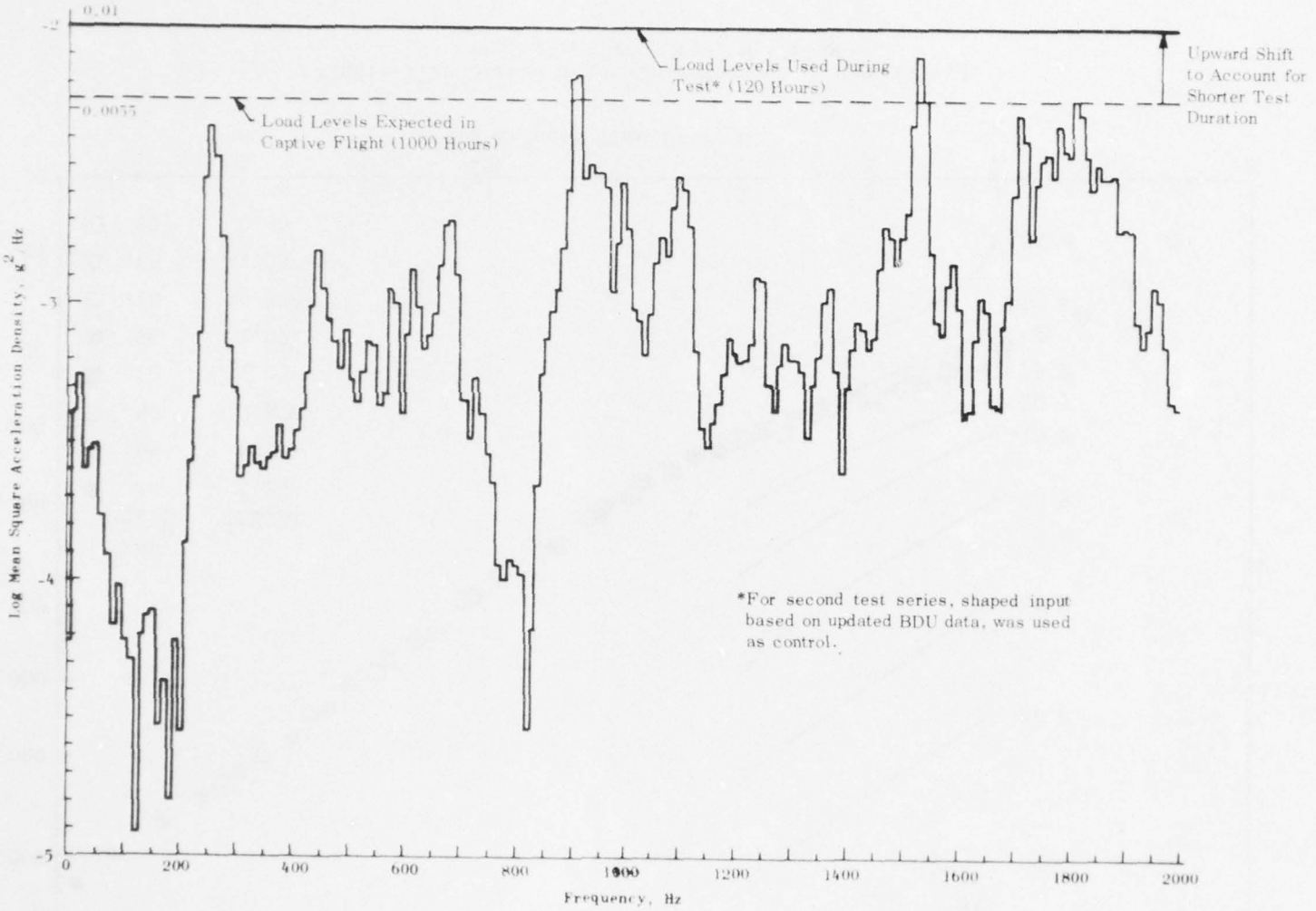

Figure 16. Power Spectral Densities on the Bomb Dummy Unit in Captive Flight

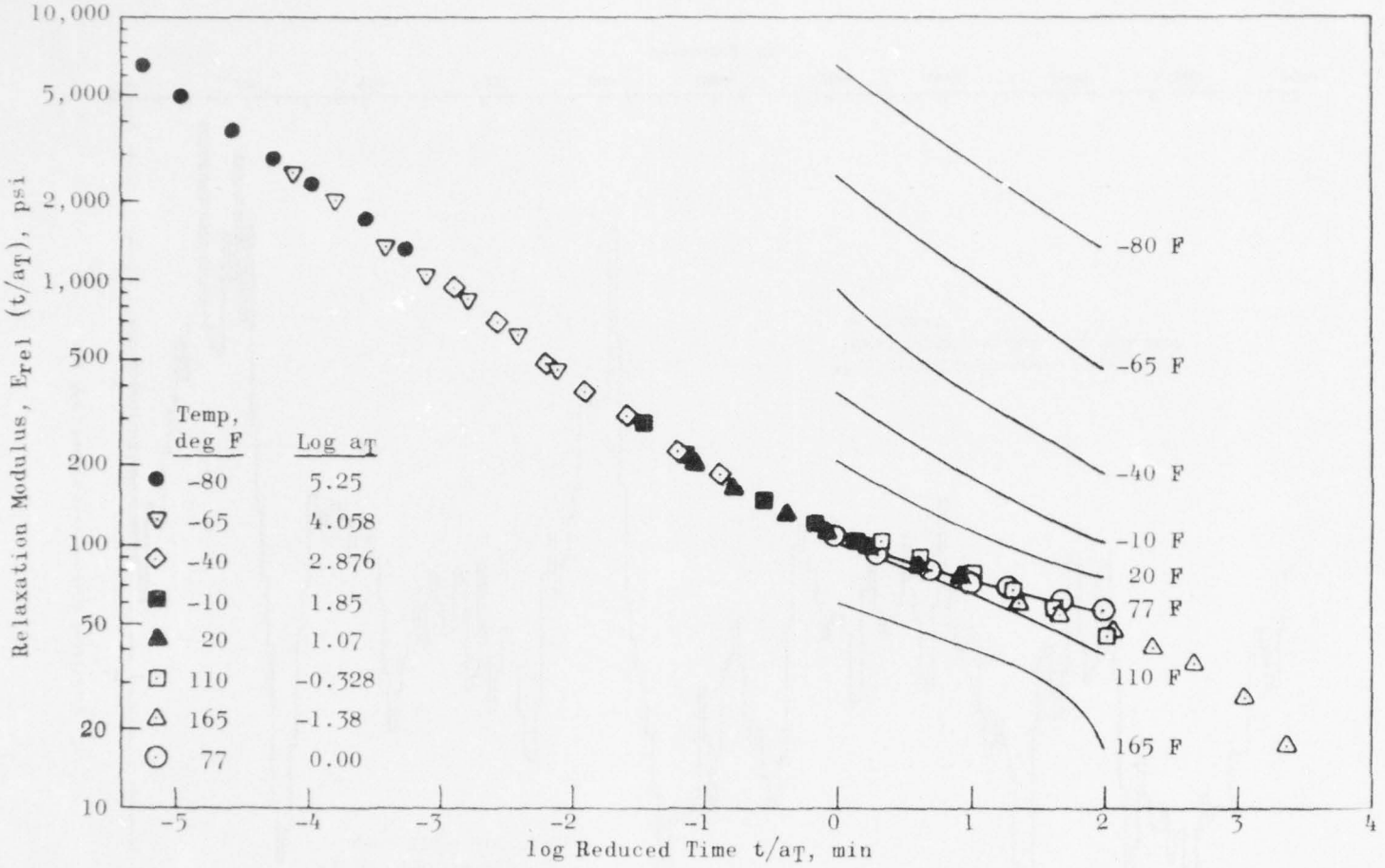

Figure 17. Stress Relaxation Modulus vs Log (t/a_T), Propellant TP-H8214, Mix L-389

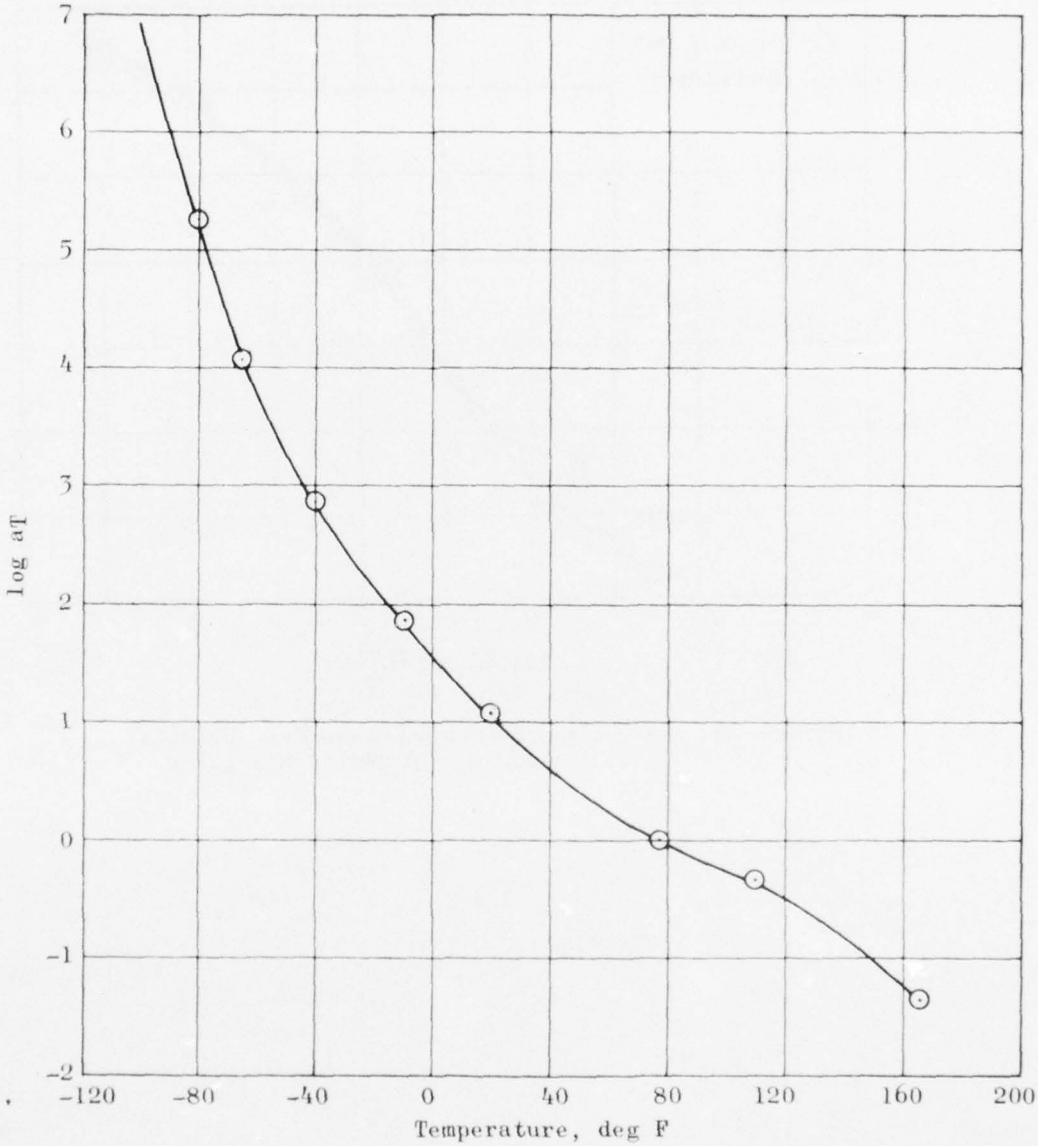

Figure 18. Log a_T vs Temperature, Propellant TP-H8214

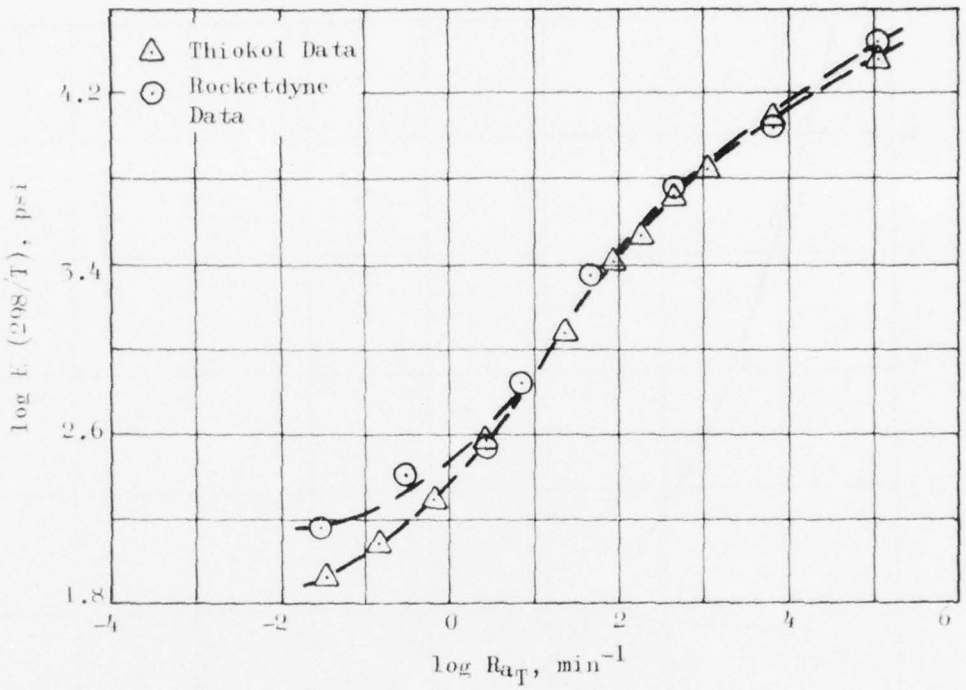

Figure 19. Base-Line Constant Strain Rate Uniaxial Tensile Modulus, TP-H8214, Mix L-389

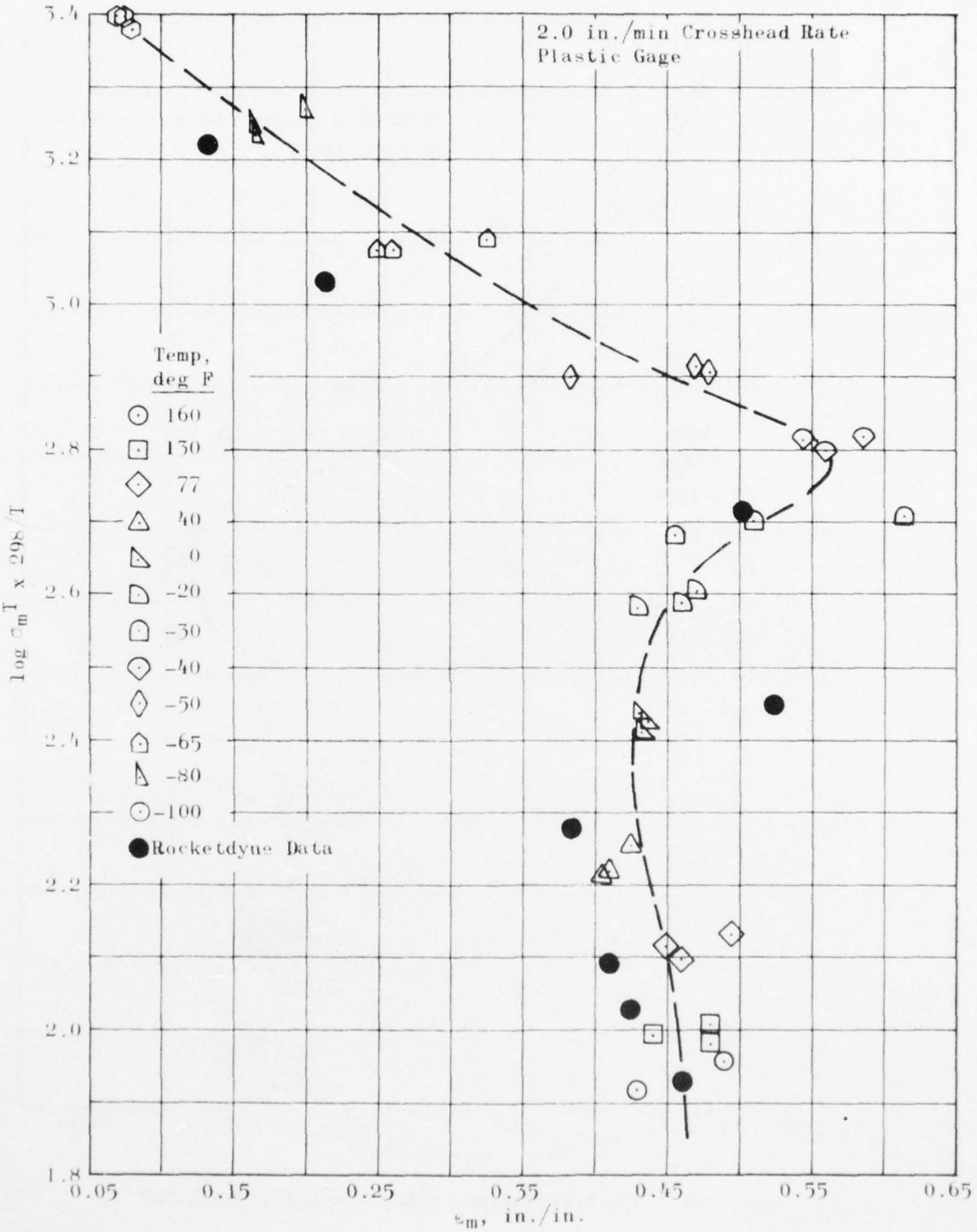

Figure 20. Uniaxial Failure Data, TP-H8214, Mix L-389, from AFRPL-TR-74-03

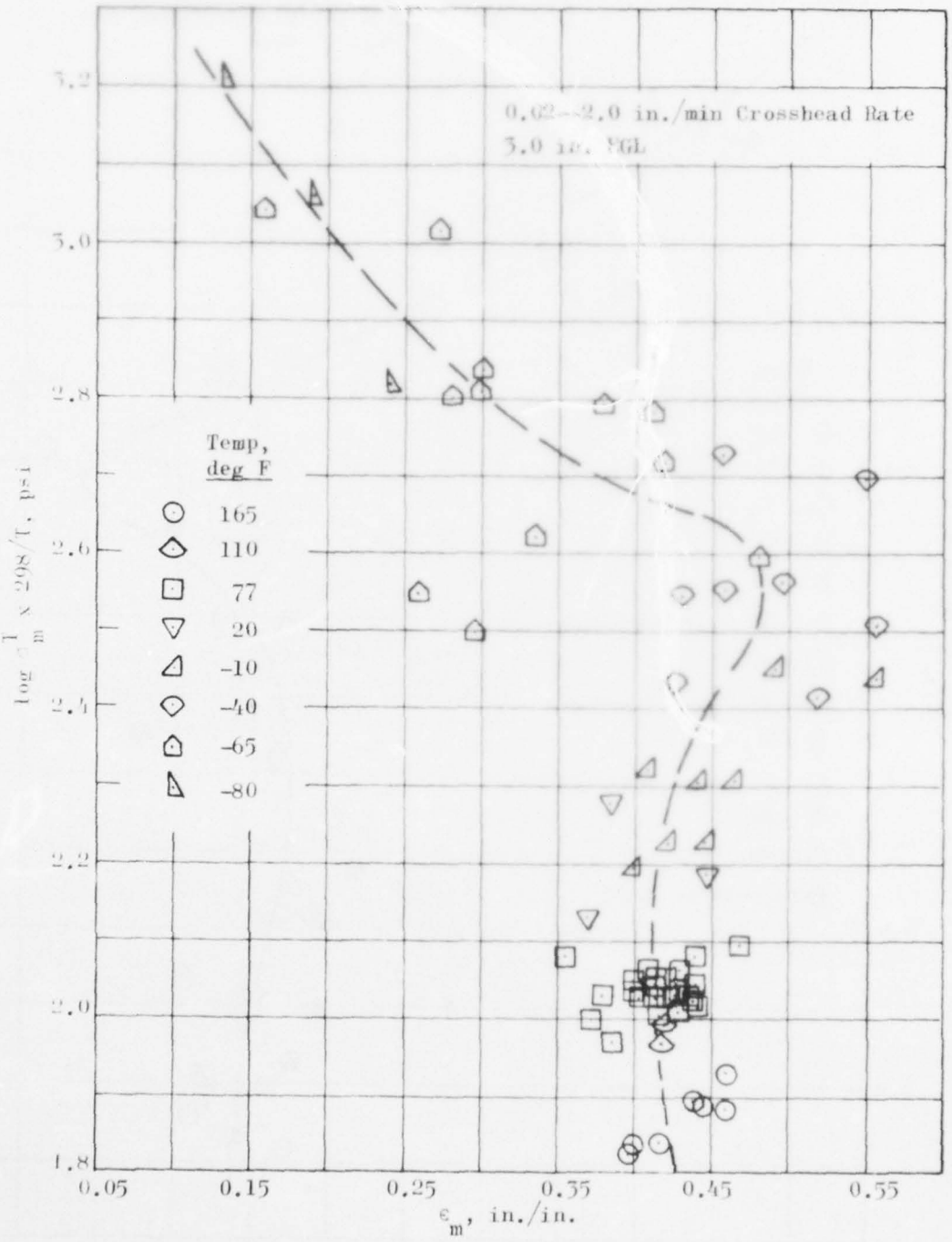

Figure 21. Uniaxial Failure Data, TP-H8214, Mix L-389

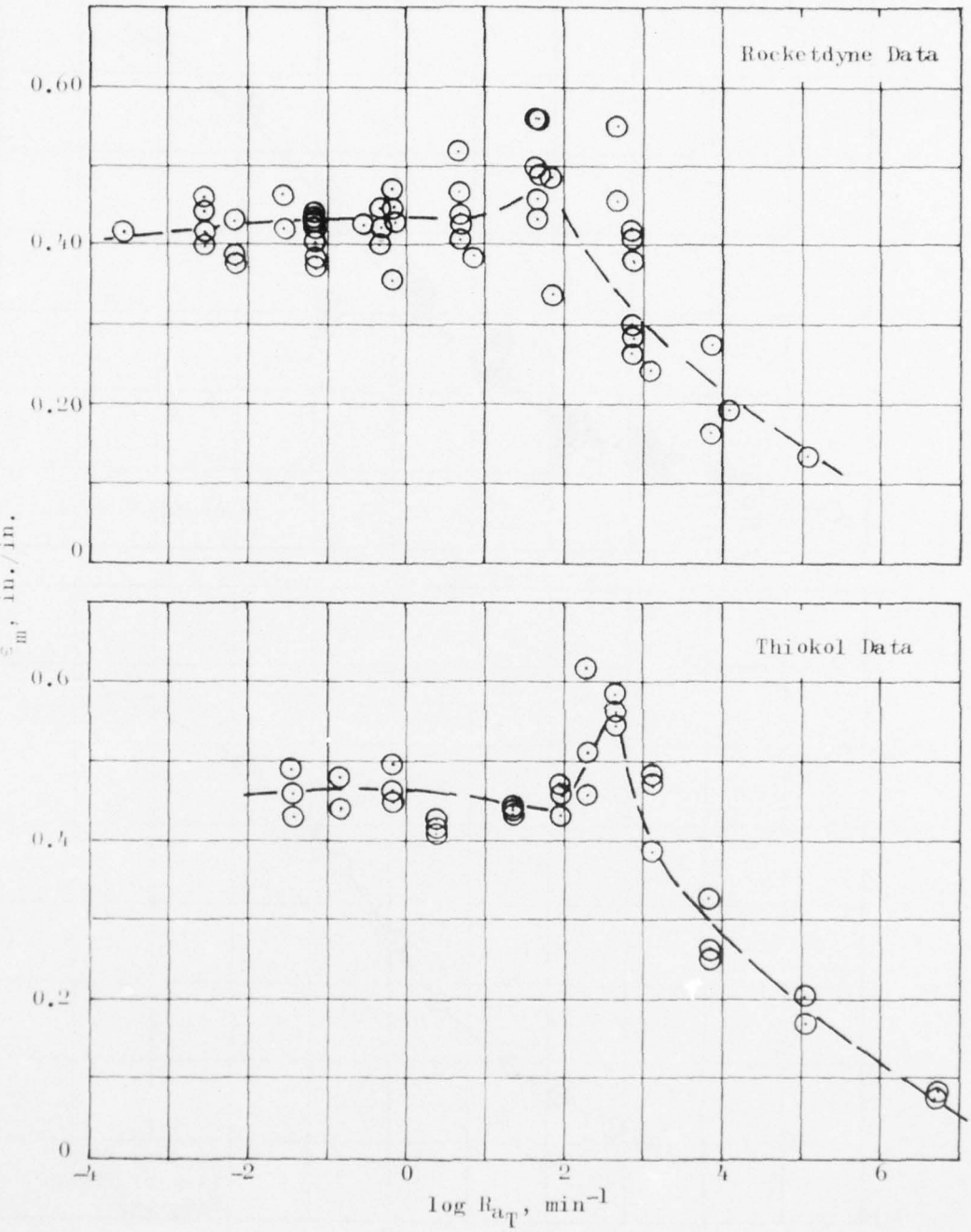

Figure 22. Strain Rate Dependence of TP-H8214, Uniaxial Strain at Maximum Stress

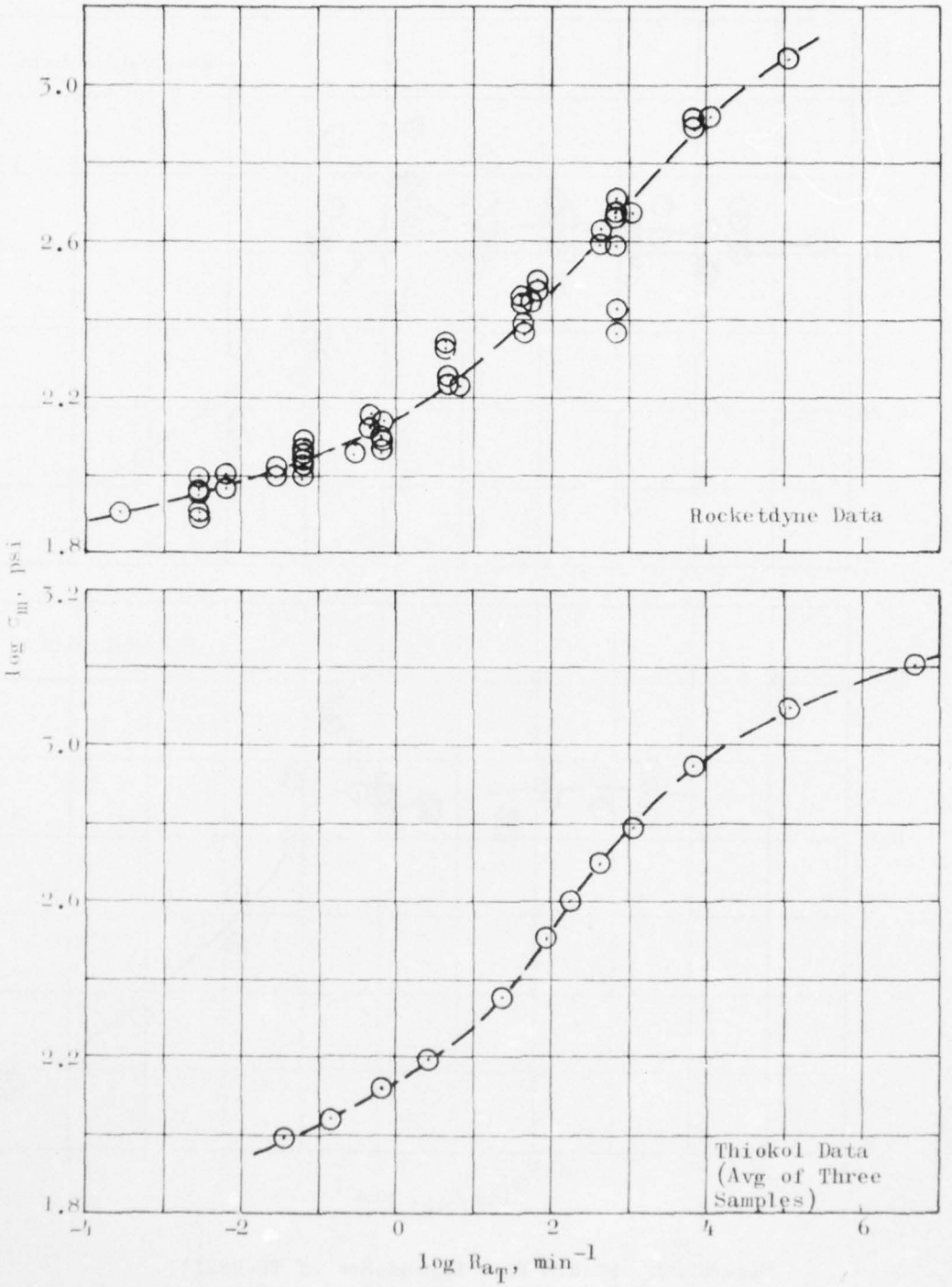

Figure 23. Strain-Rate Dependence of TP-H8214, Maximum Tensile Strength

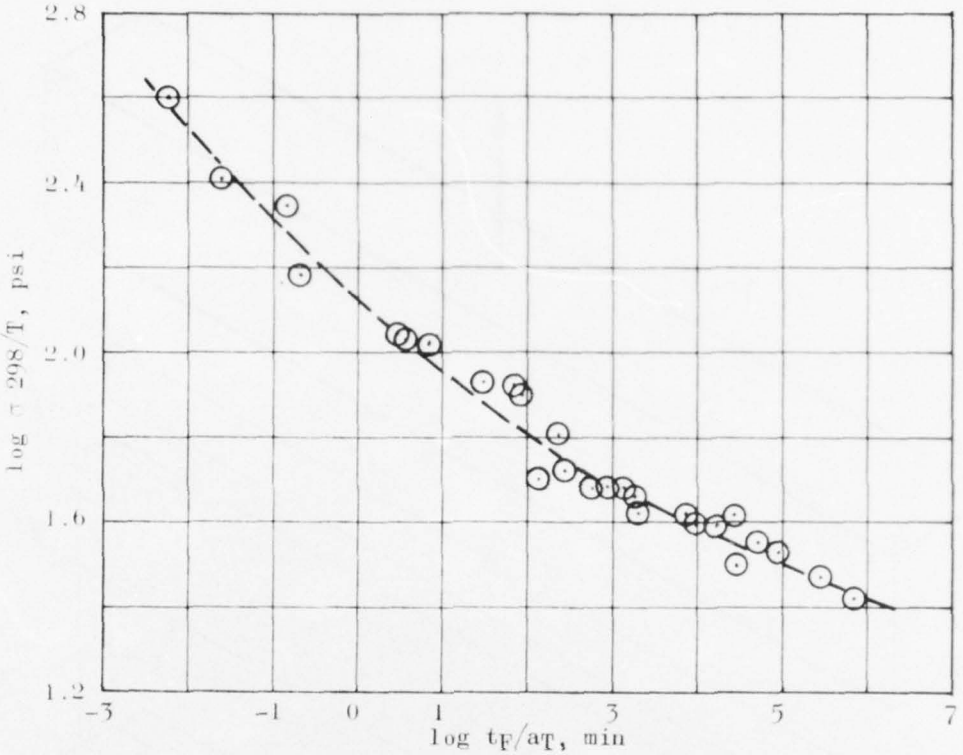

Figure 24. Uniaxial Constant Load to Failure, TP-H8214

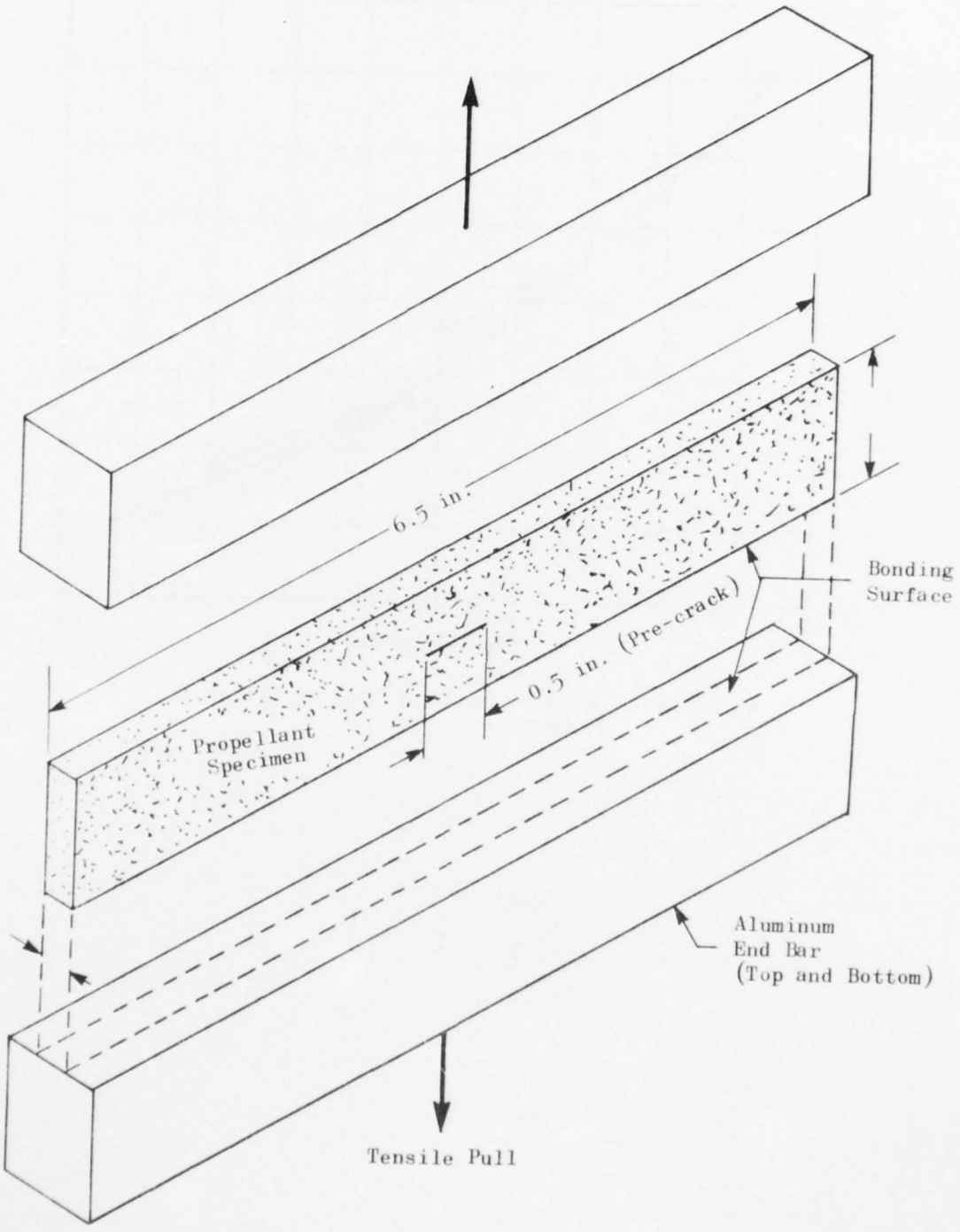

Figure 25. Biaxial Test Specimen

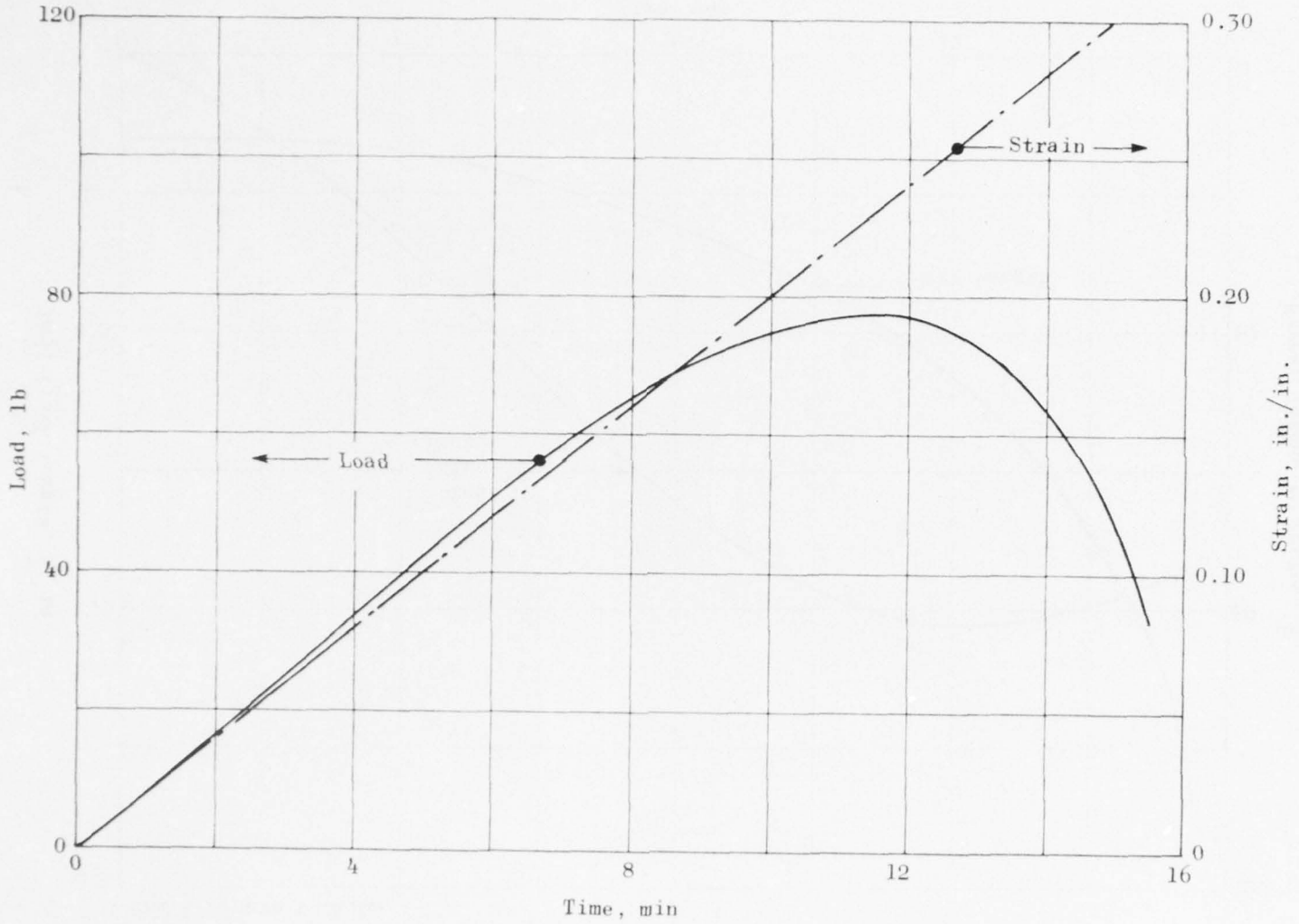

Figure 26. Typical Plot of Load and Strain vs Time

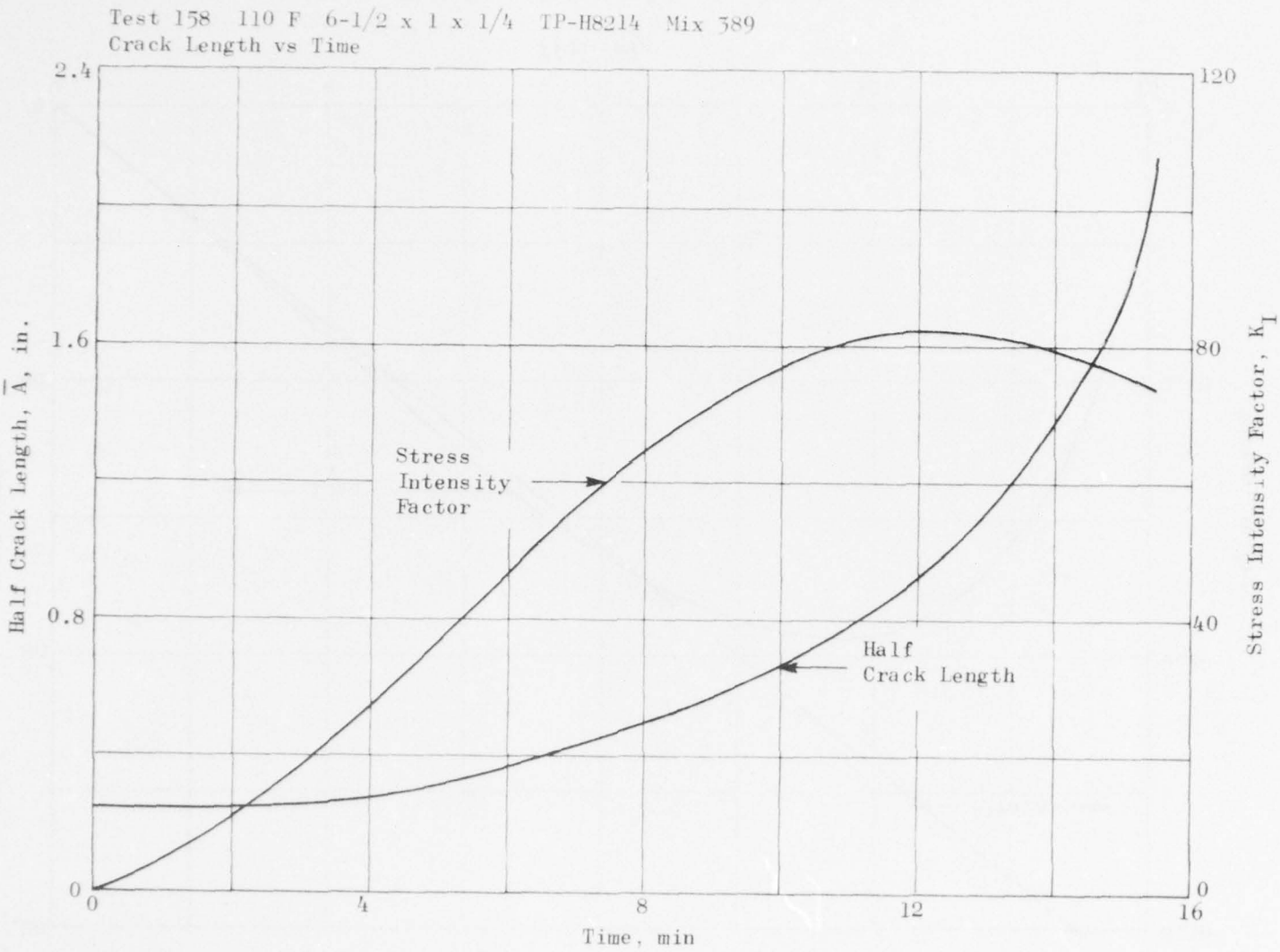

Figure 27. Typical Plot of Half Crack Length and Reduced Stress Intensity Factor vs Time

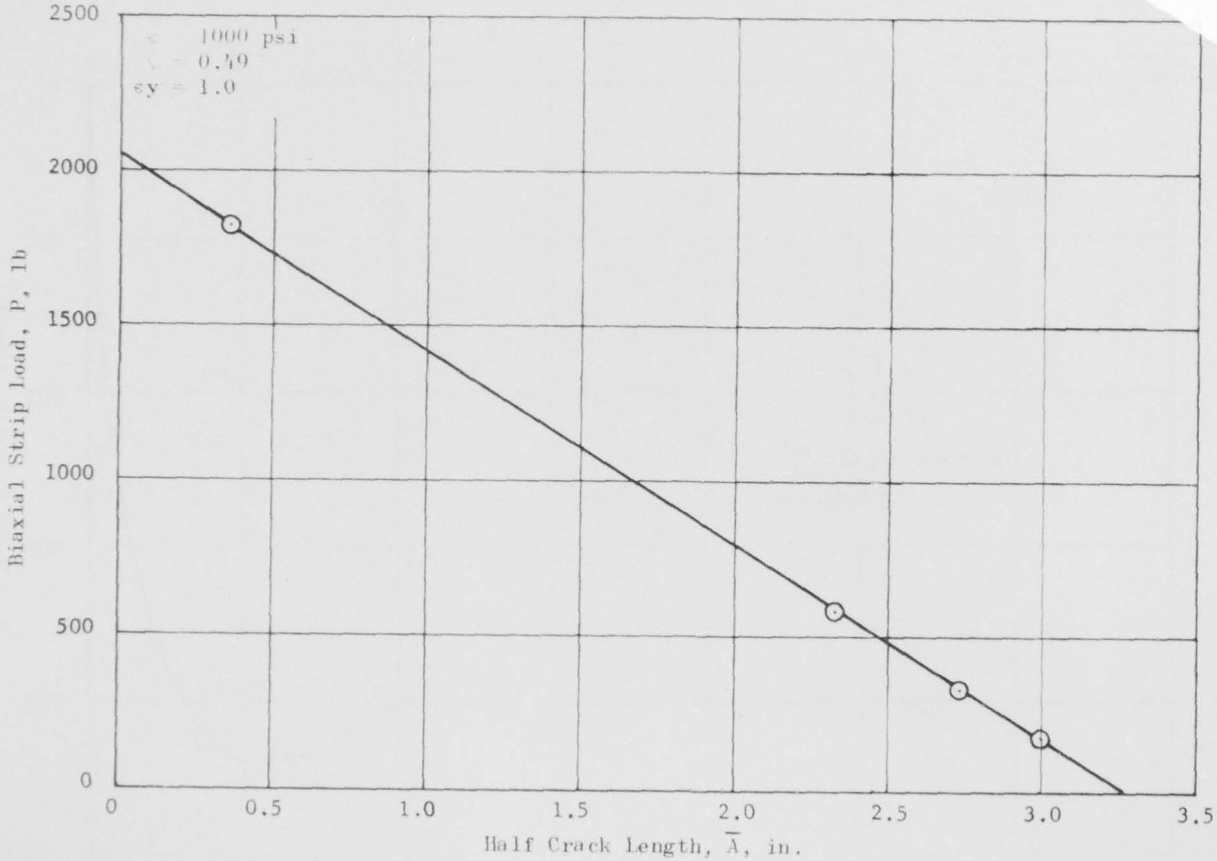

Figure 28. Biaxial Strip Load vs Half Crack Length

AD-A037 102 ROCKWELL INTERNATIONAL MCGREGOR TEX ROCKETDYNE DIV F/G 21/9.2
AIR LAUNCH INSTRUMENTED VEHICLES EVALUATION (ALIVE).(U)
FEB 77 J D BURTON F04611-74-C-0009
UNCLASSIFIED R-4939 AFRPL-TR-76-101 NL

2 OF 3
AD
A037102

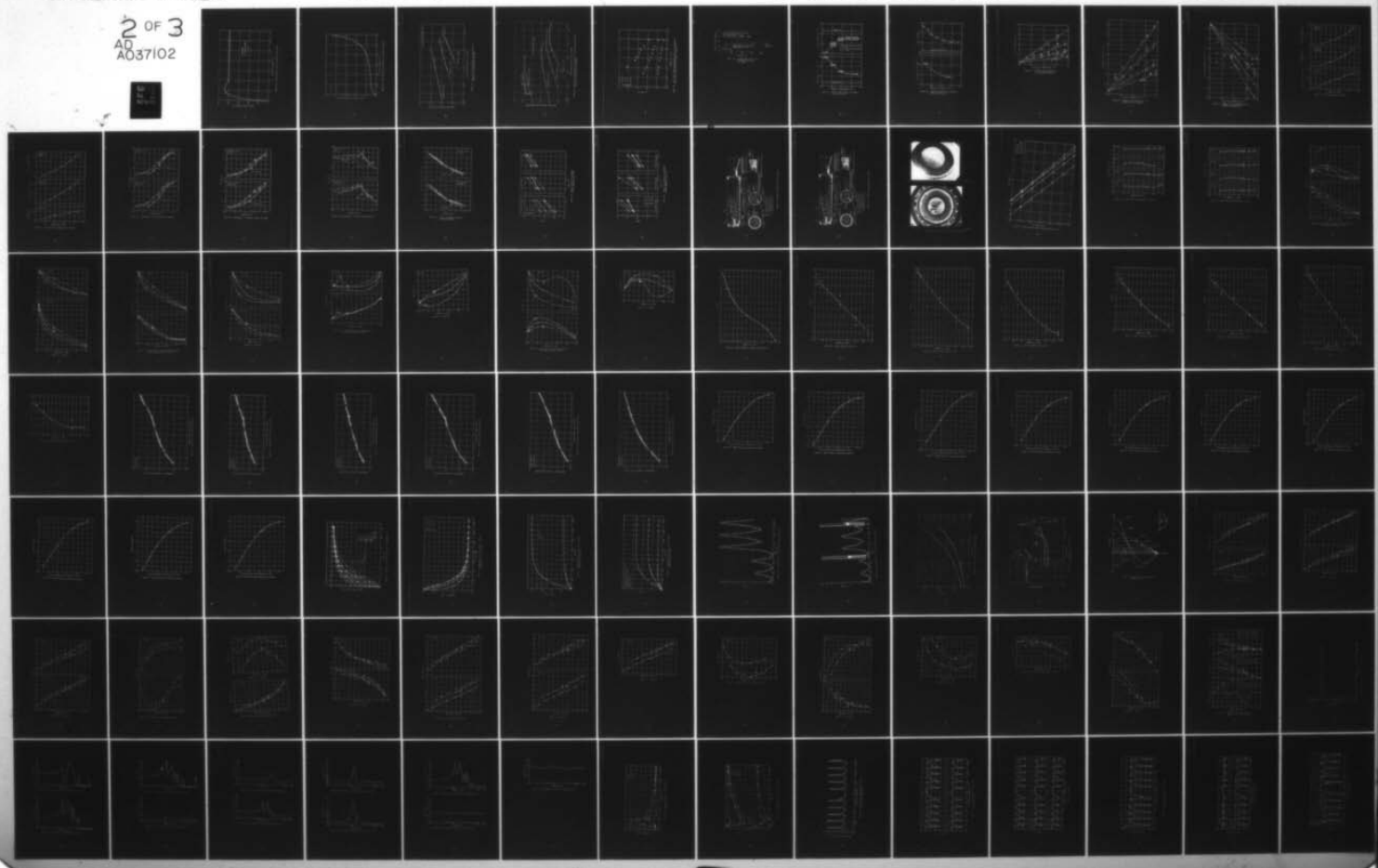

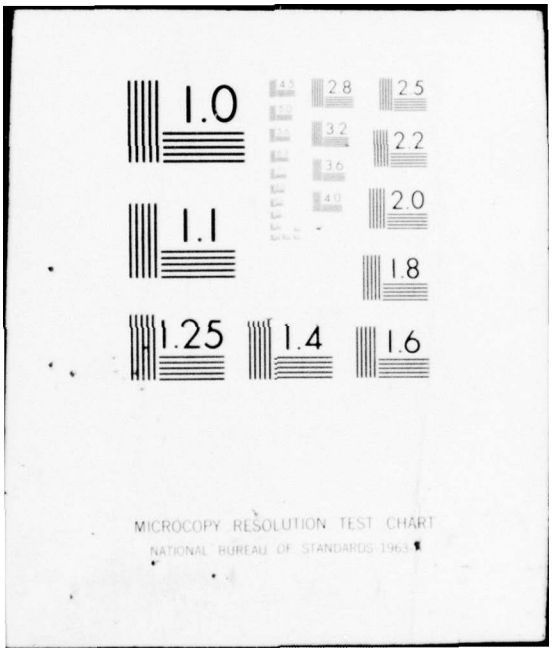
1.0
1.1
1.25
1.4
1.6
1.8
2.0
2.2
2.5
2.8
3.2
3.6
4.0
4.5
MICROCOPY RESOLUTION TEST CHART
NATIONAL BUREAU OF STANDARDS-1963

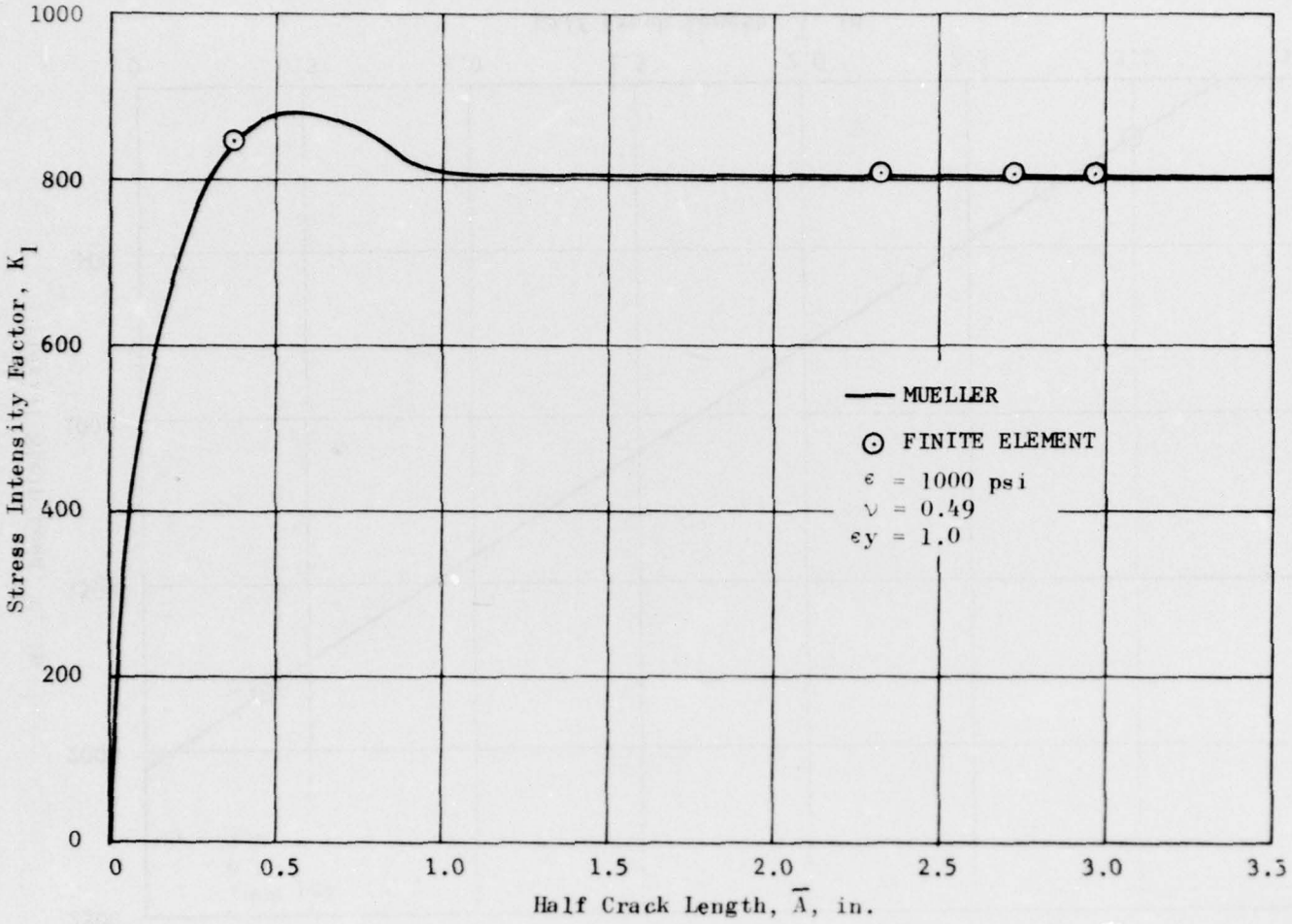

Figure 29. Stress Intensity Factor vs Half Crack Length

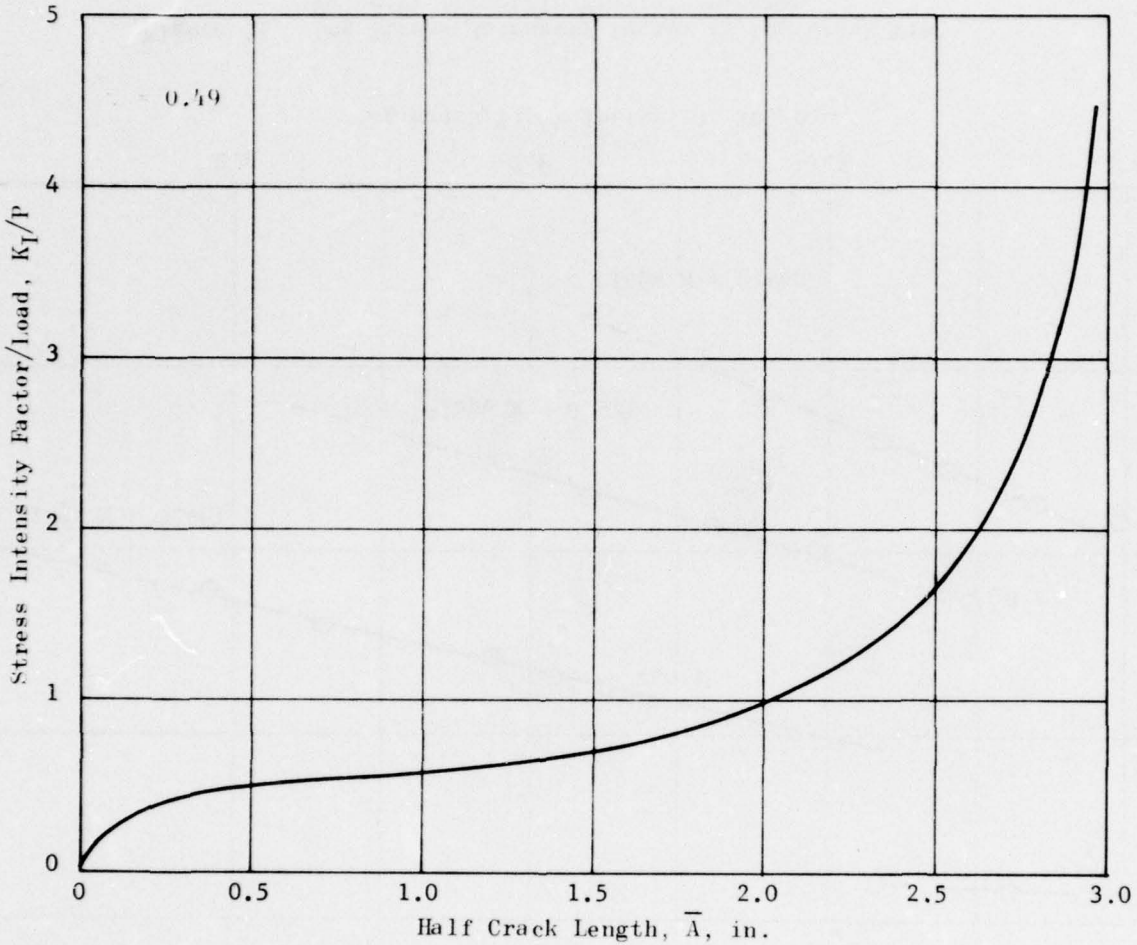

Figure 30. Stress Intensity Factor/Load vs Half Crack Length

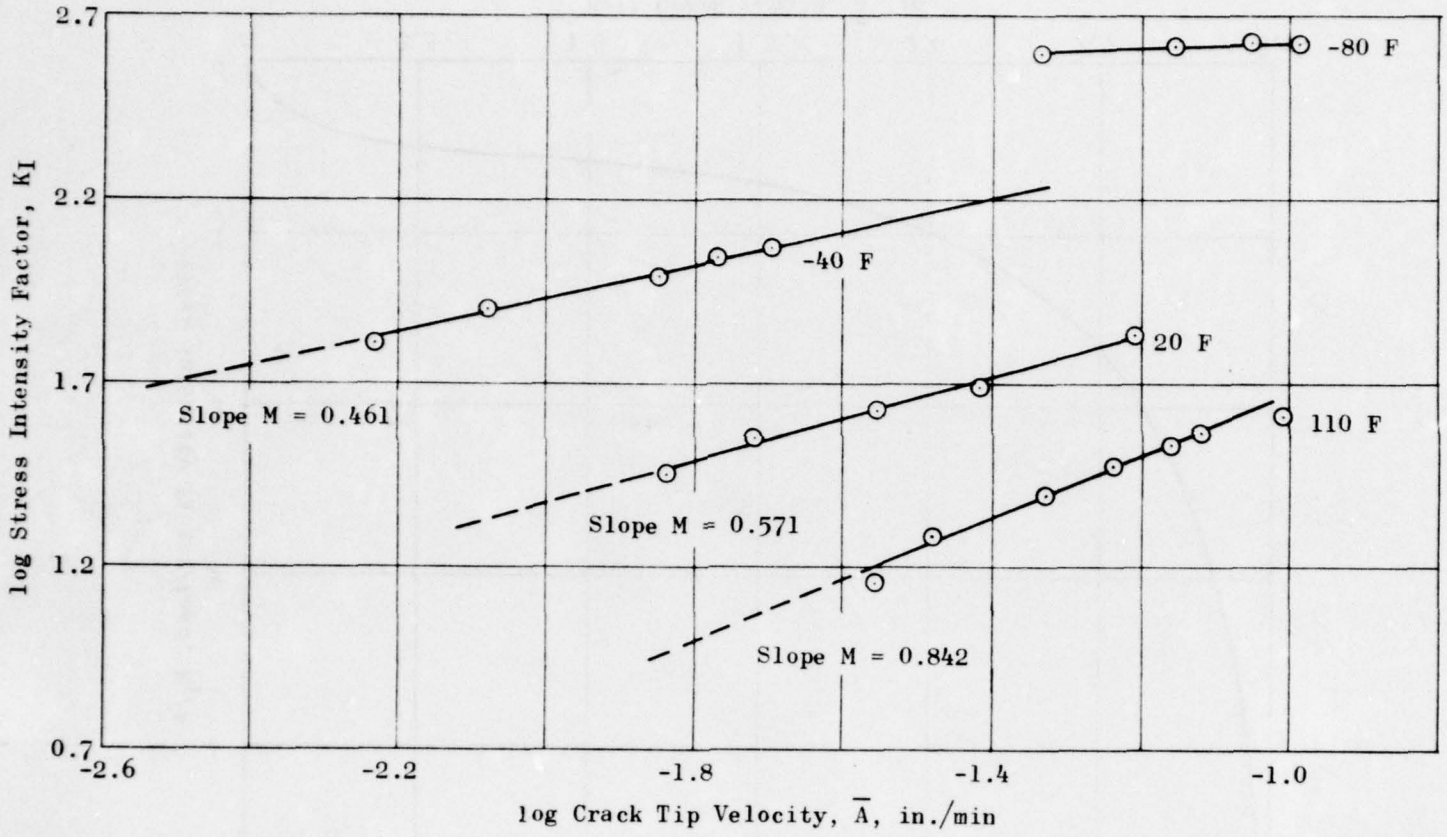

Figure 31. Log Stress Intensity Factor vs Log Crack Tip Velocity for Strip Biaxial Specimen

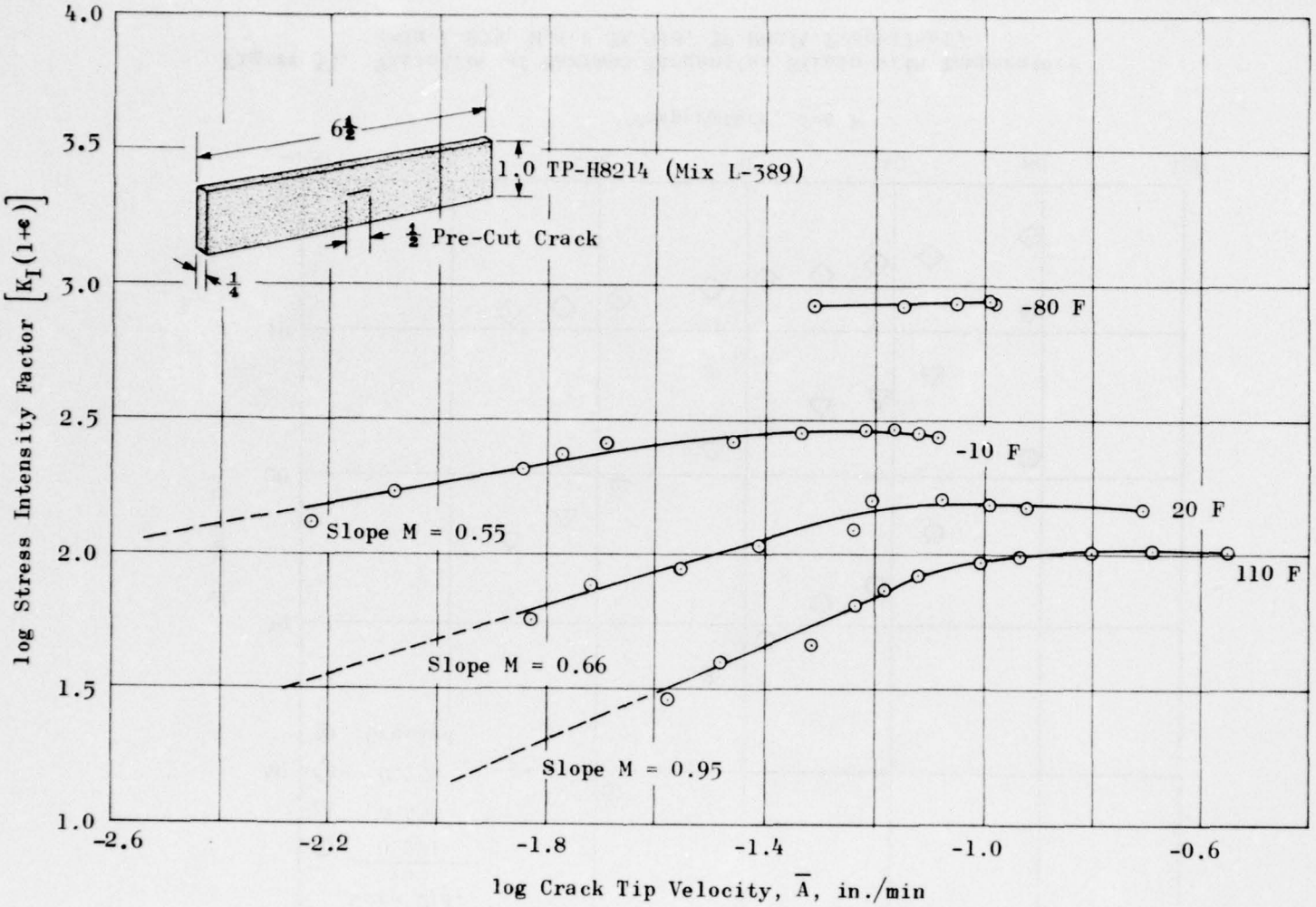

Figure 32. Log Stress Intensity Factor Adjusted for Strain vs Log Crack Tip Velocity for Strip Biaxial Specimen

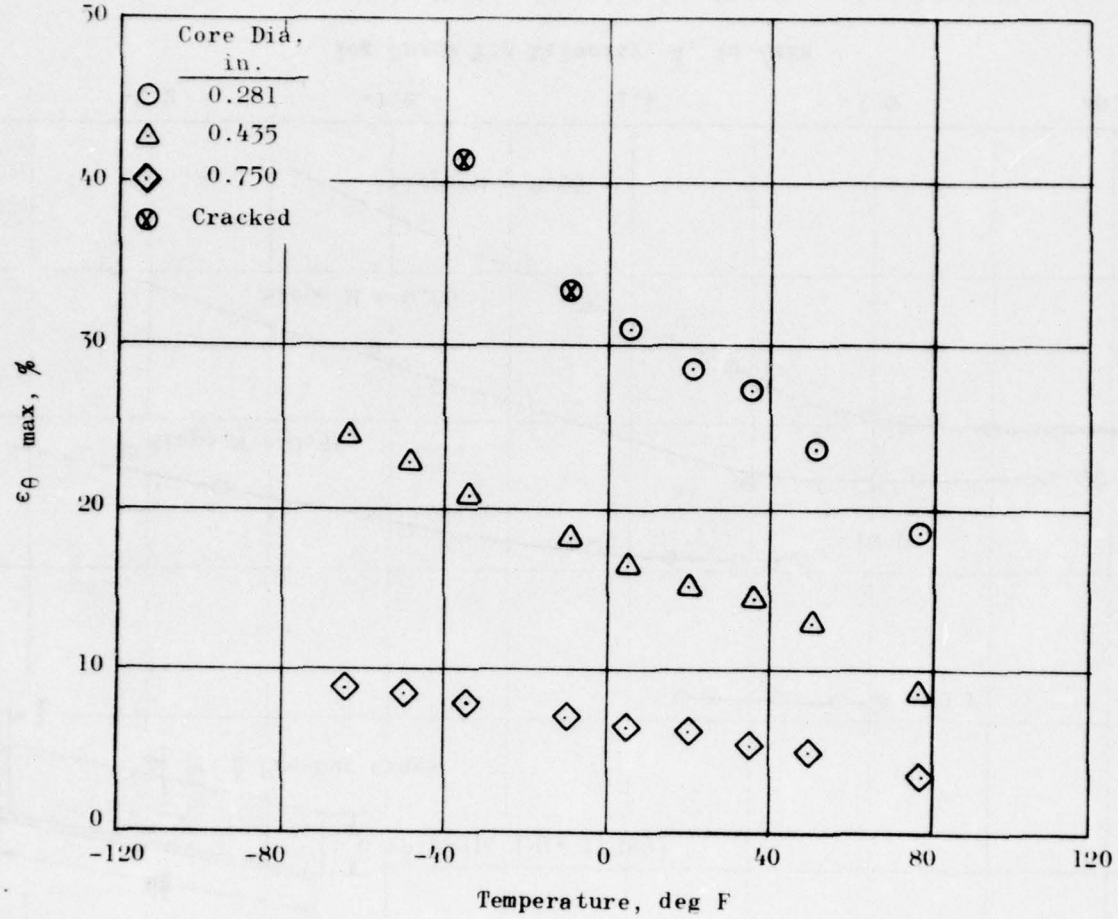

Figure 33. Variation of Maximum Tangential Strain with Temperature (Mix L-275, Motor TX-318, TP-H8214 Propellant)

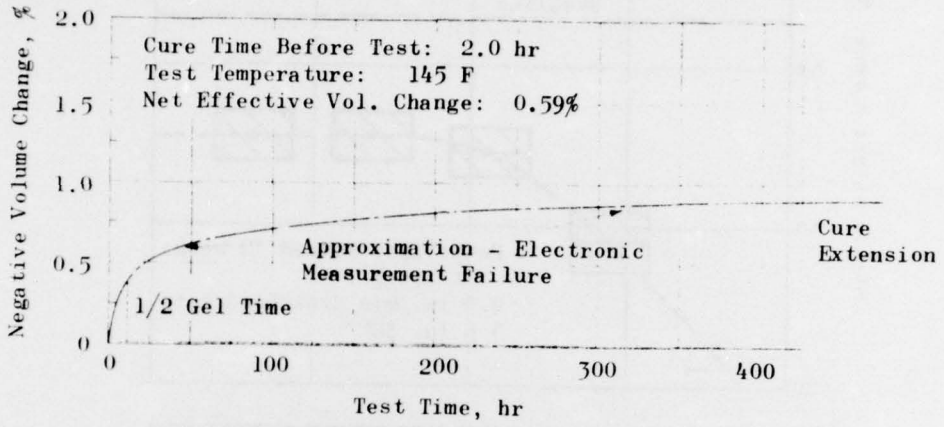

Figure 34. Volume Change During Cure (TP-H8214 Propellant, Mix L-389)

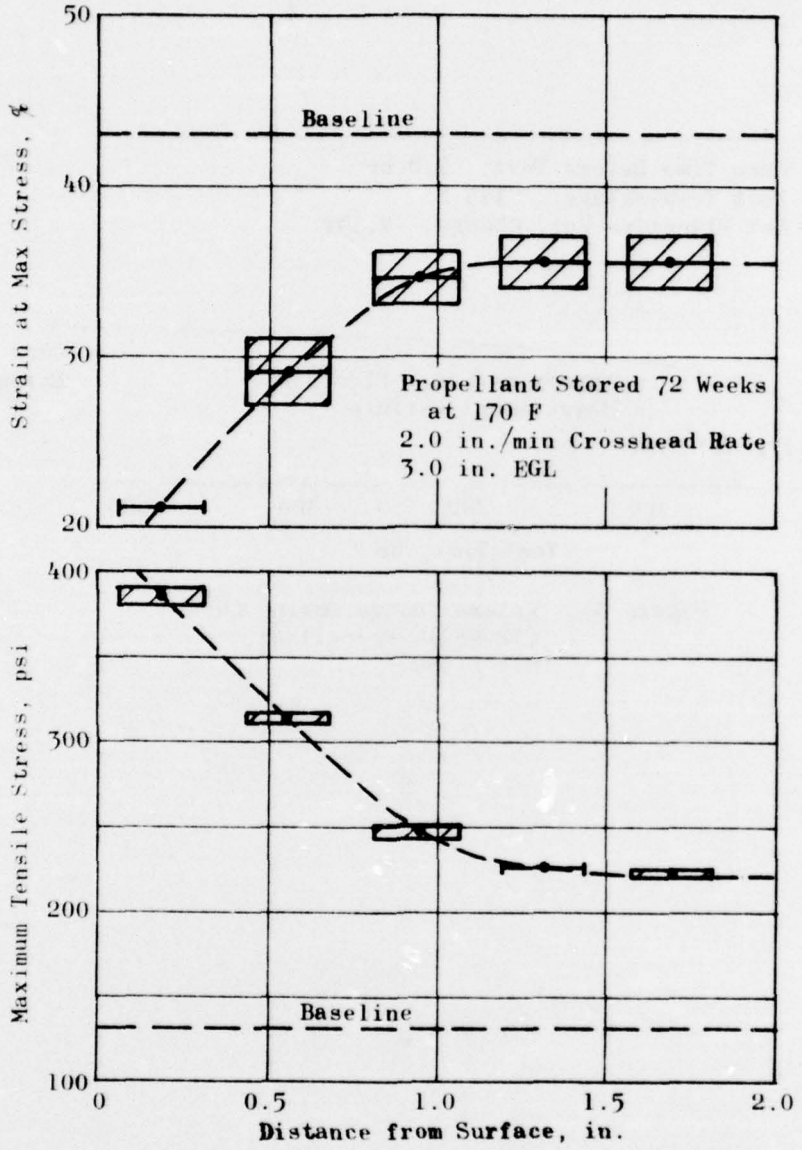

Figure 35. Surface Aging Effect on TP-H8214 Tensile Properties

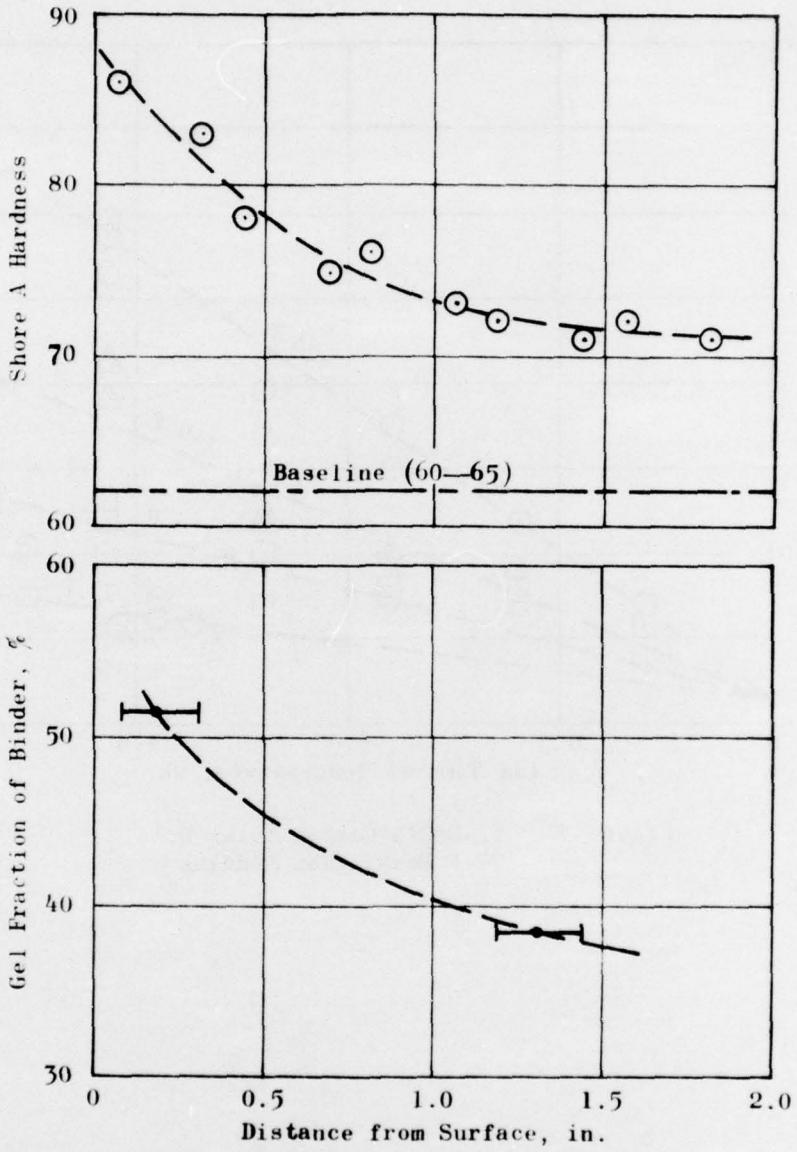

Figure 36. Surface Aging Effect on TP-H8214, Bulk Characteristics

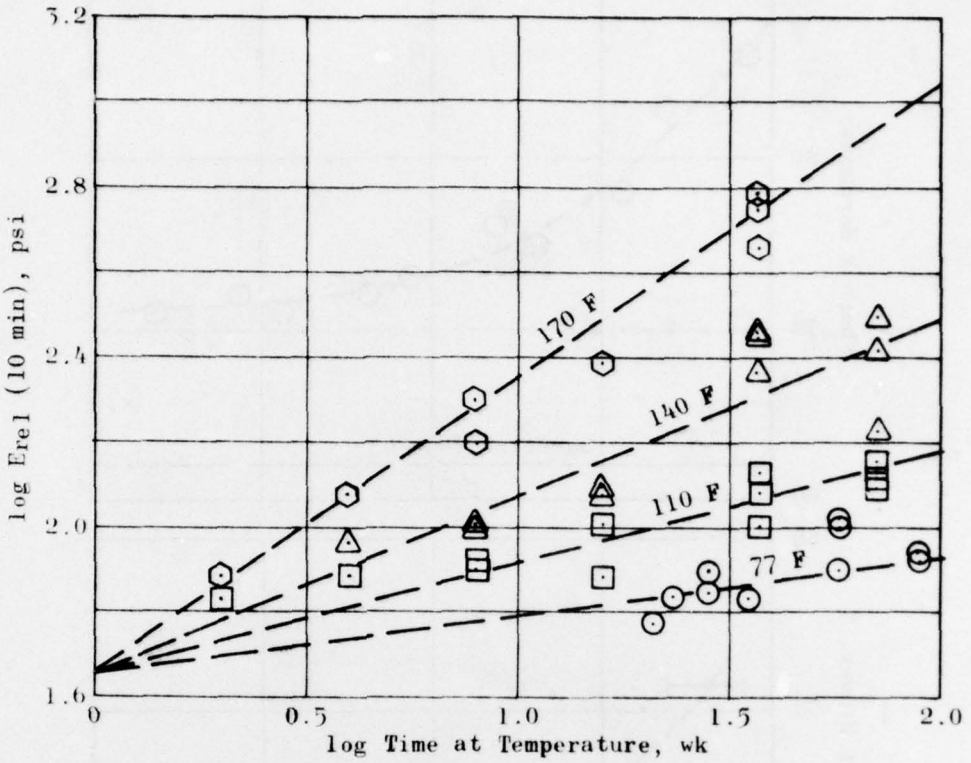

Figure 37. TP-H8214 Carton Aging Data, 77 F Rexaxation Modulus

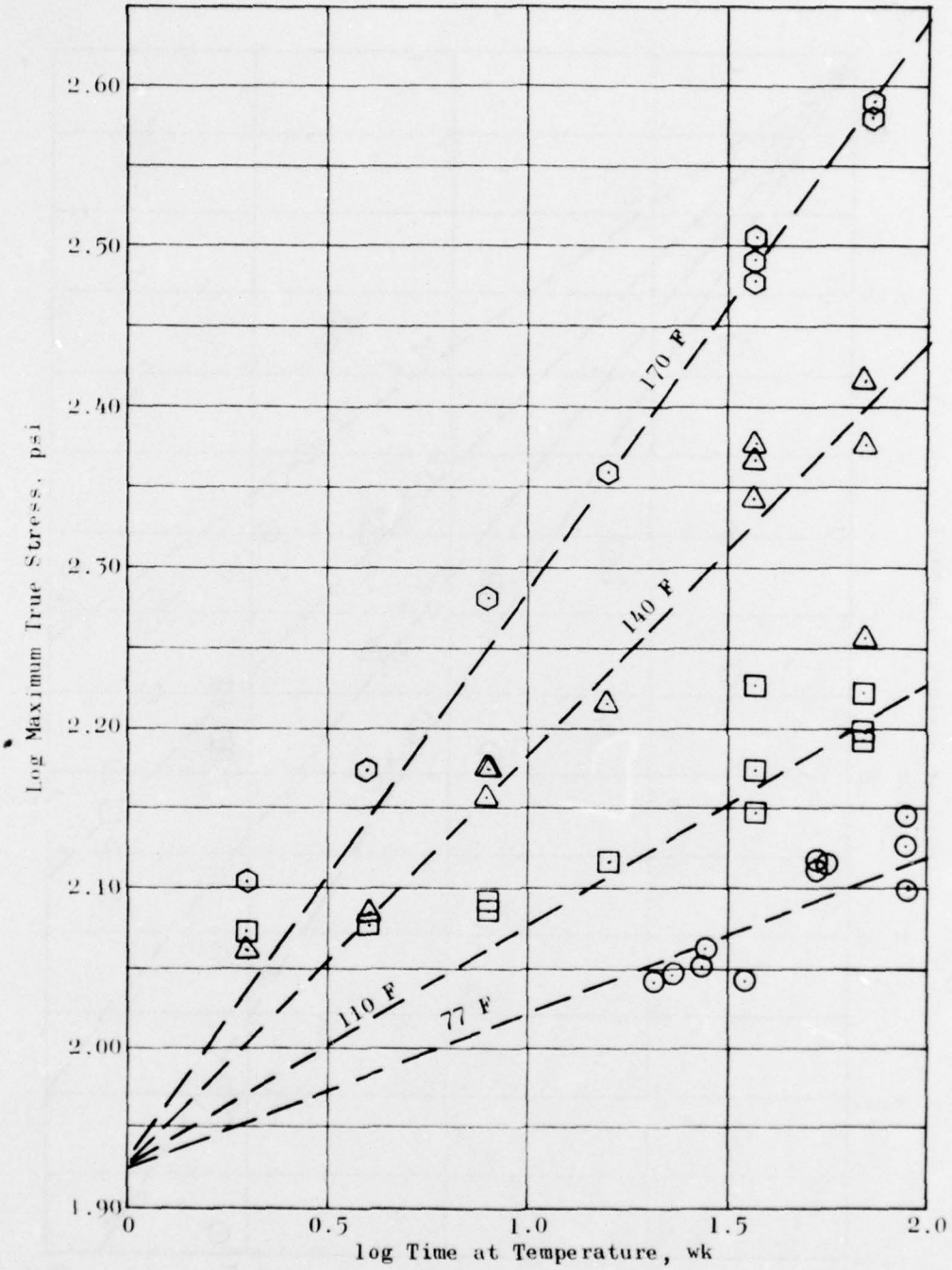

Figure 38. TP-H8214 Carton Aging Data, 77 F
Uniaxial Tensile Strength

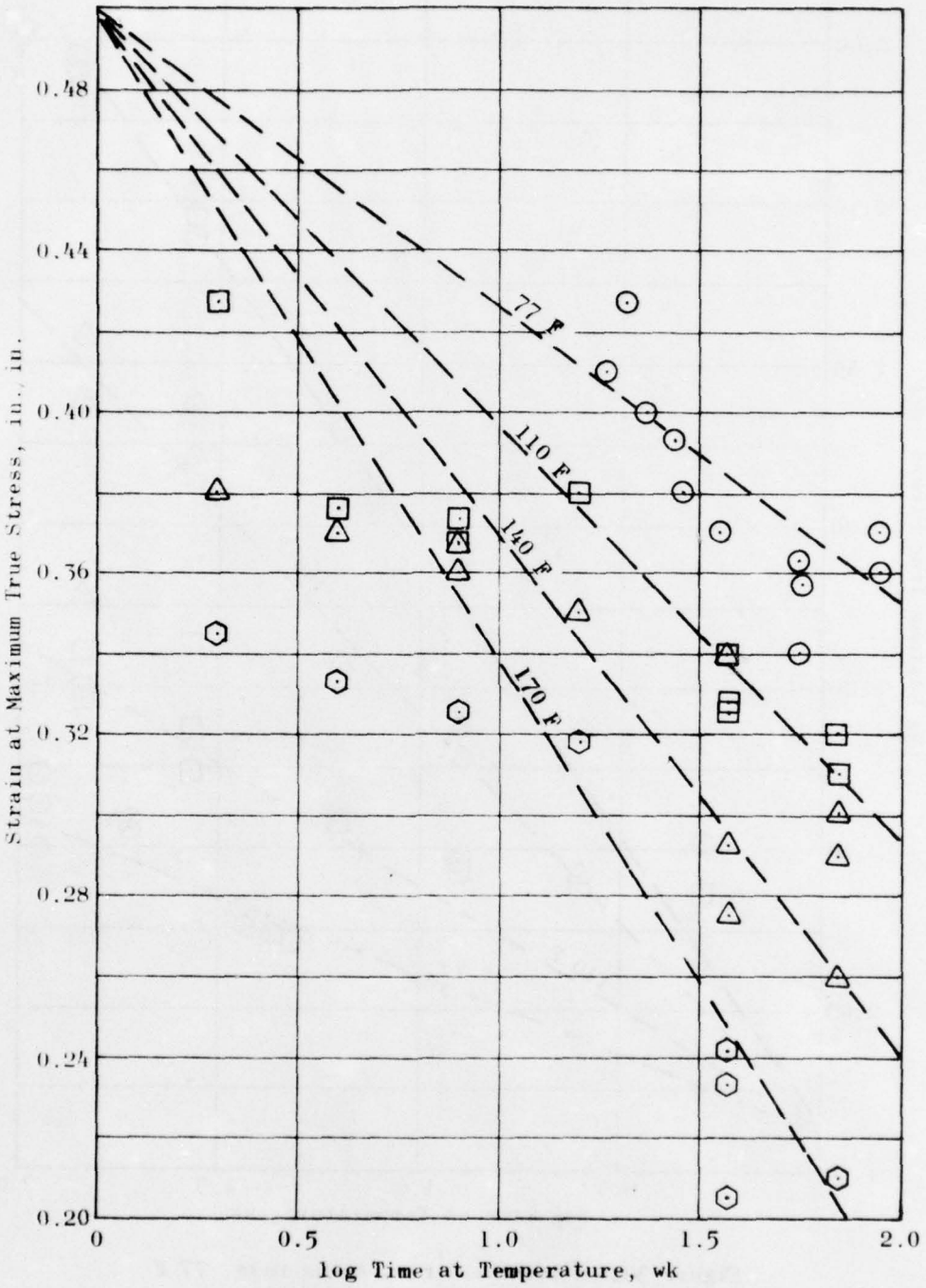

Figure 39. TP-H8214 Carton Aging Data, 77 F Strain at Maximum Stress

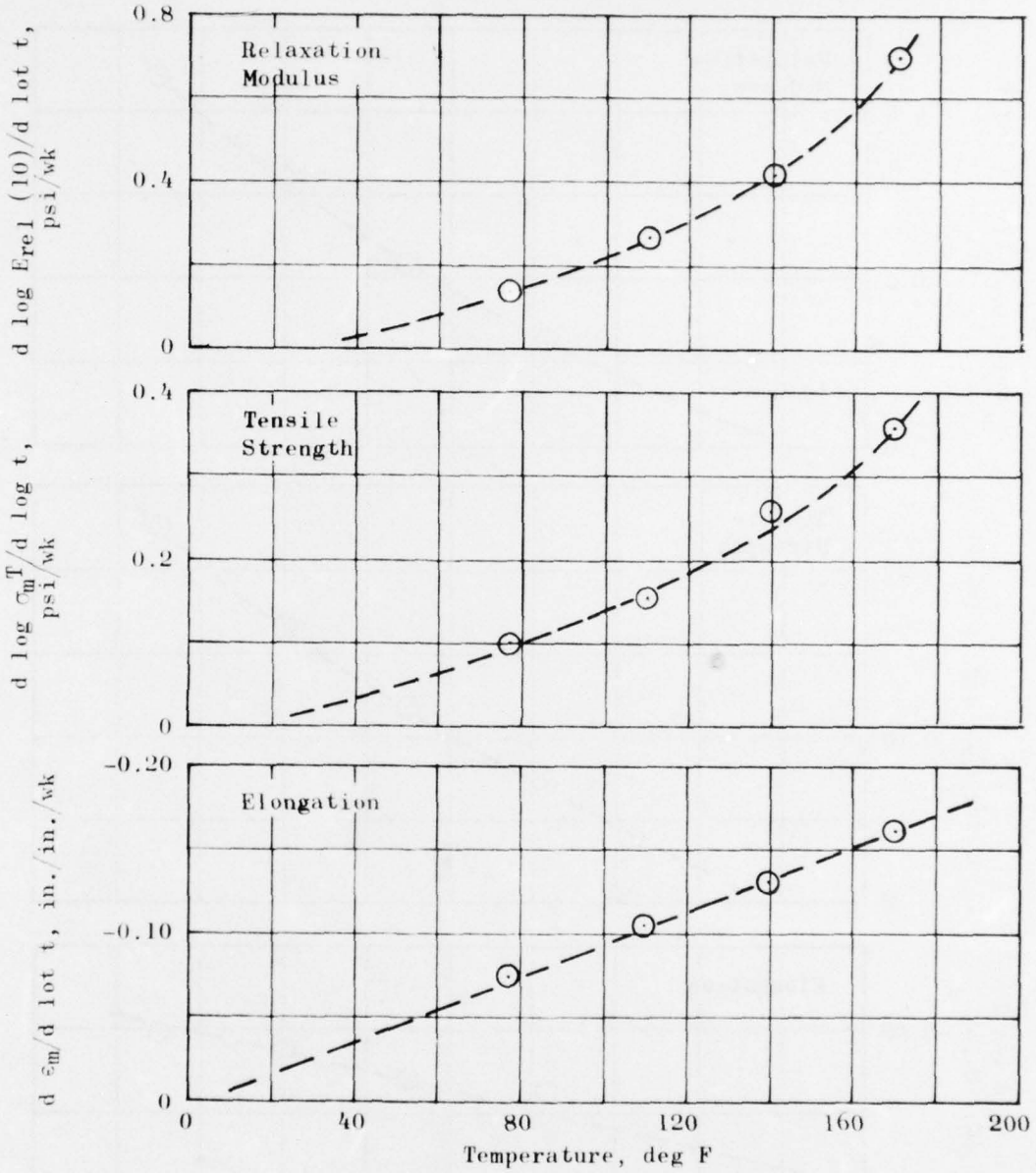

Figure 40. Surface Aging Rate, TP-H8214

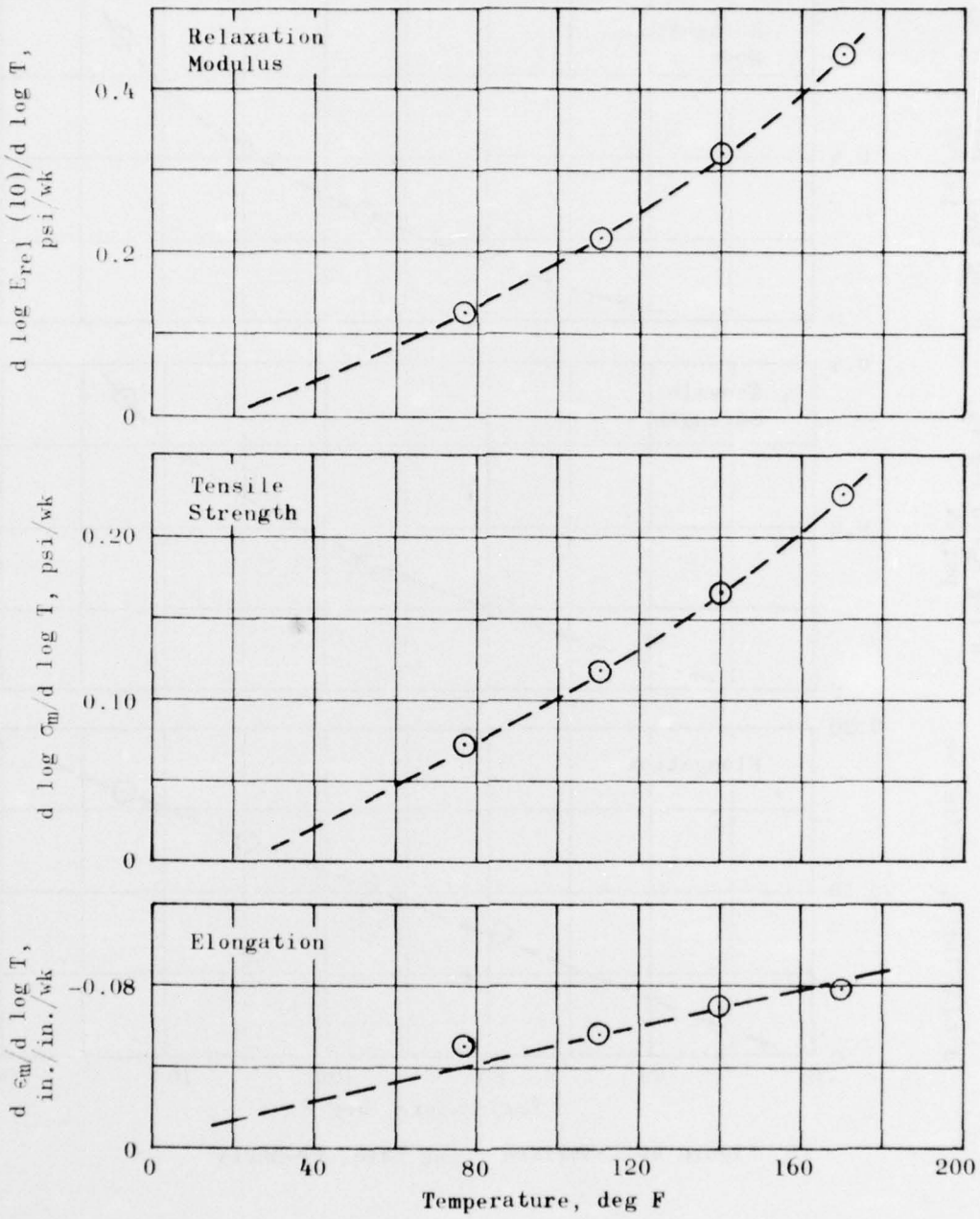

Figure 41. Estimated Bulk Aging Rate for TP-H8214

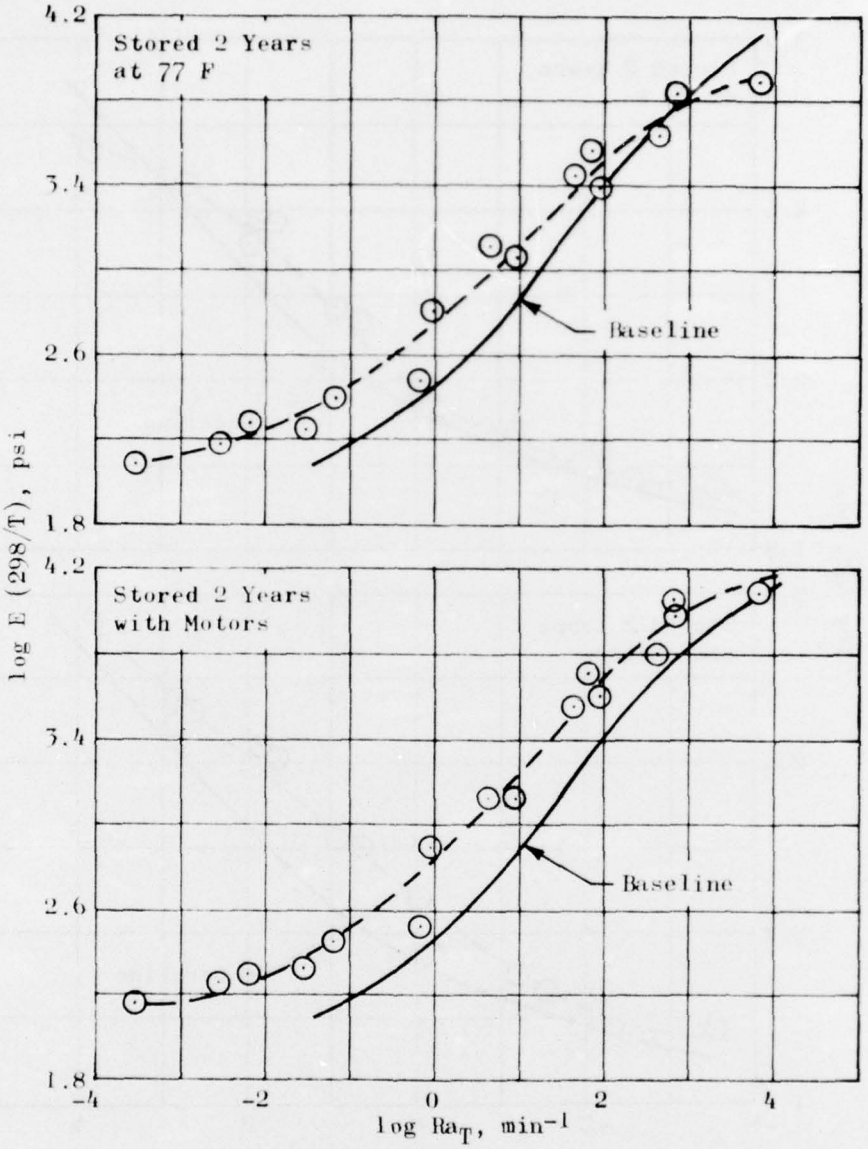

Figure 42. Aging Effect on Uniaxial Tensile Modulus

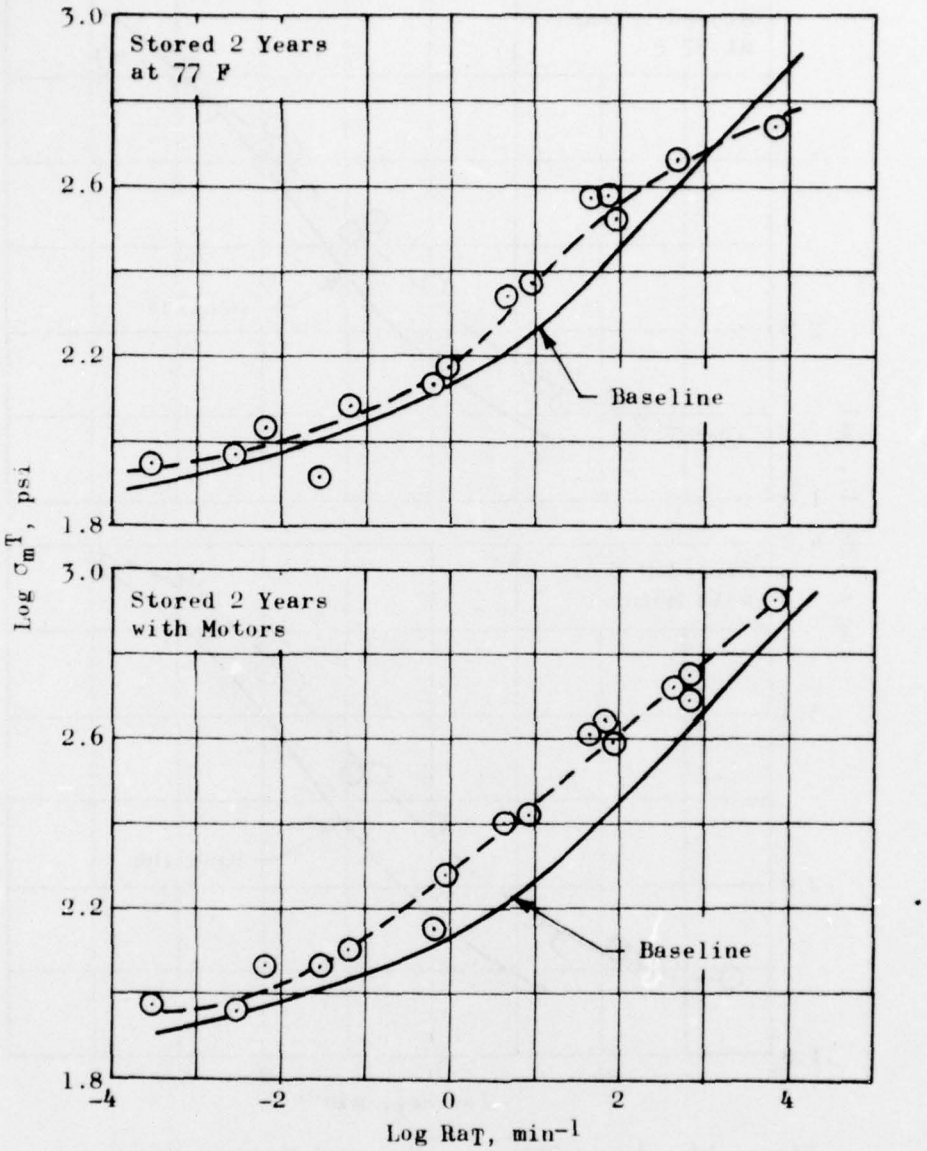

Figure 43. Aging Effect on Uniaxial Tensile Strength

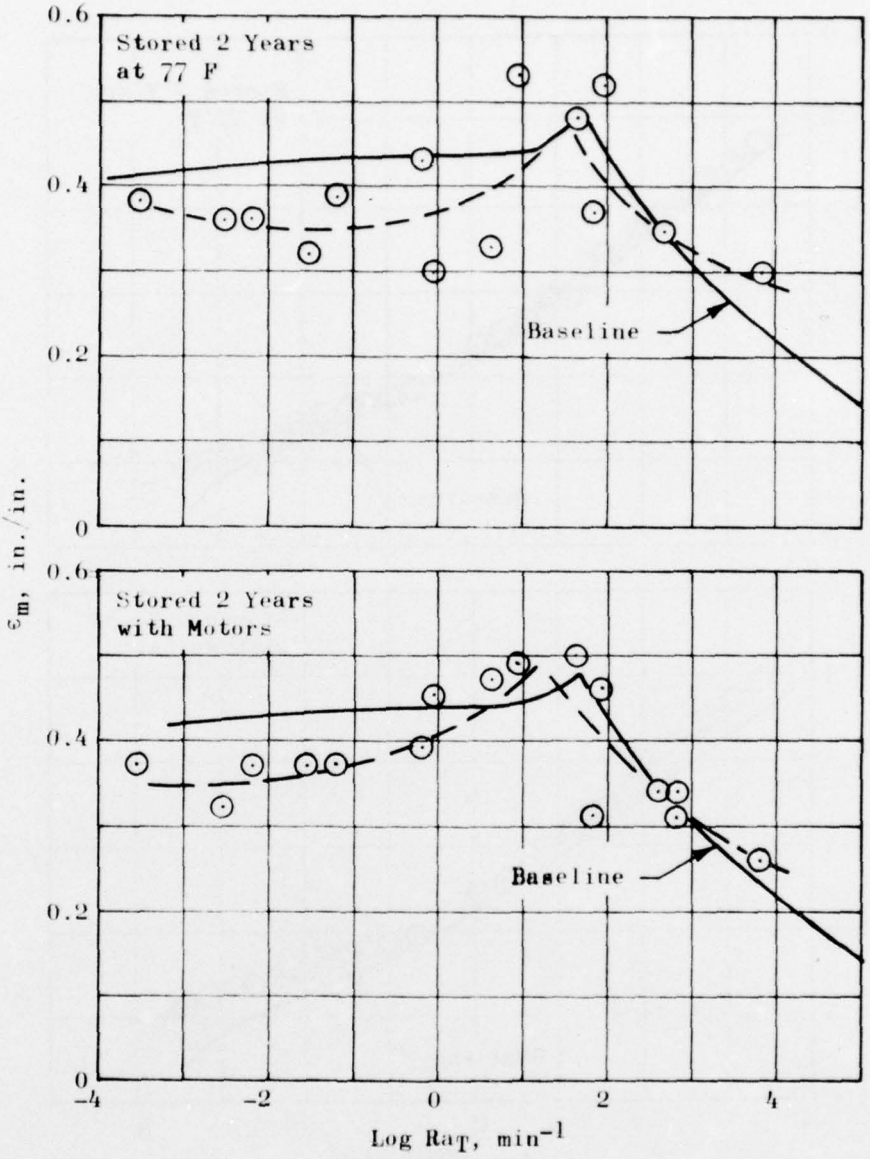

Figure 44. Aging Effect on Strain at Maximum Stress

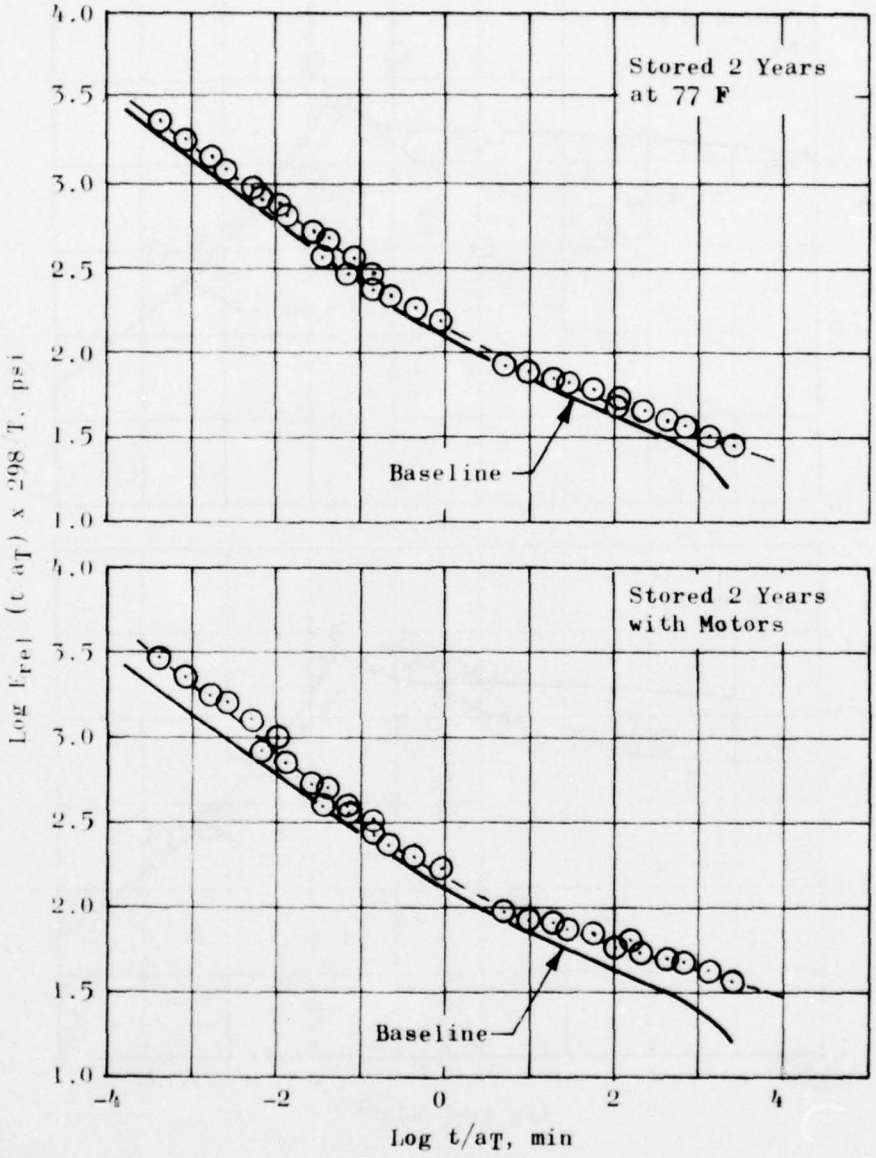

Figure 45. Effect of Aging on Uniaxial Relaxation Modulus

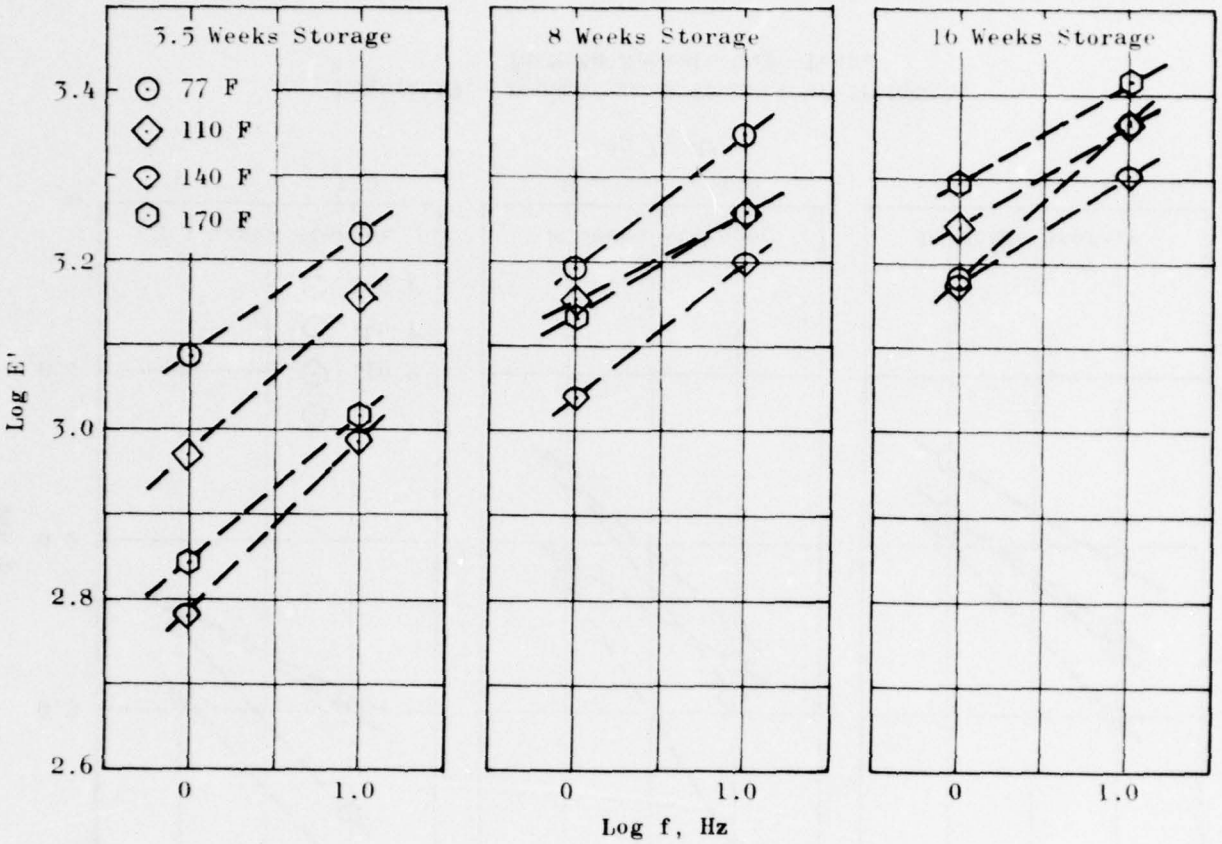

Figure 46. Dynamic Modulus of TP-H8214, In-Situ Dynamic Gage Tests

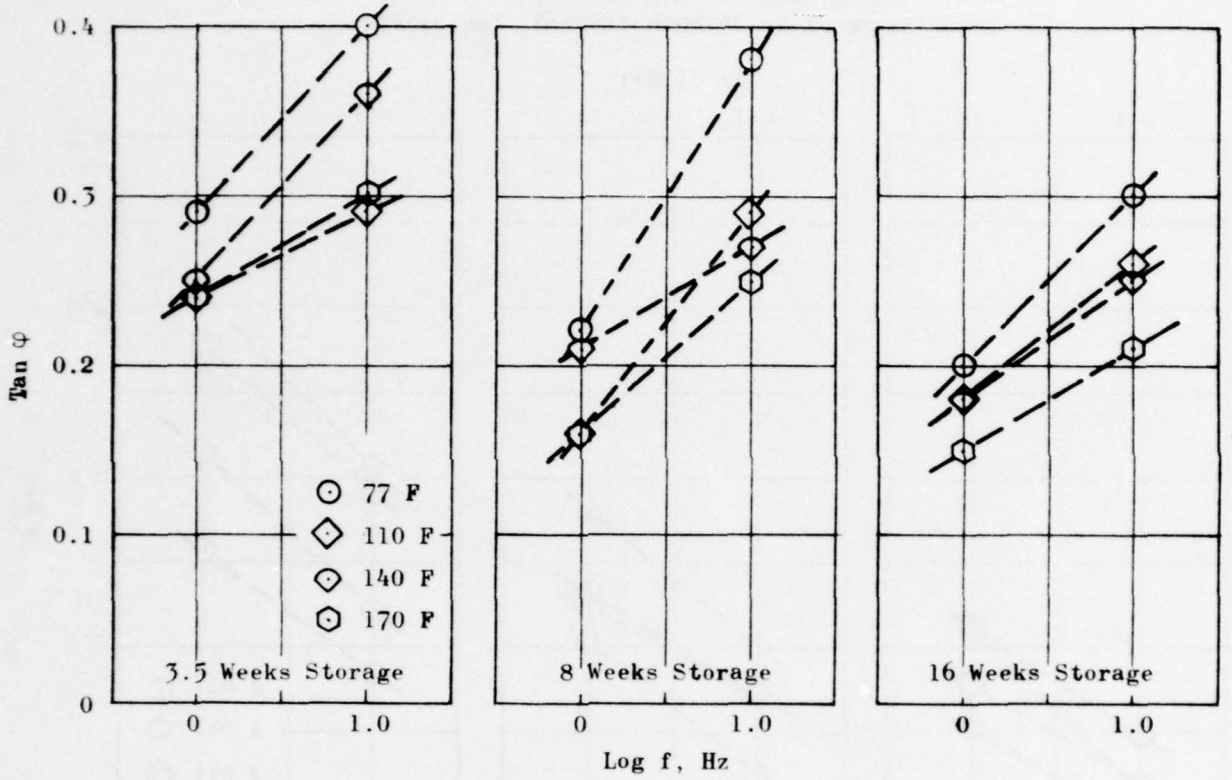

Figure 47. Dynamic Loss Tangent of TP-H8214, In-Situ Dynamic Gage Tests

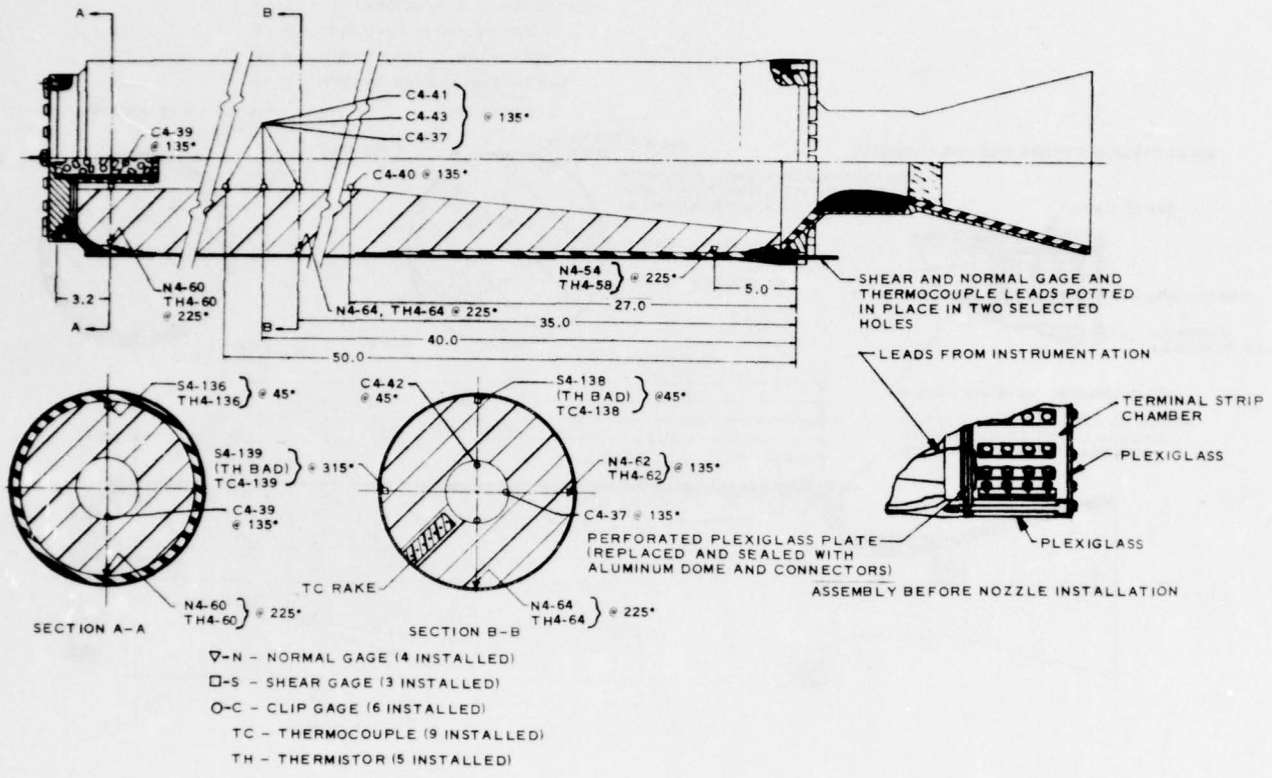

Figure 48. TX-606-4 Instrumented Motor Layout

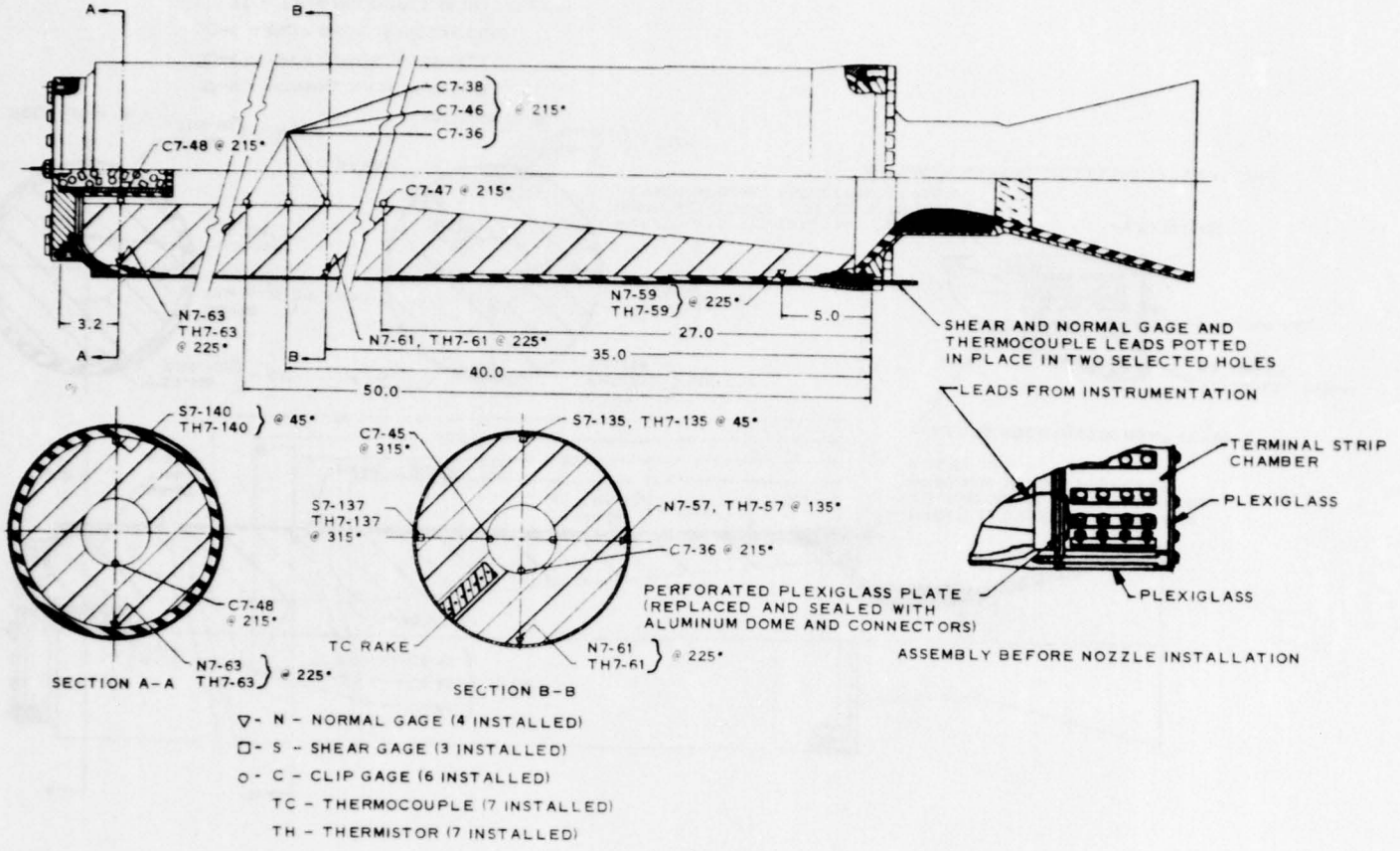

Figure 49. TX-606-7 Instrumented Motor Layout

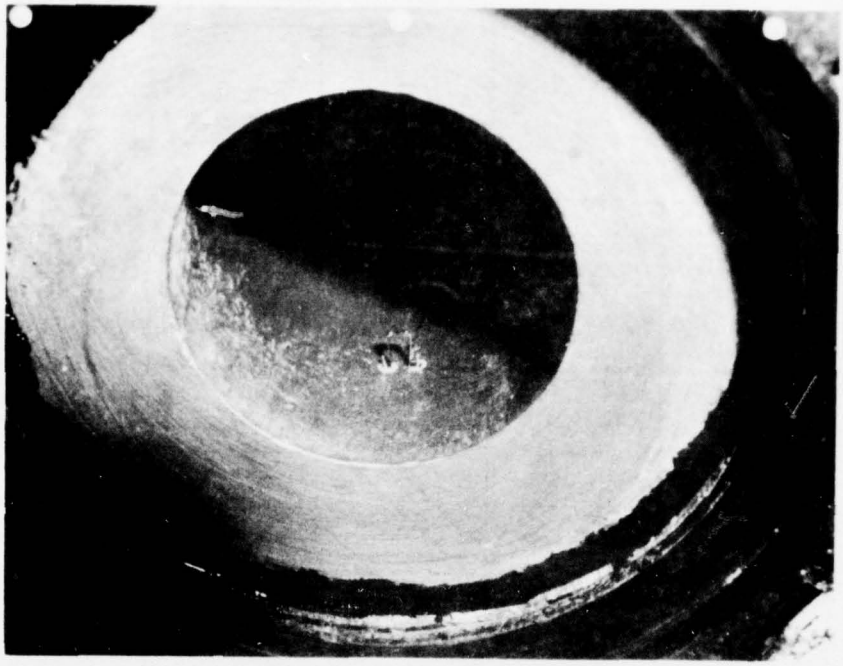

CN 3290

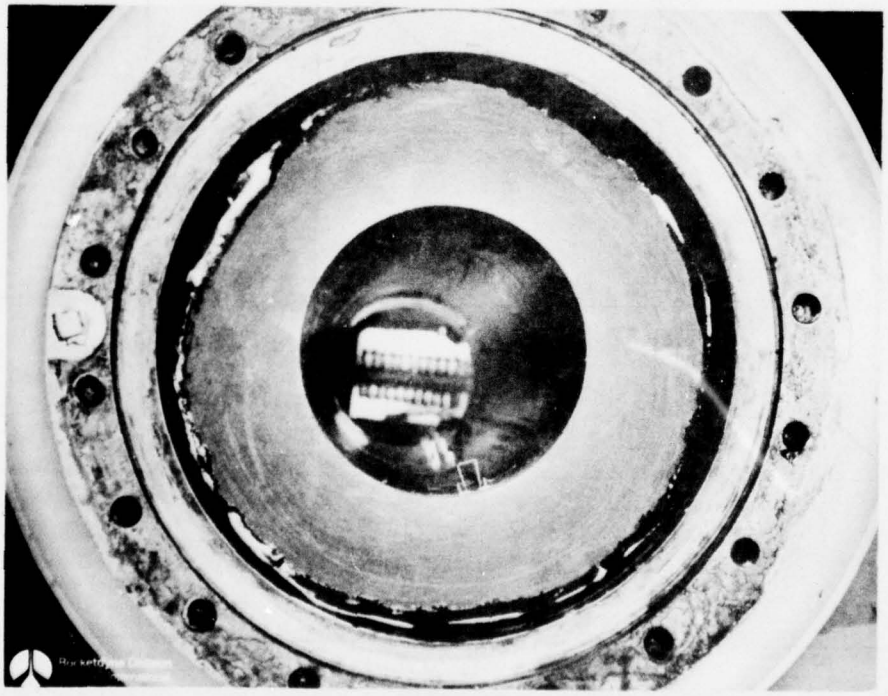

76-154

Figure 50. Inner Bore Clip Gage Installation

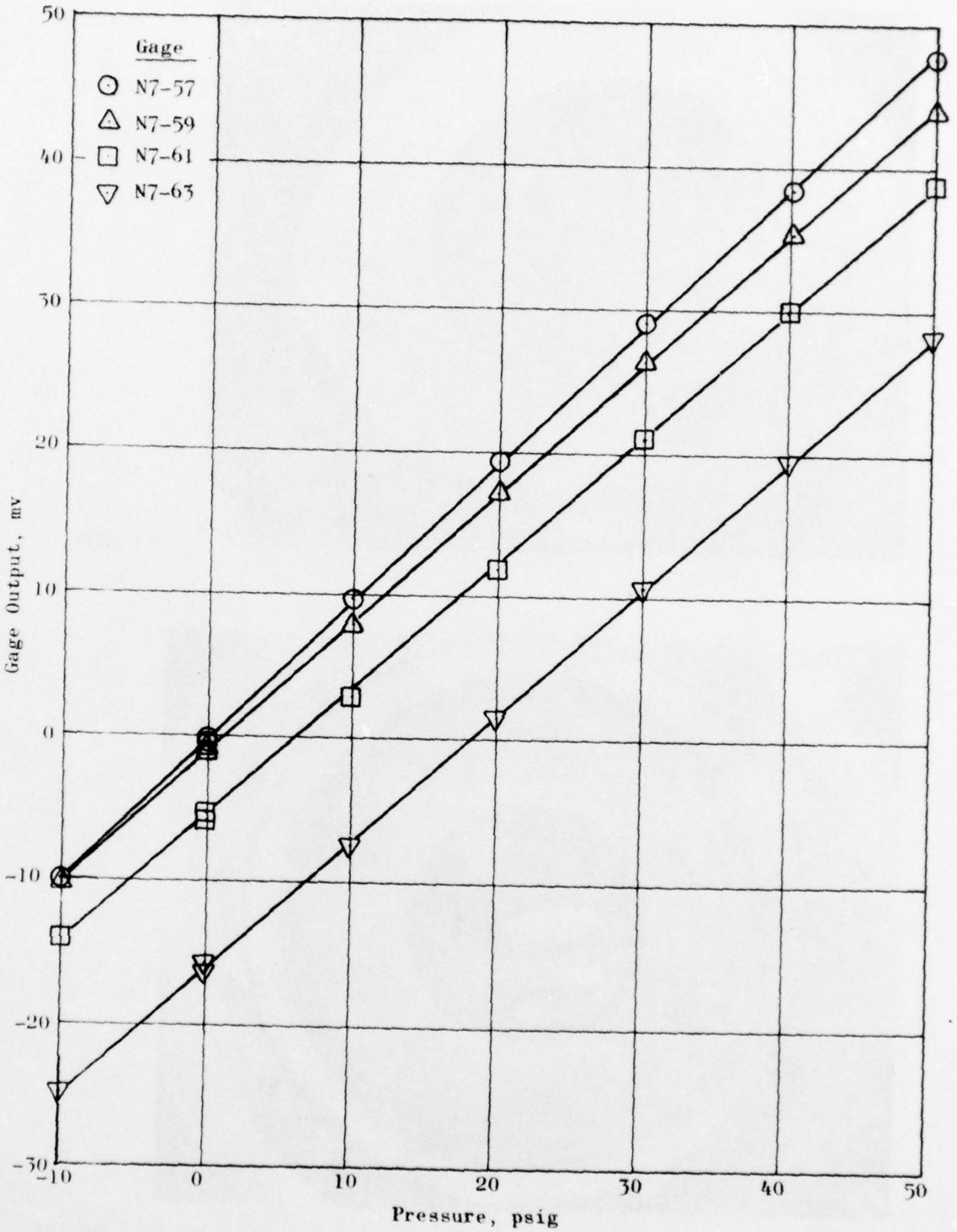

Figure 51. Typical Normal Gage Pressure Response, Motor 7

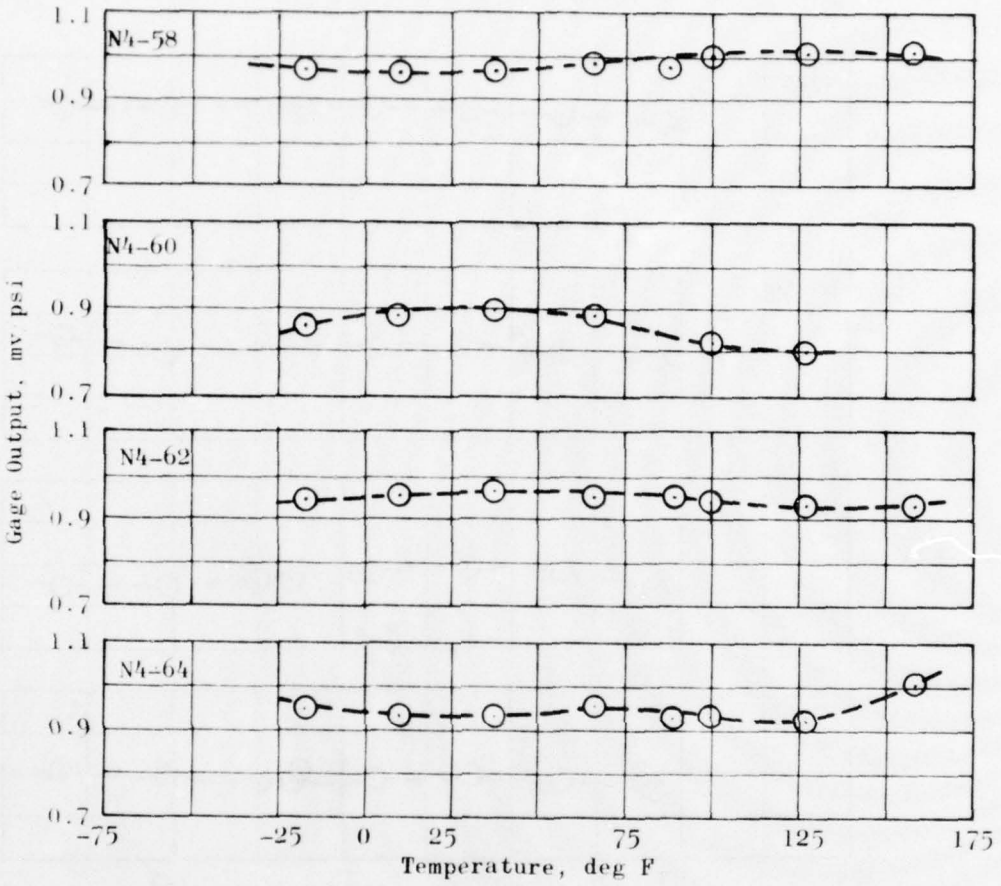

Figure 52. Normal Stress Gage Sensitivity, Motor 4

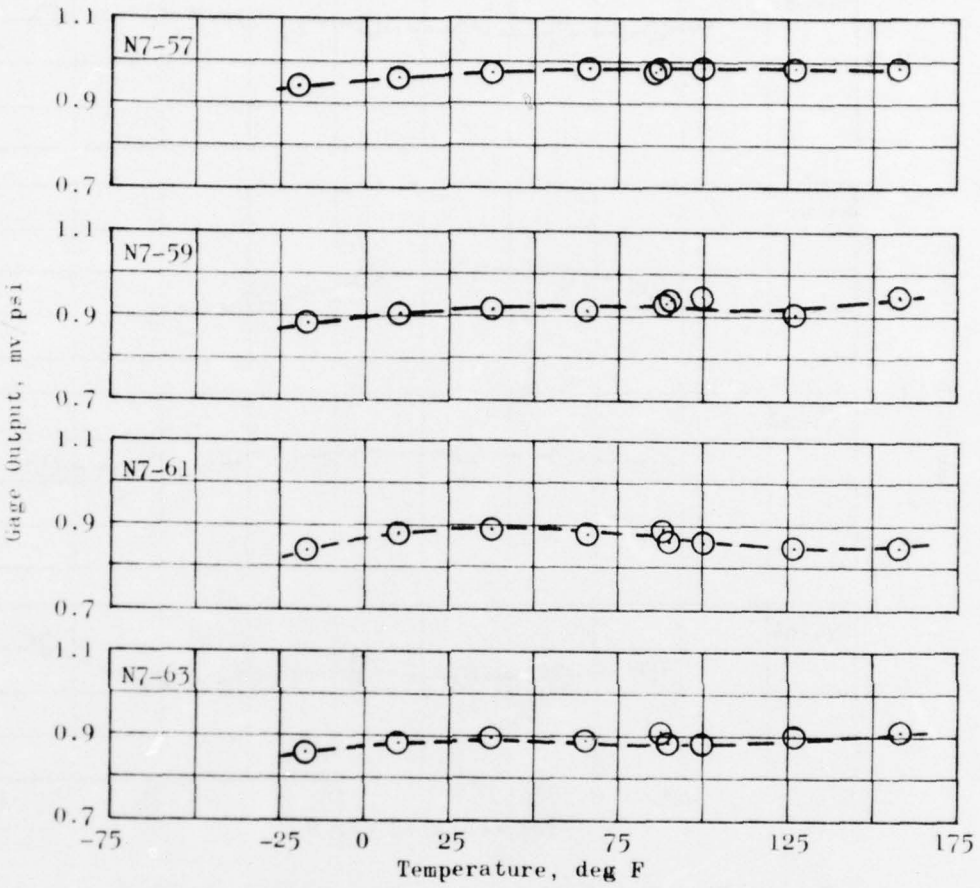

Figure 53. Normal Stress Gage Sensitivity, Motor 7

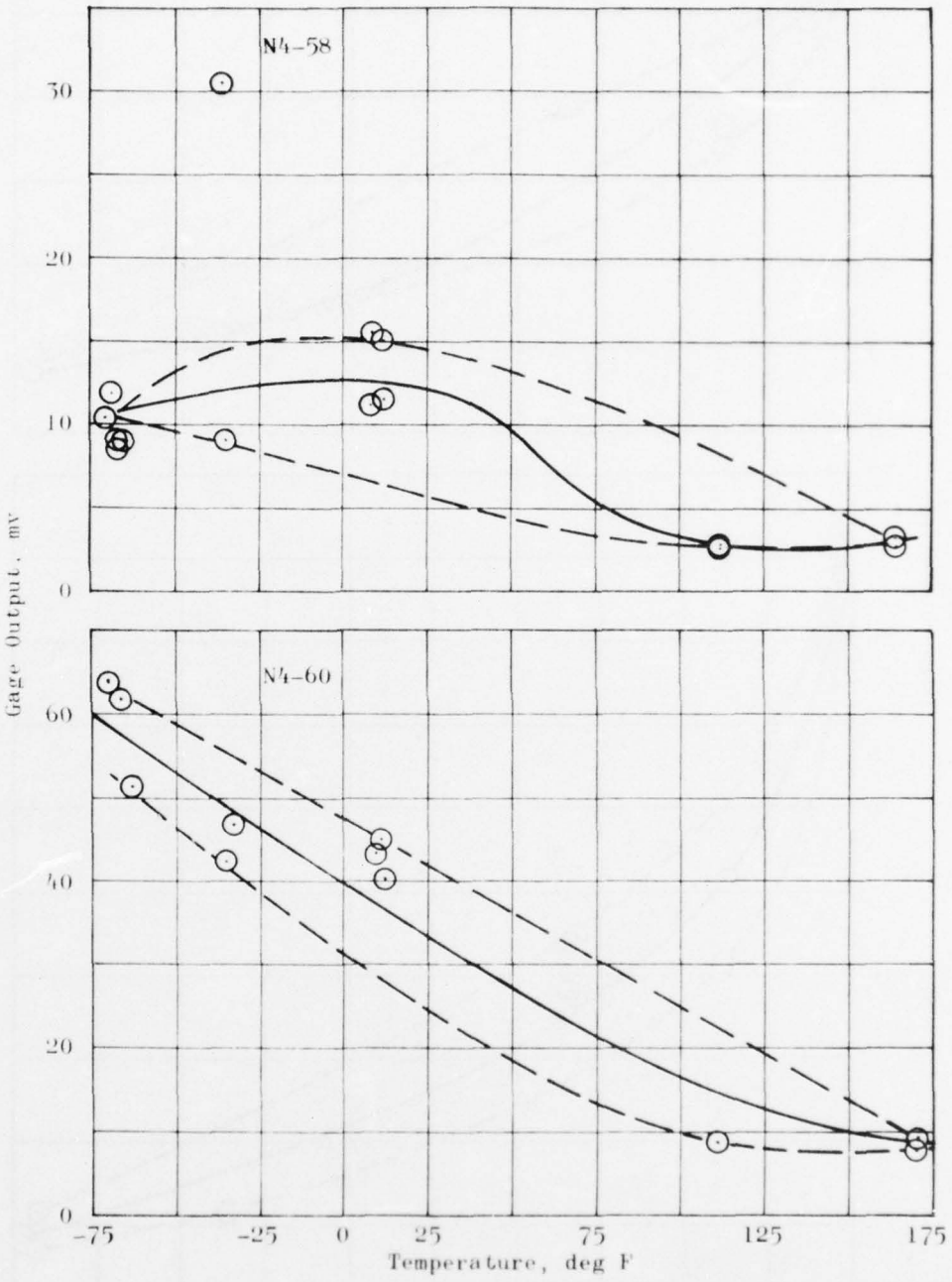

Figure 54. Normal Stress Gage Pre-cast No-Load Data as Determined by Thiokol, Motor 4

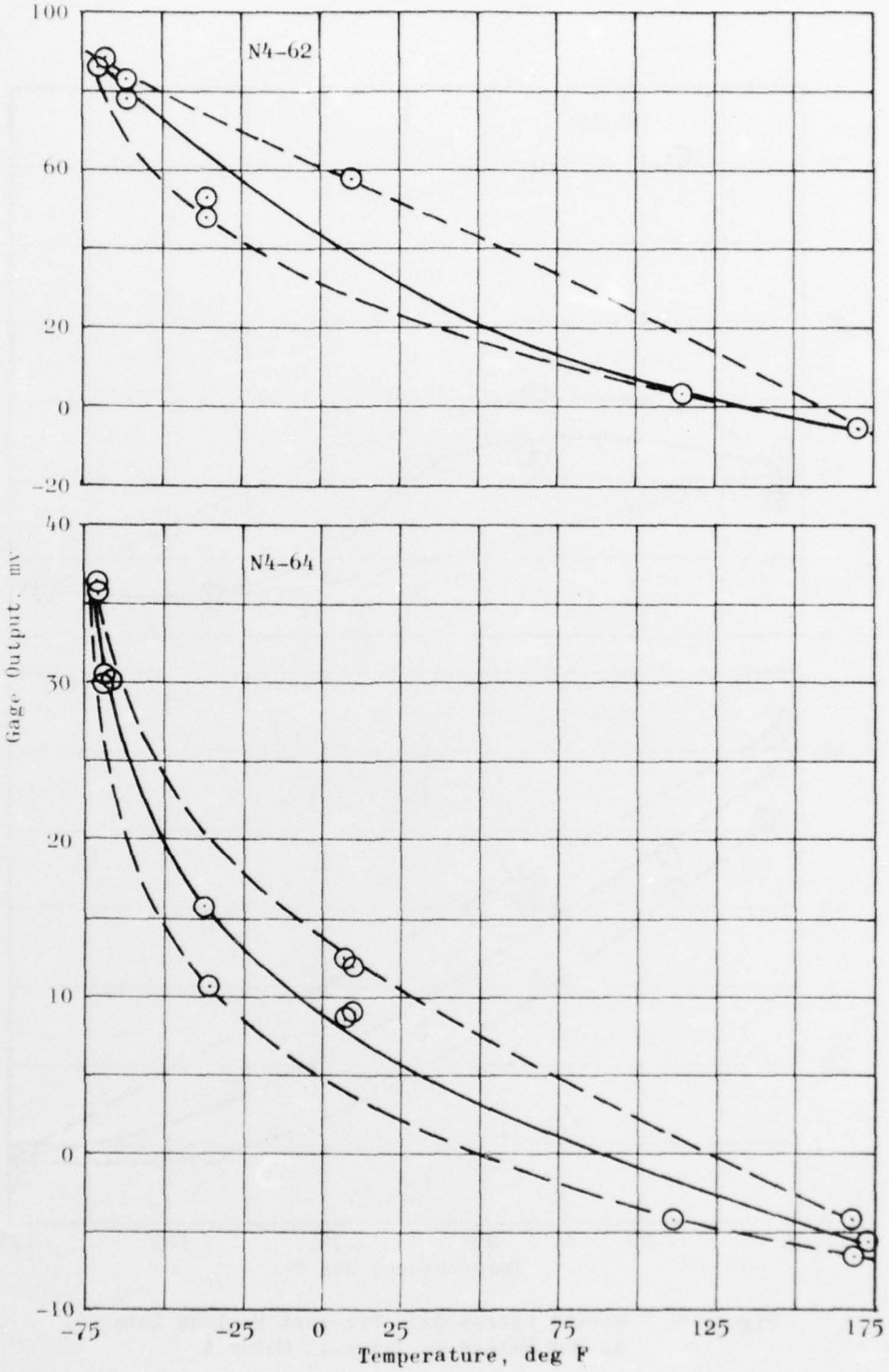

Figure 54. Continued

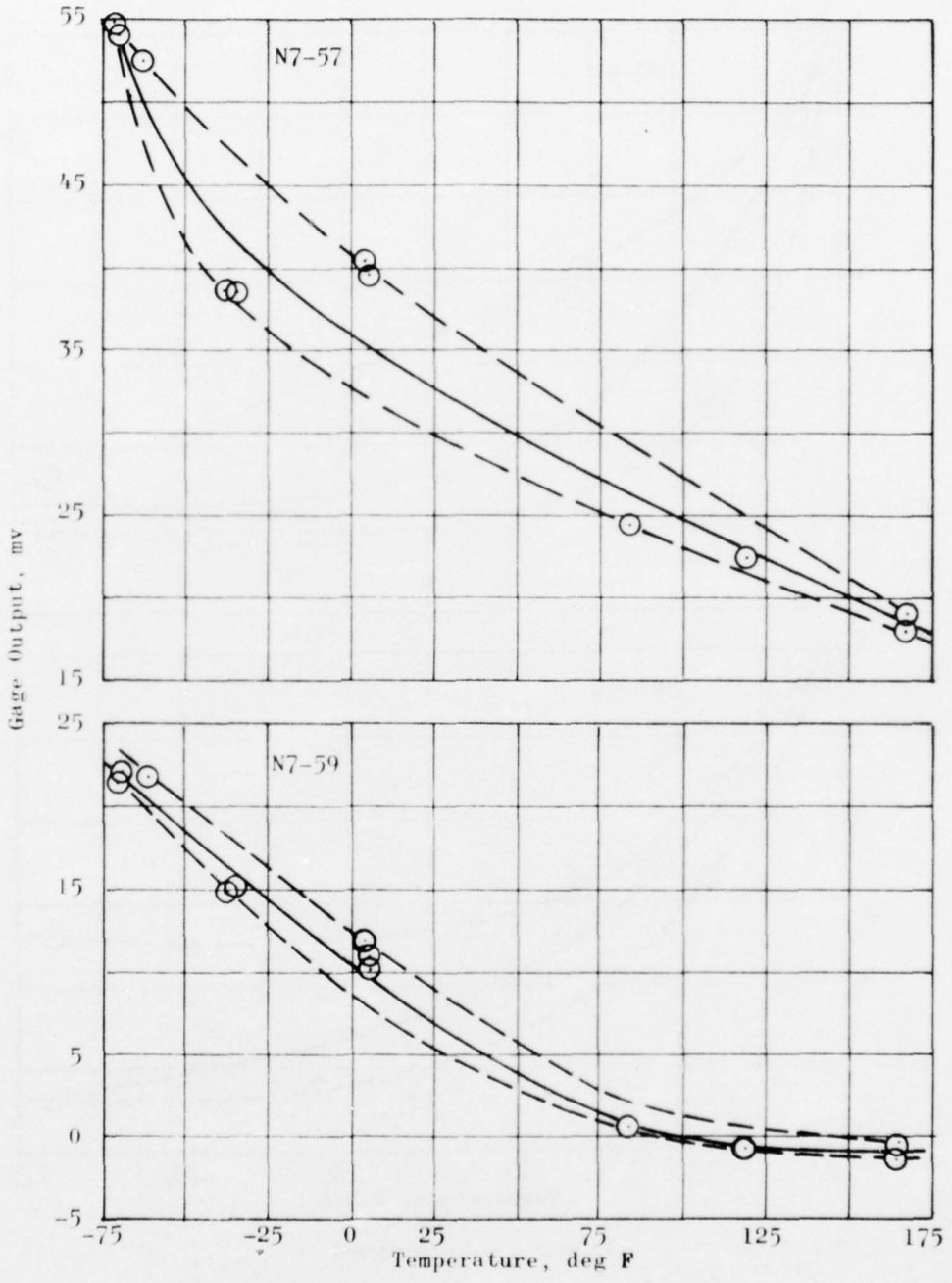

Figure 55. Normal Stress Gage Pre-cast No-Load Data as Determined by Thiokol, Motor 7

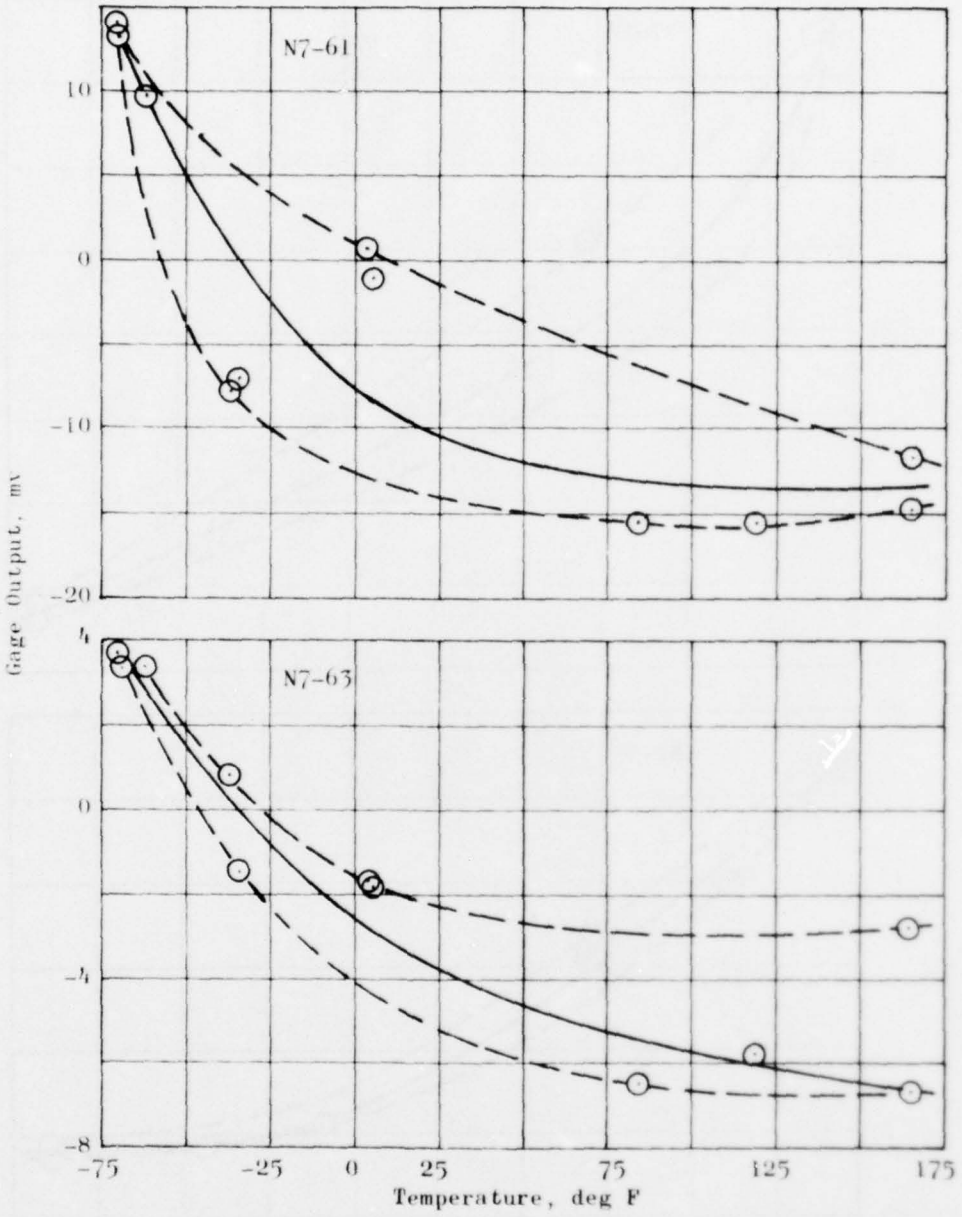

Figure 55. Continued

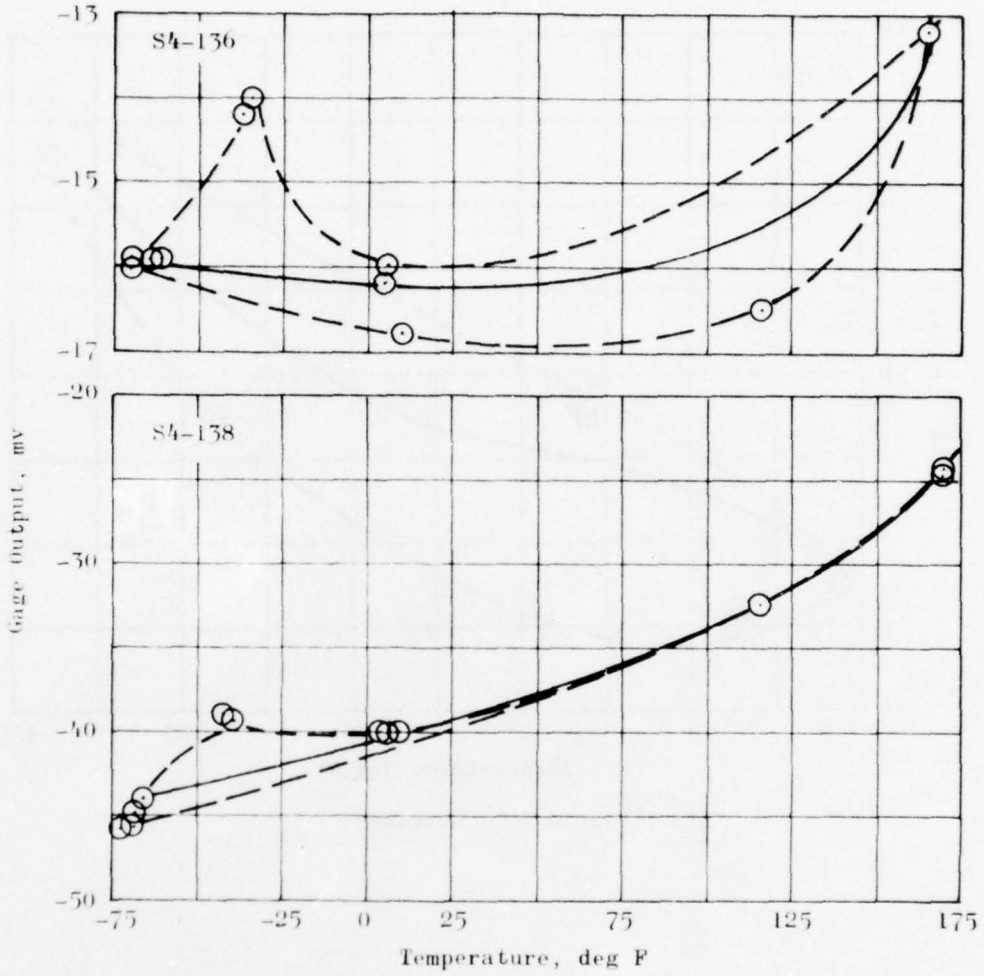

Figure 56. Shear Gage Pre-cast No-Load Data as Determined by Thiokol, Motor 4

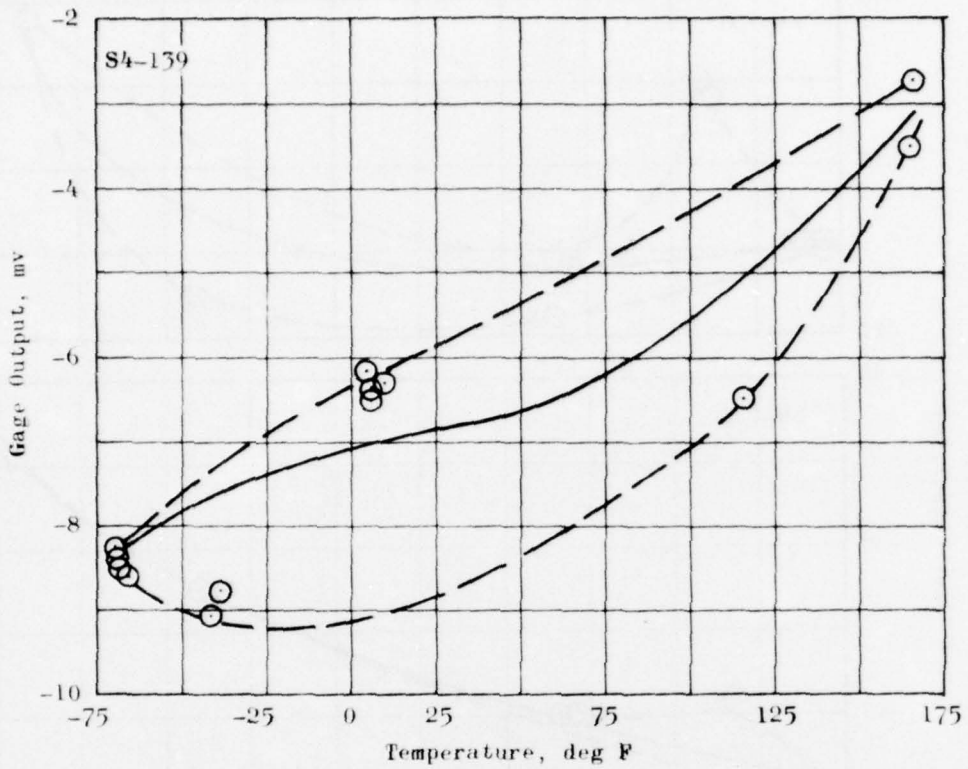

Figure 56. Continued

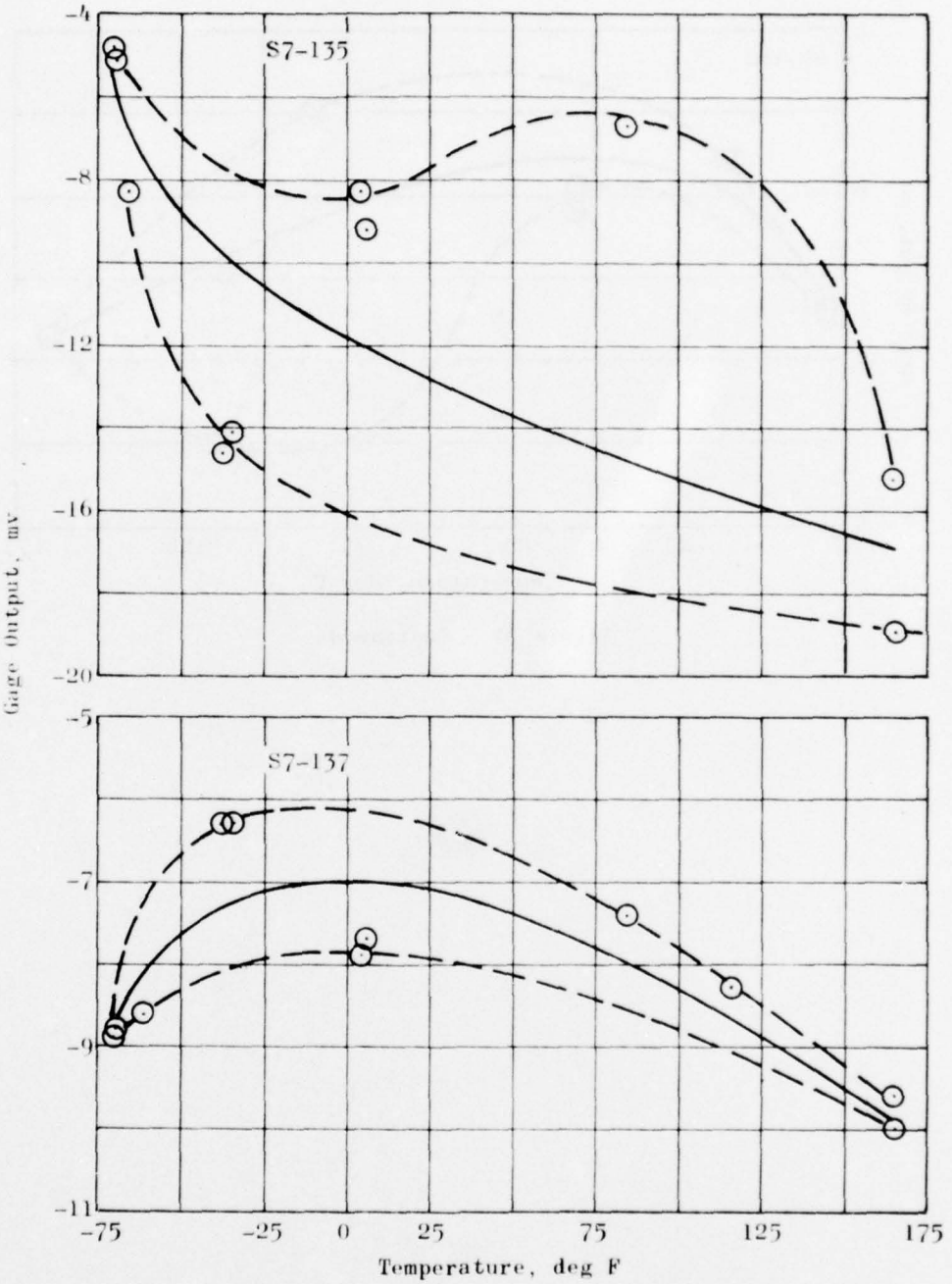

Figure 57. Shear Gage Pre-cast No-Load Data as Determined by Thiokol, Motor 7

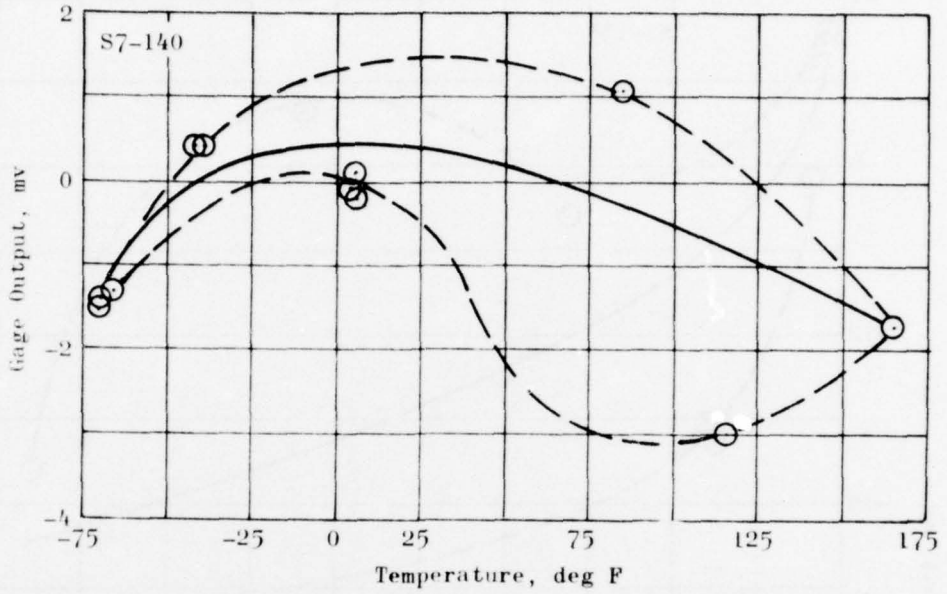

Figure 57. Continued

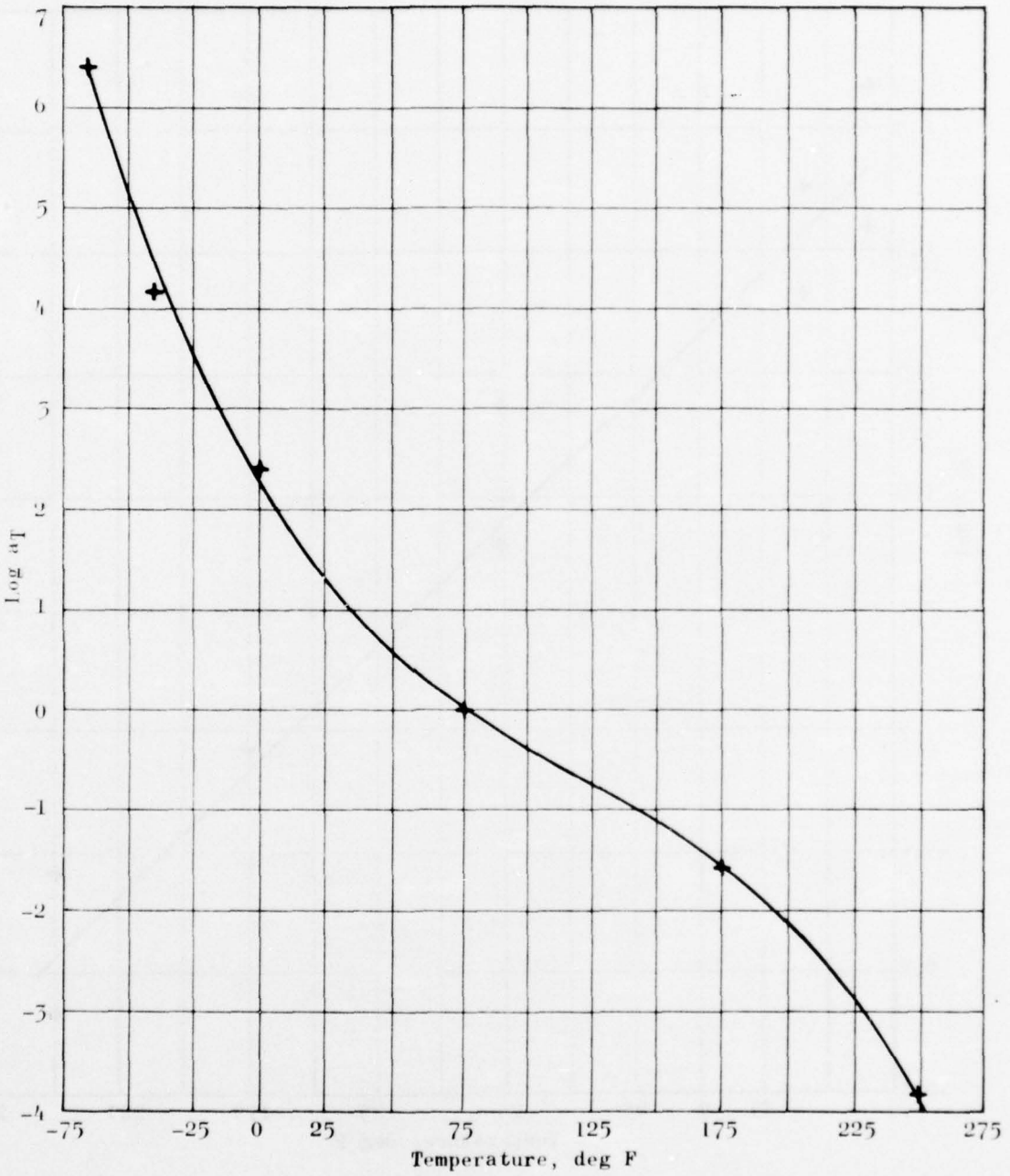

Figure 58. Bench Calibration, Gages 134 through 139

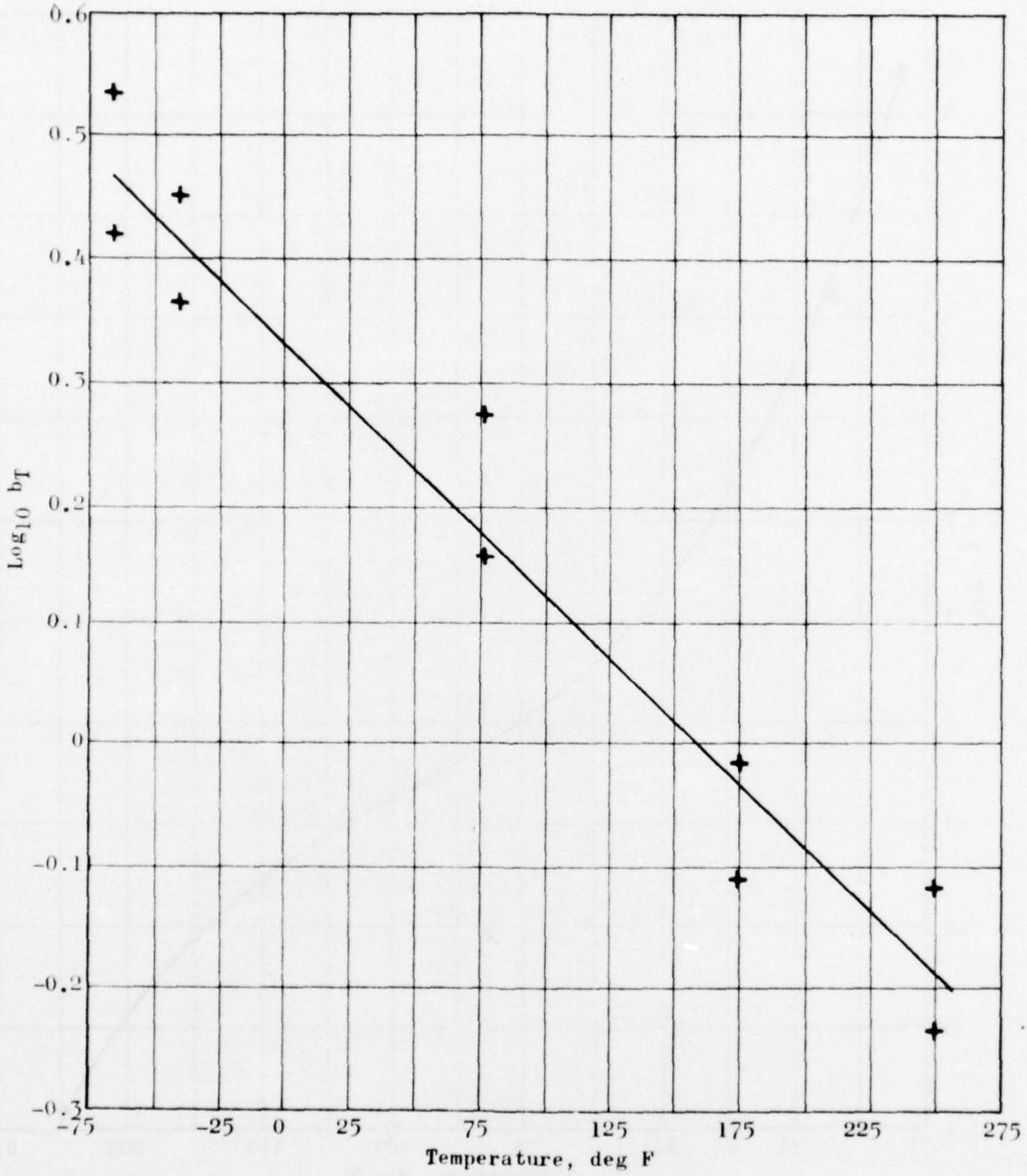

Figure 59. Bench Calibration, Gage 134

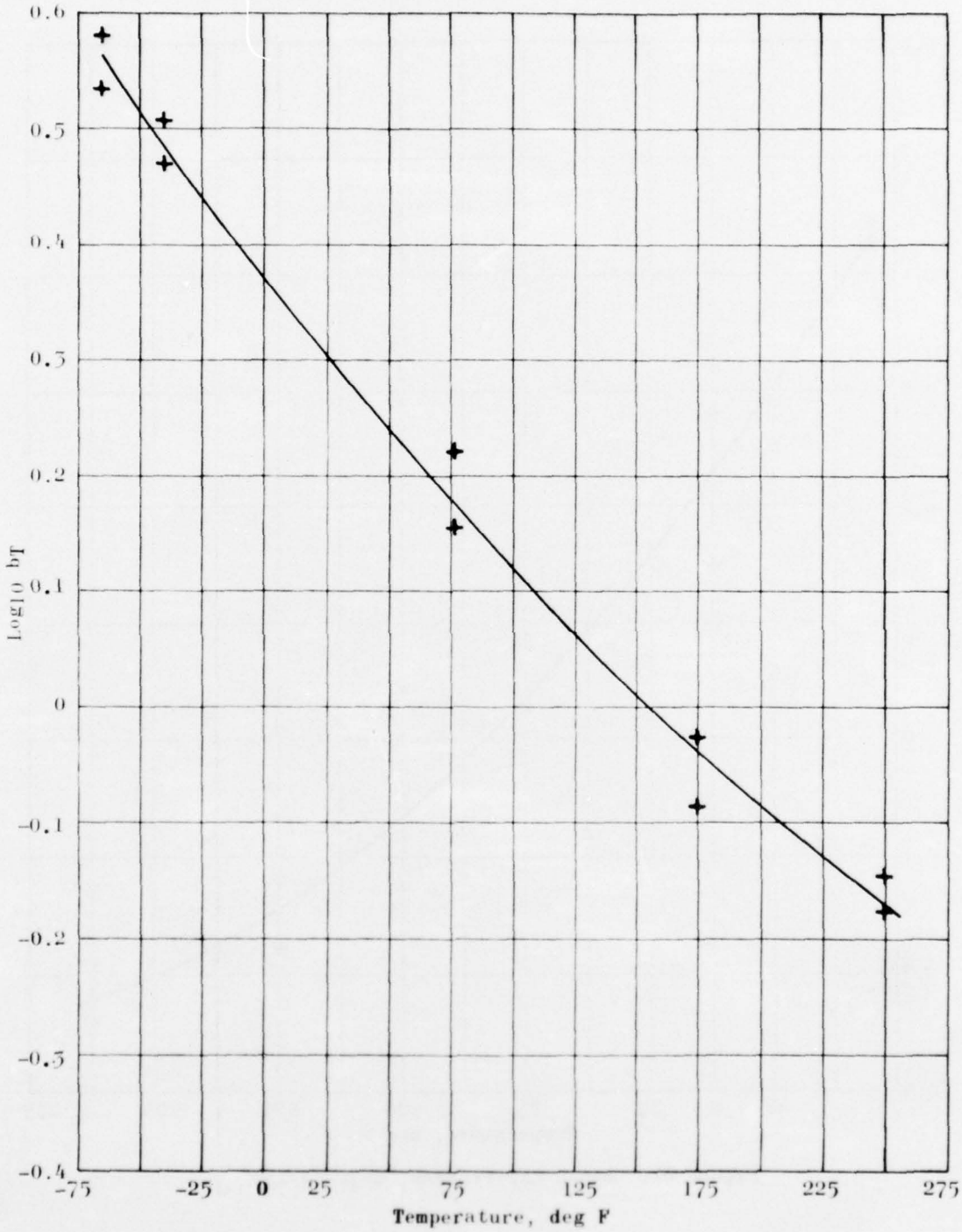

Figure 60. Bench Calibration, Gage S7-135

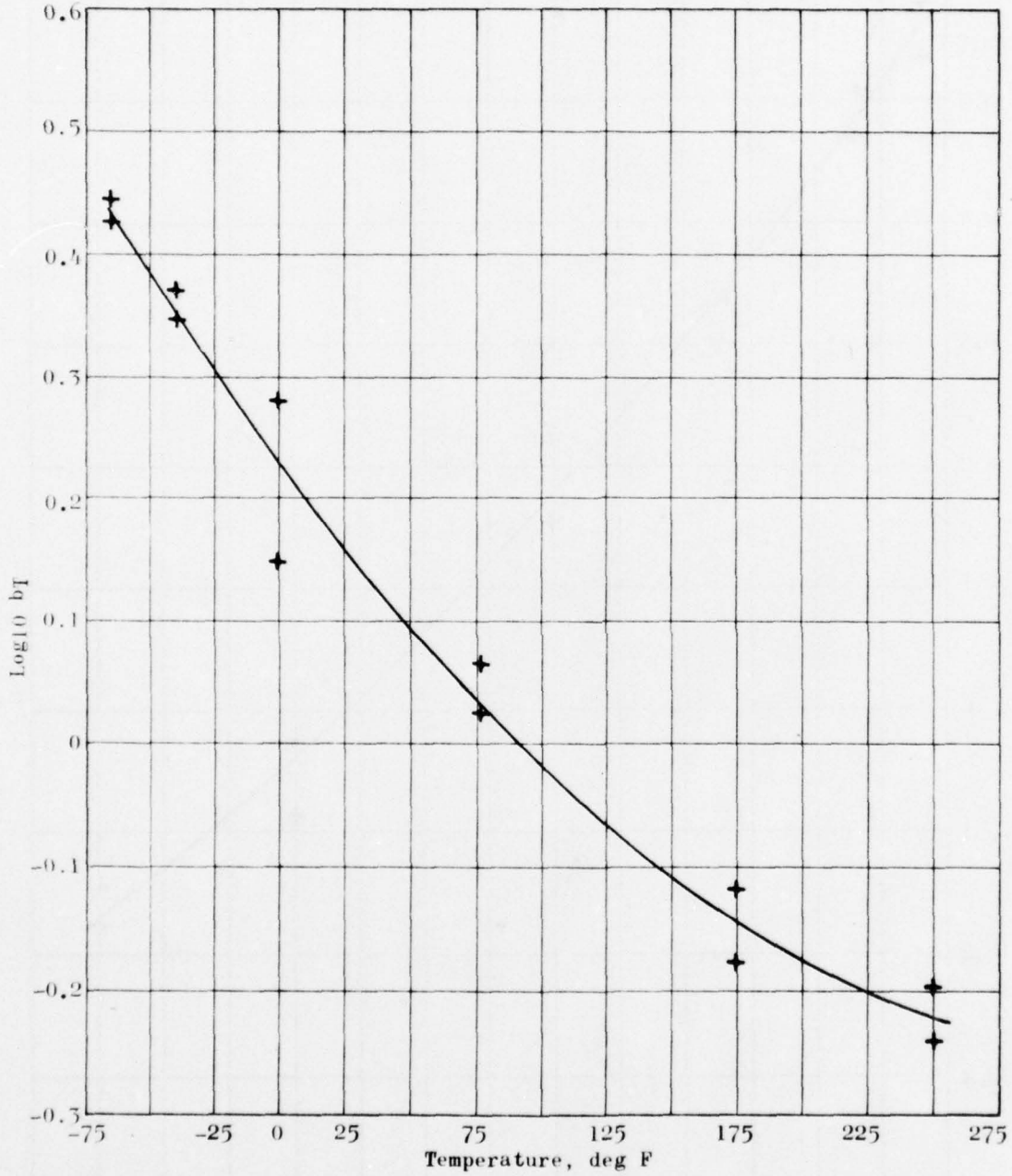

Figure 61. Bench Calibration, Gage S4-136

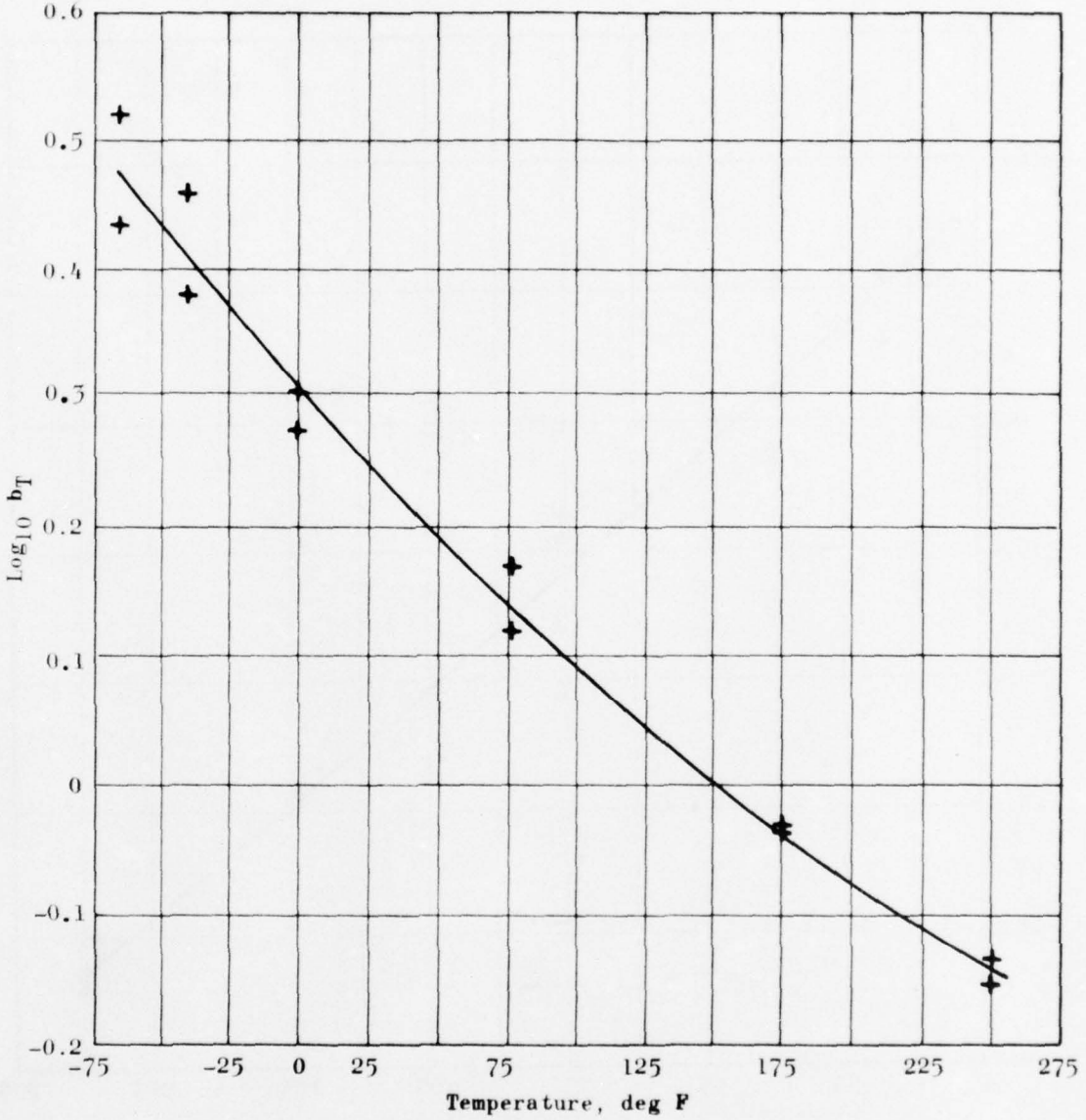

Figure 62. Bench Calibration, Gage S7-137

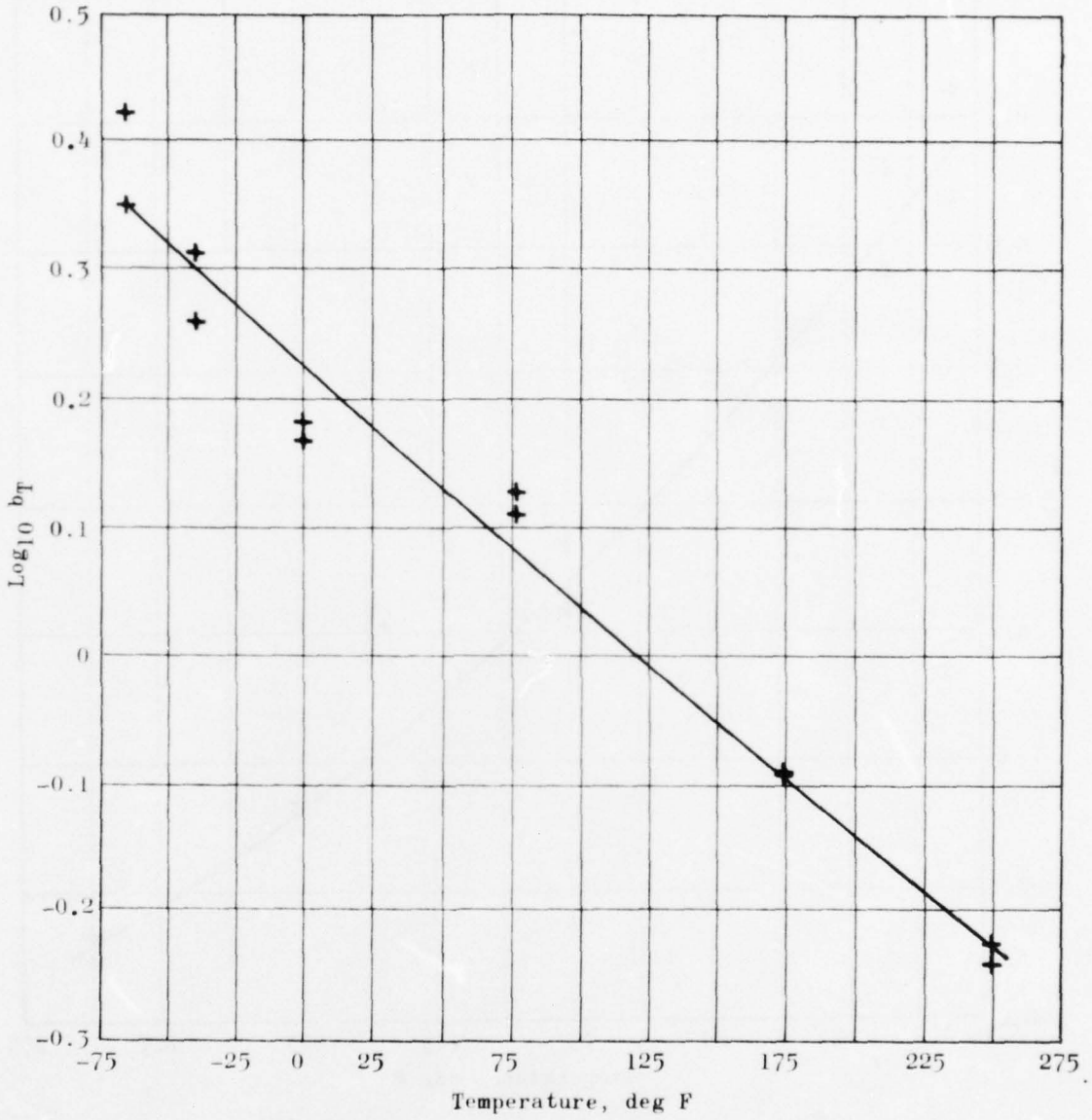

Figure 63. Bench Calibration, Gage S4-138

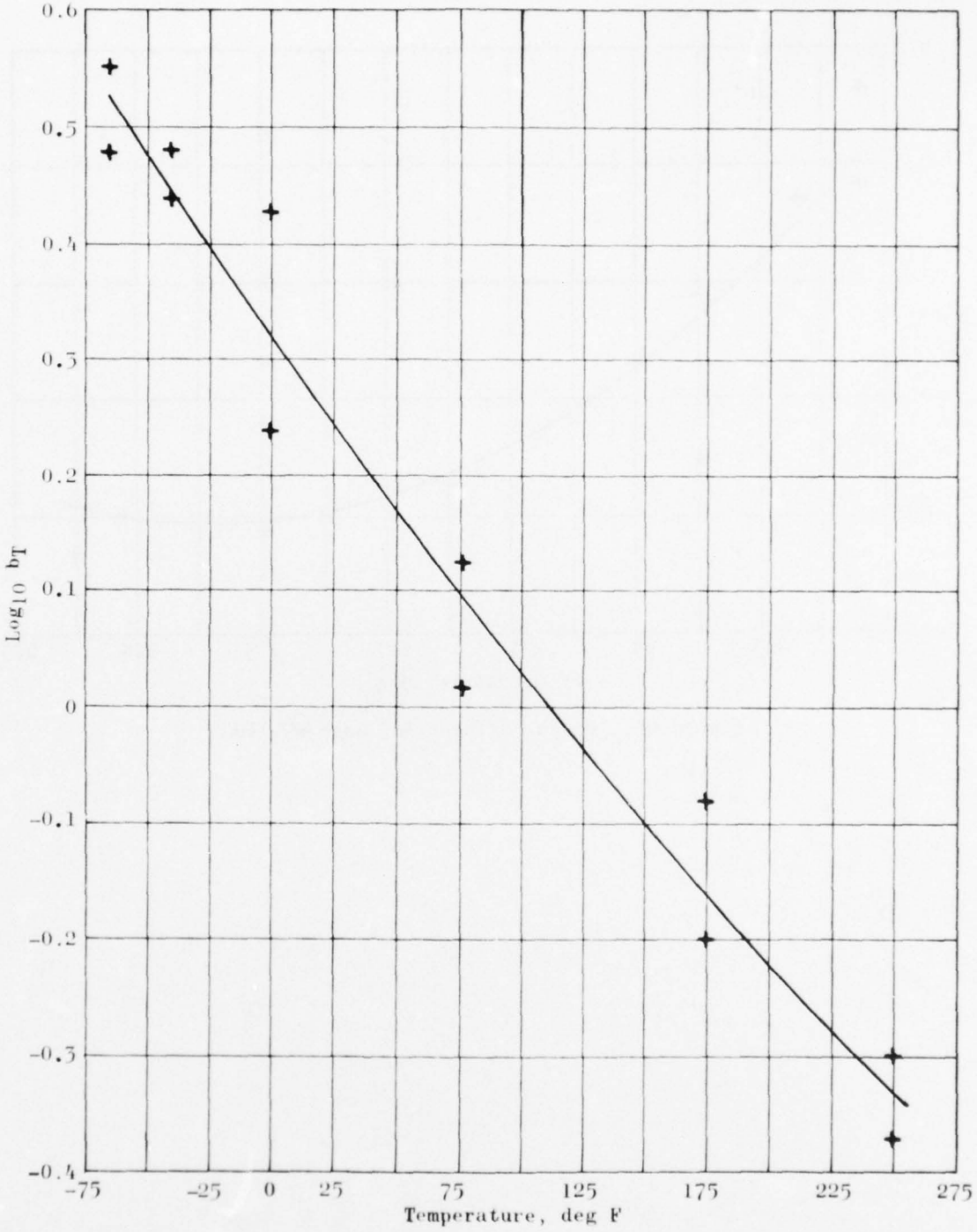

Figure 64. Bench Calibration, Gage S4-139

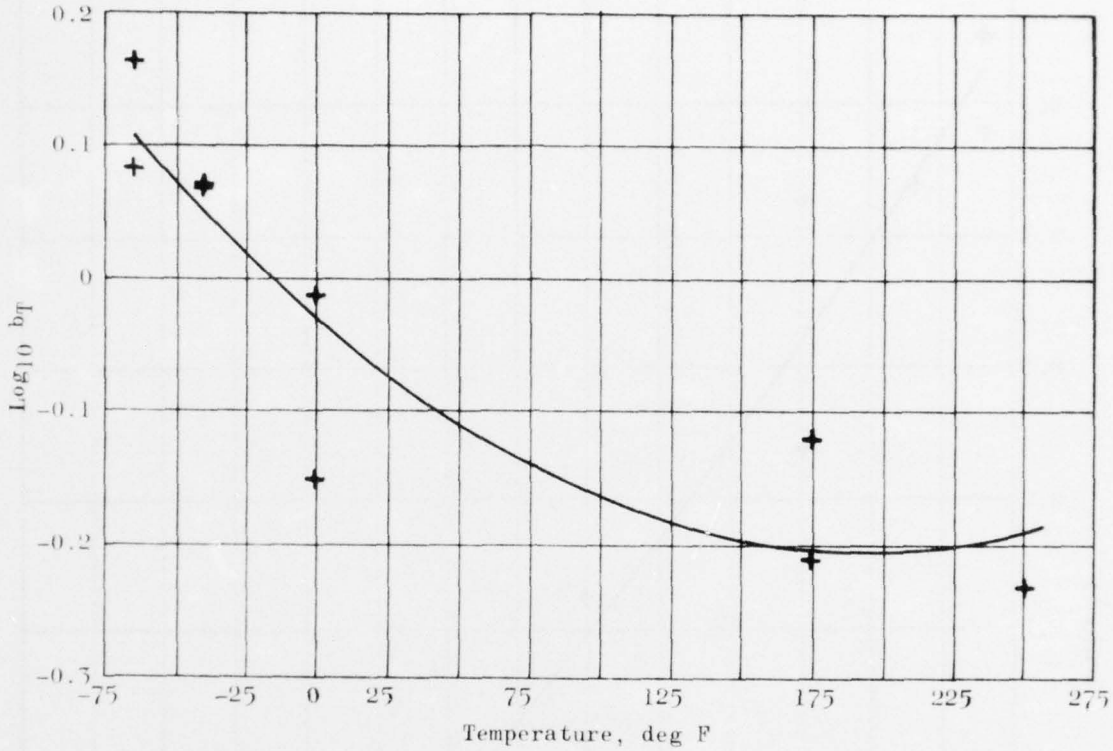

Figure 65. Bench Calibration, Gage S7-140

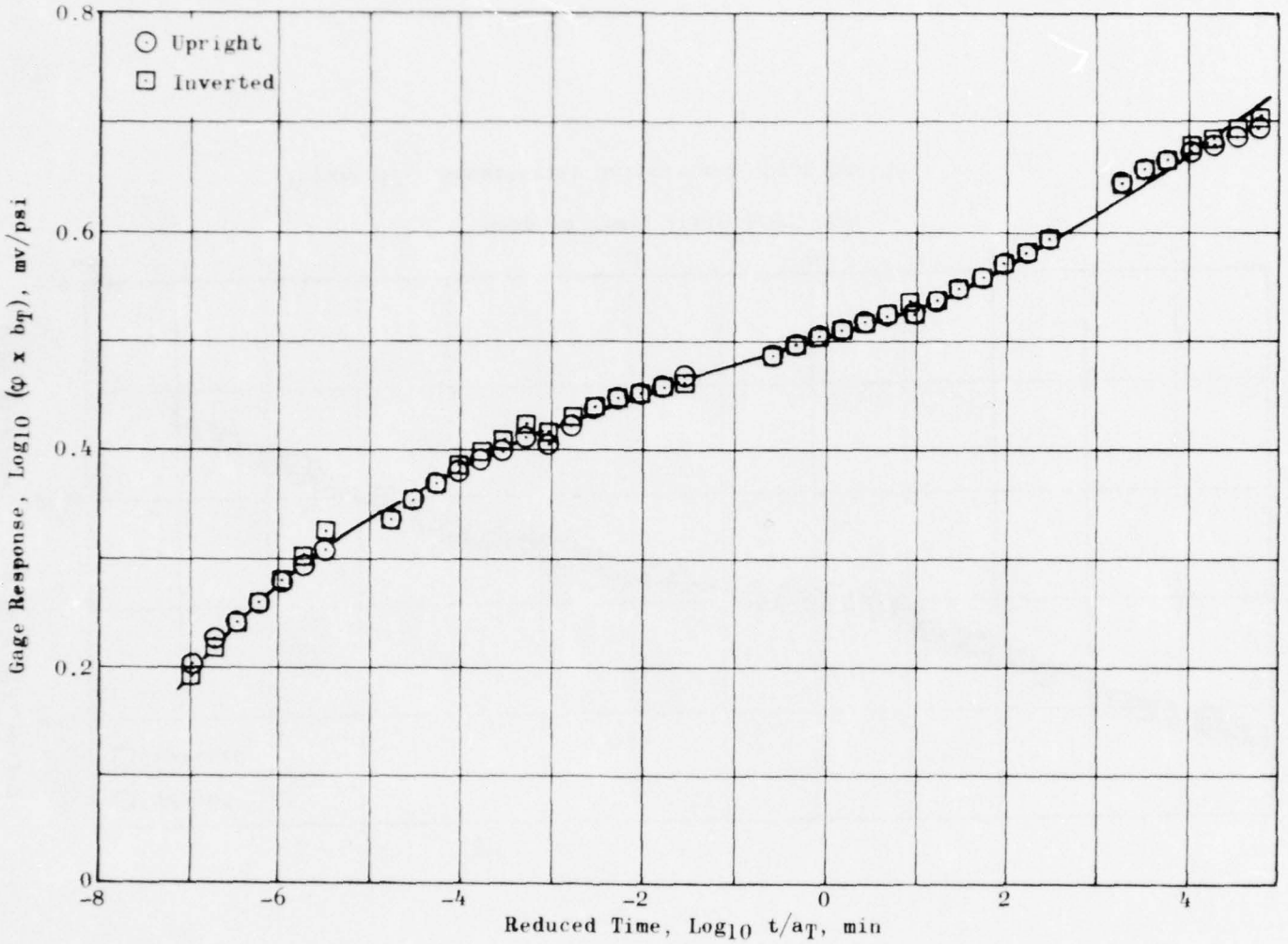

Figure 66. Sensitivity Calibration, Gage S4-136

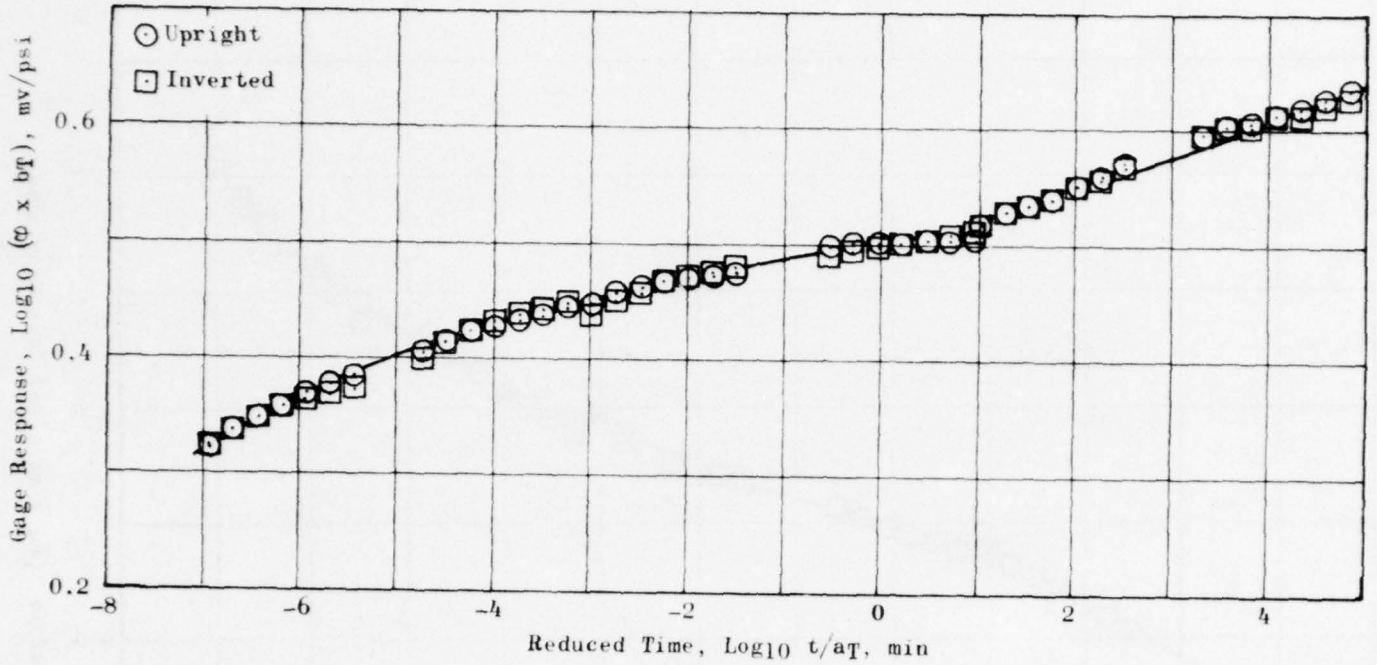

Figure 67. Sensitivity Calibration, Gage S4-138

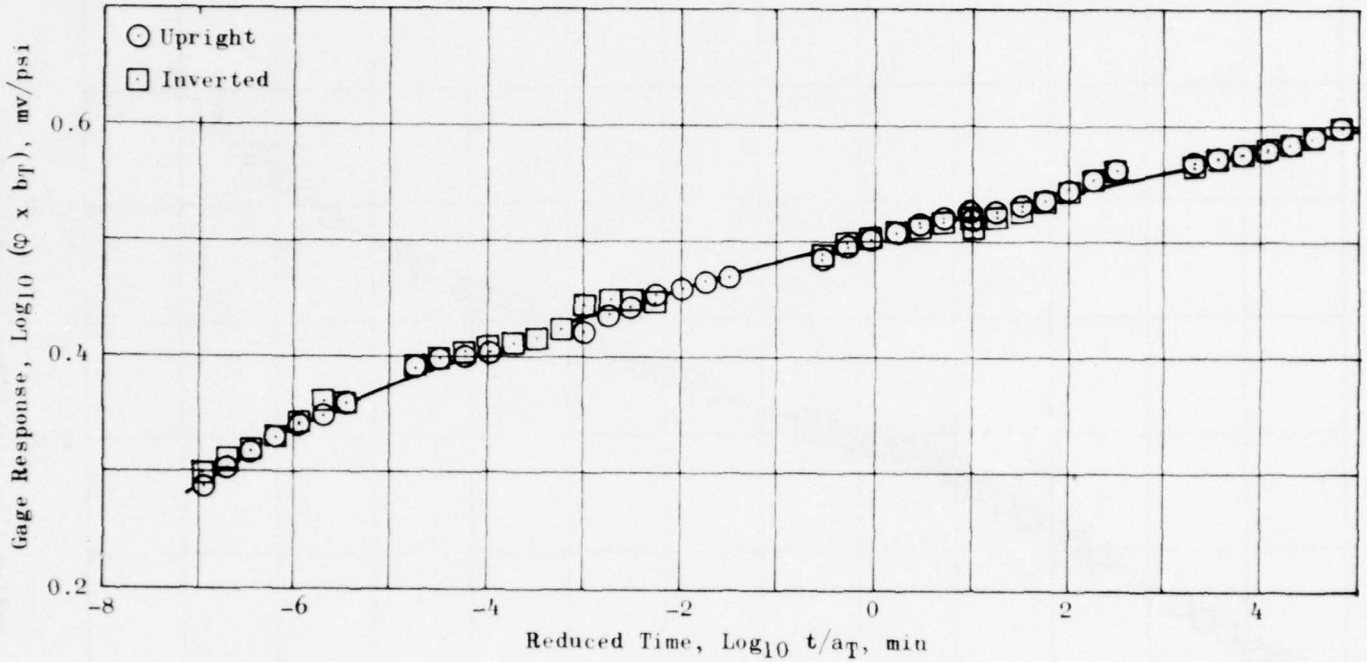

Figure 68. Sensitivity Calibration, Gage S4-139

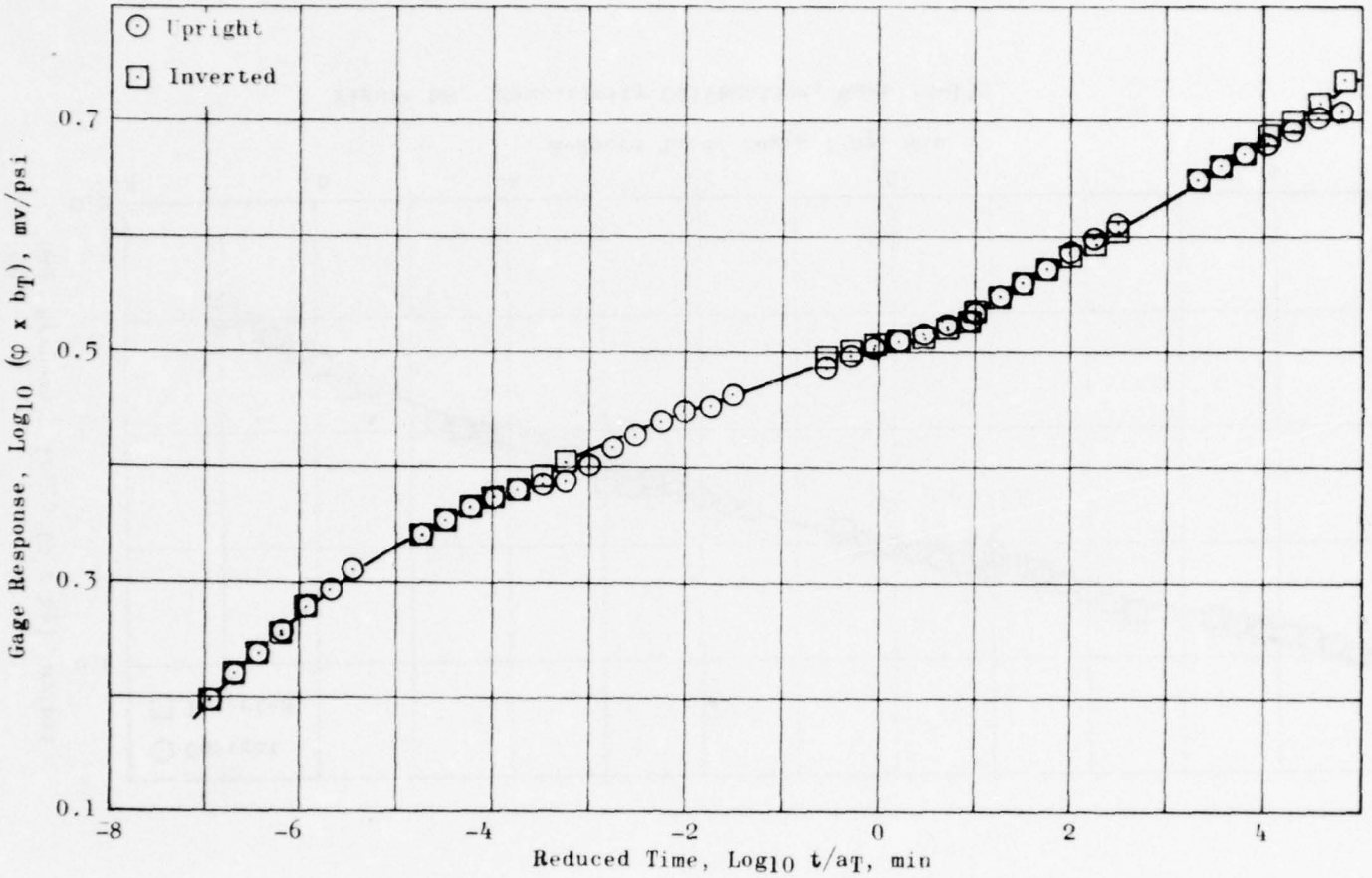

Figure 69. Sensitivity Calibration, Gage S7-135

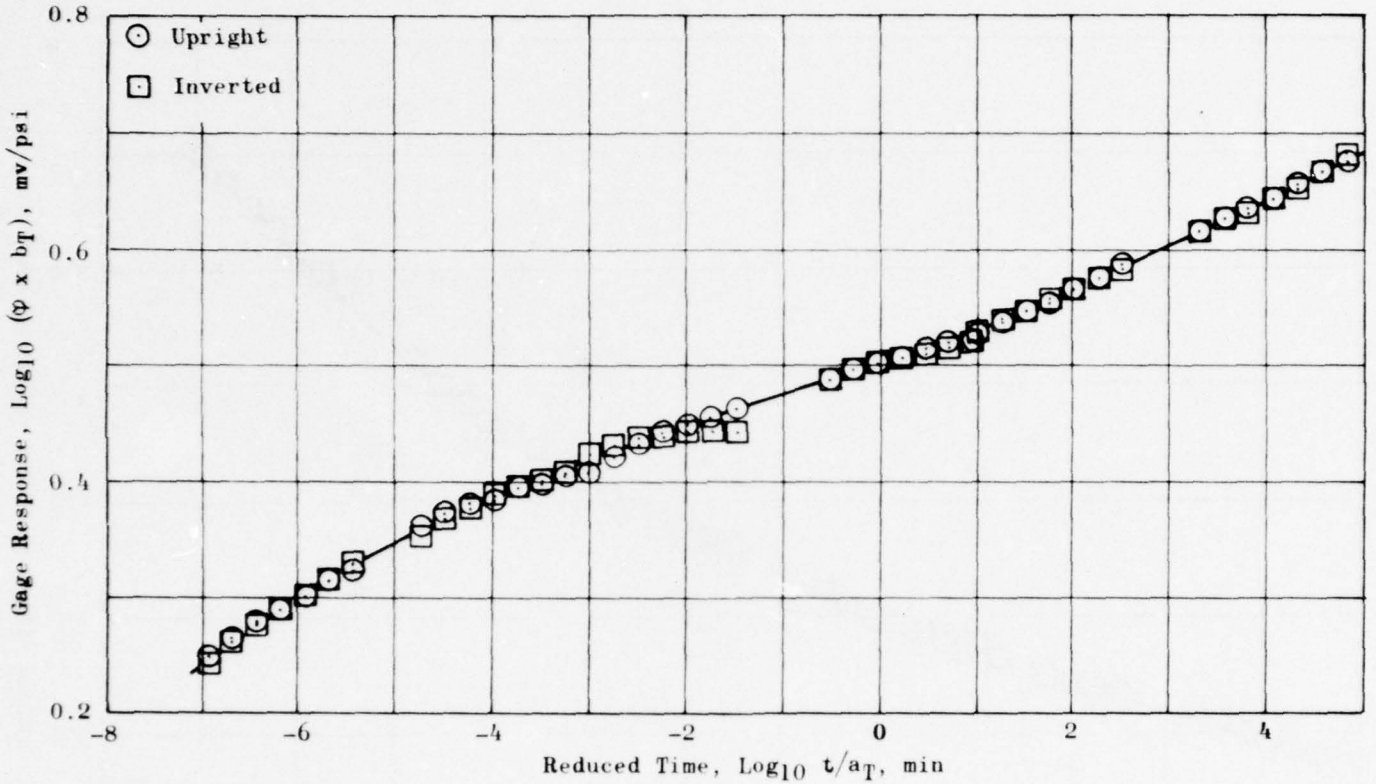

Figure 70. Sensitivity Calibration, Gage S7-137

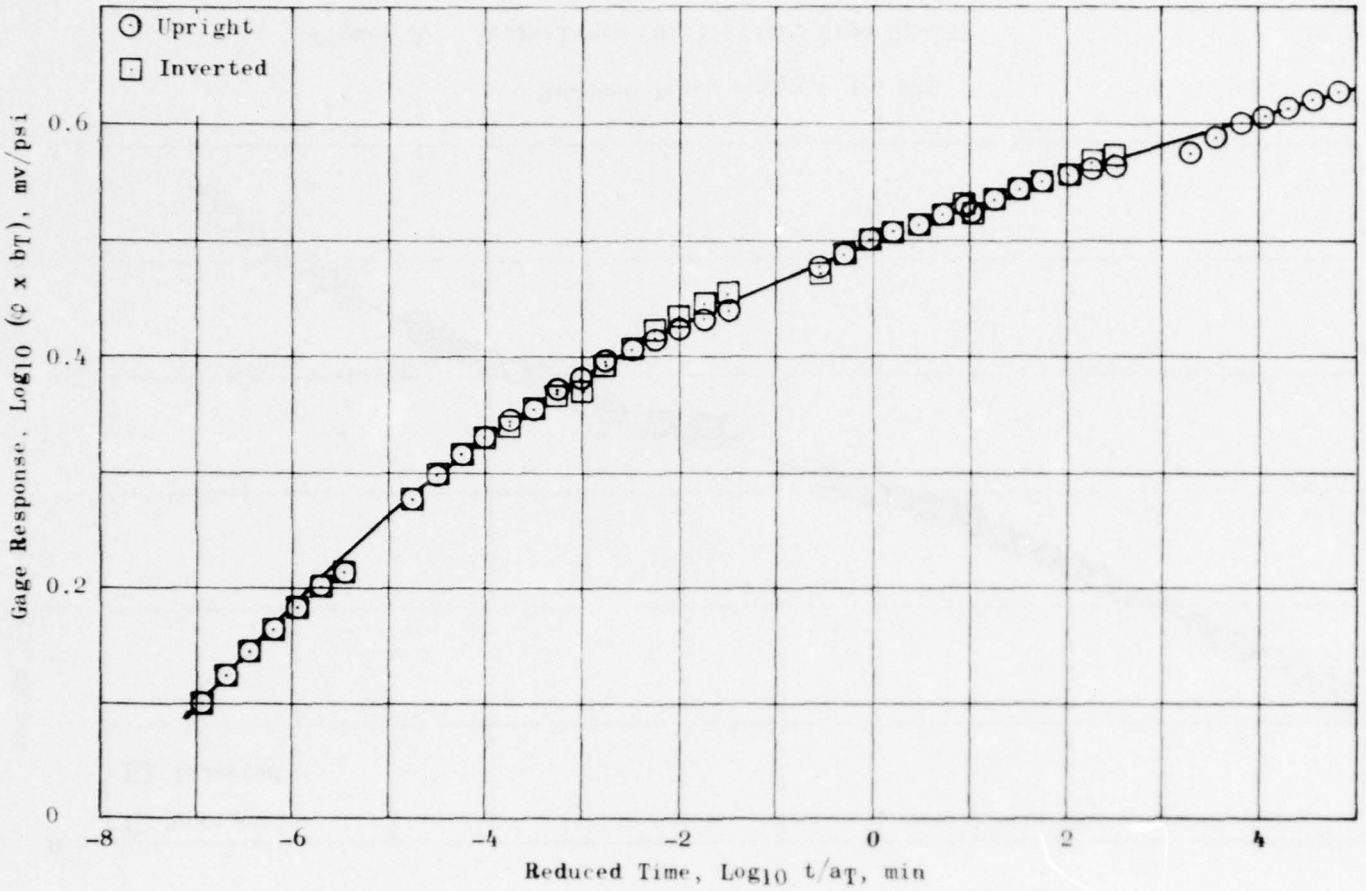

Figure 71. Sensitivity Calibration, Gage S7-140

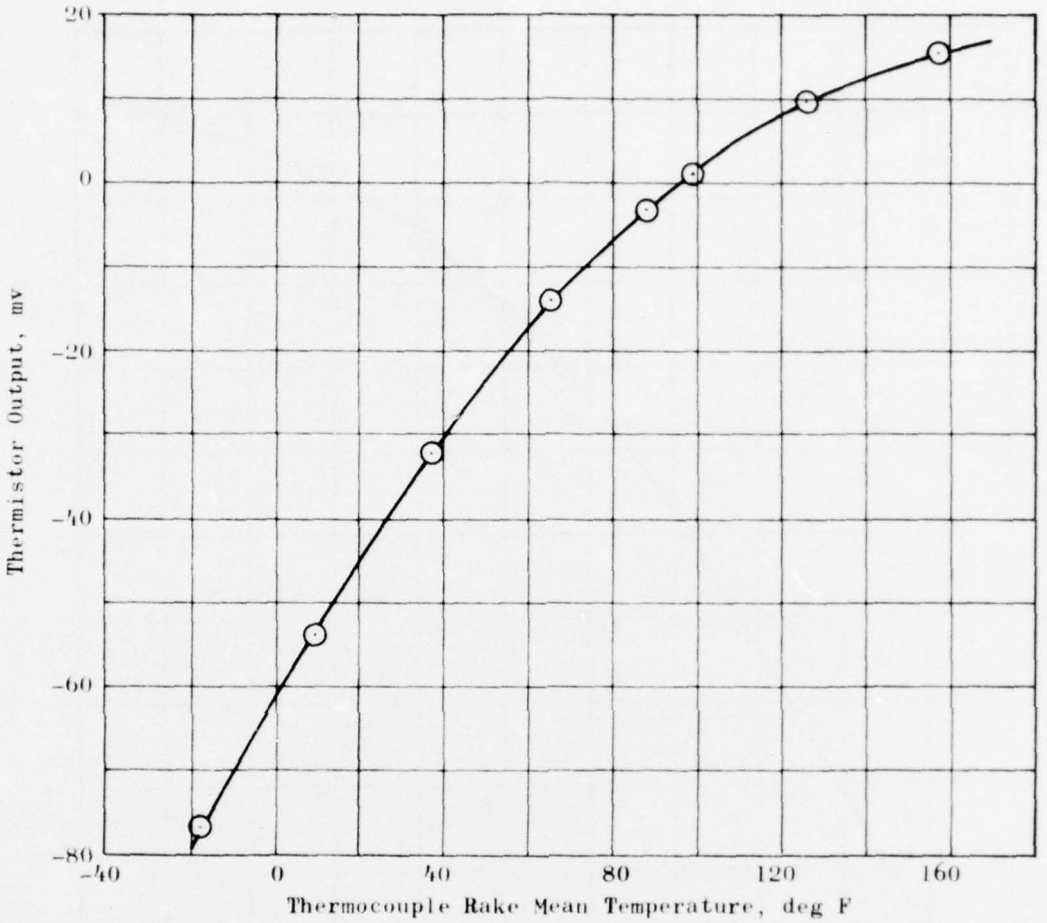

Figure 72. TH4-60 Response during Motor Checkout

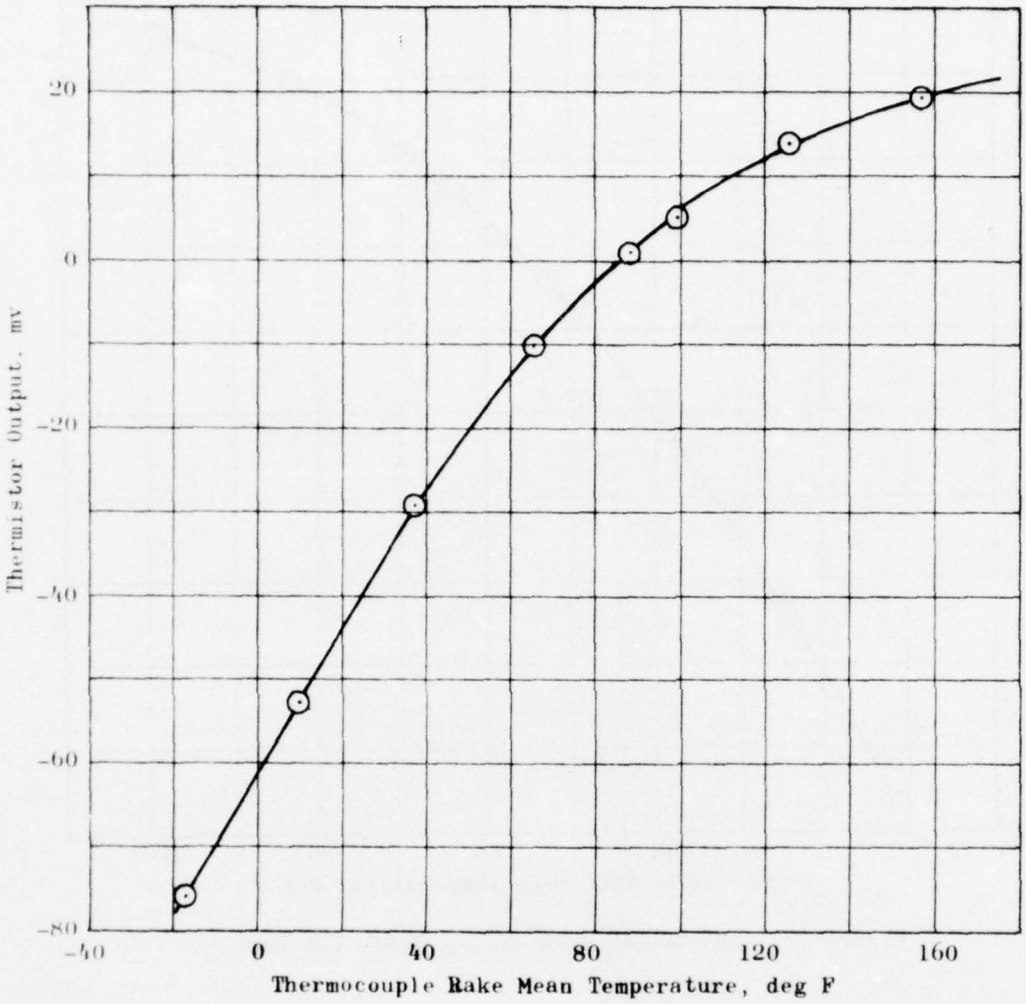

Figure 73. TH4-64 Response during Motor Checkout

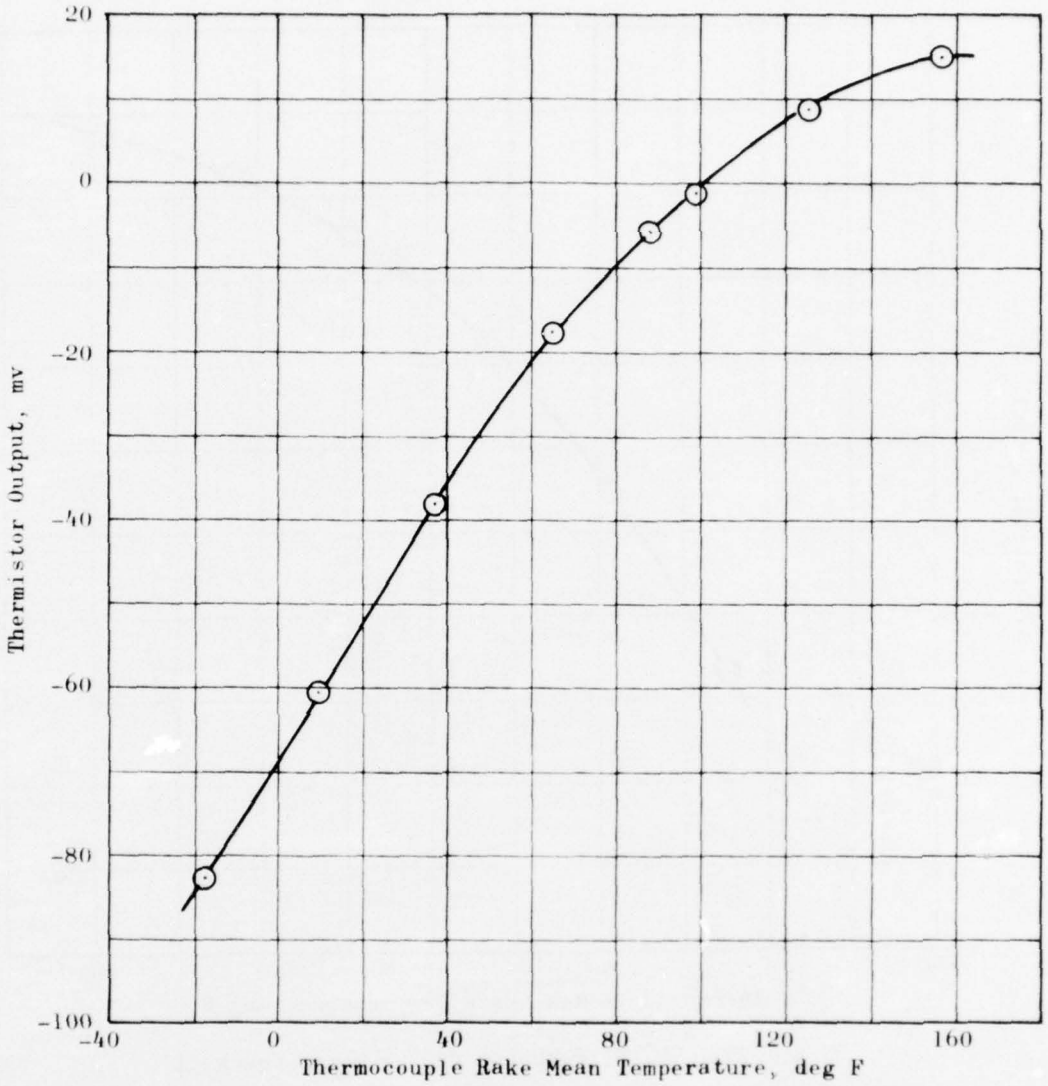

Figure 74. TH4-136 Response during Motor Checkout

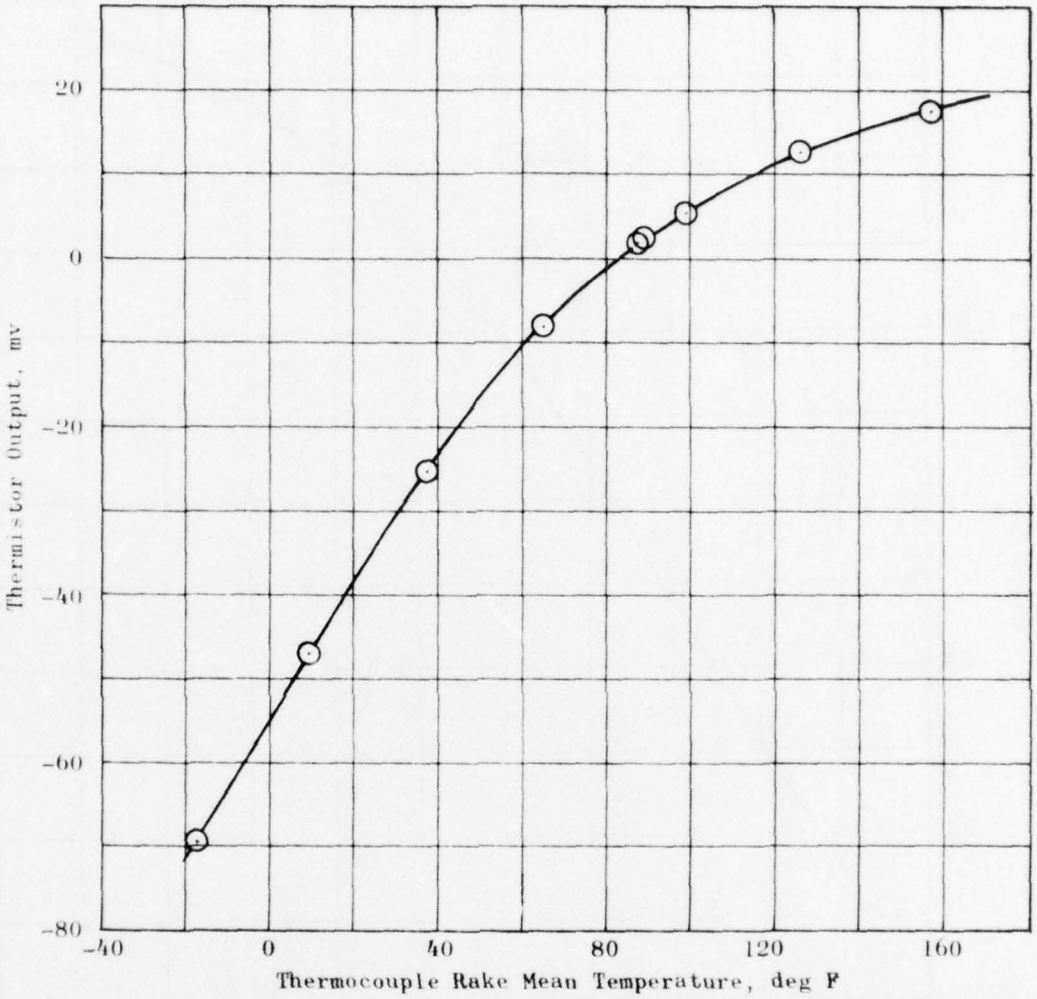

Figure 75. TH7-57 Response during Motor Checkout

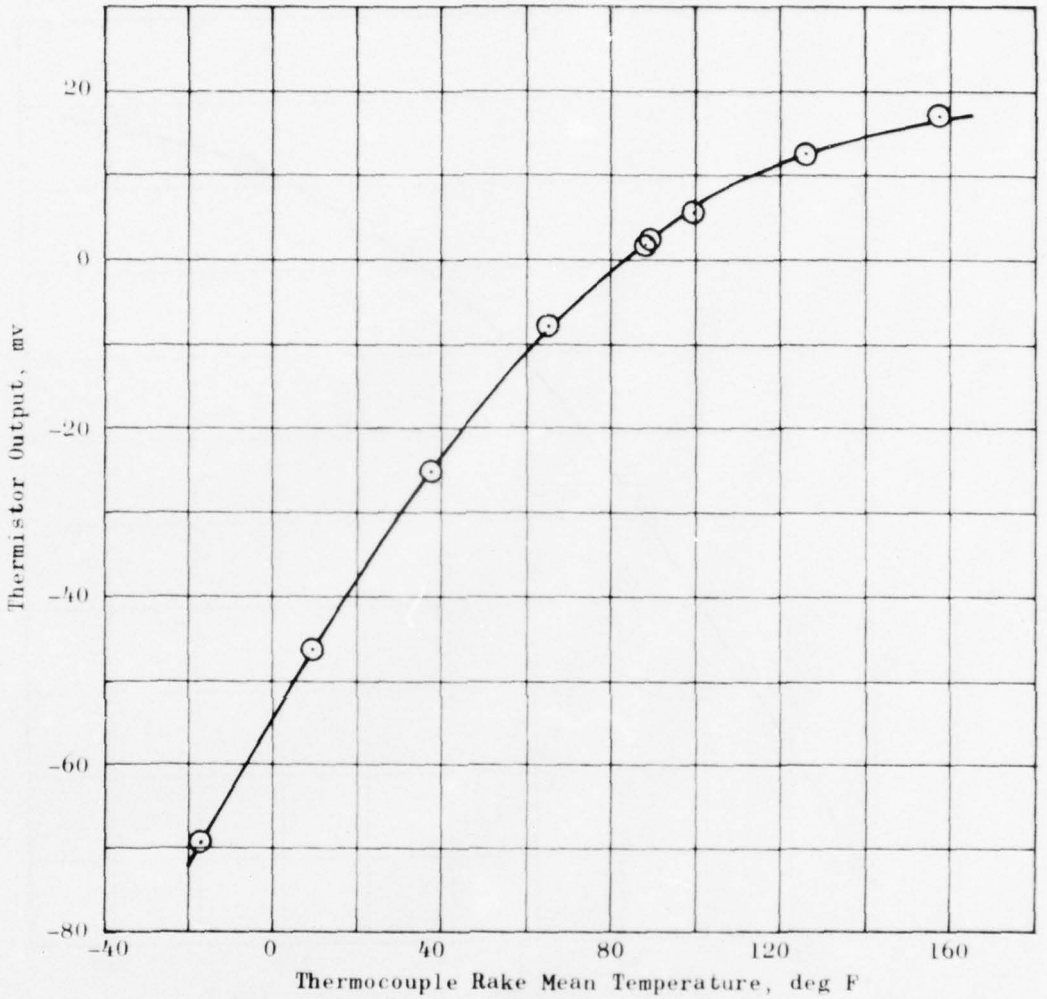

Figure 76. TH7-59 Response during Motor Checkout

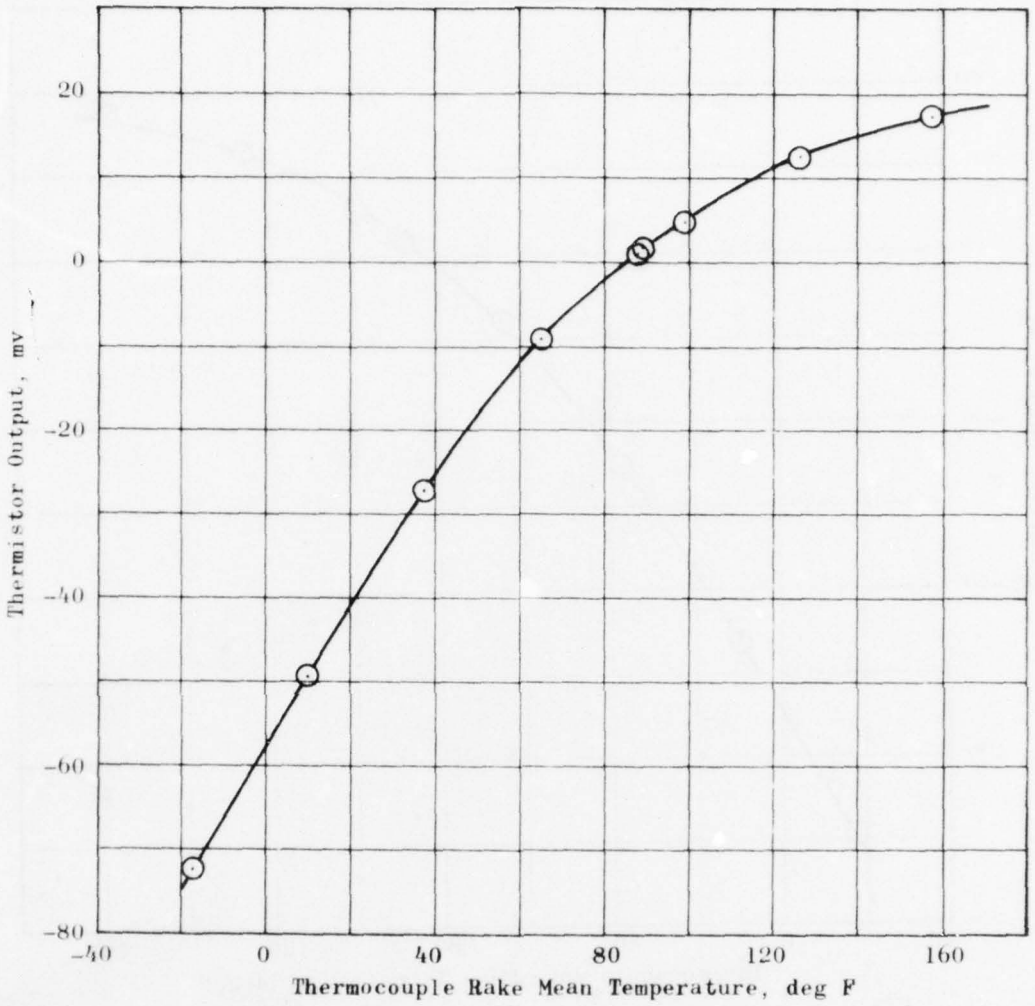

Figure 77. TH7-61 Response during Motor Checkout

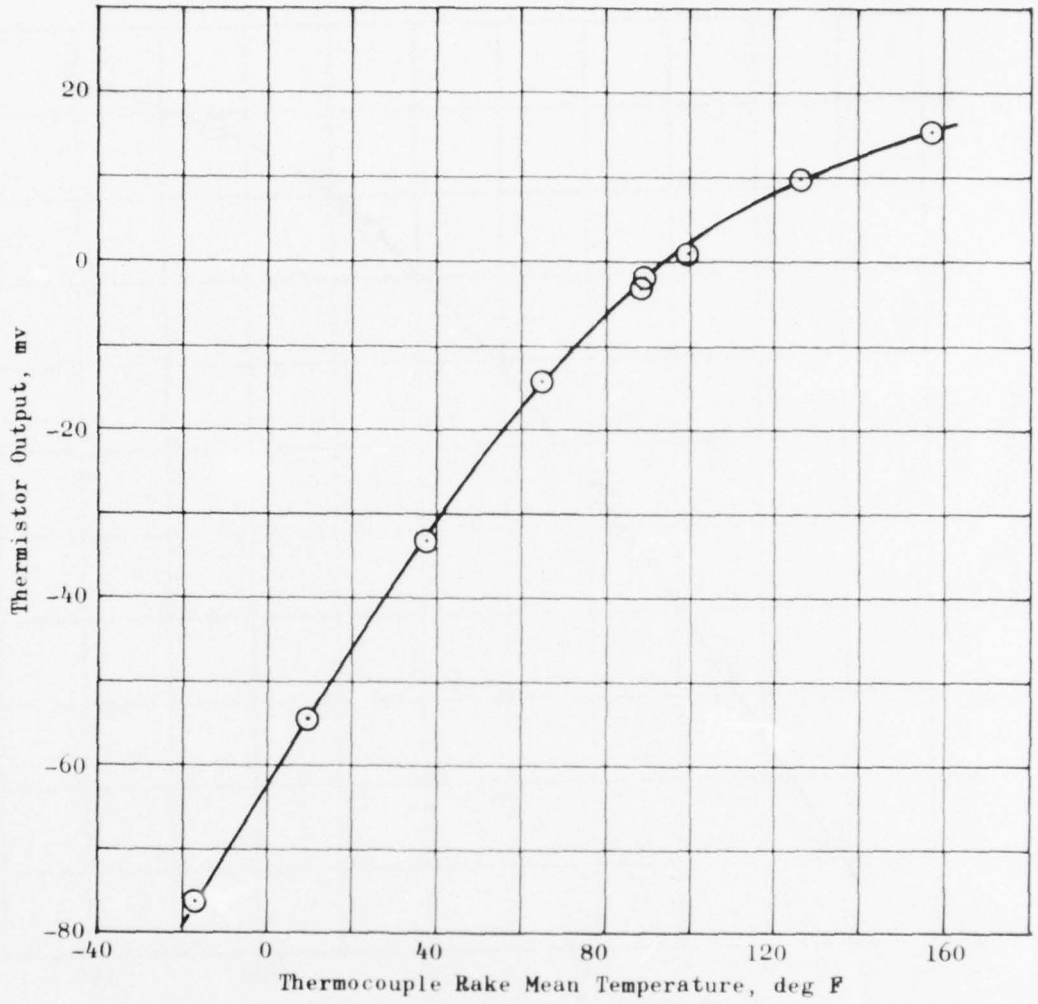

Figure 78. TH7-63 Response during Motor Checkout

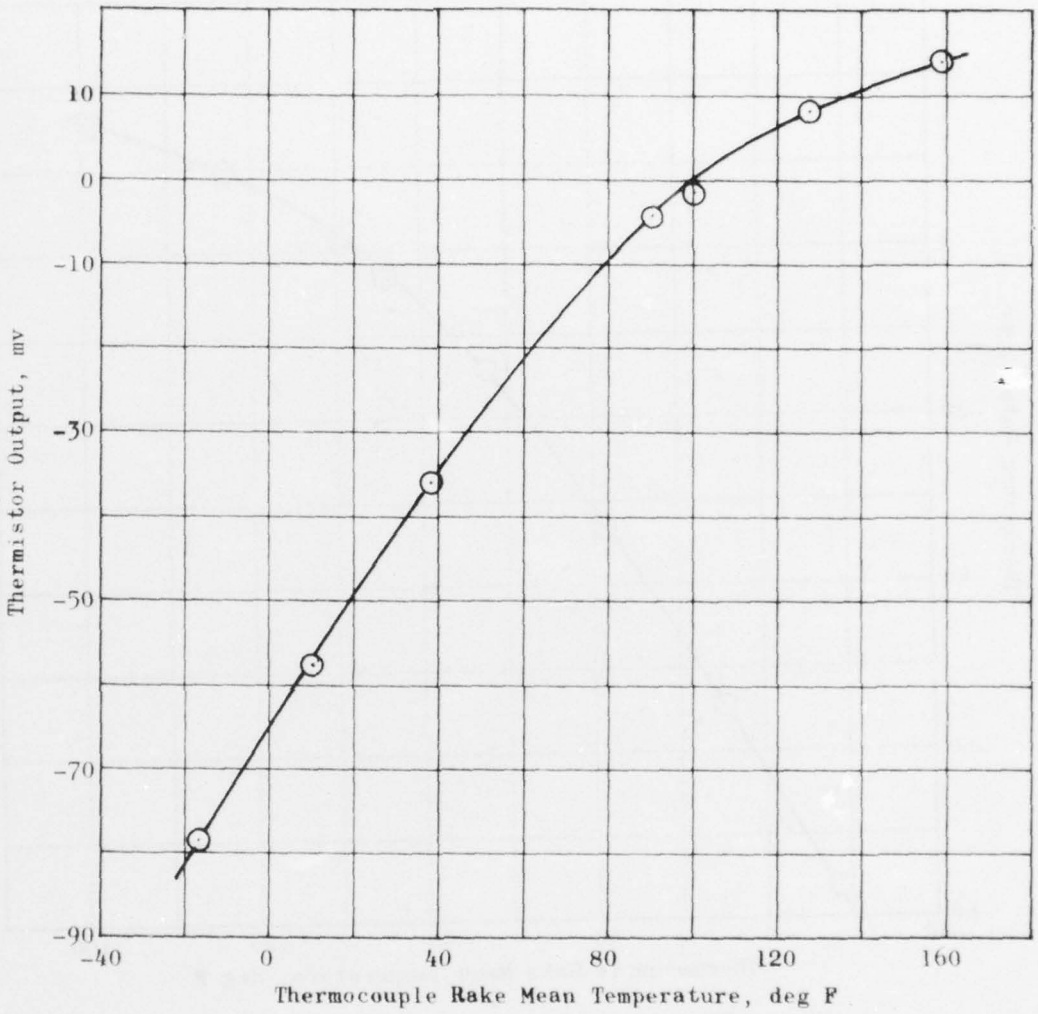

Figure 79. TH7-135 Response during Motor Checkout

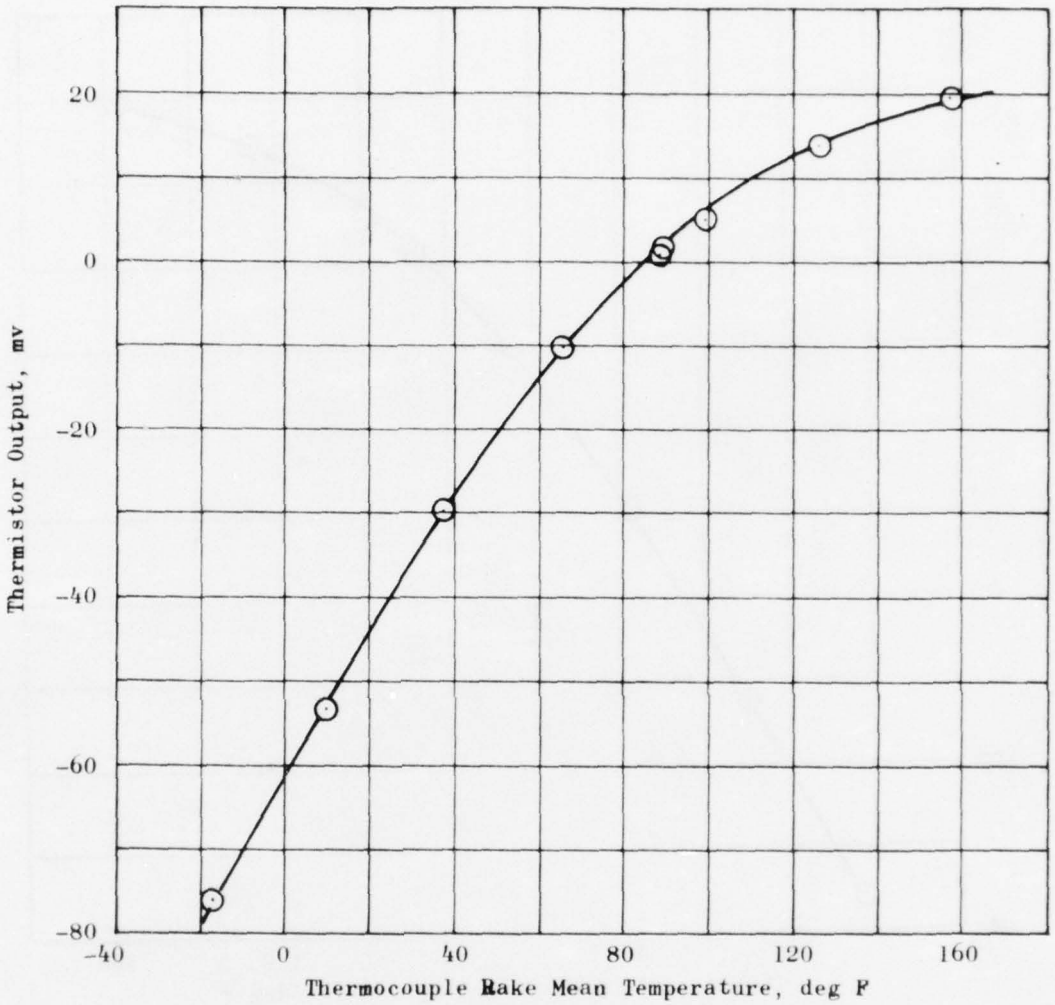

Figure 80. TH7-137 Response during Motor Checkout

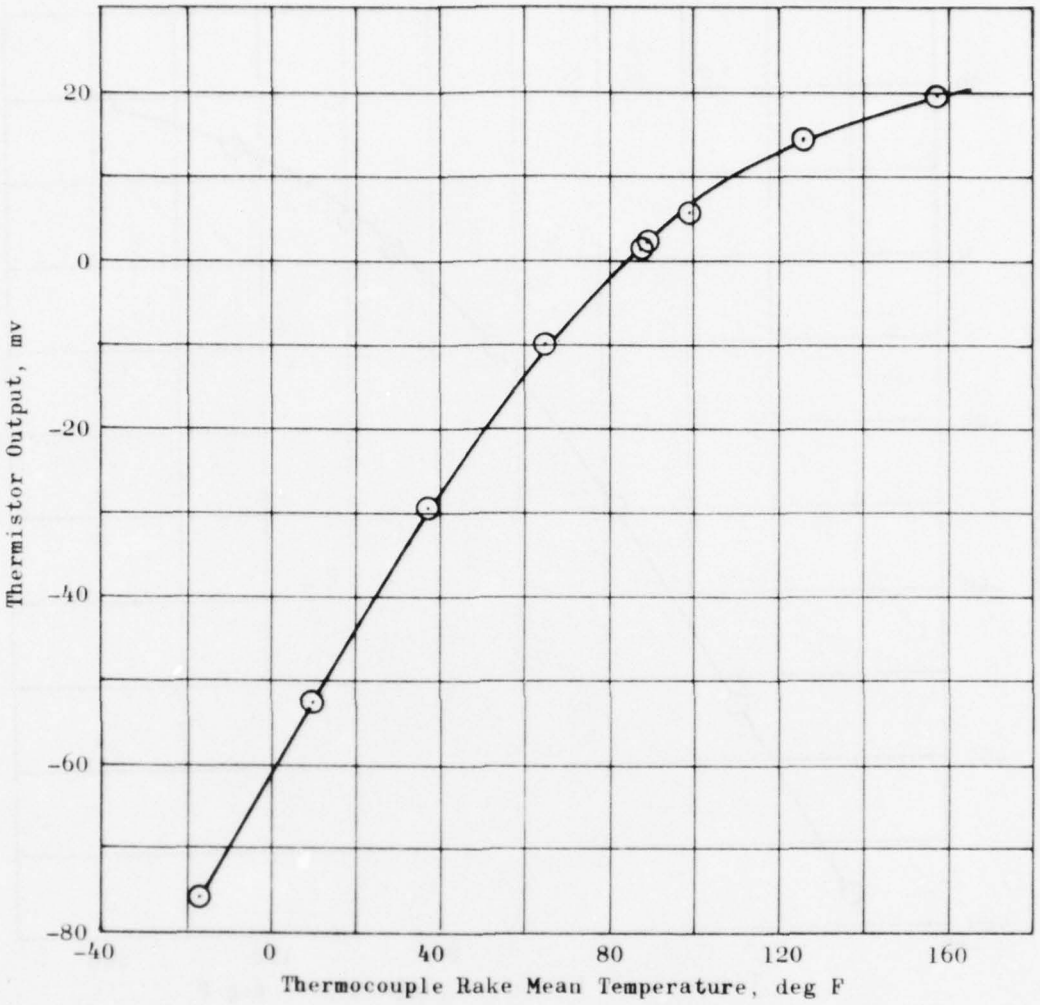

Figure 81. TH7-140 Response during Motor Checkout

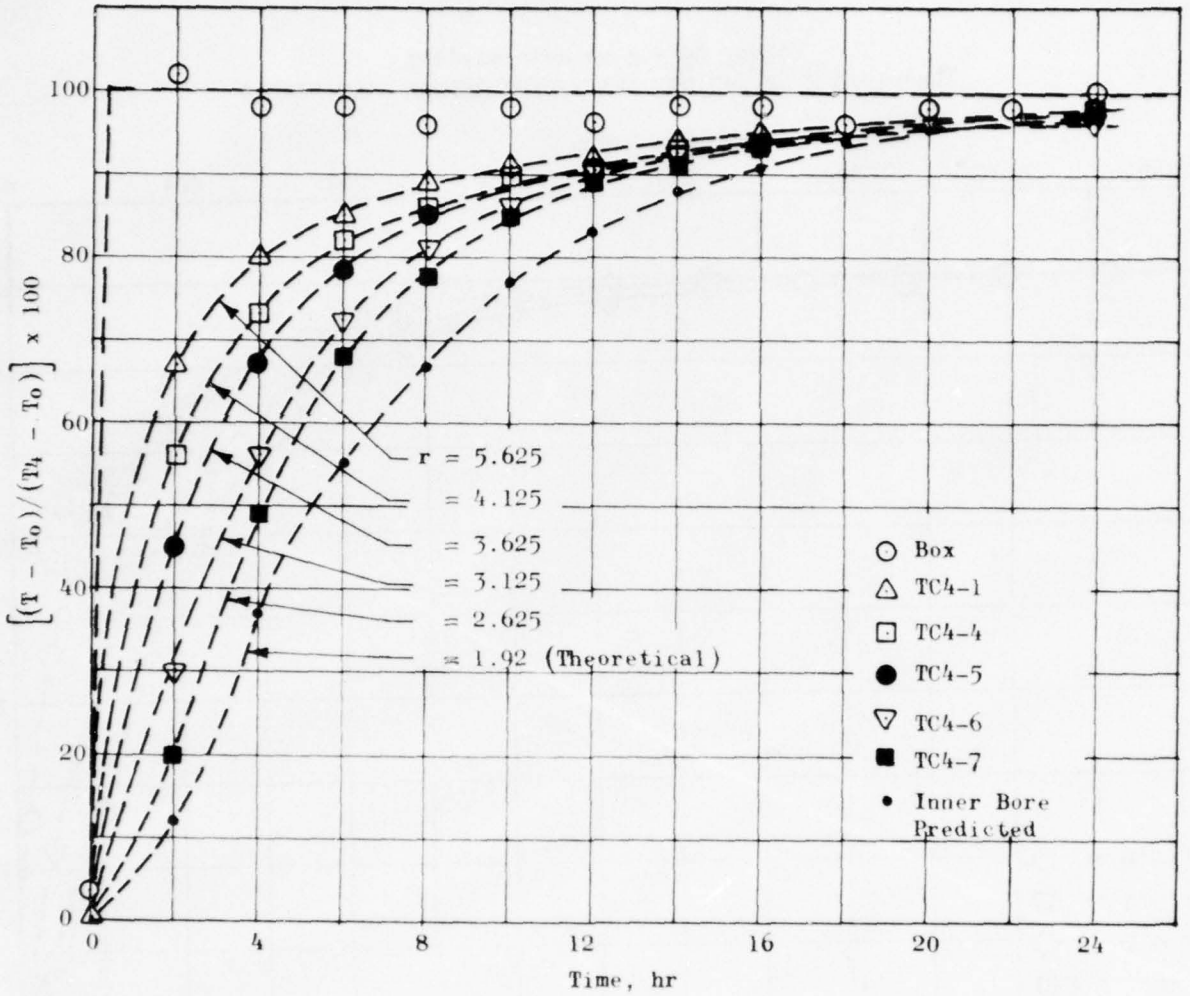

Figure 82. Temperature Conditioning Behavior of SRBDM Motors

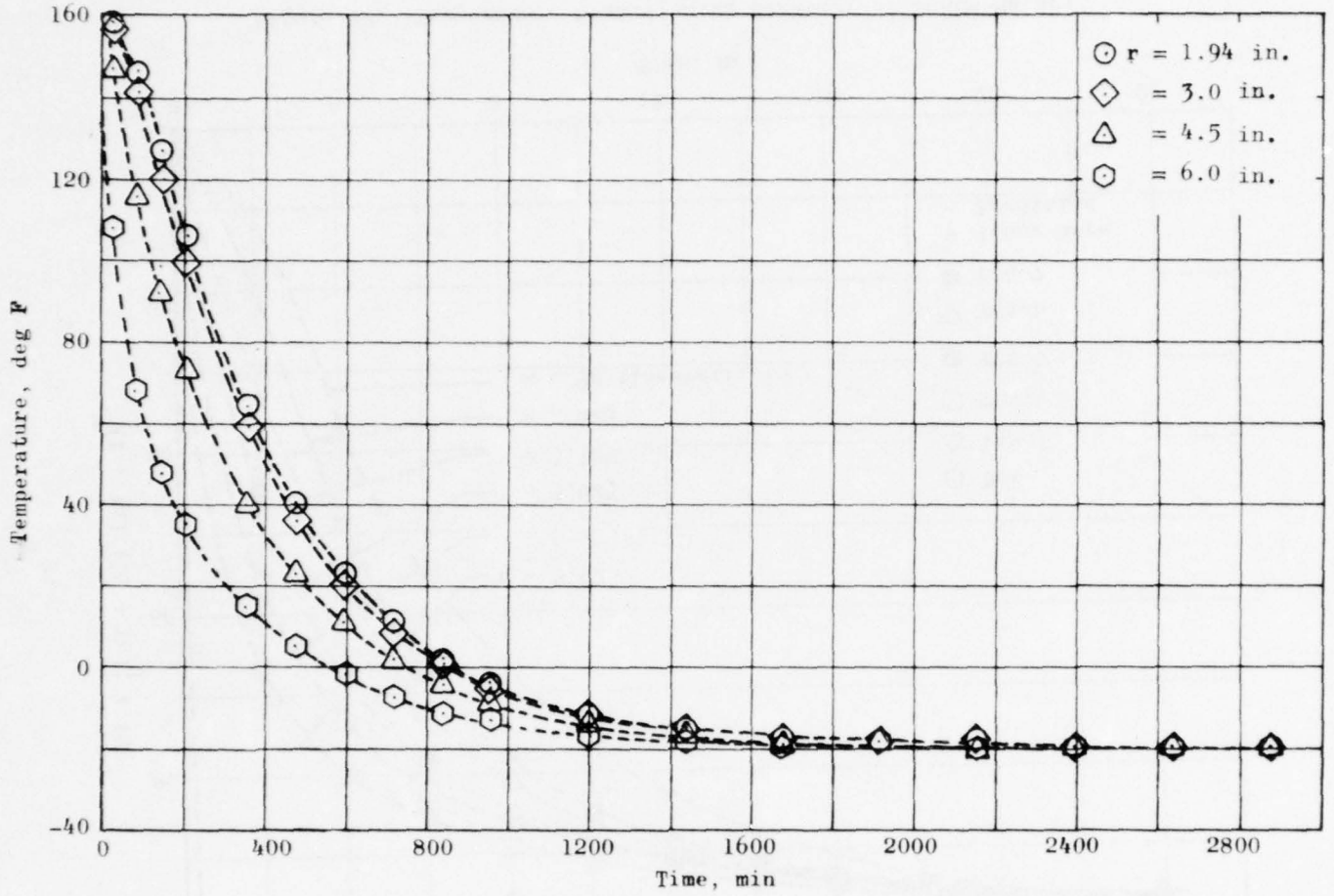

Figure 83. THVINC Result for 160 to -20 F Cooldown, Temperatures at Z = 33 Inches

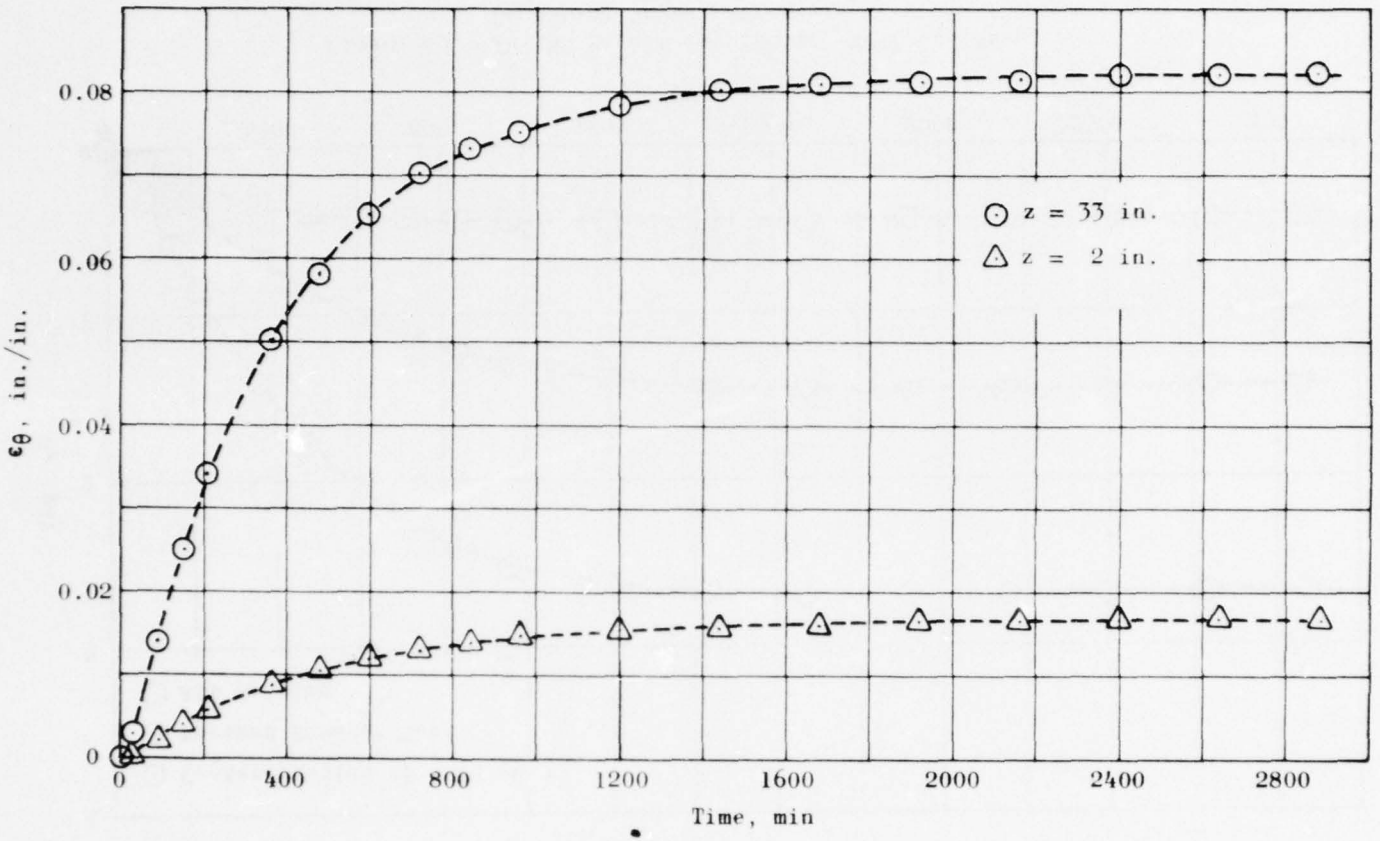

Figure 84. THVINC Result for 160 to -20 F Cooldown, Inner-Bore Hoop Strains

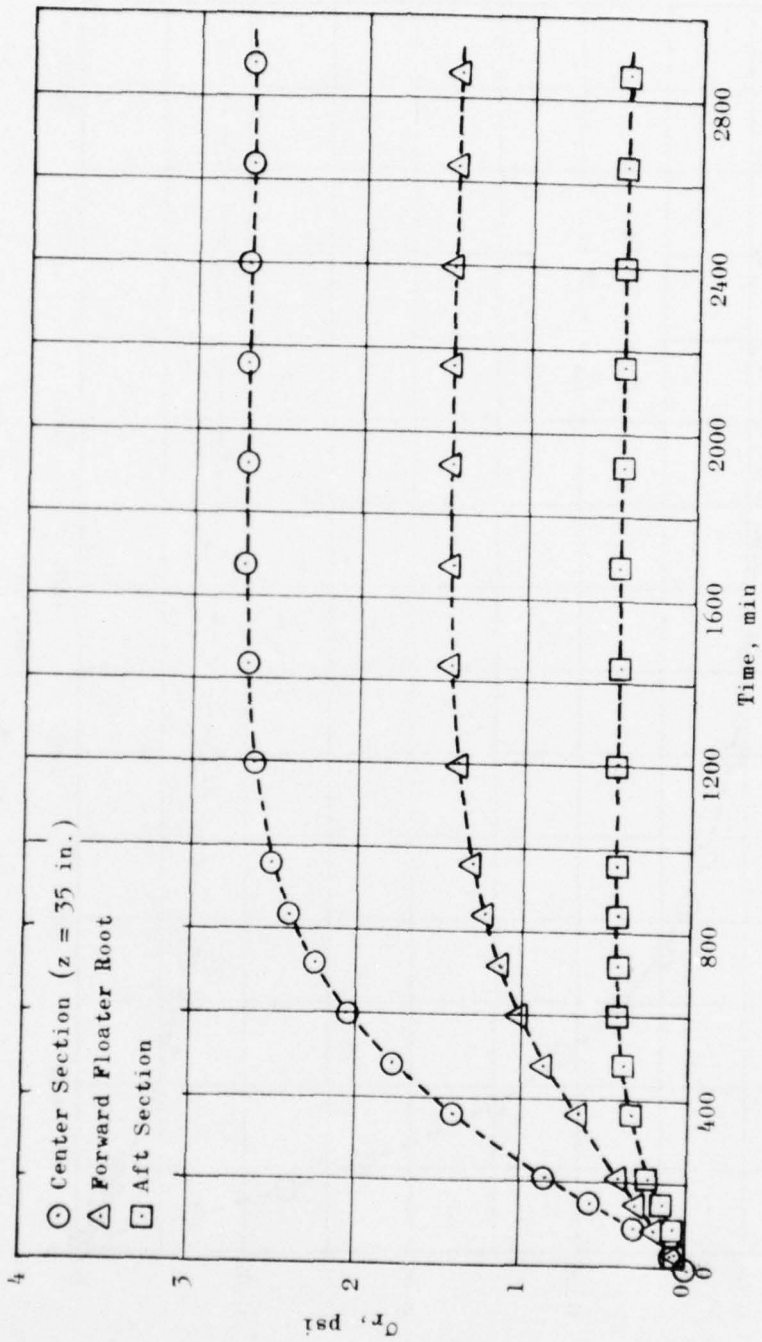

Figure 85. THVINC Result for 160 to -20 F Cooldown, Bond-Line Normal Stresses

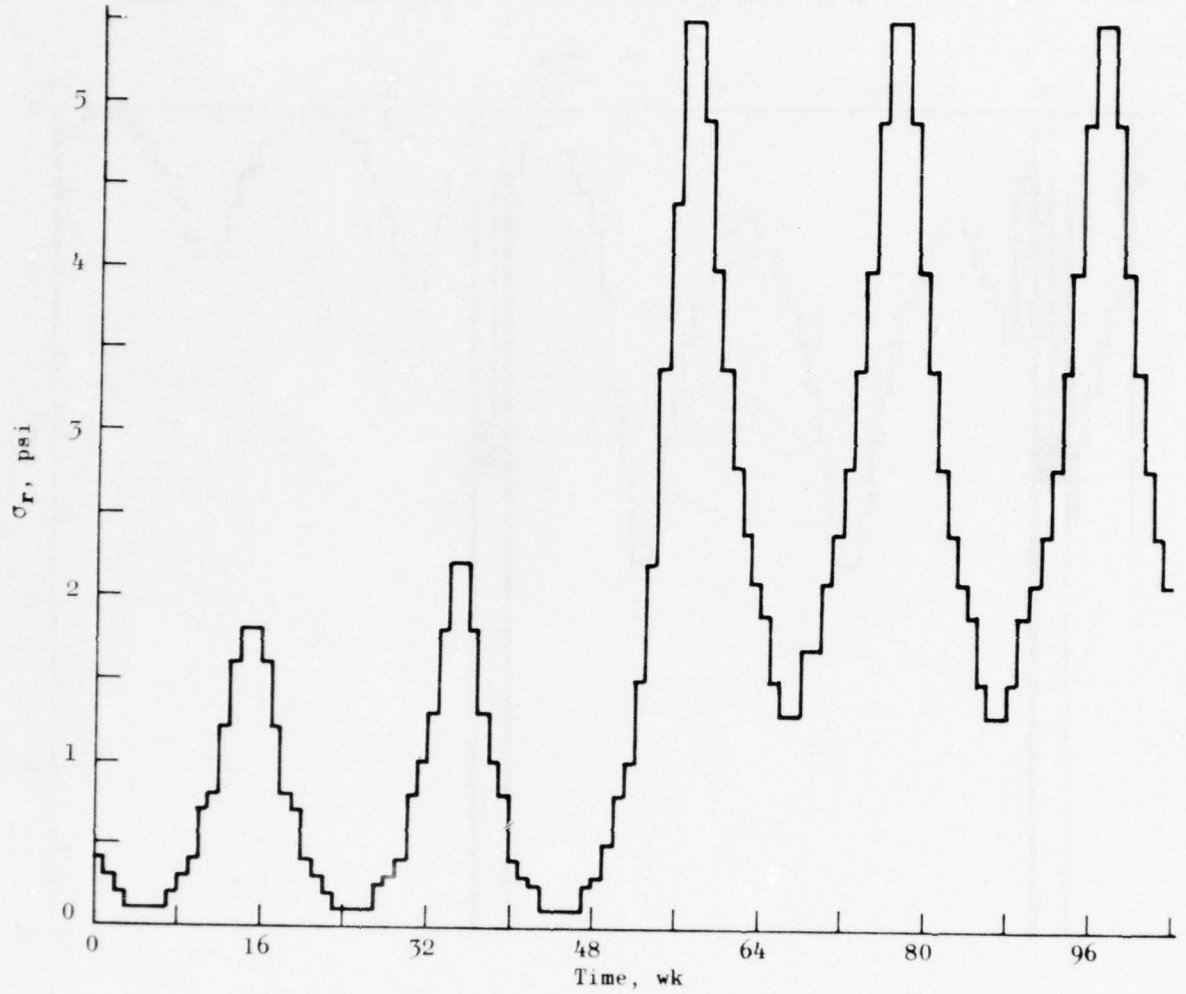

Figure 86. Predicted Motor 4 Center-Plane Thermal Bond Stress

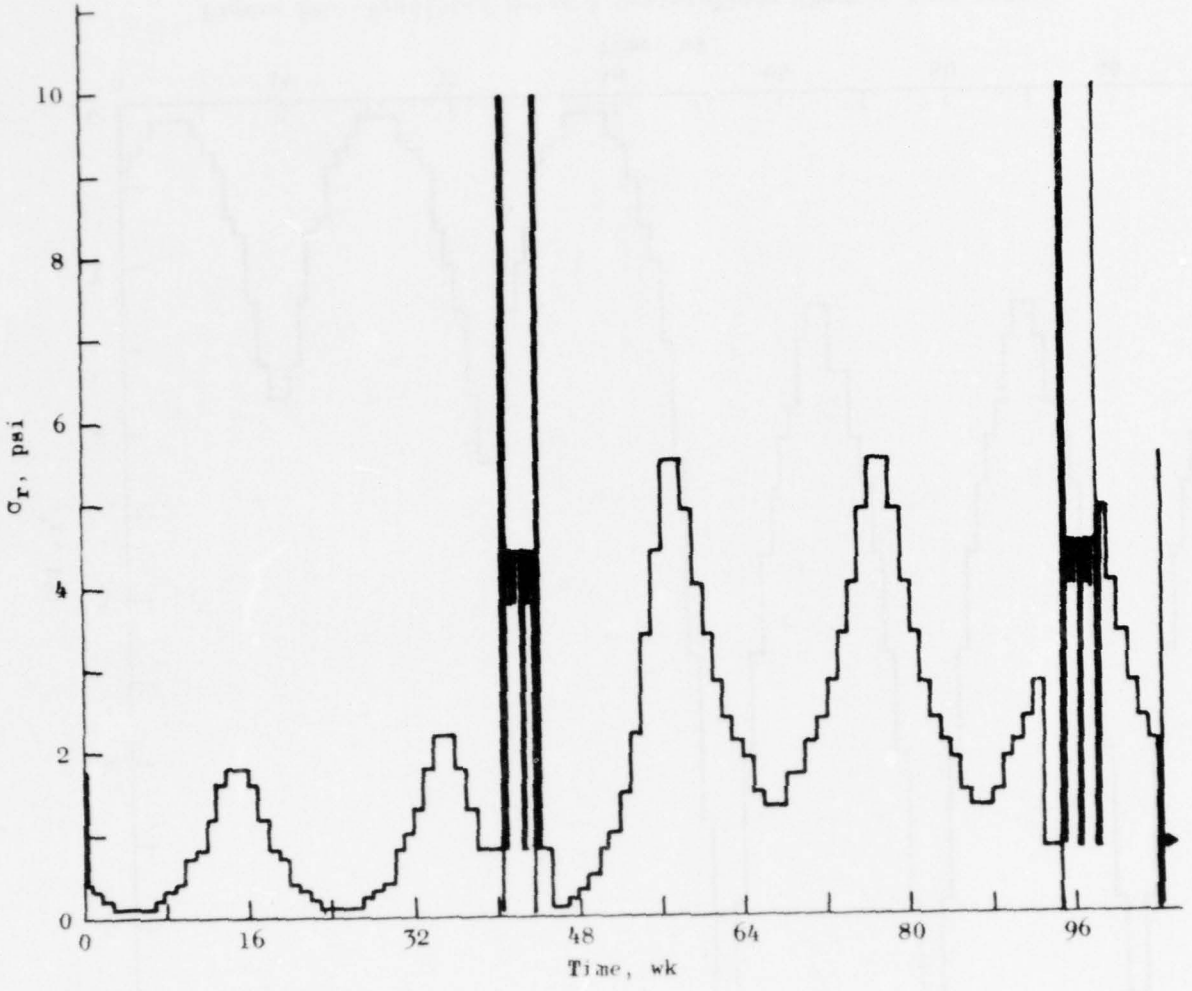

Figure 87. Predicted Motor 7 Center-Plane Thermal Bond Stress

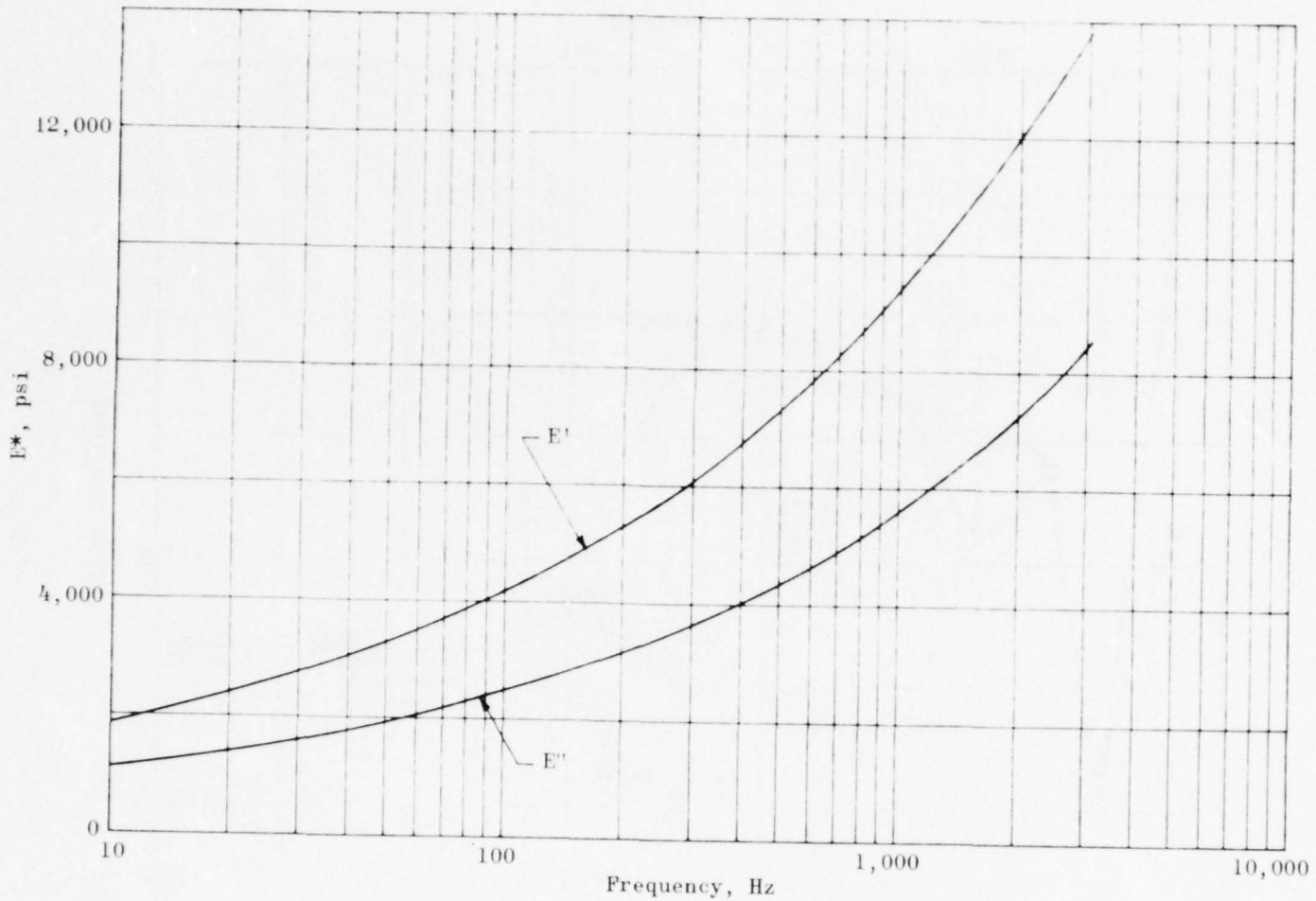

Figure 88. Dynamic Modulus of Propellant TP-H8214

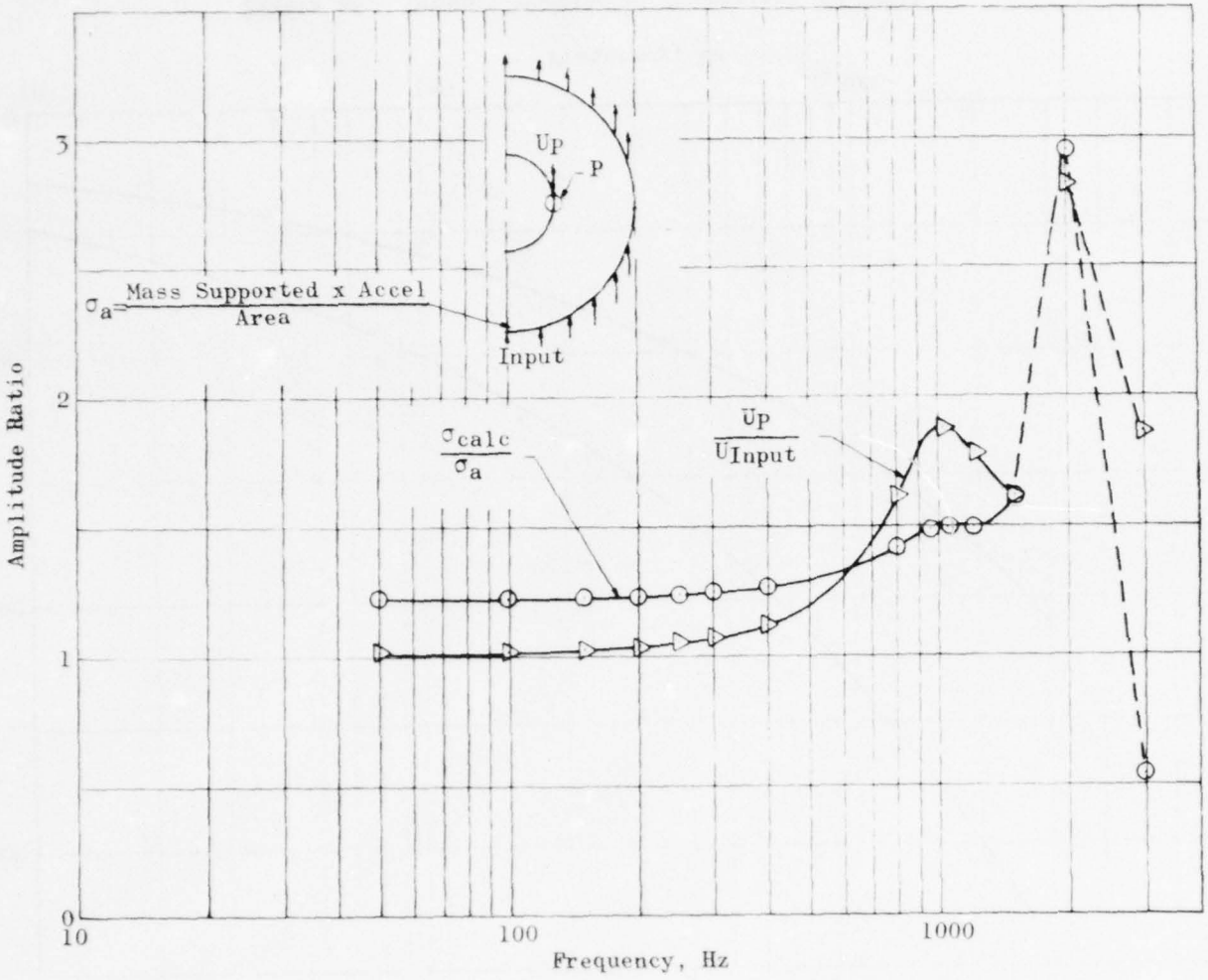

Figure 89. Calculated Stress and Displacement Amplitude Ratios

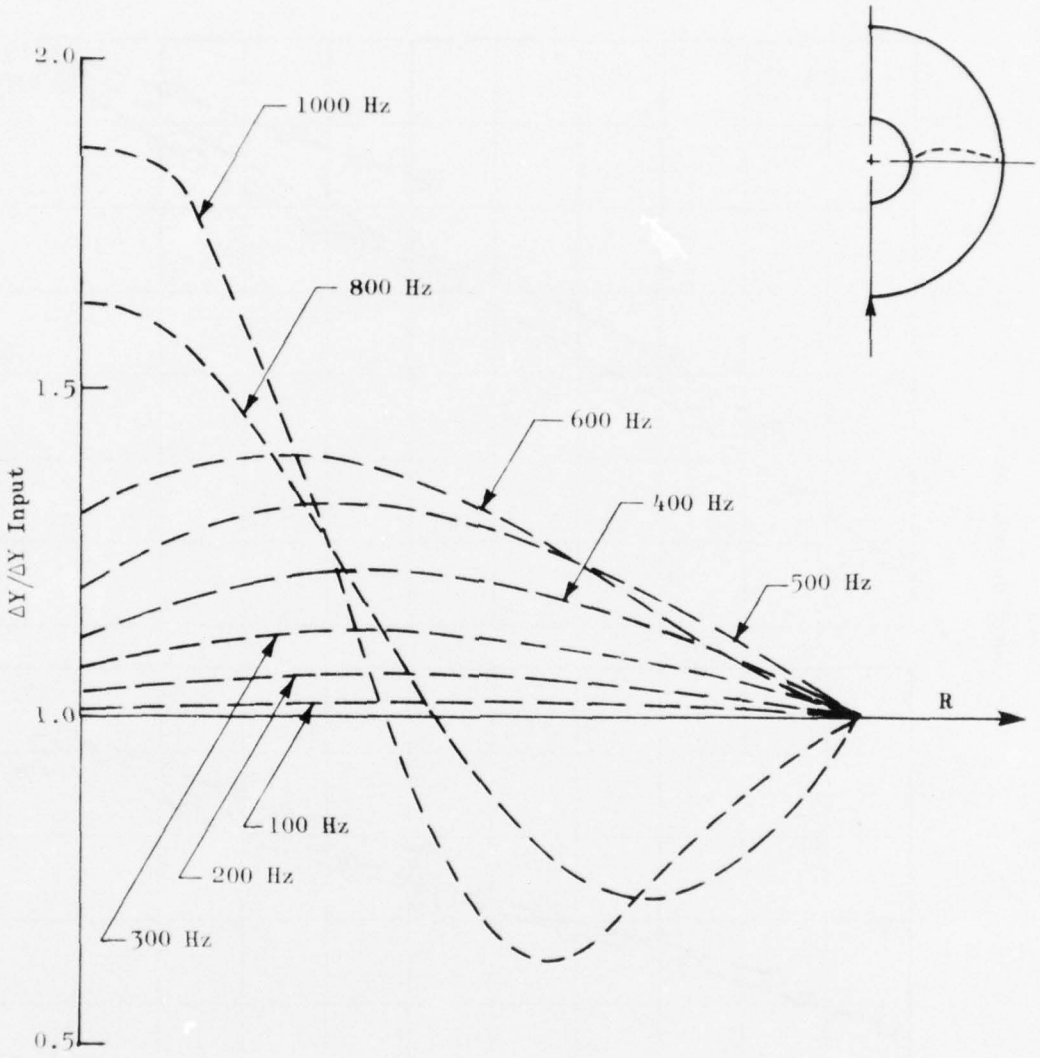

Figure 90. Displacement Configuration for Nodes at Y = 0

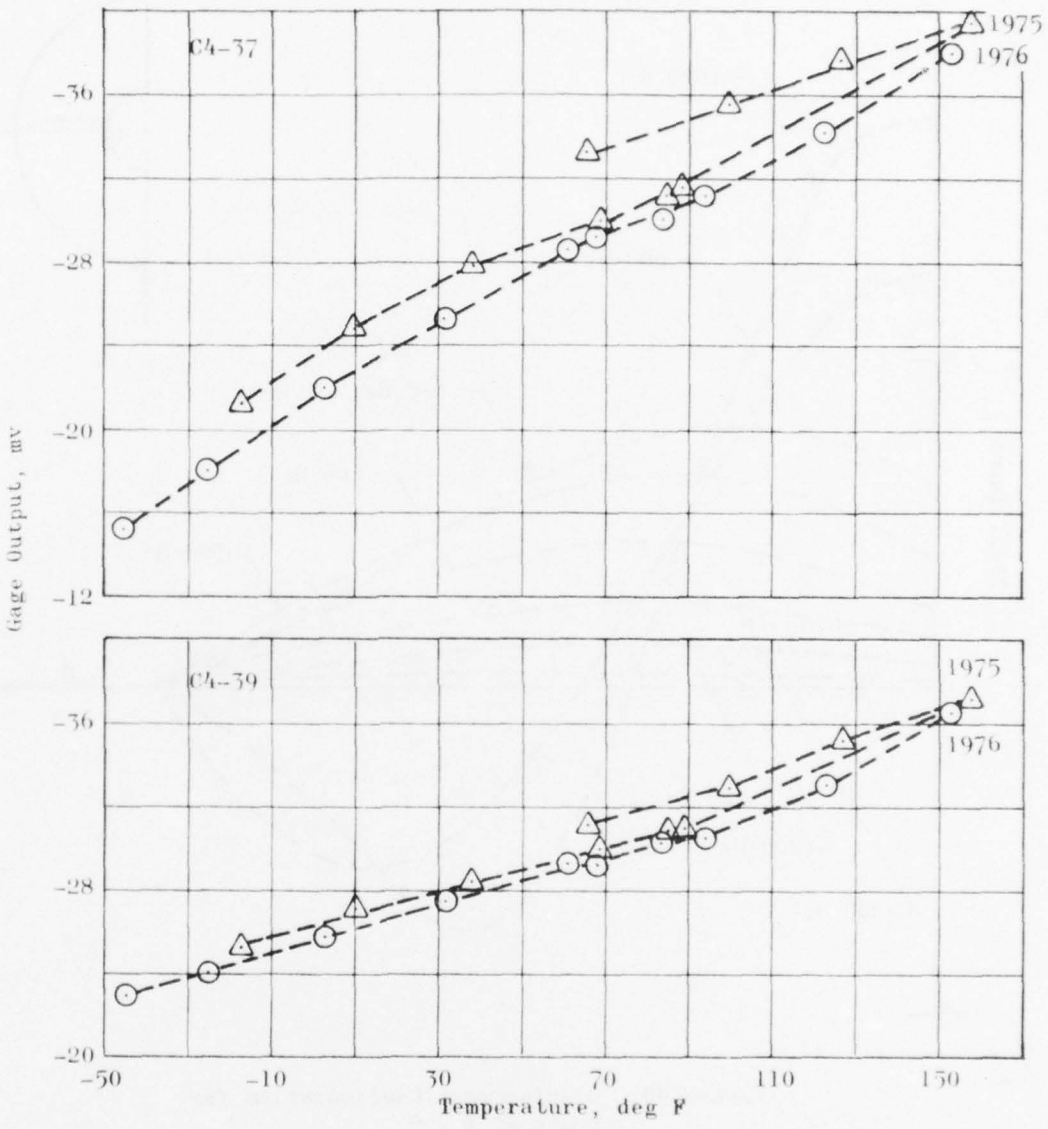

Figure 91. Clip Gage Response, Motor 4

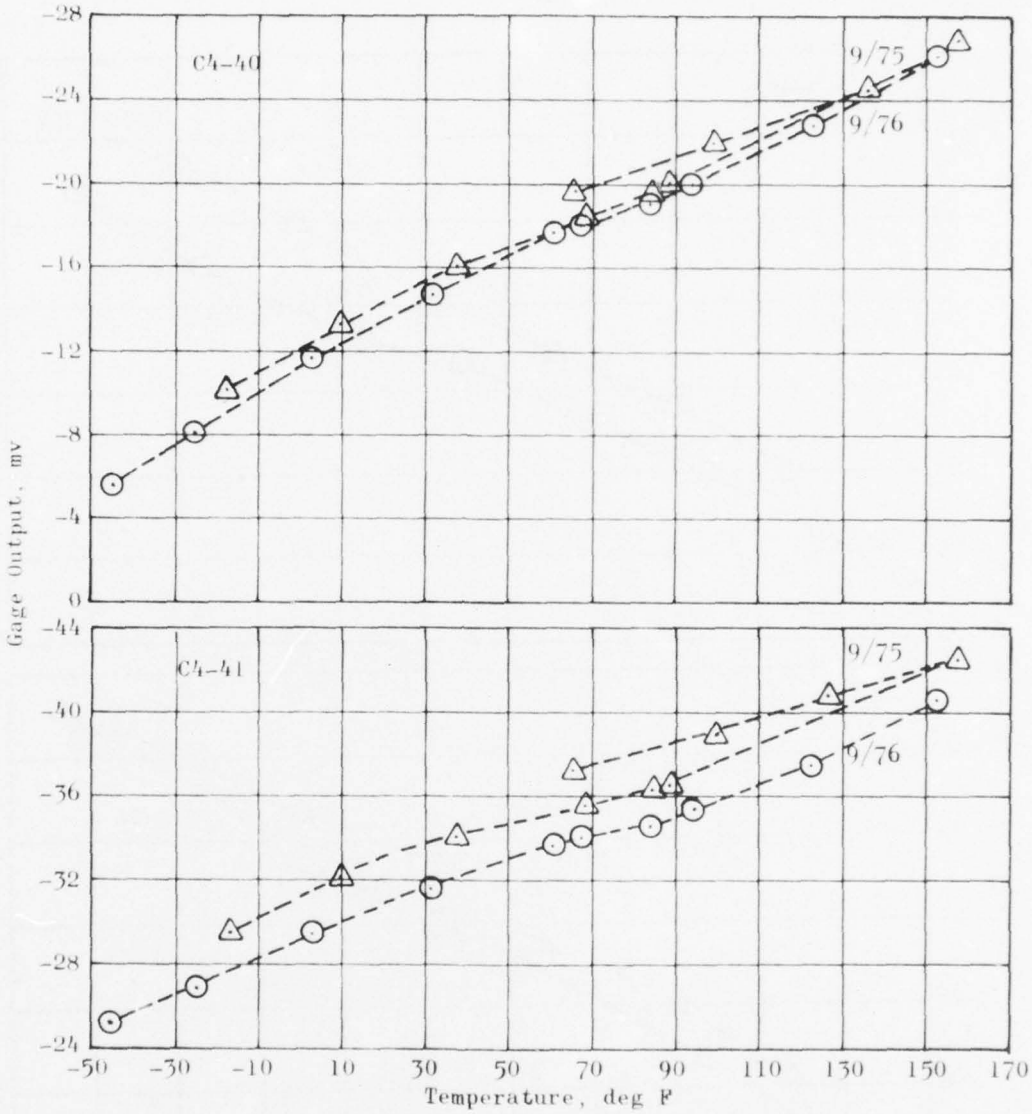

Figure 91. Continued

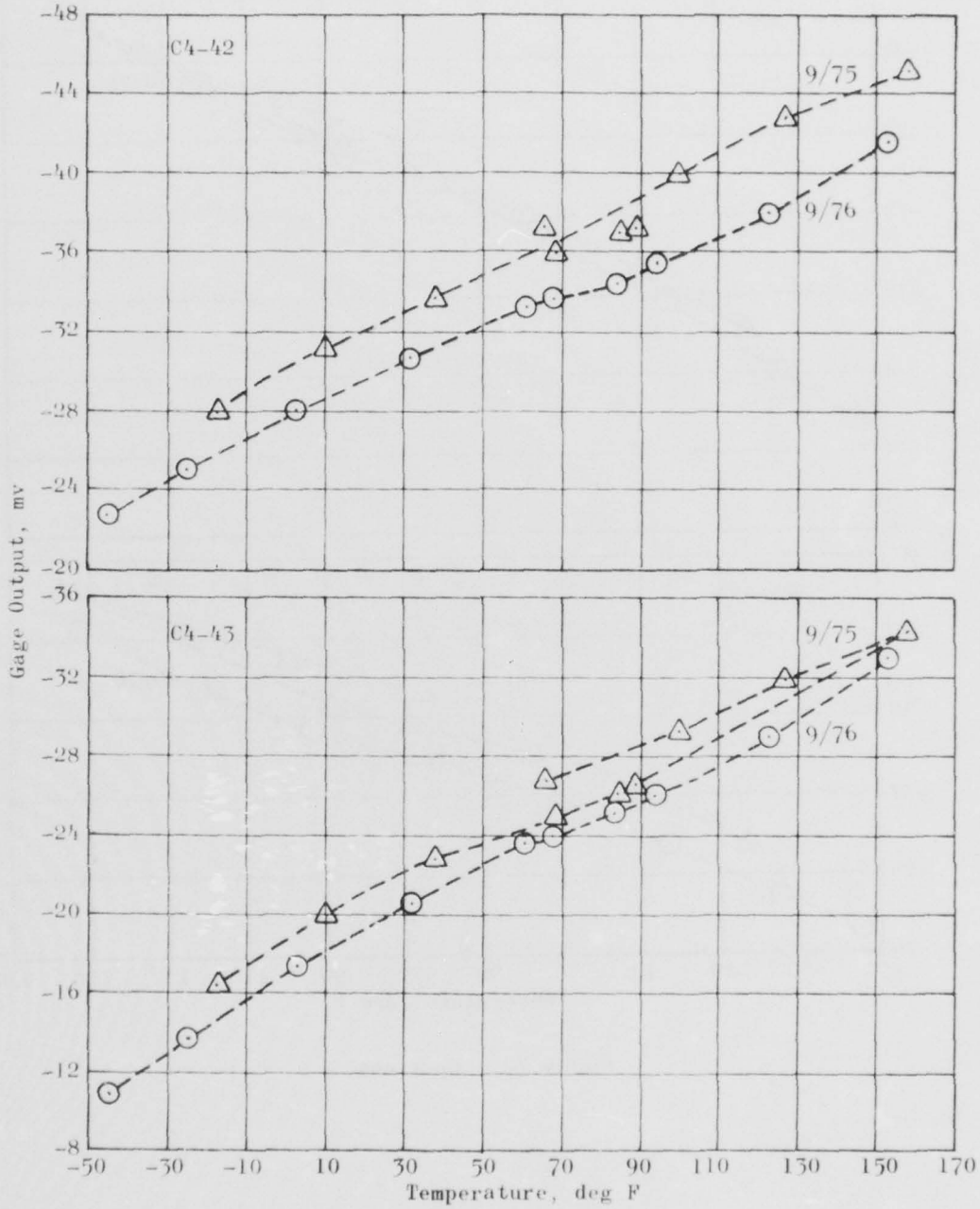

Figure 91. Continued

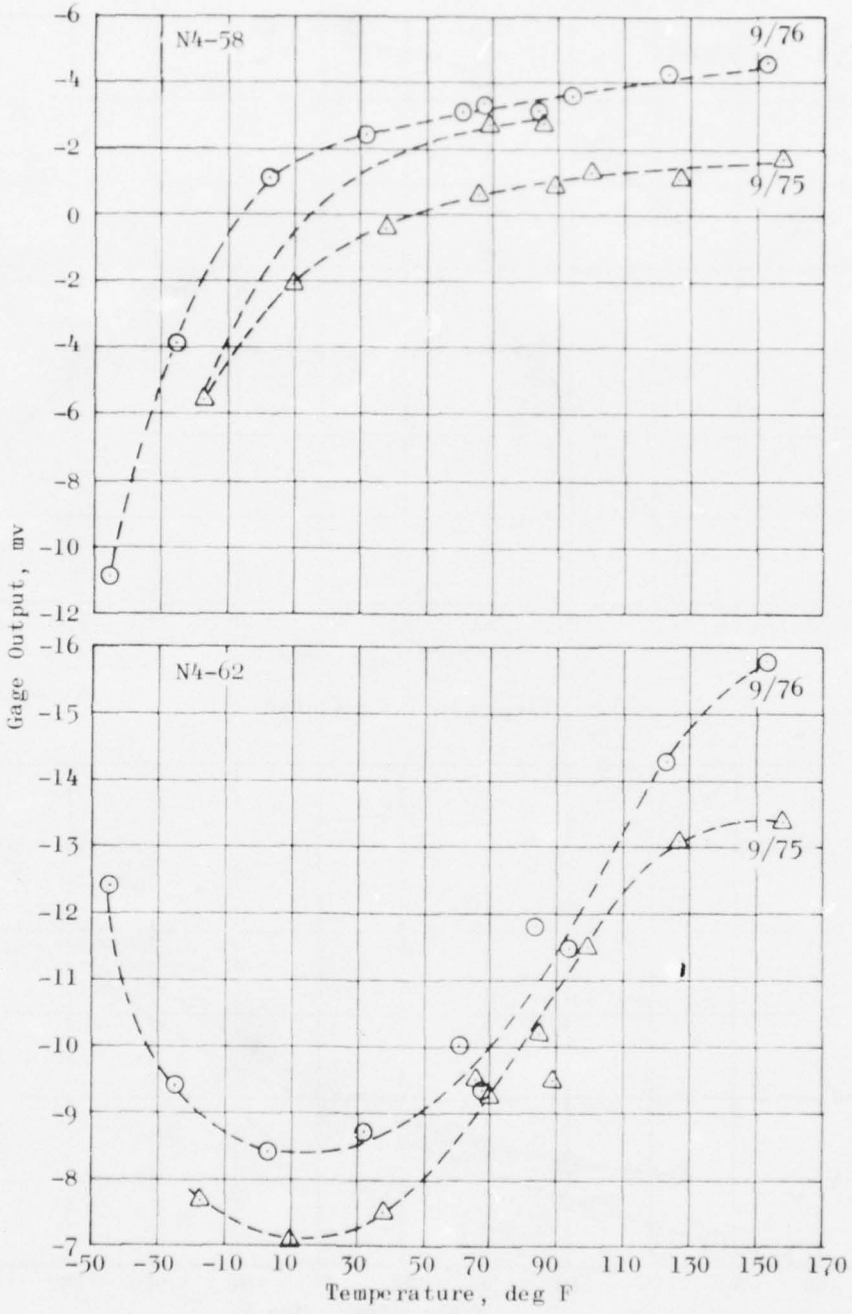

Figure 92. Normal Stress Gage Response, Motor 4

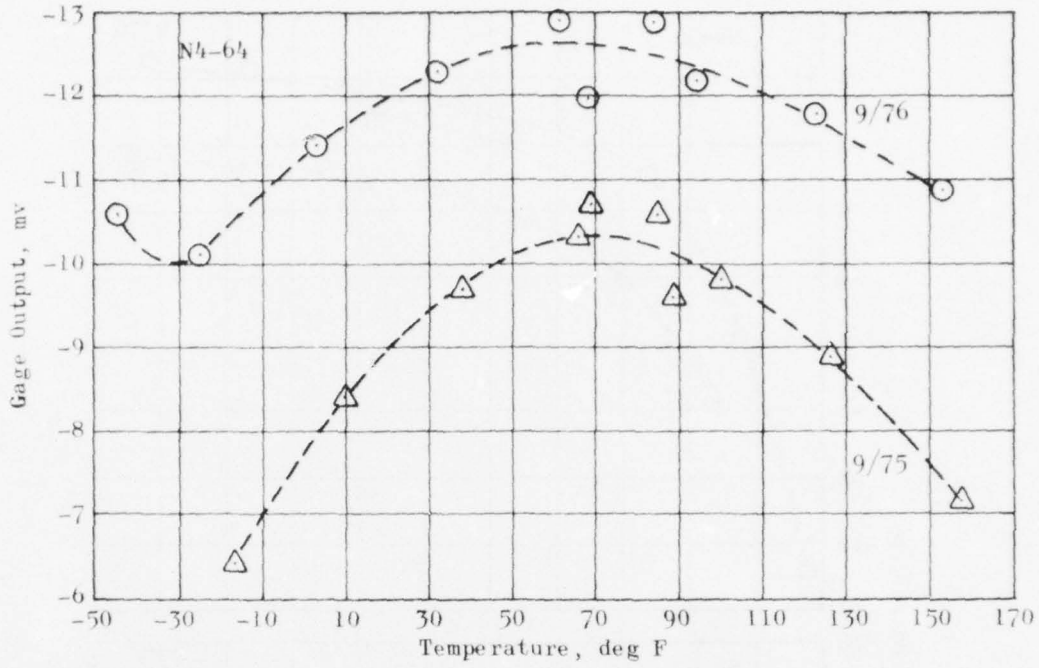

Figure 92. Continued

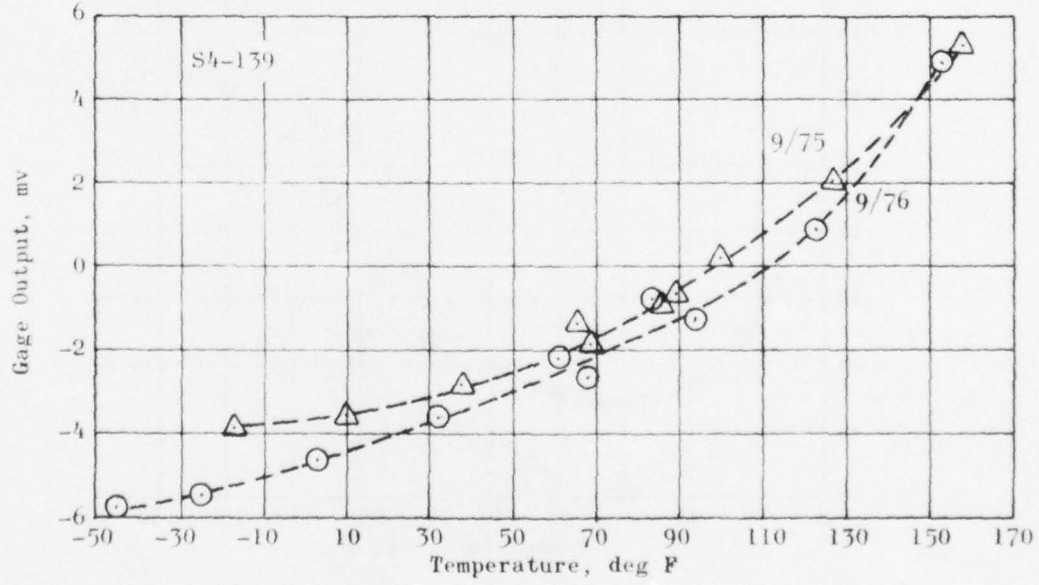

Figure 93. Shear Stress Gage Response, Motor 4

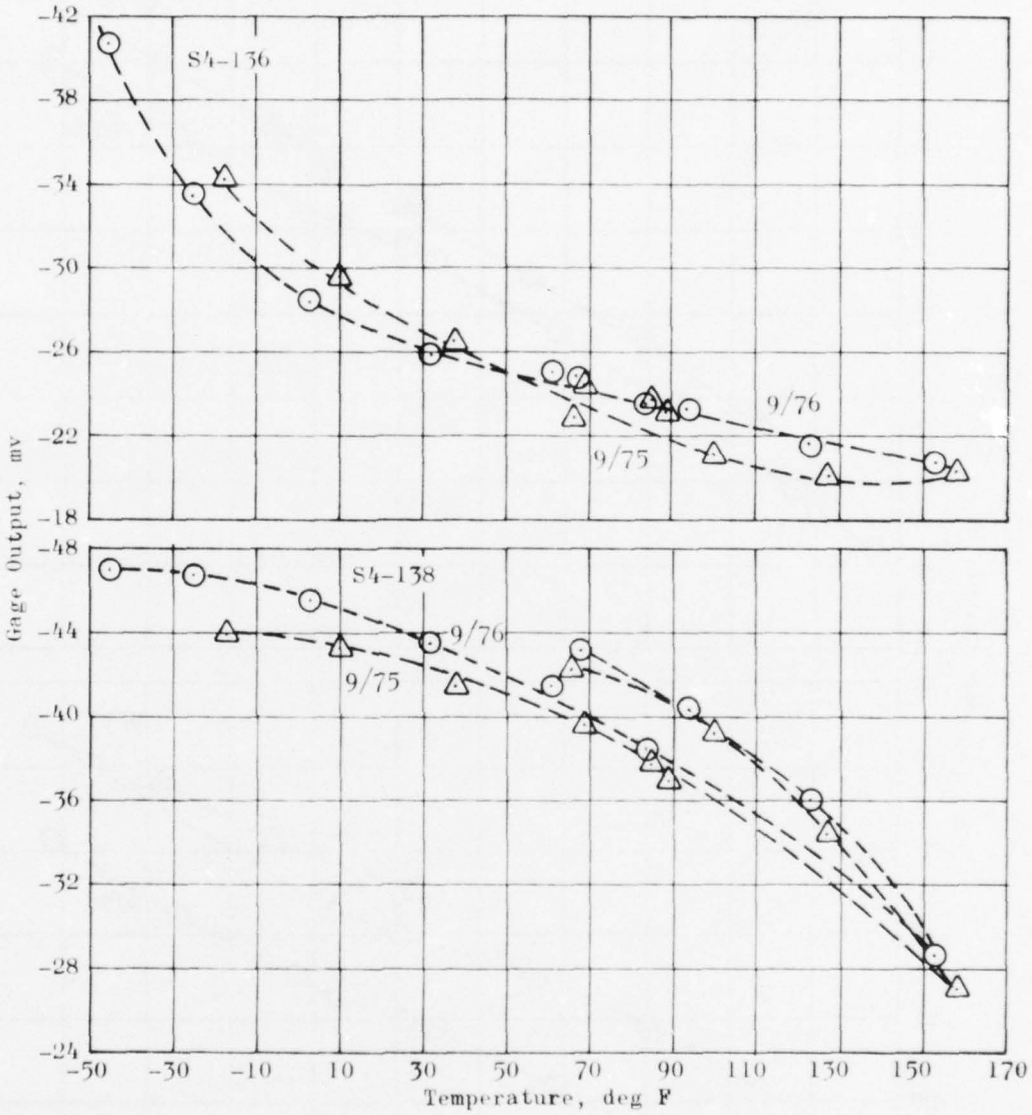

Figure 93. Continued

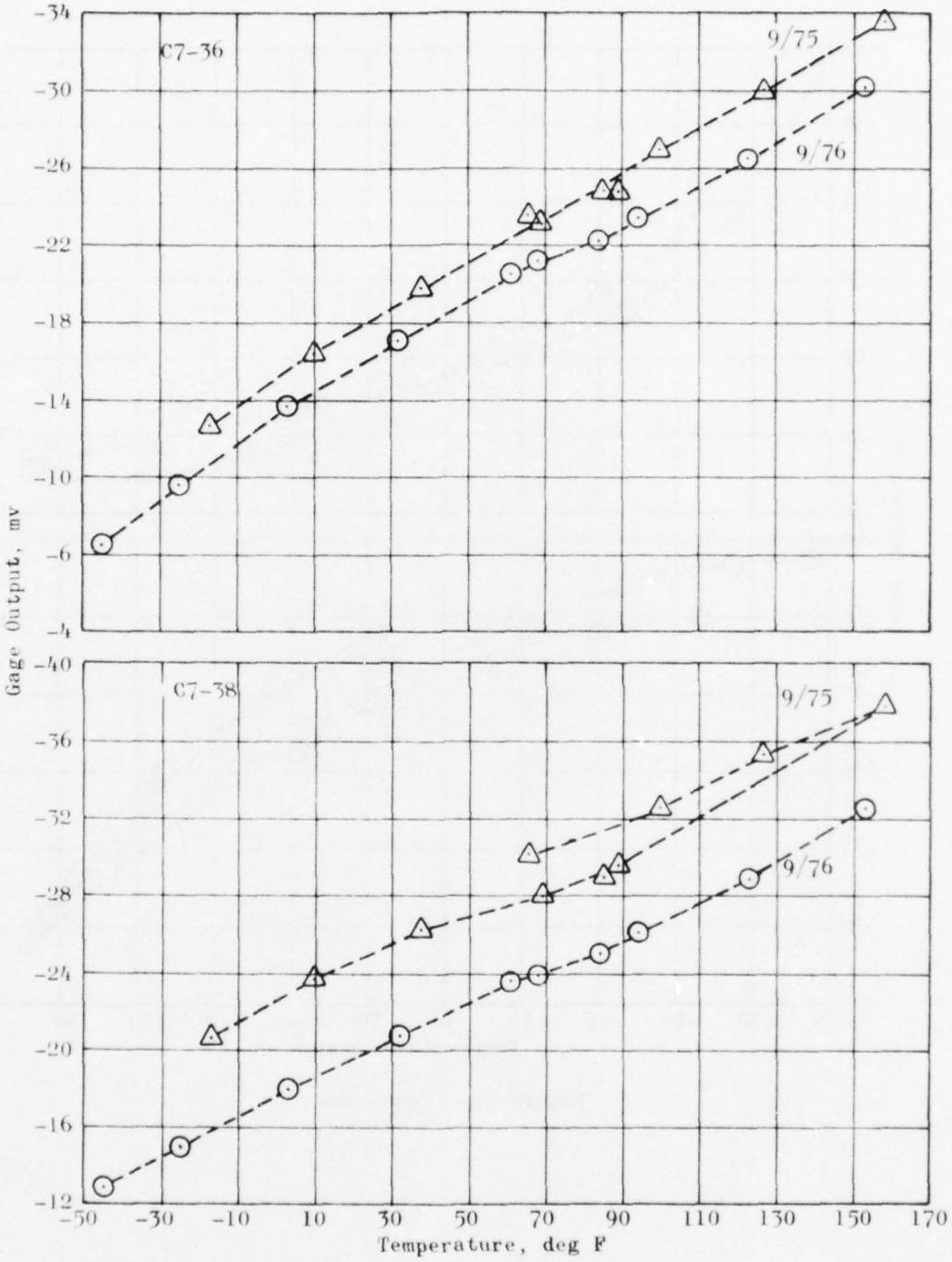

Figure 94. Clip Gage Response, Motor 7

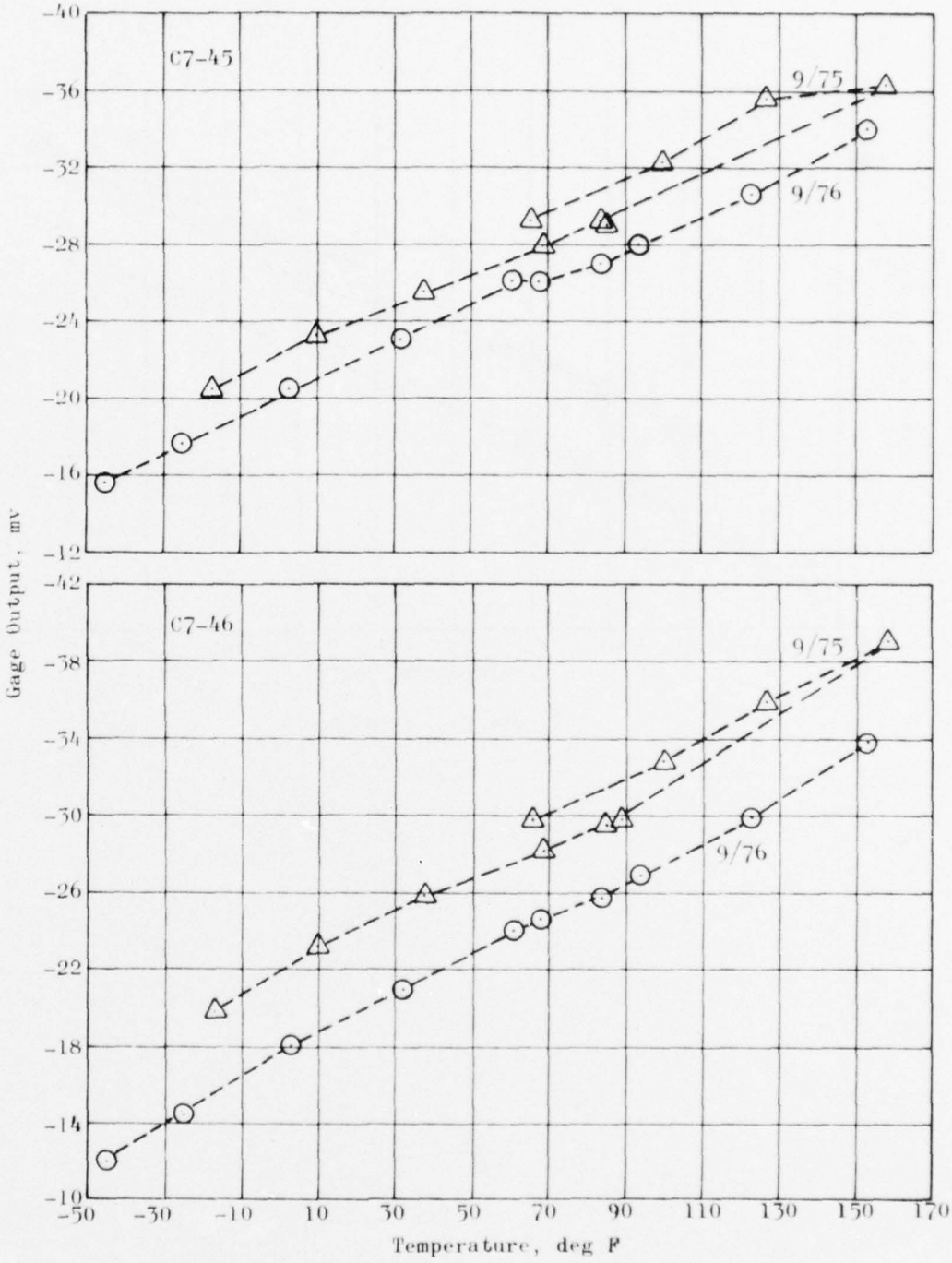

Figure 94. Continued

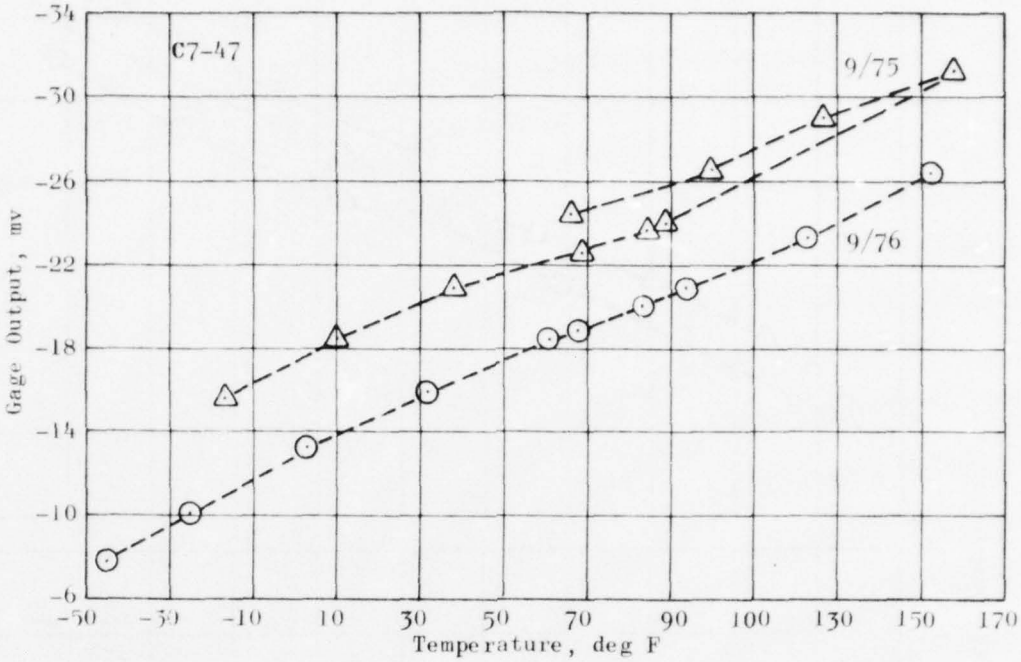

Figure 94. Continued

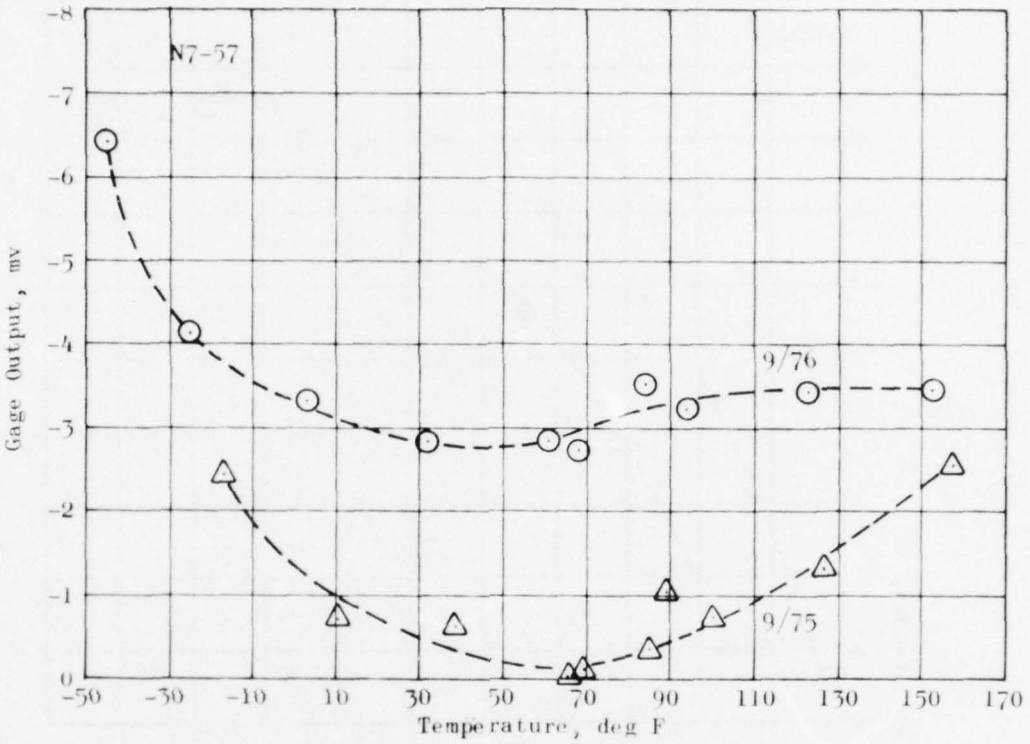

Figure 95. Normal Stress Gage Response, Motor 7

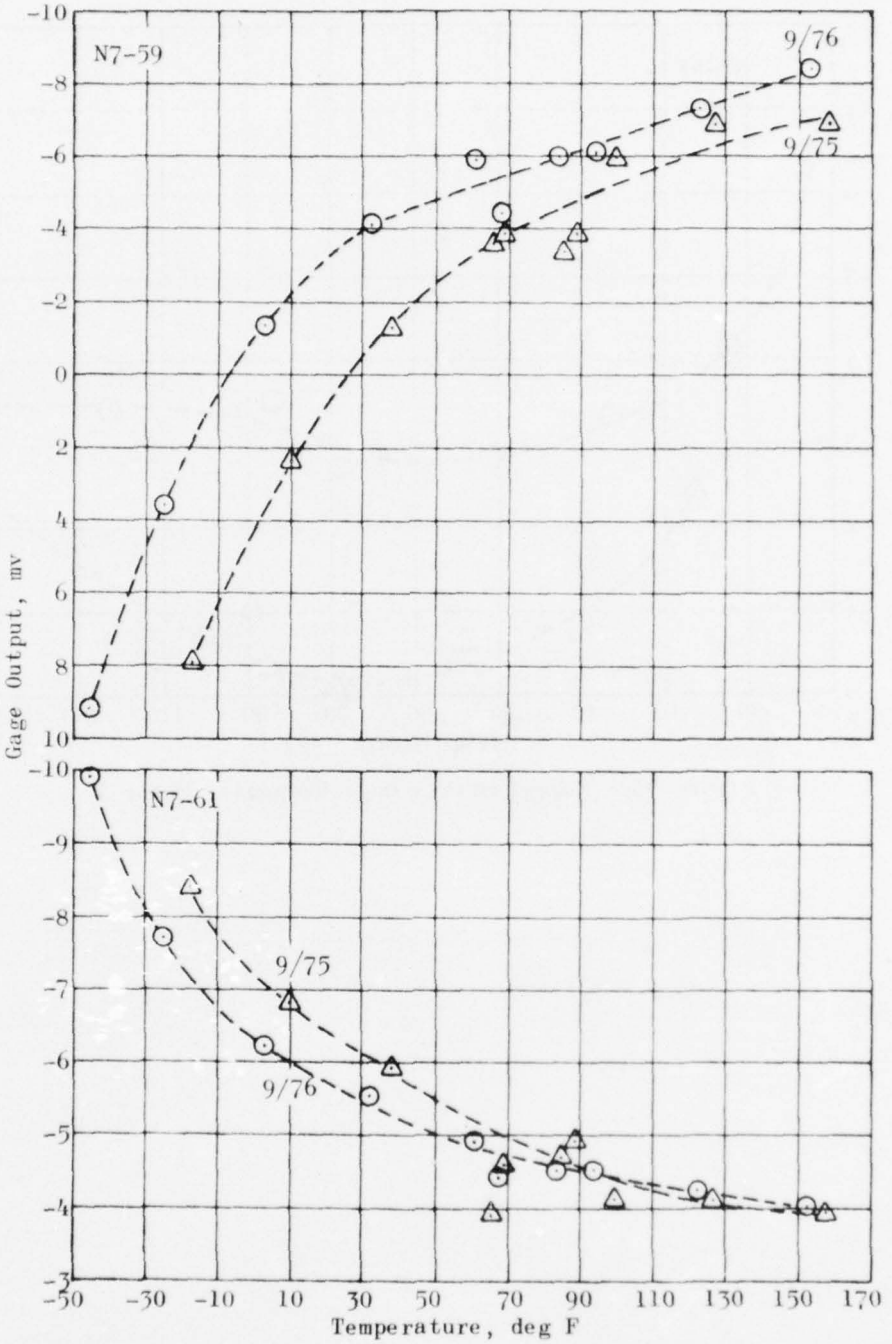

Figure 95. Continued

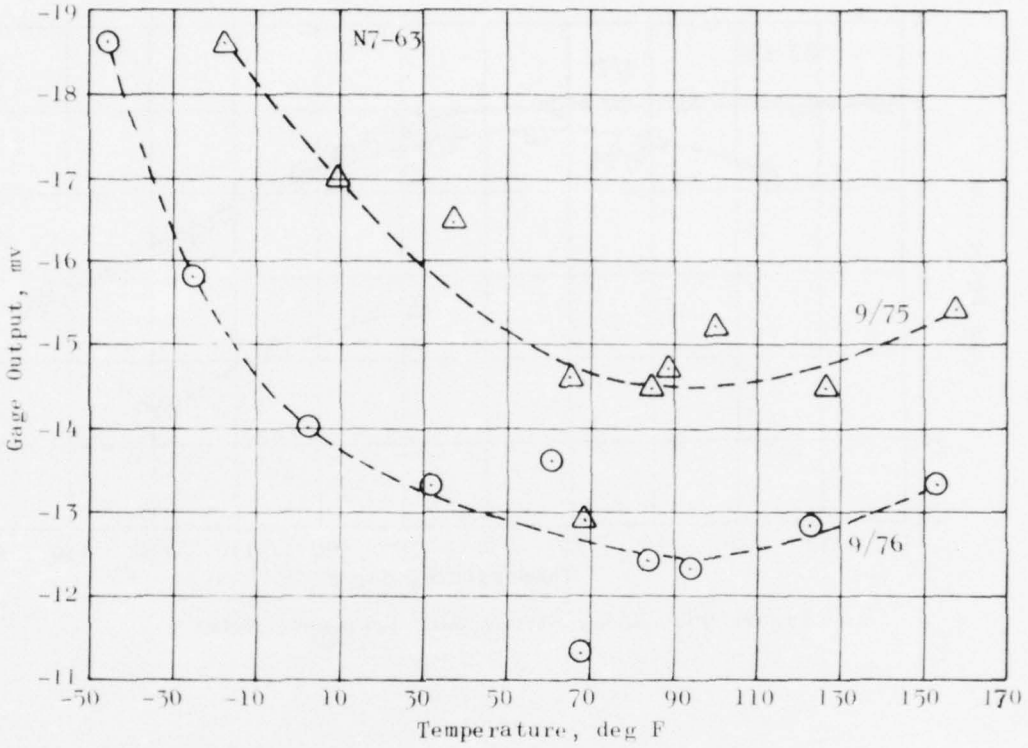

Figure 95. Continued

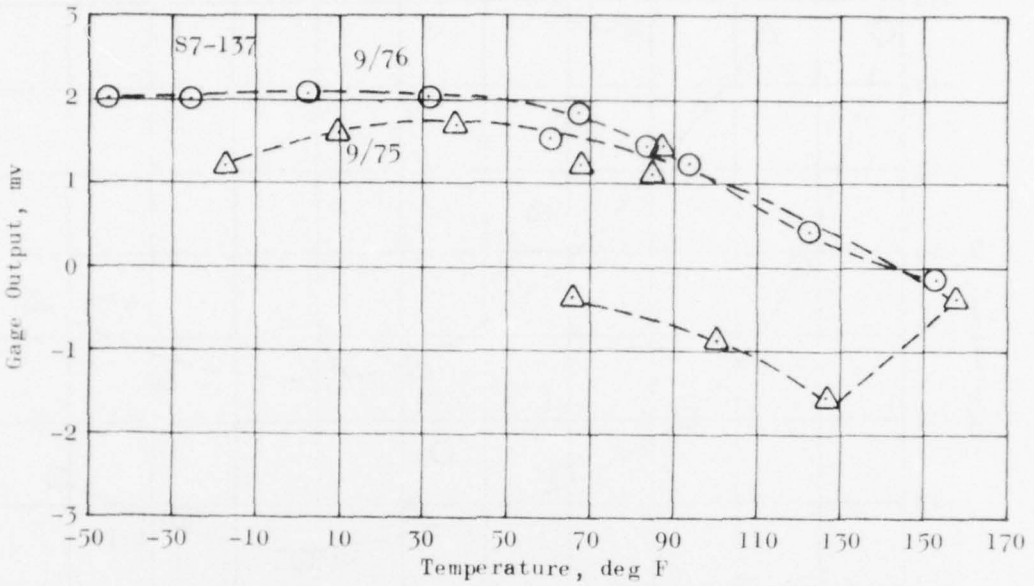

Figure 96. Shear Stress Gage Response, Motor 7

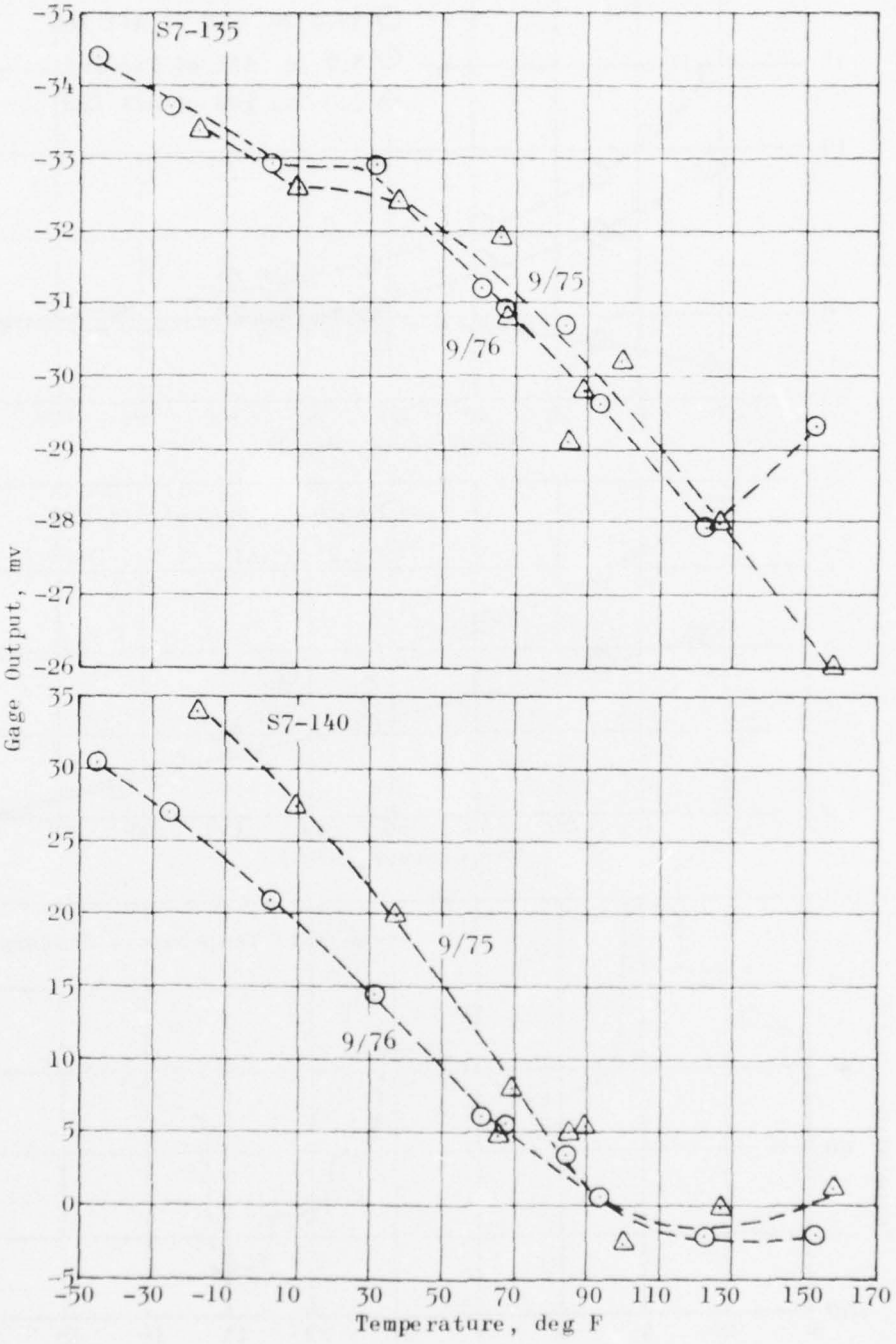

Figure 96. Continued

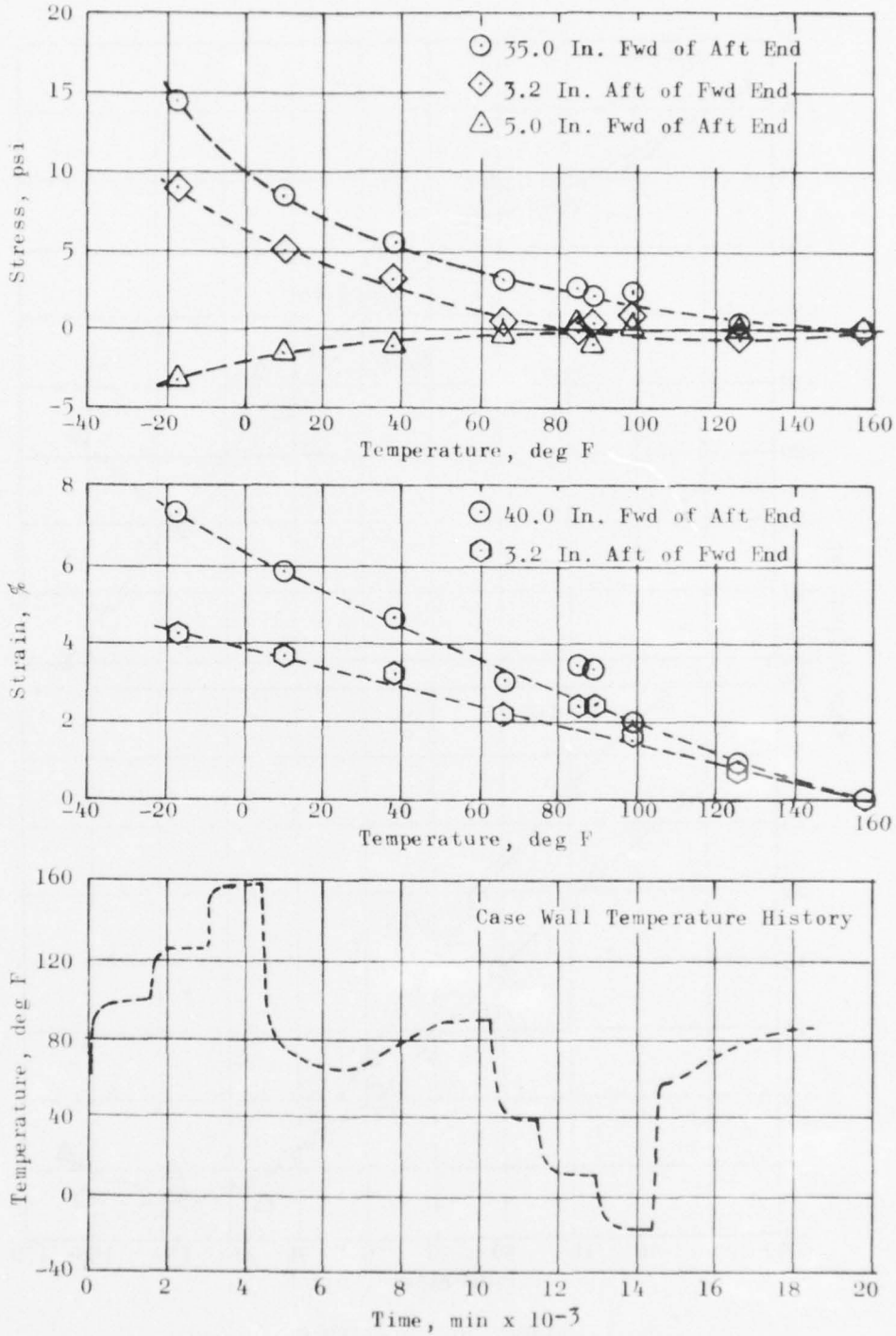

Figure 97. Summary of Pressure Calibration Thermal Cycle, Motors 4 and 7

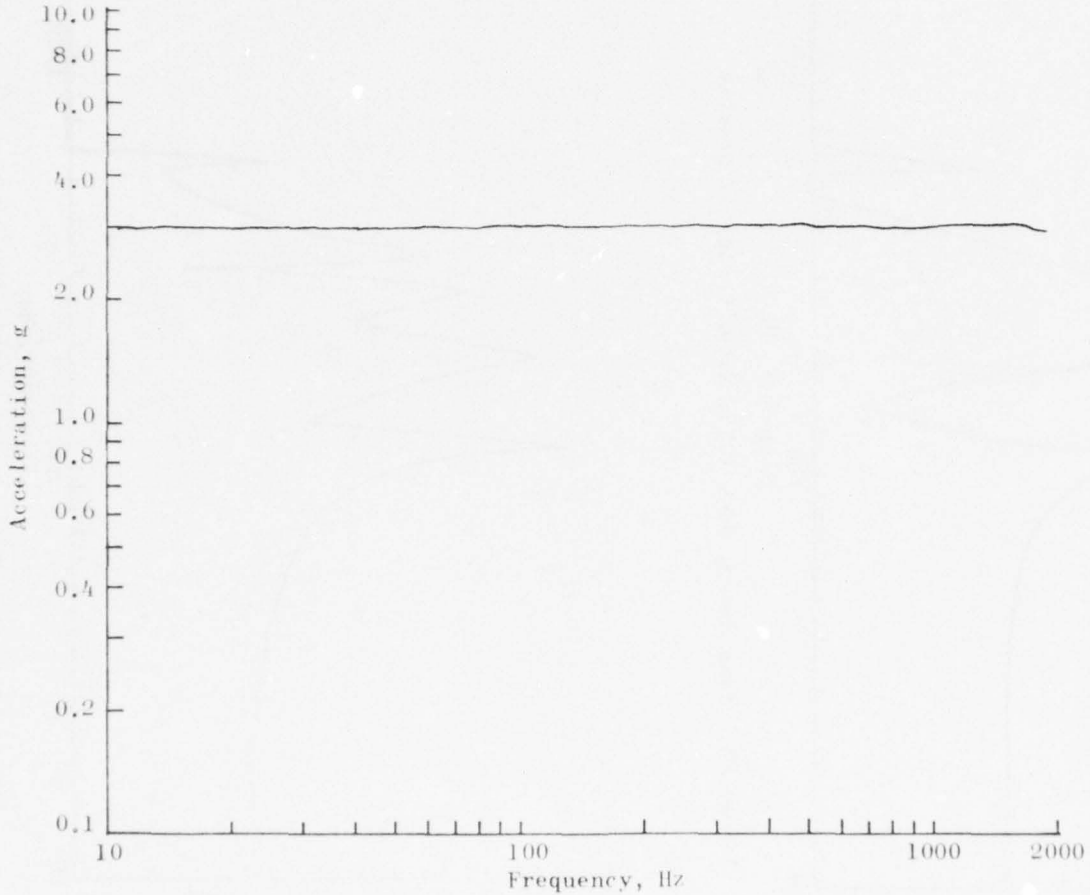

Figure 98. Sine Sweep 1, June 1975, Input Control

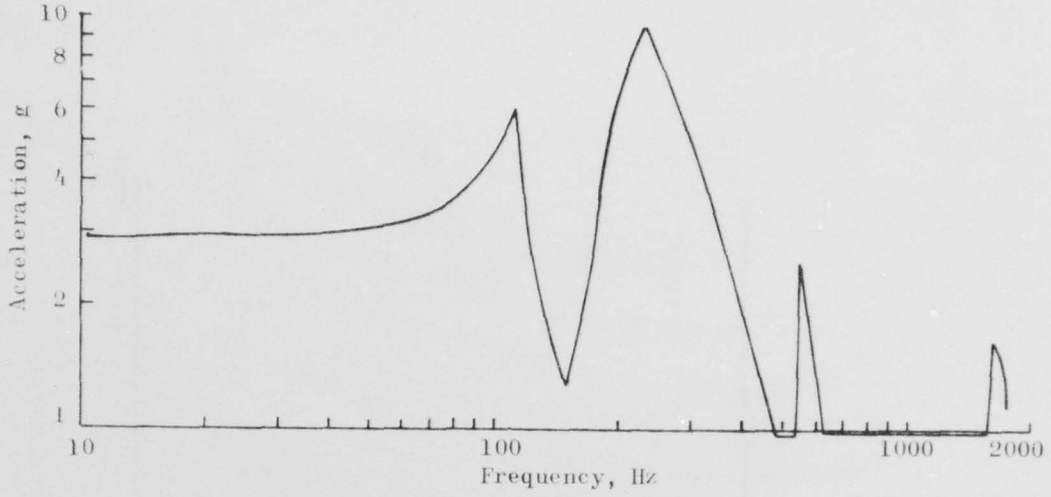

Figure 99. Sine Sweep, June 1975, Motor Center of Gravity

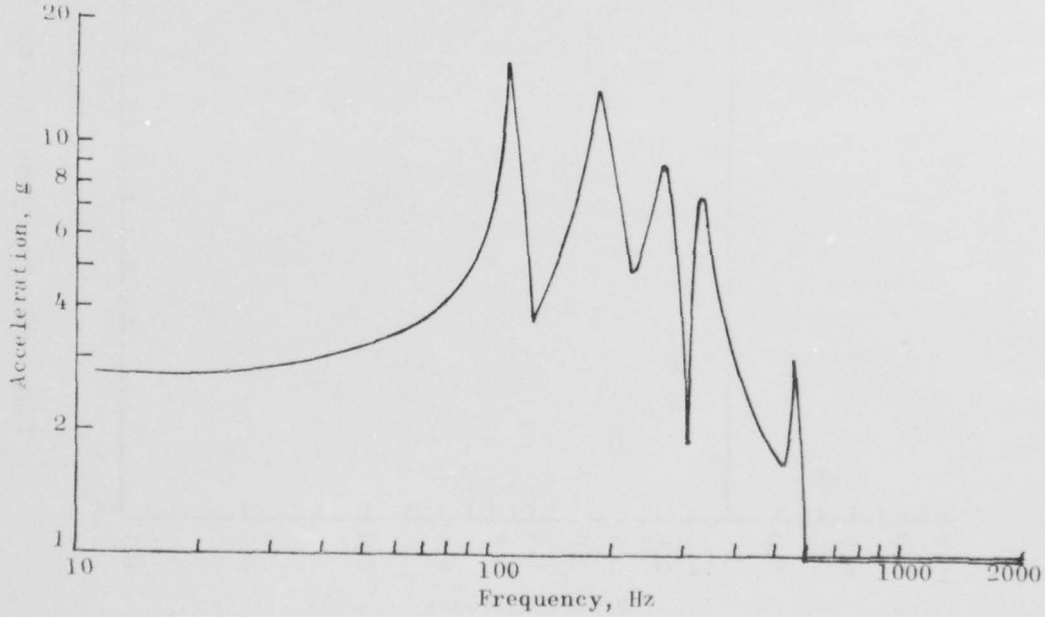

Figure 100. Sine Sweep 1, June 1975, Motor Interior

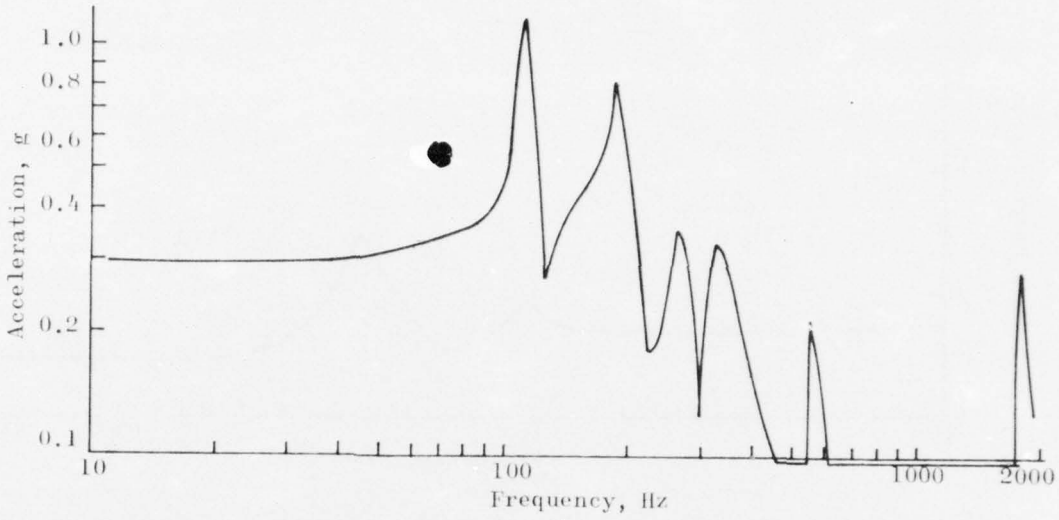

Figure 101. Sine Sweep 1, June 1975, Motor Forward End

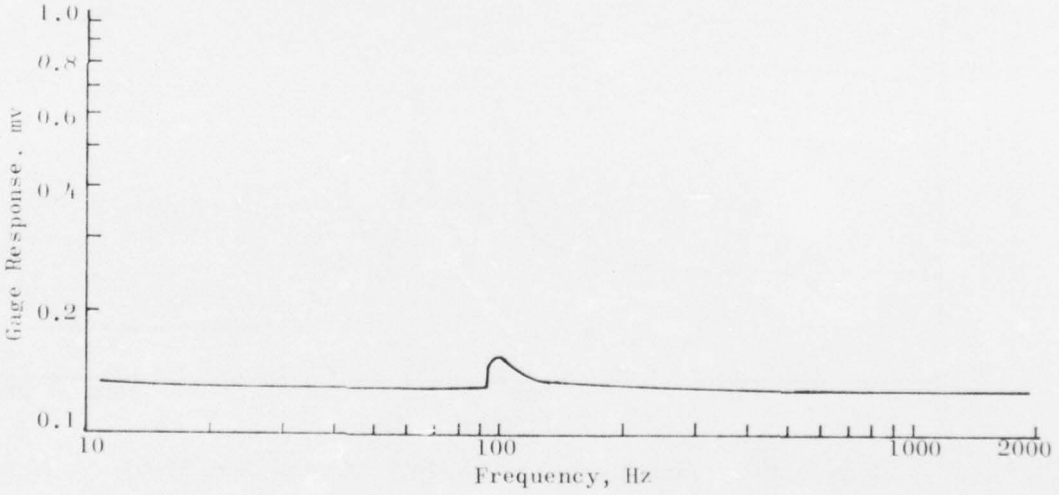

Figure 102. Sine Sweep 2, June 1975, Normal Gage N7-59

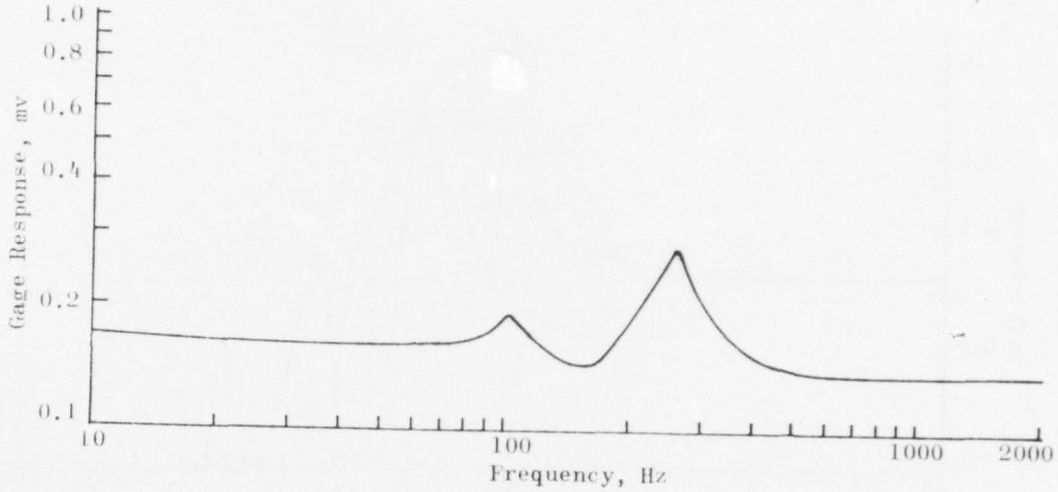

Figure 103. Sine Sweep 2, June 1975, Normal Gage N7-61

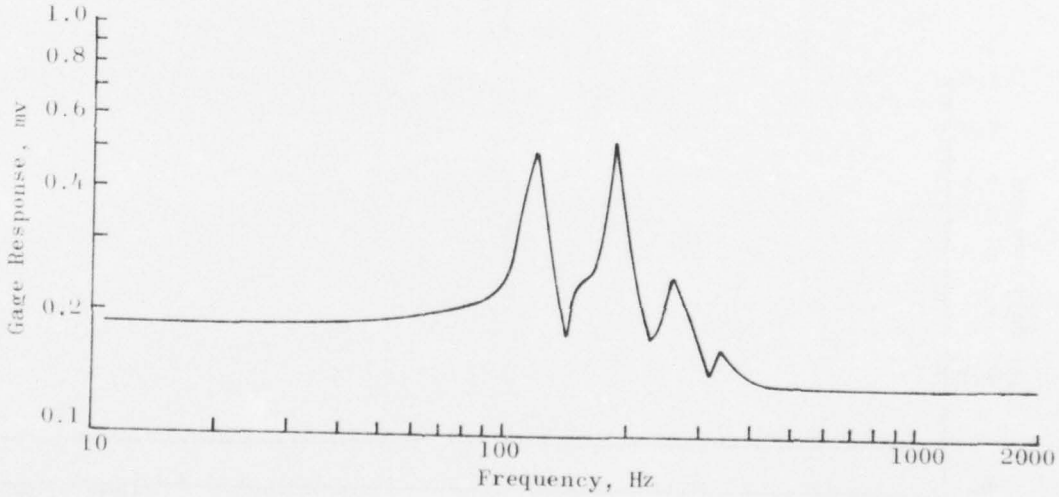

Figure 104. Sine Sweep 2, June 1975, Normal Gage N7-63

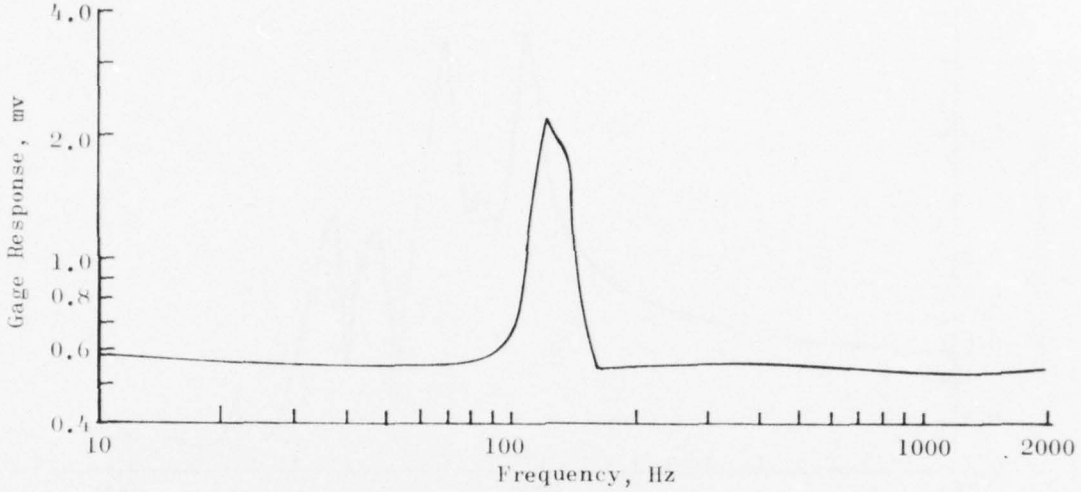

Figure 105. Sine Sweep 2, June 1975, Stress Gage S7-135

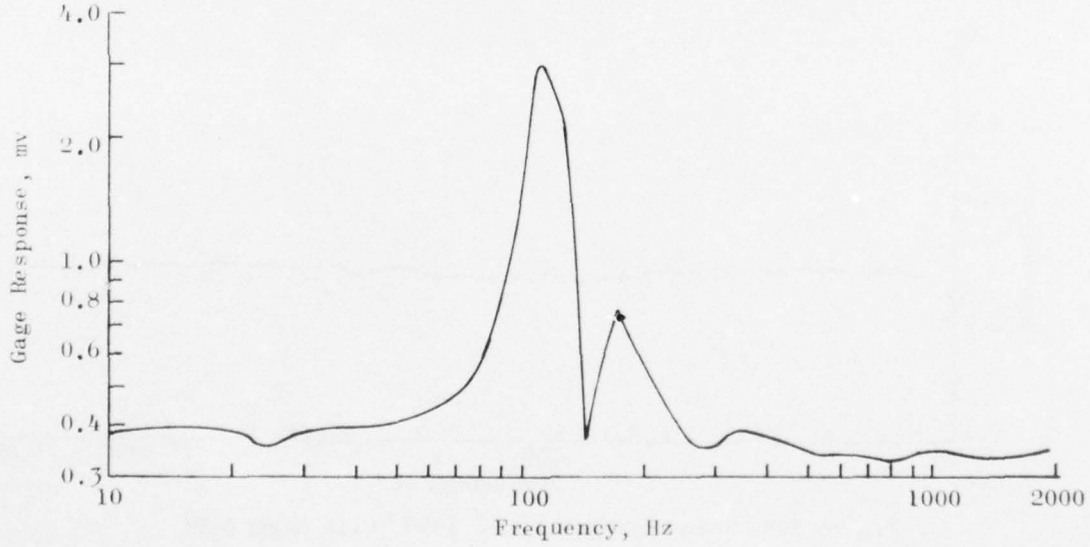

Figure 106. Sine Sweep 2, June 1975, Stress Gage S7-137

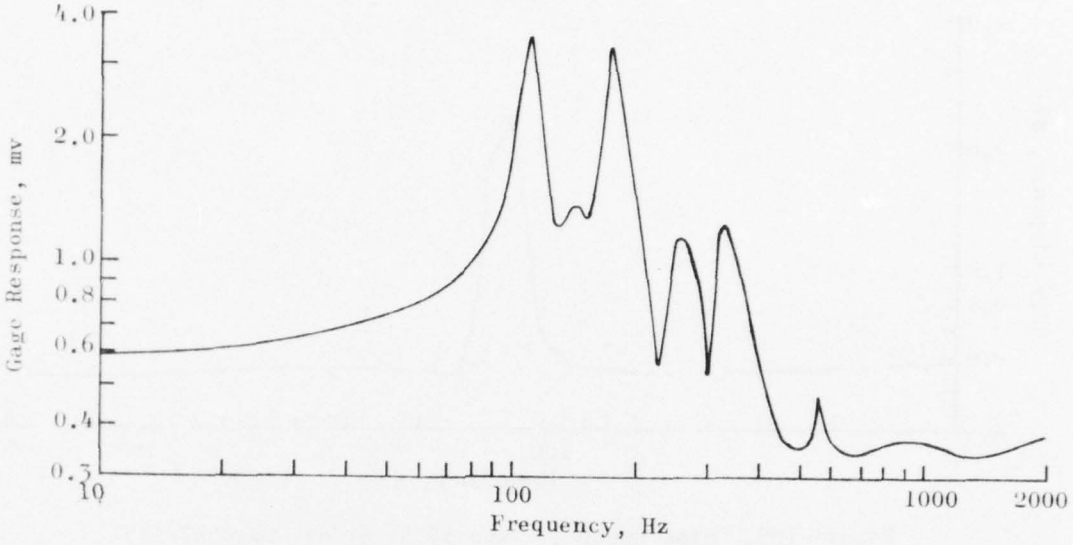

Figure 107. Sine Sweep 2, June 1975, Stress Gage S7-140

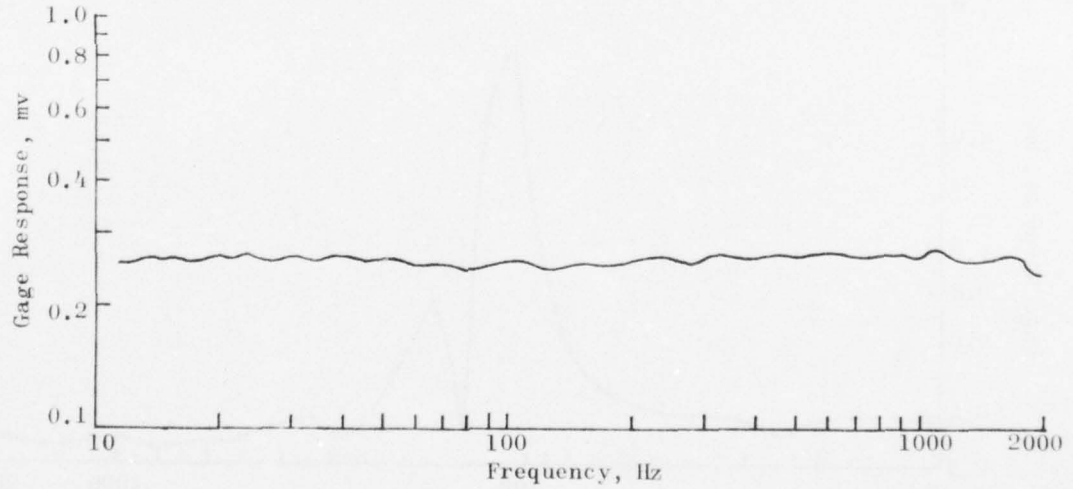

Figure 108. Sine Sweep 1, June 1975, Clip Gage 7-38

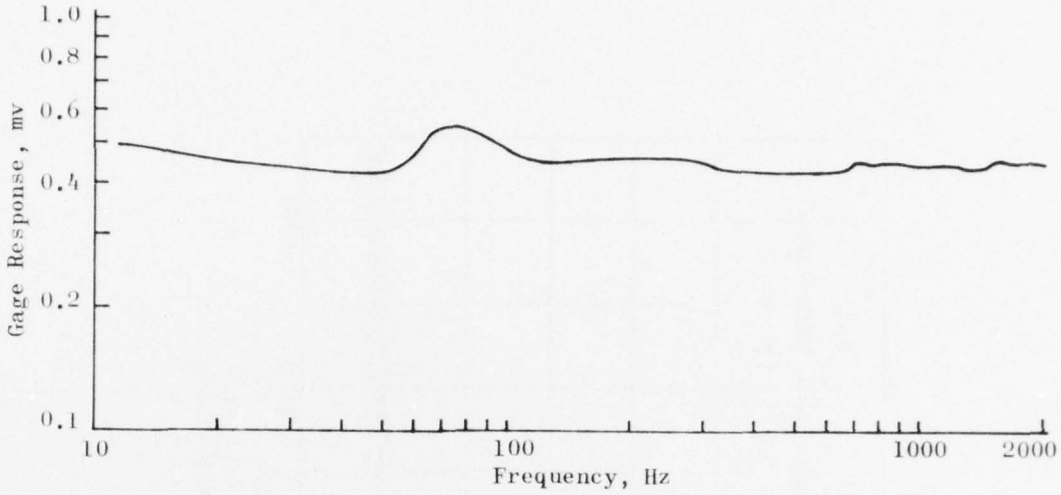

Figure 109. Sine Sweep 1, June 1975, Clip Gage C7-47

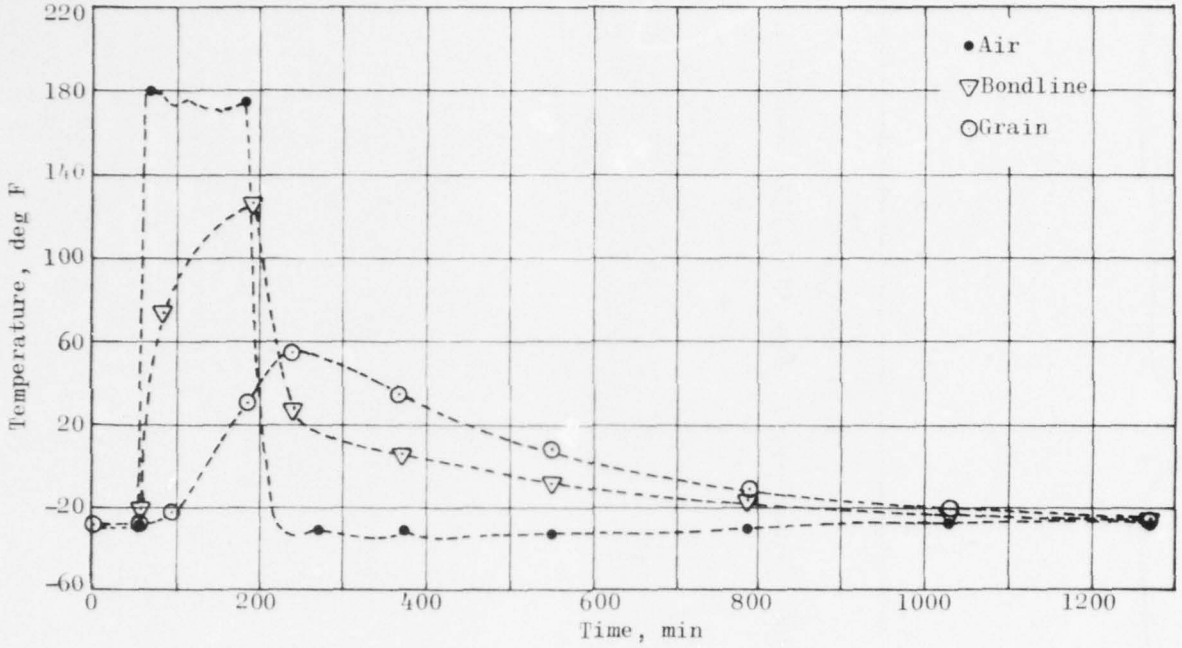

Figure 110. Temperature Response, Aeroheat Cycle, June 1975

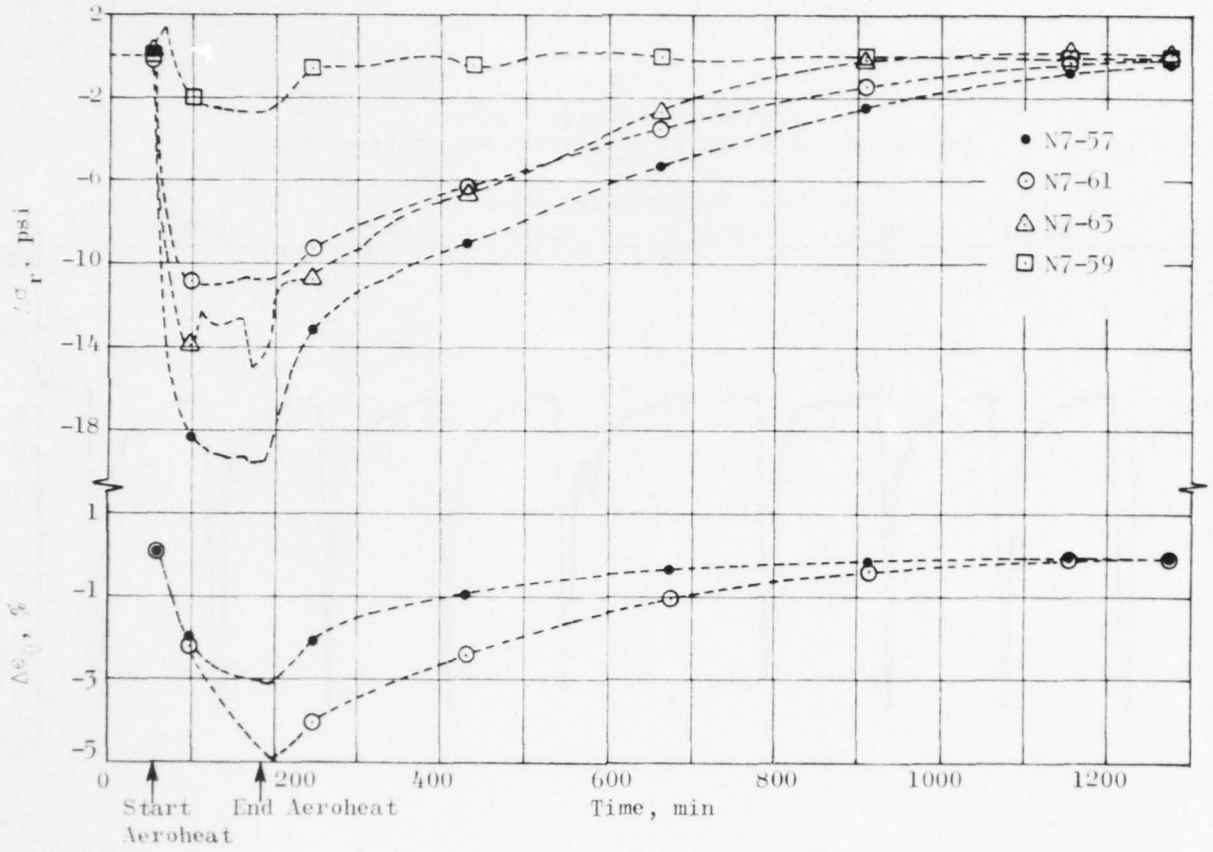

Figure 111. Stress/Strain Response, Aeroheat Cycle, June 1975

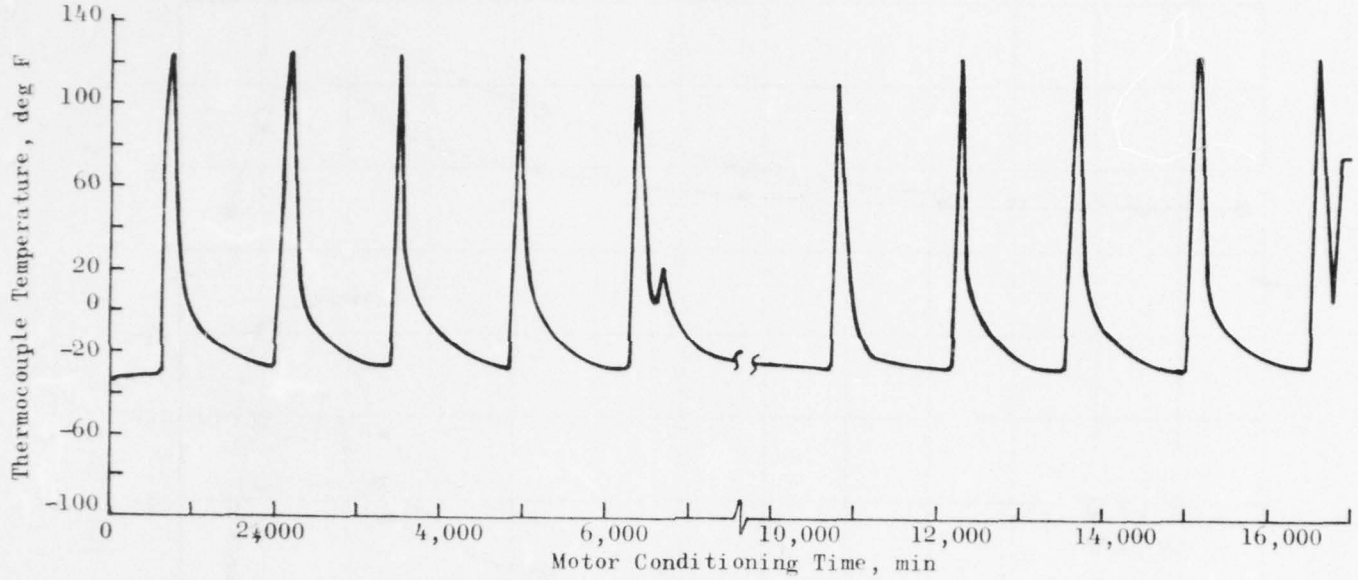

Figure 112. Thermocouple 1 (Grain/Liner) Response, Captive-Flight Simulation

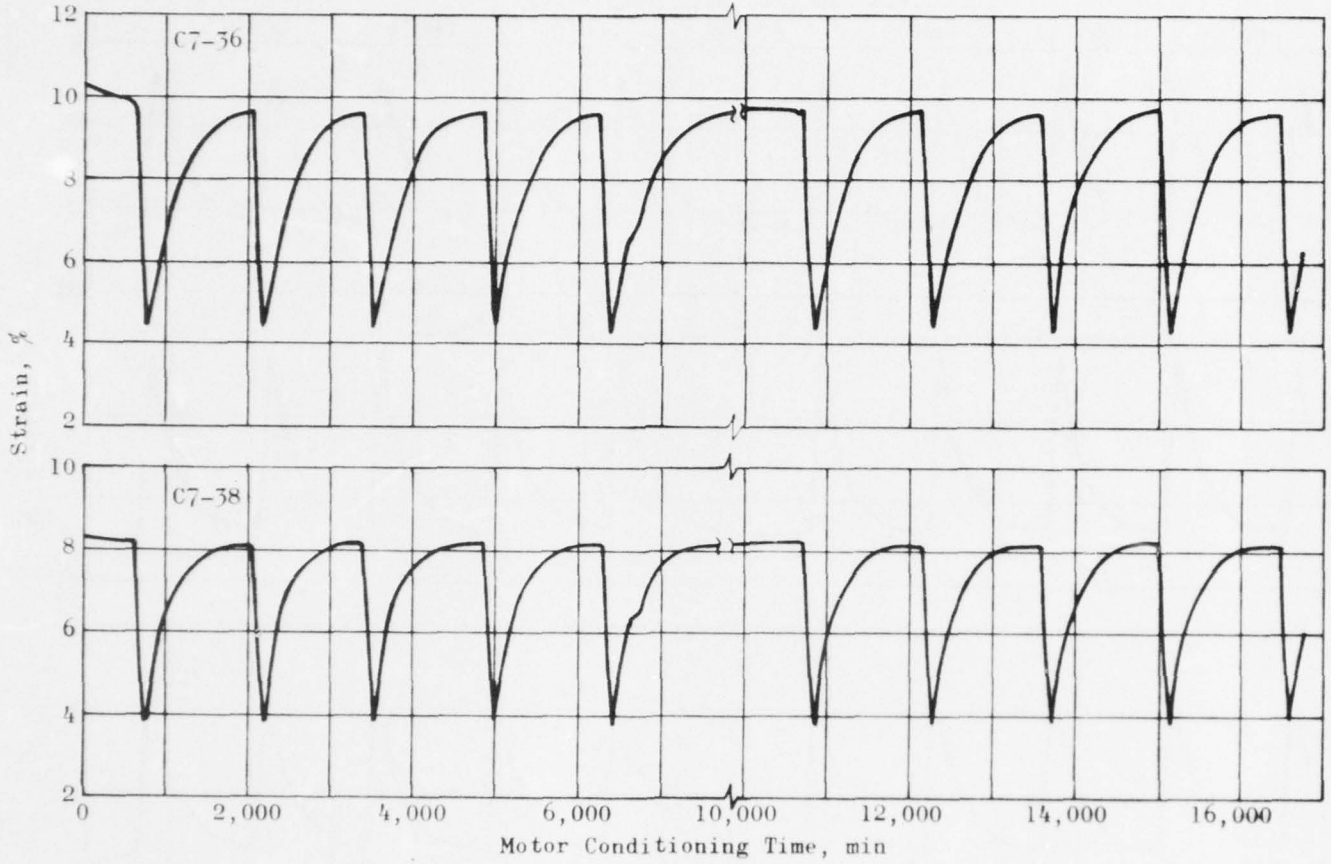

Figure 113. Bore Strain History, Captive-Flight Simulation Tests

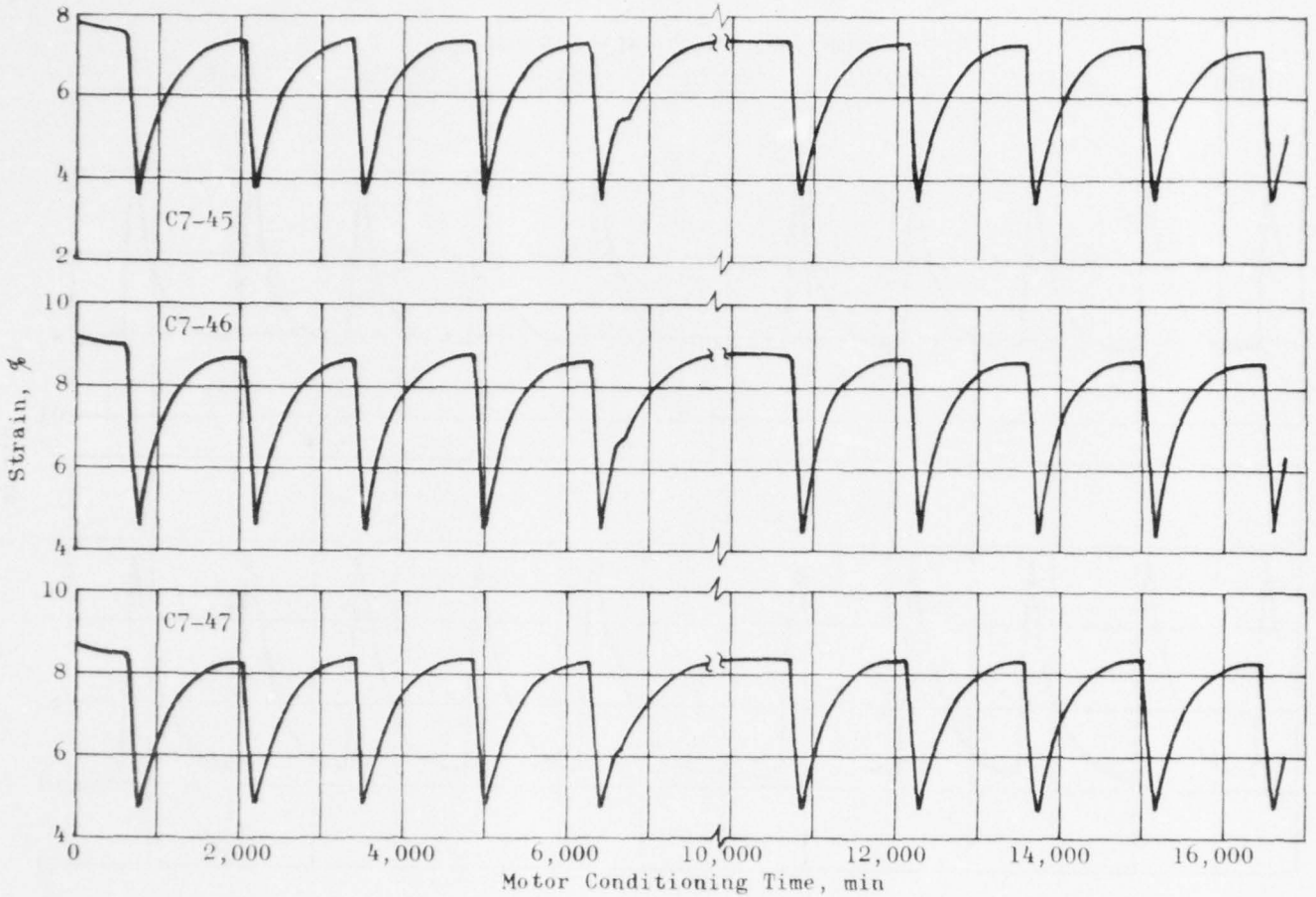

Figure 113. Continued

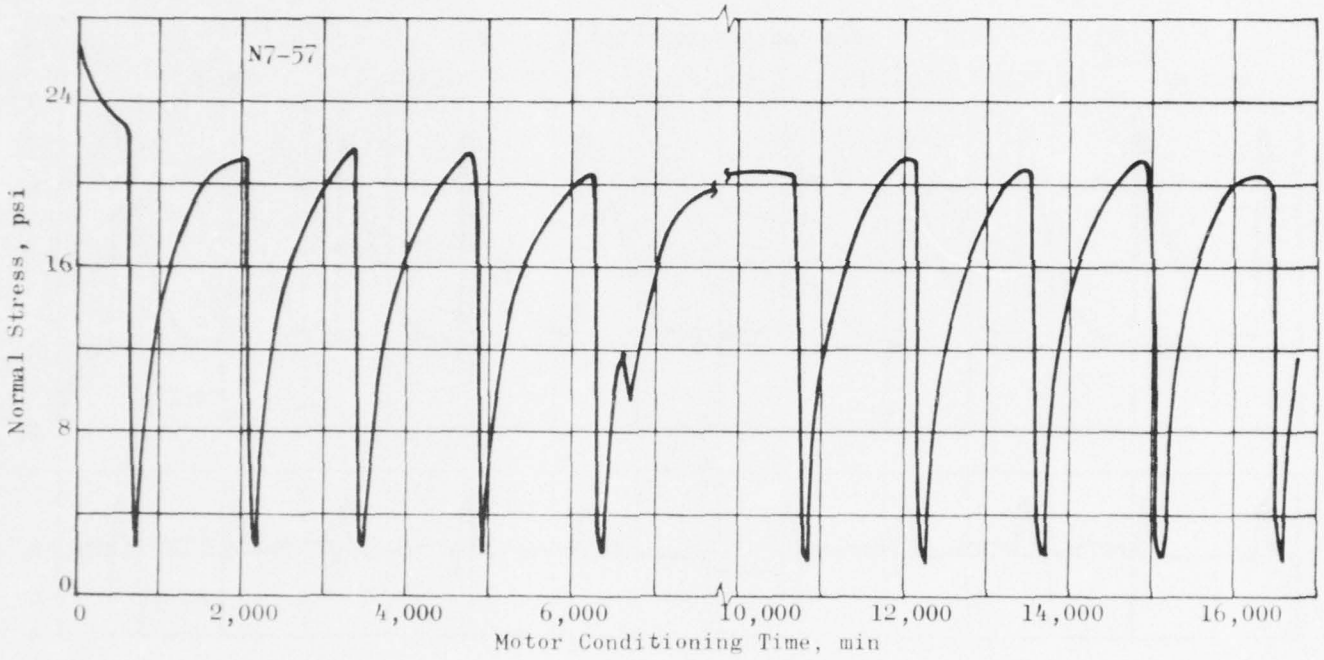

Figure 114. Normal Bond Stress, Captive-Flight Simulation Tests

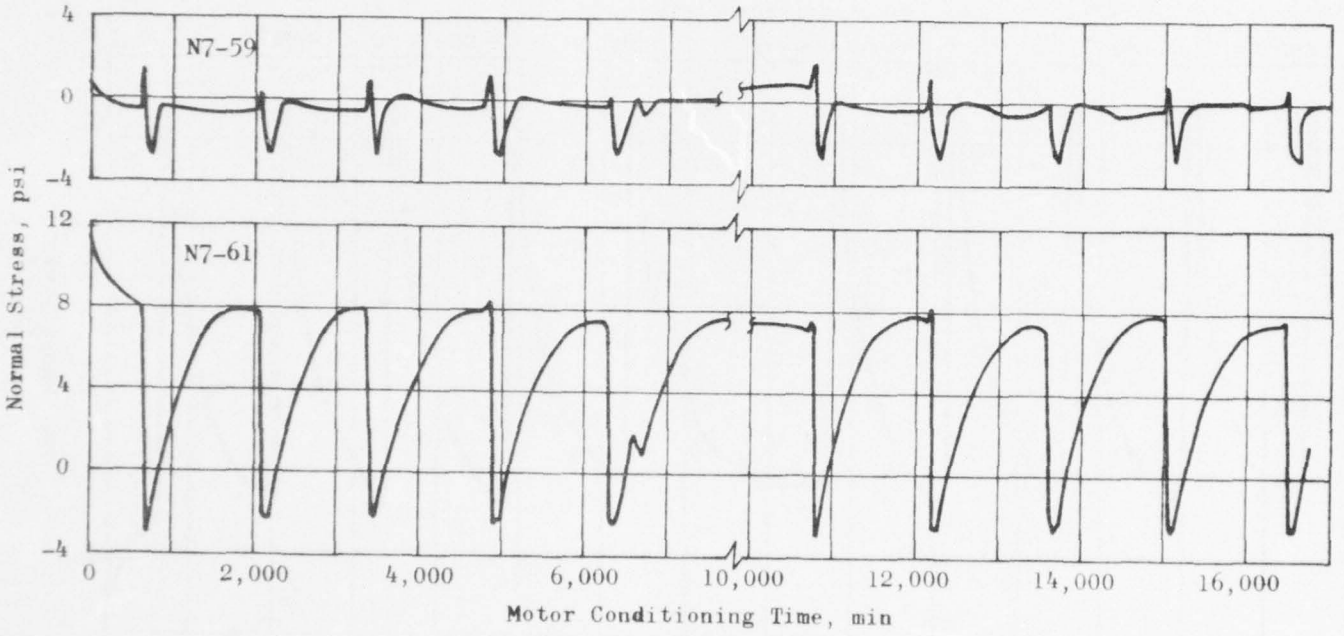

Figure 114. Continued

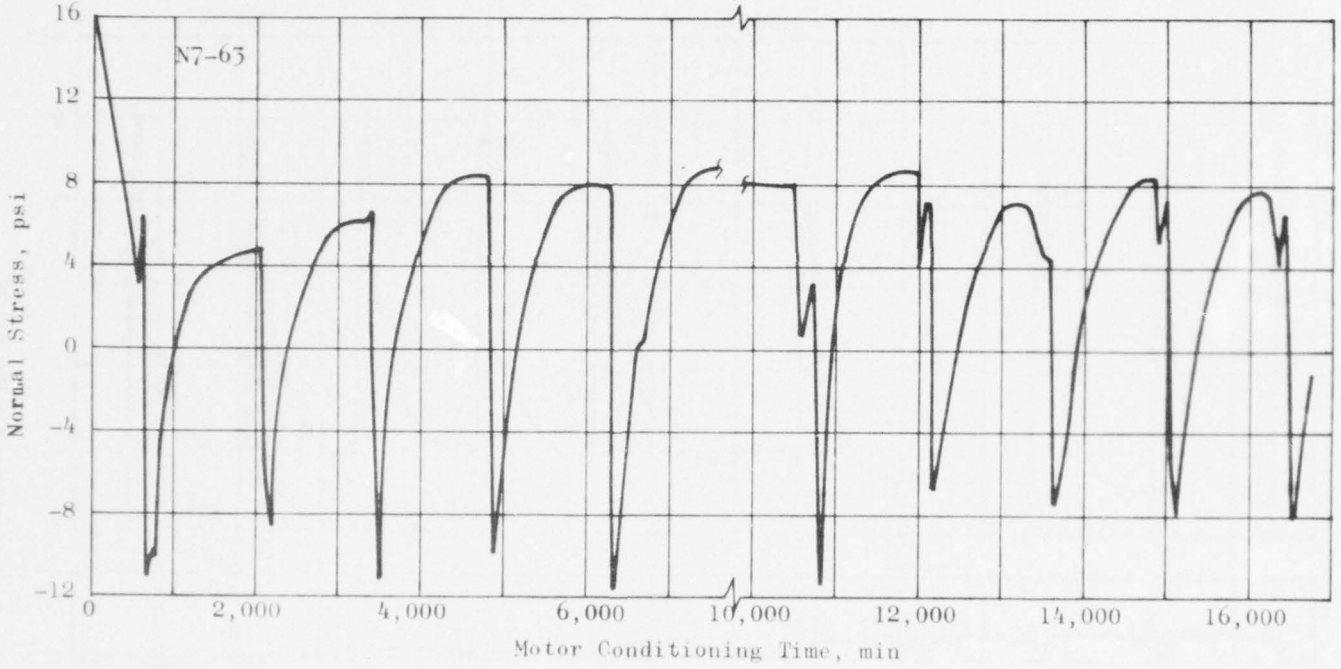

Figure 114. Continued

AD-A037 102 ROCKWELL INTERNATIONAL MCGREGOR TEX ROCKETDYNE DIV F/G 21/9.2
AIR LAUNCH INSTRUMENTED VEHICLES EVALUATION (ALIVE).(U)
FEB 77 J D BURTON F04611-74-C-0009
UNCLASSIFIED R-4939 AFRPL-TR-76-101 NL

3 OF 3
AD
A037102

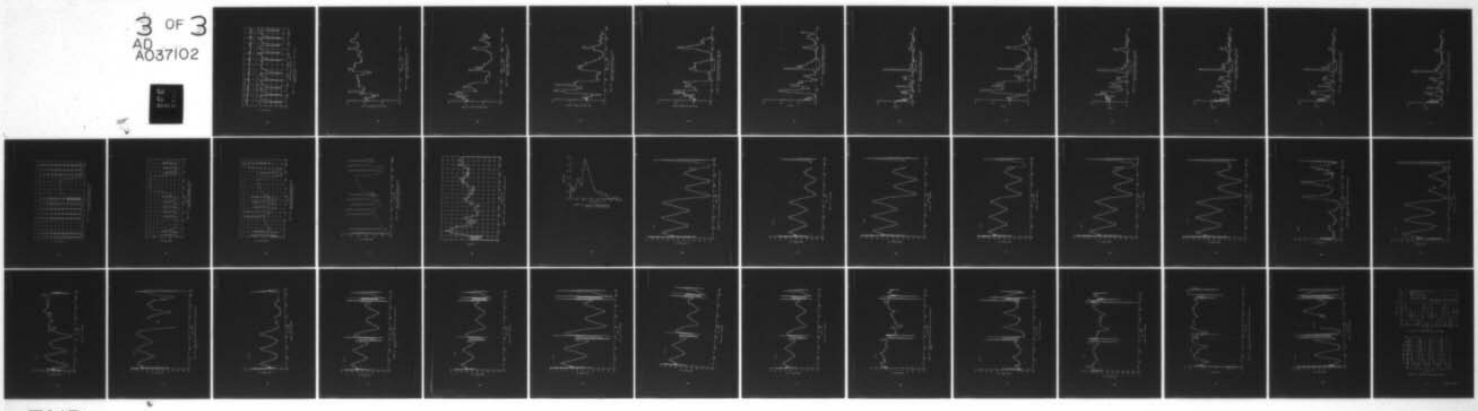

END

DATE
FILMED
4-77

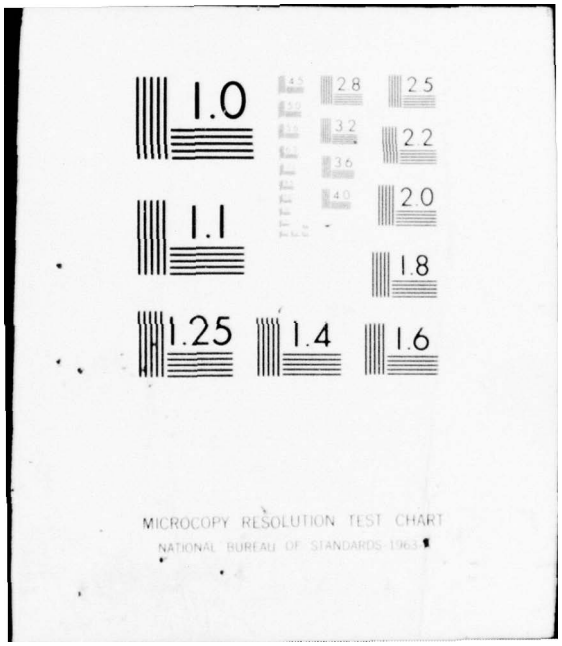
1.0
1.1
1.25
1.4
1.6
1.8
2.0
2.2
2.5
2.8
3.2
3.6
4.0
MICROCOPY RESOLUTION TEST CHART
NATIONAL BUREAU OF STANDARDS-1963

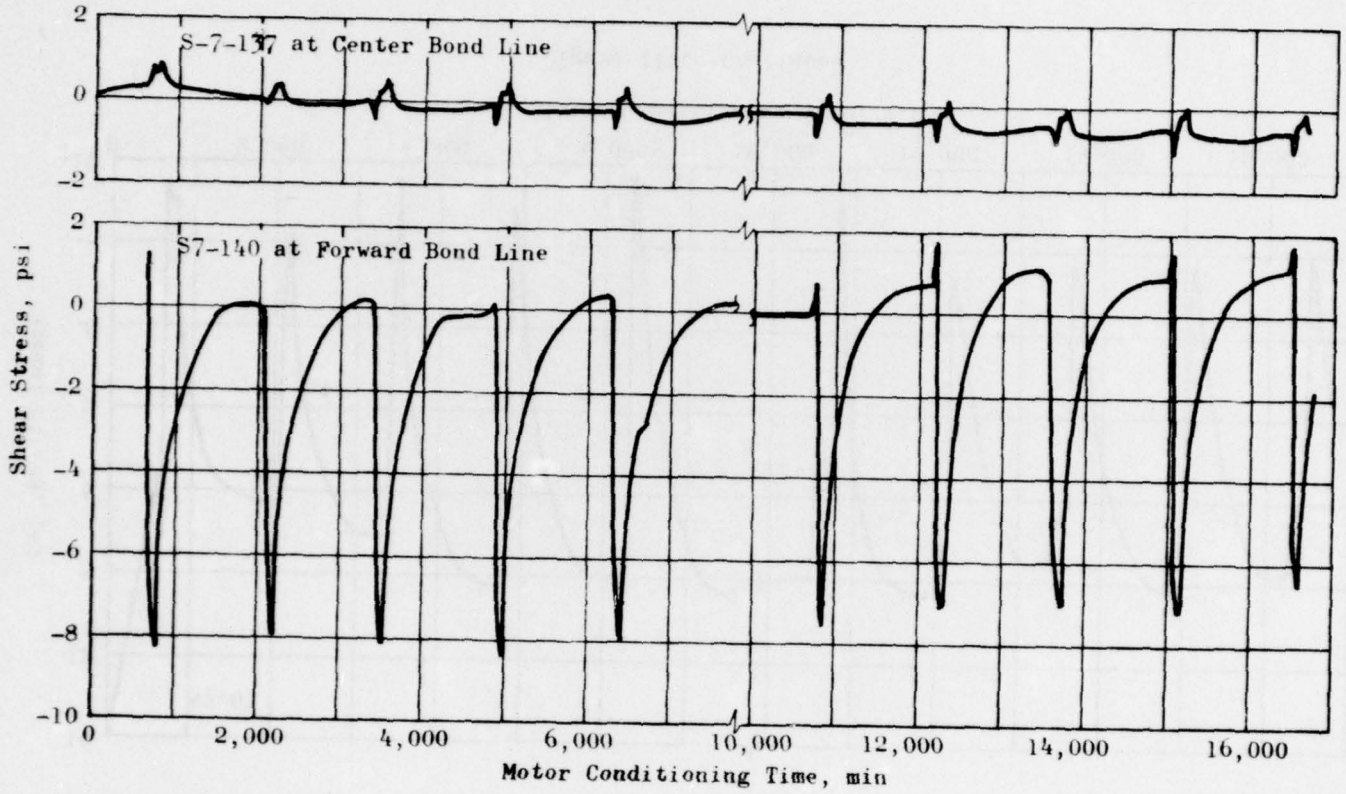

Figure 115. Longitudinal Shear Stress, Captive-Flight Simulation Tests

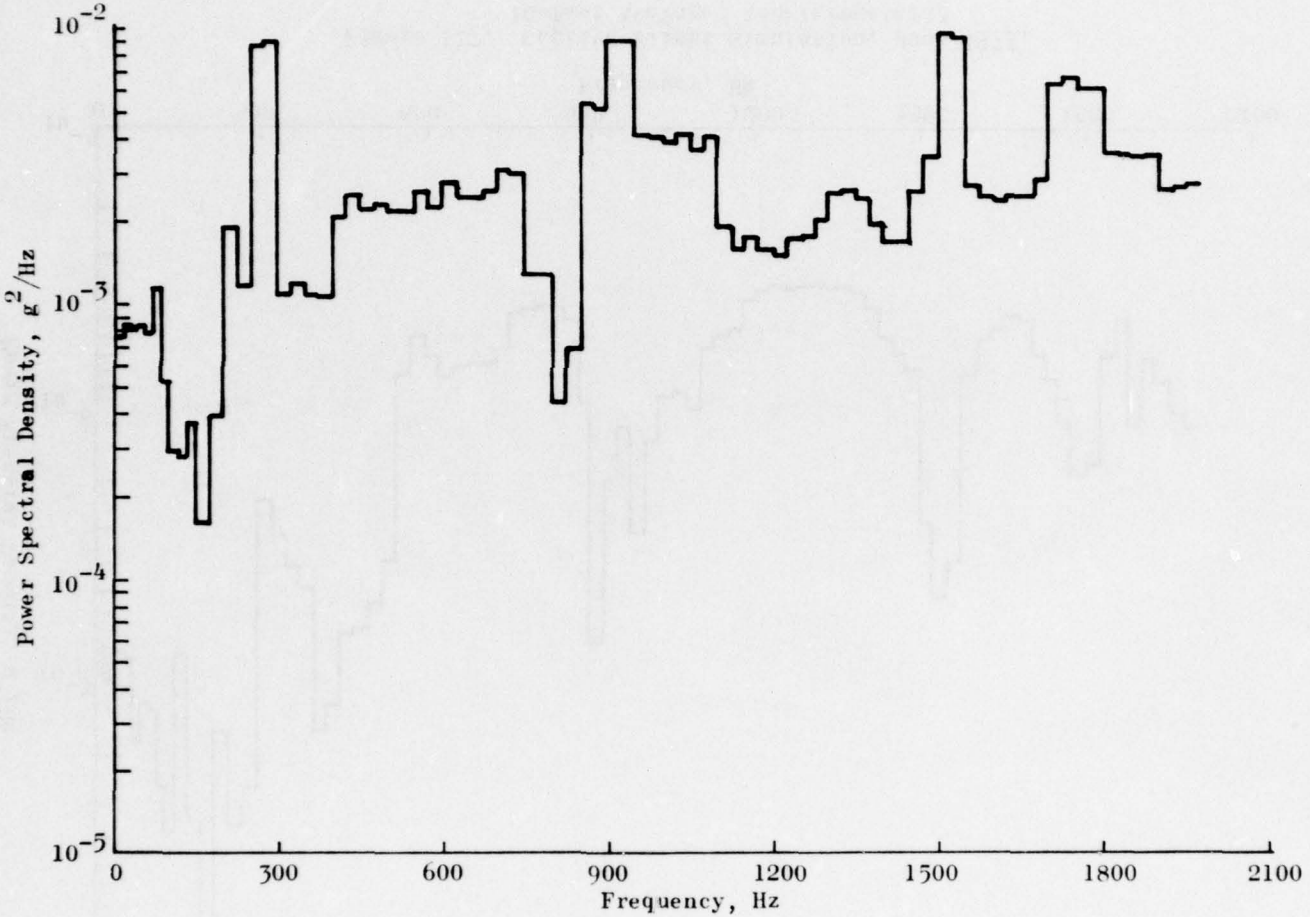

Figure 116. Captive Flight Simulation, June 1975, 10-Test Average, Input Control

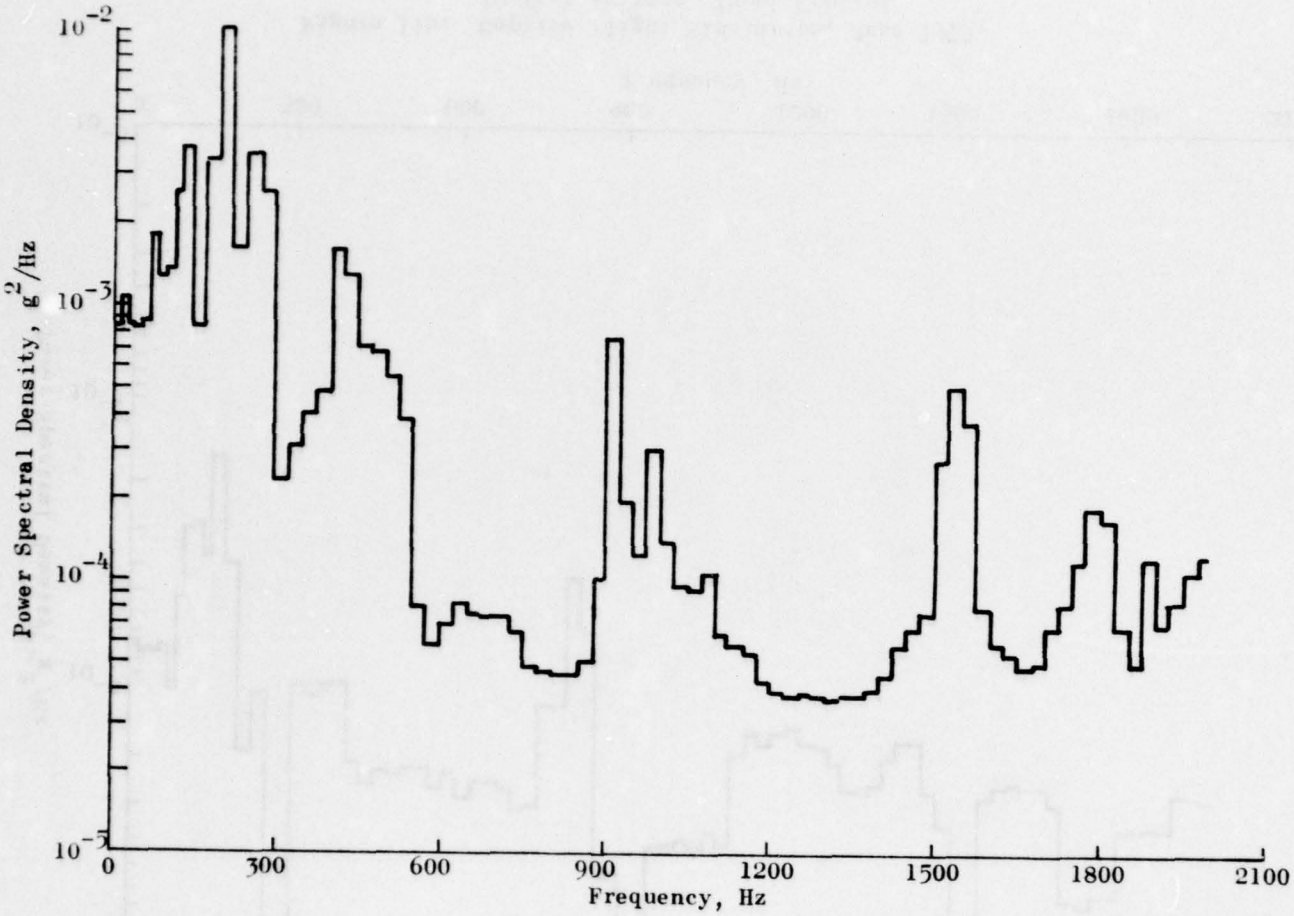

Figure 117. Captive-Flight Simulation, June 1975, 10-Test Average, Accelerometer 3

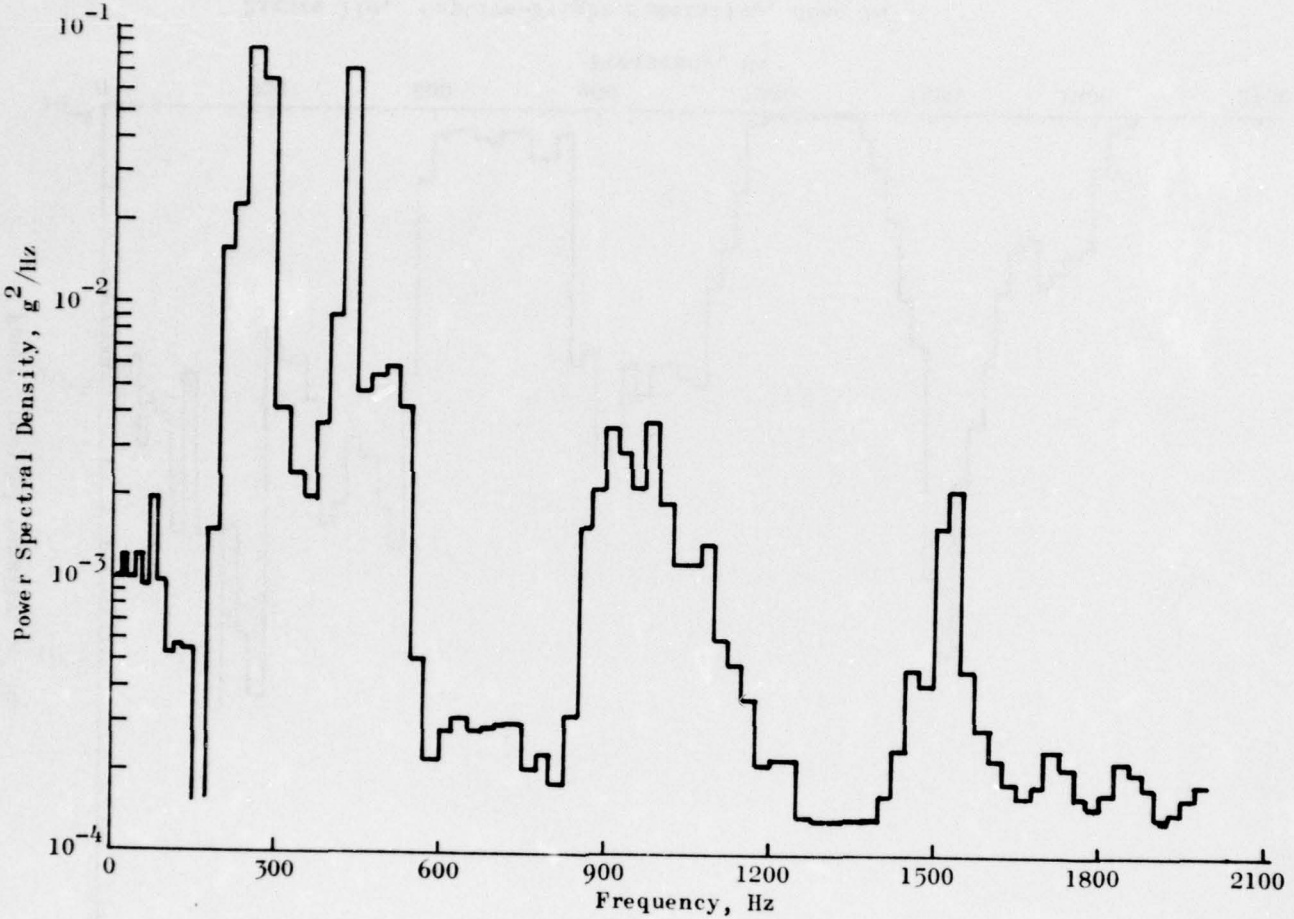

Figure 118. Captive-Flight Simulation, June 1975, 10-Test Average, Accelerometer 4

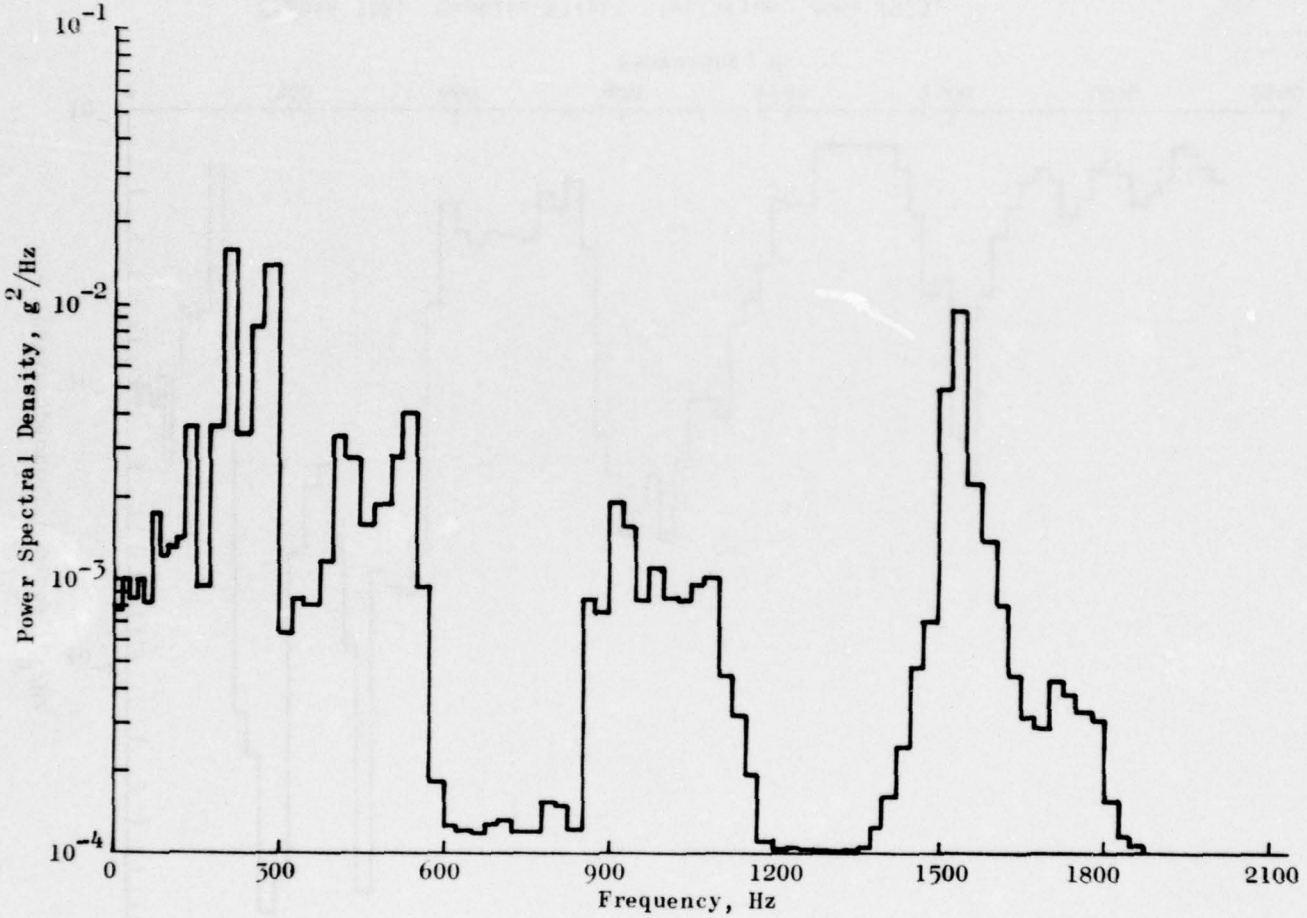

Figure 119. Captive-Flight Simulation, June 1975, 10-Week Test Average, Accelerometer 5

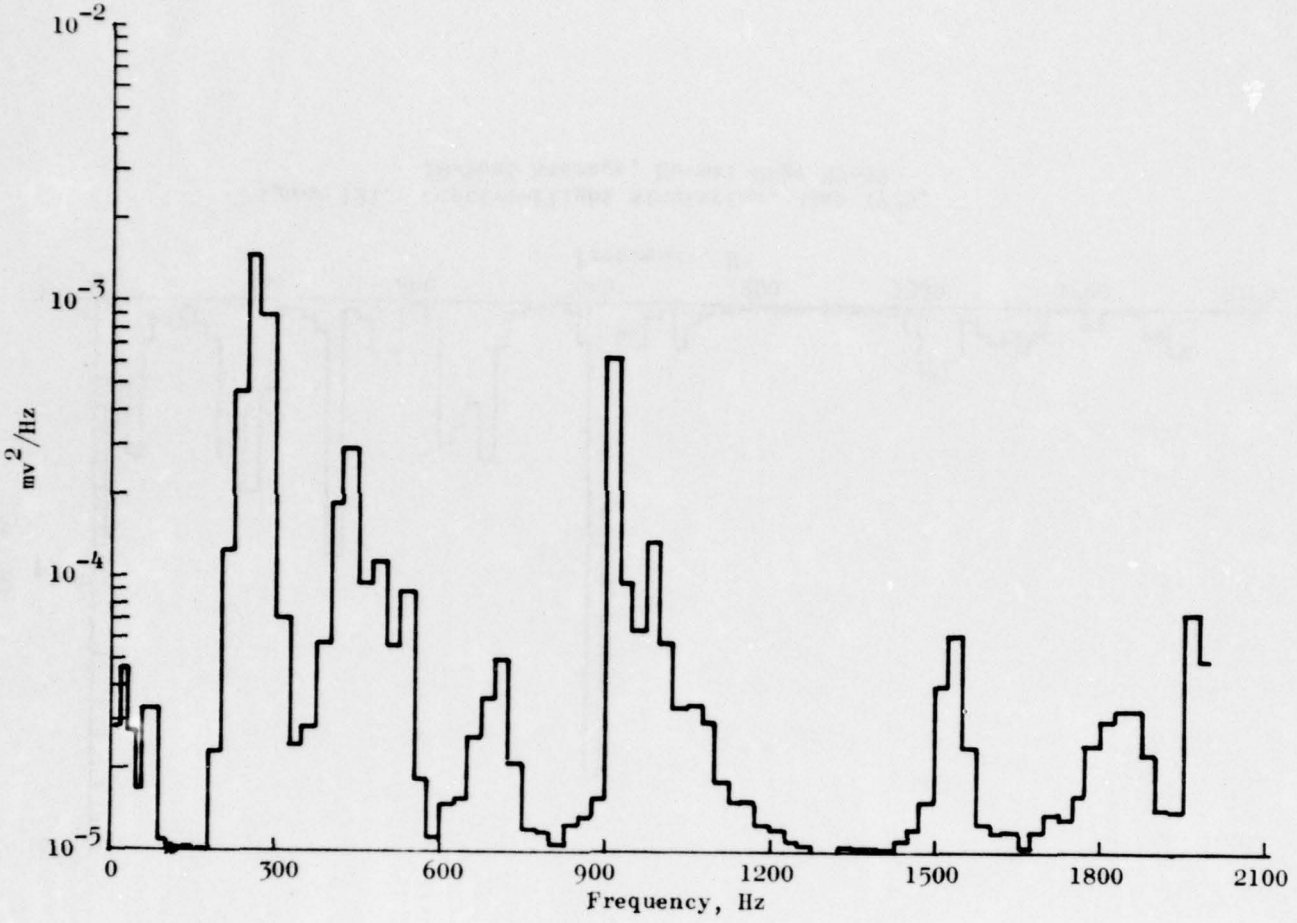

Figure 120. Captive-Flight Simulation, June 1975, 10-Test Average, Normal Gage N7-57

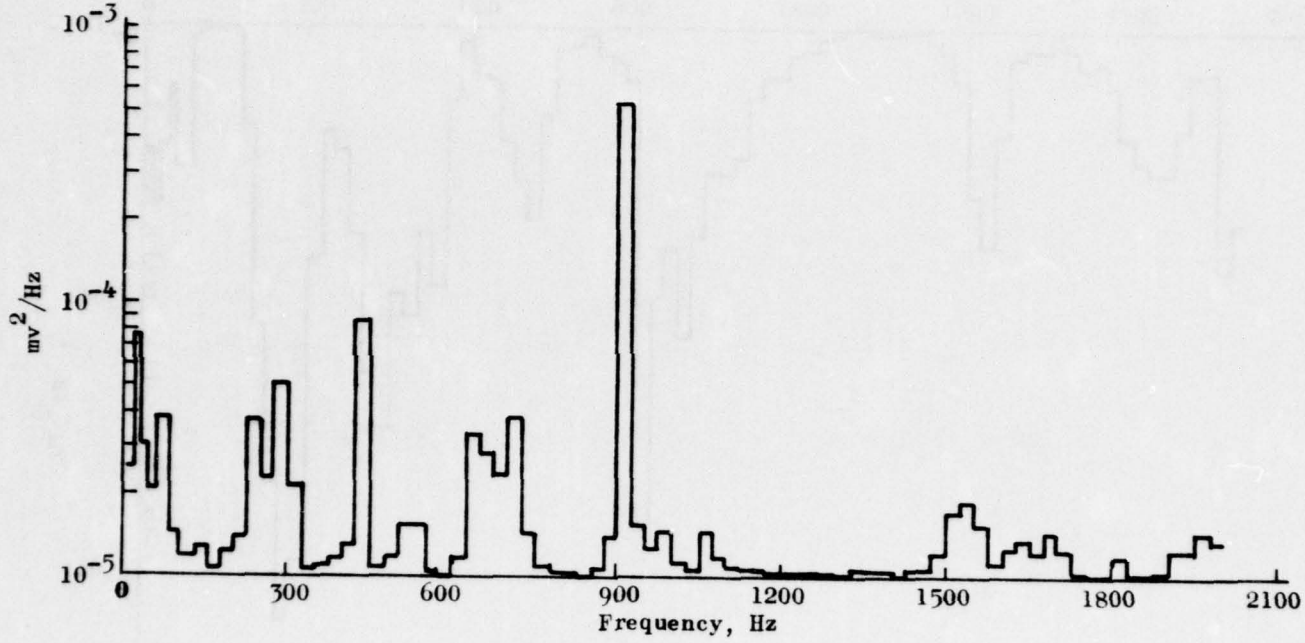

Figure 121. Captive-Flight Simulation, June 1975, 10-Test Average, Novmal Gage N7-59

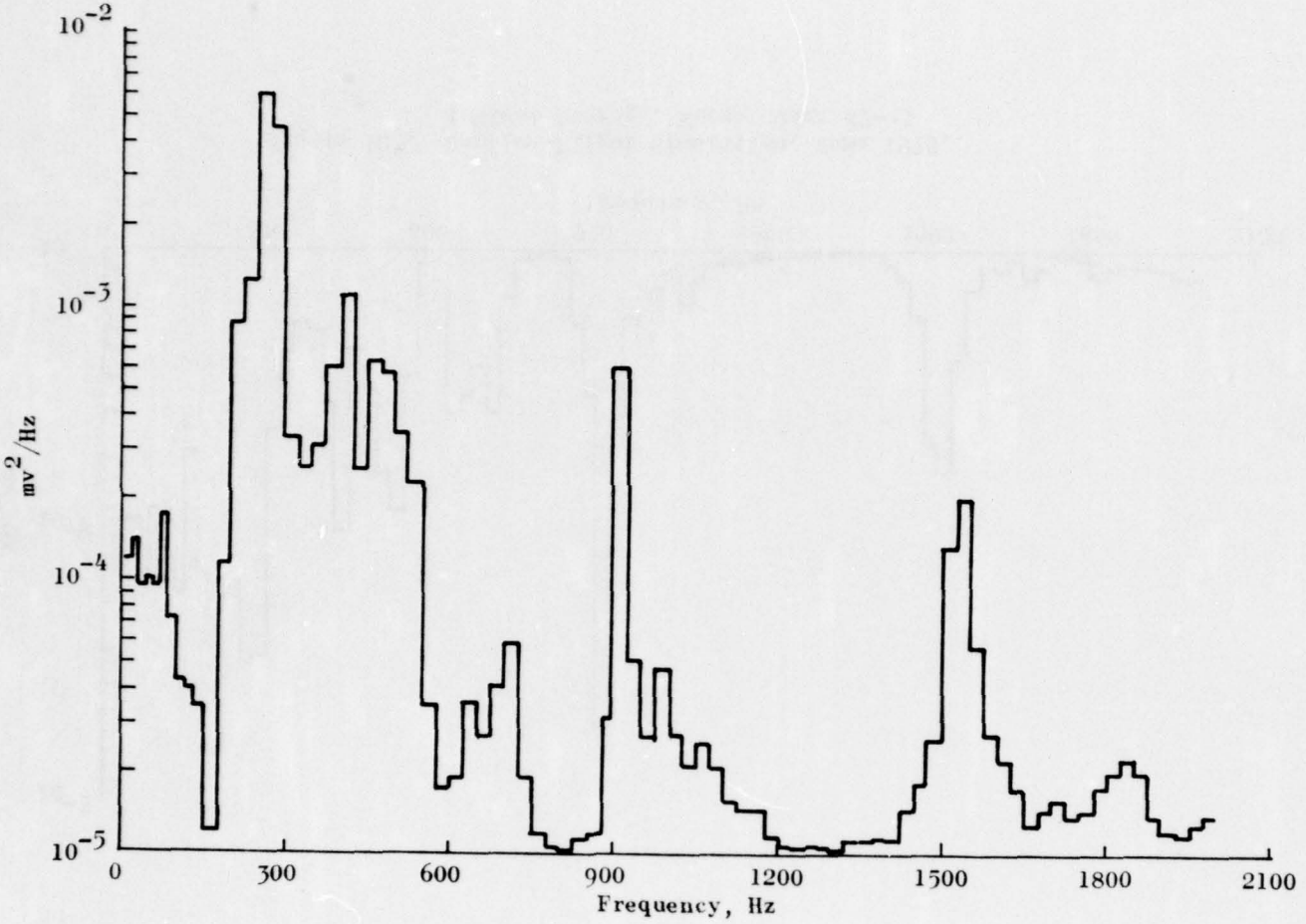

Figure 122. Captive-Flight Simulation, June 1975, 10-Test Average, Normal Gage N7-61

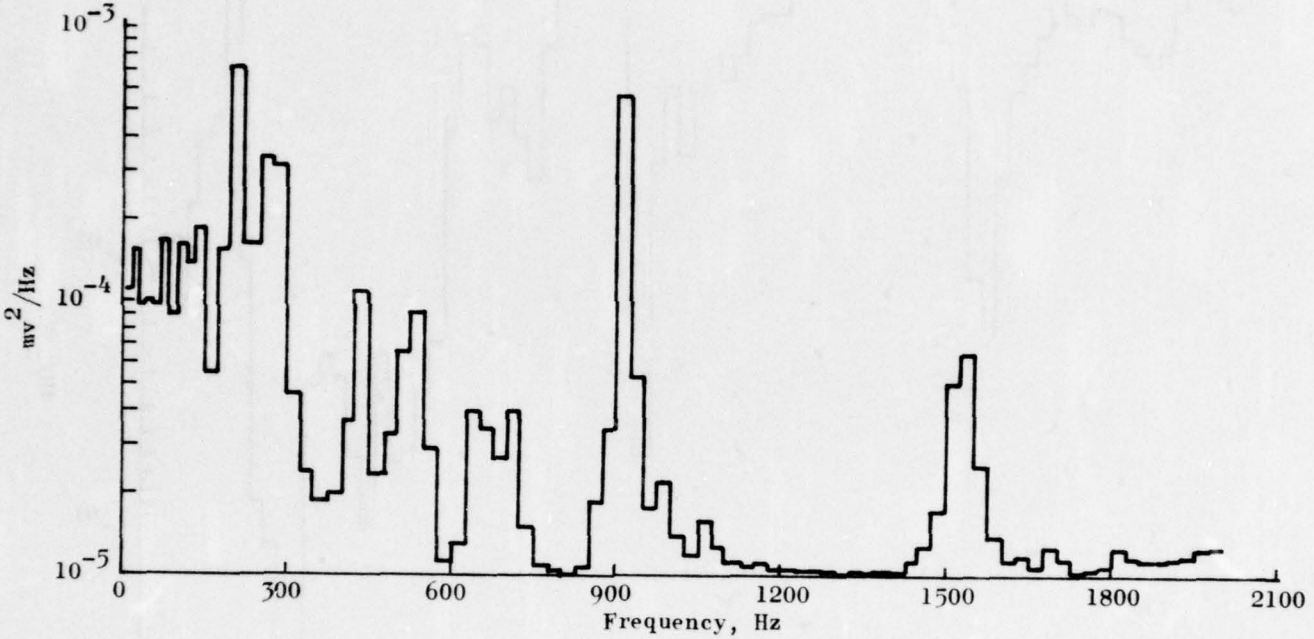

Figure 123. Captive-Flight Simulation, June 1975, 10-Test Average, Normal Gage N7-63

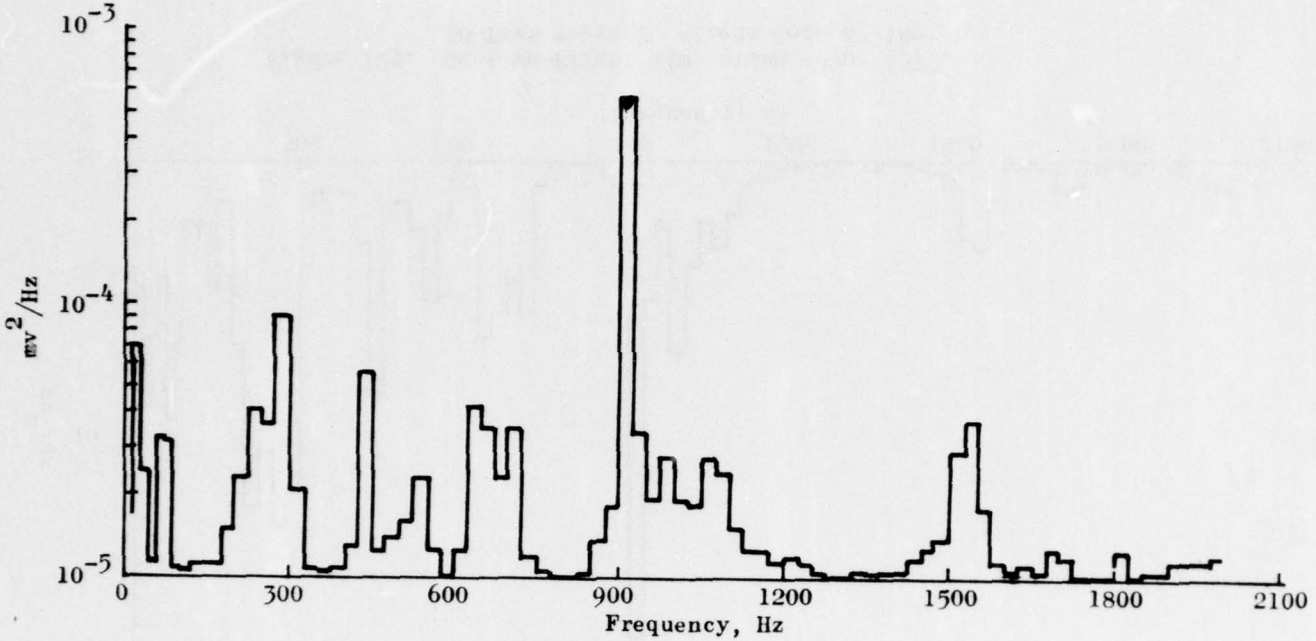

Figure 124. Captive-Flight Simulation, June 1975, 10-Test Average, Stress Gage S7-137

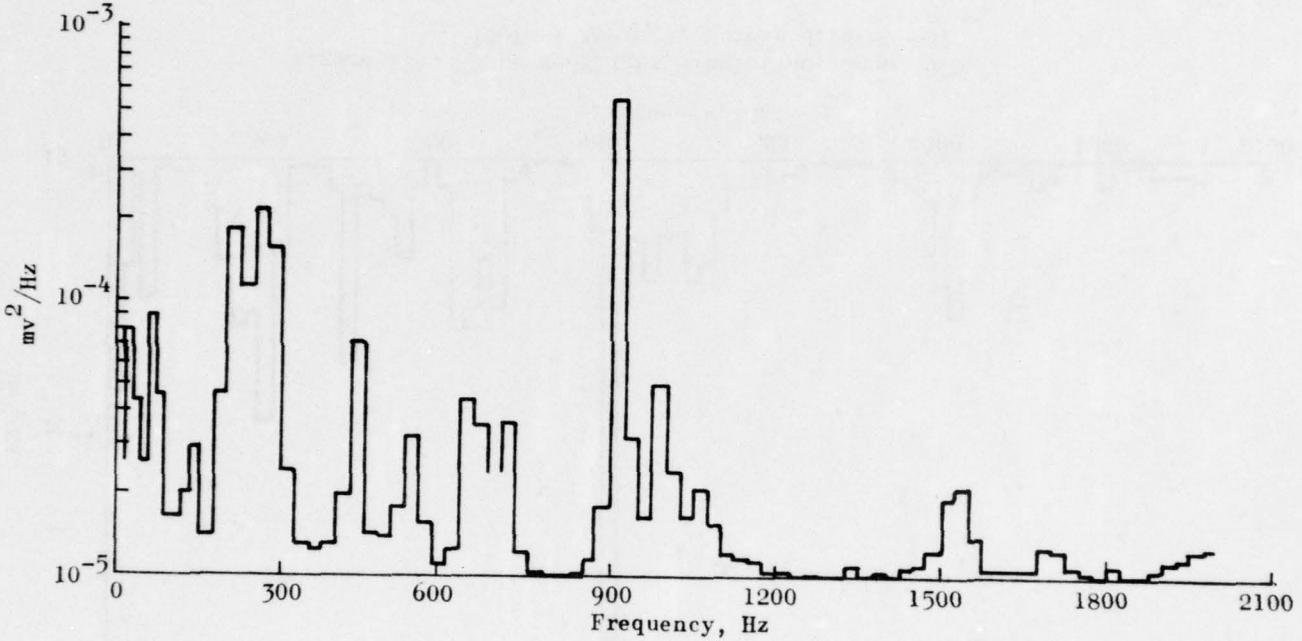

Figure 125. Captive-Flight Simulation, June 1975, 10-Test Average, Stress Gage S7-140

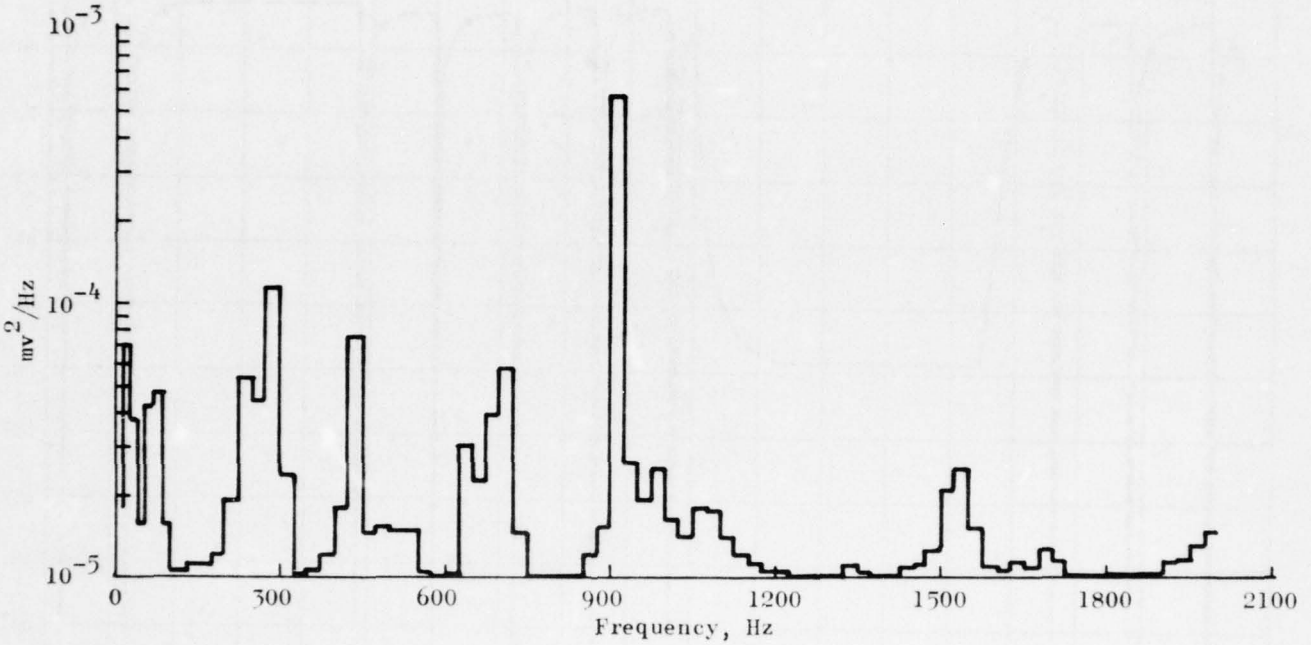

Figure 126. Captive-Flight Simulation, June 1975, 10-Test Average, Stress Gage S7-135

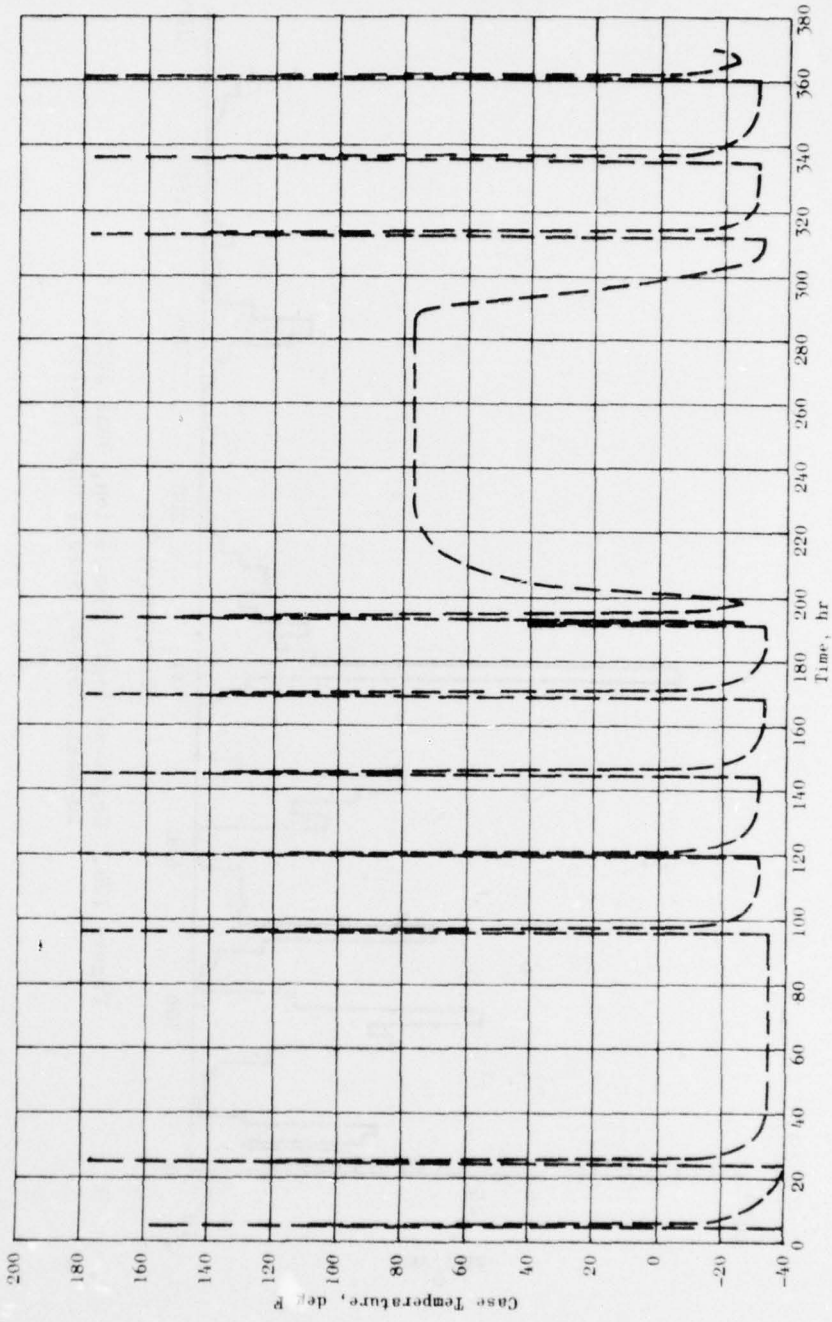

Figure 127. Case Temperature Response, Second Captive-Flight Simulation Test

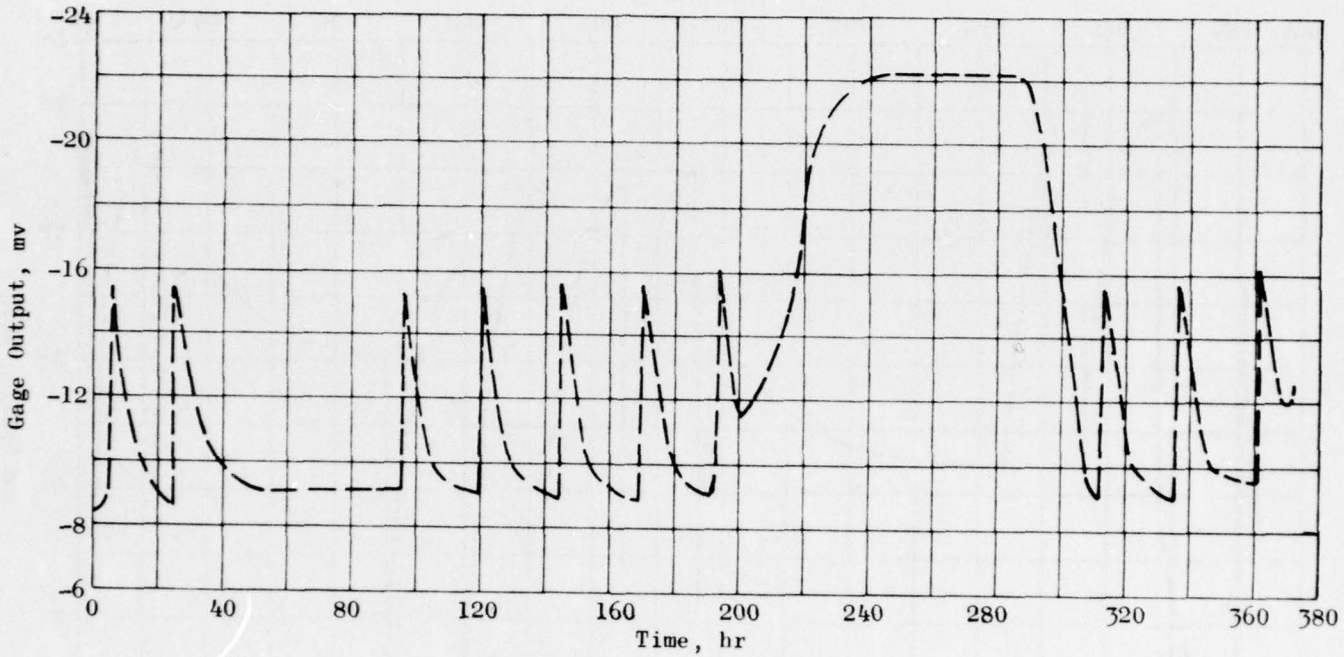

Figure 128. Clip Gage C7-36 Response, Second Captive-Flight Simulation Test

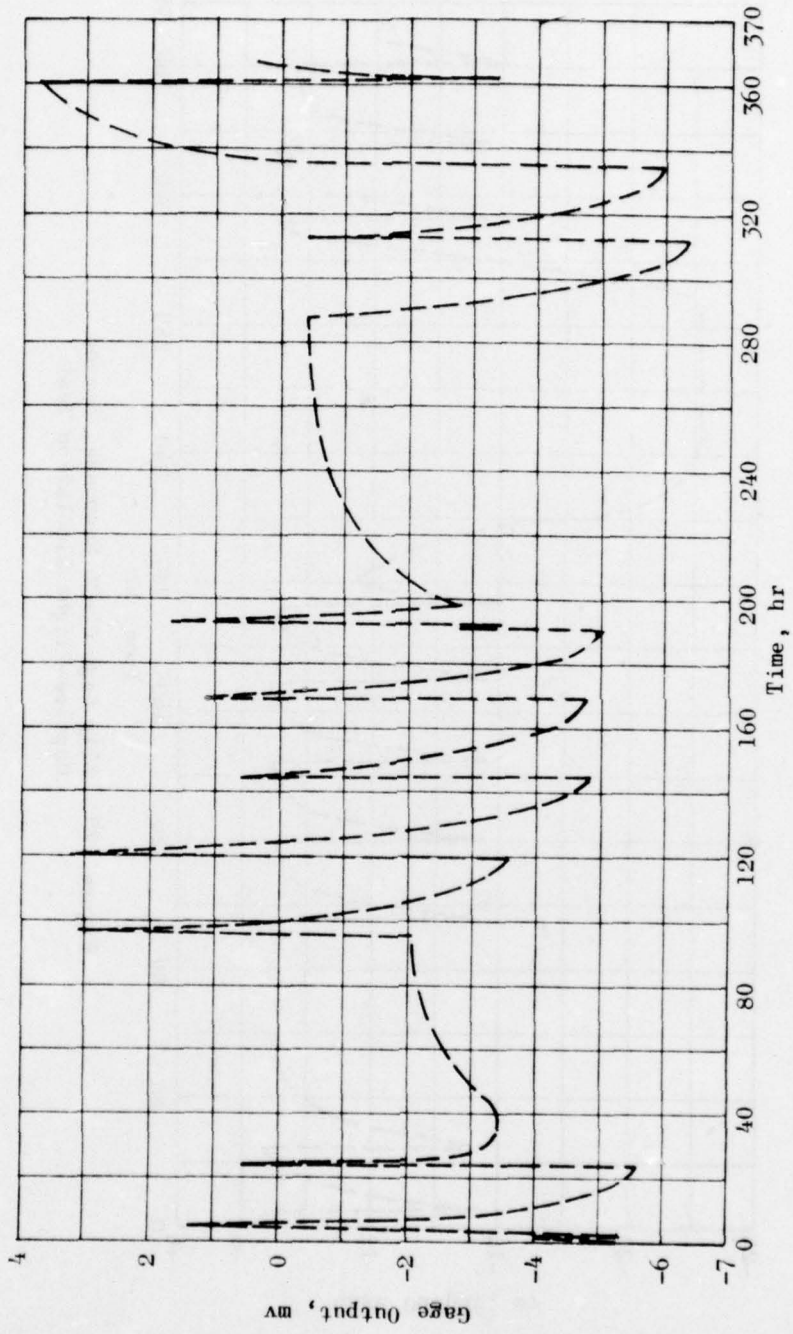

Figure 129. Normal Gage N7-61 Response, Second Captive-Flight Simulation Test

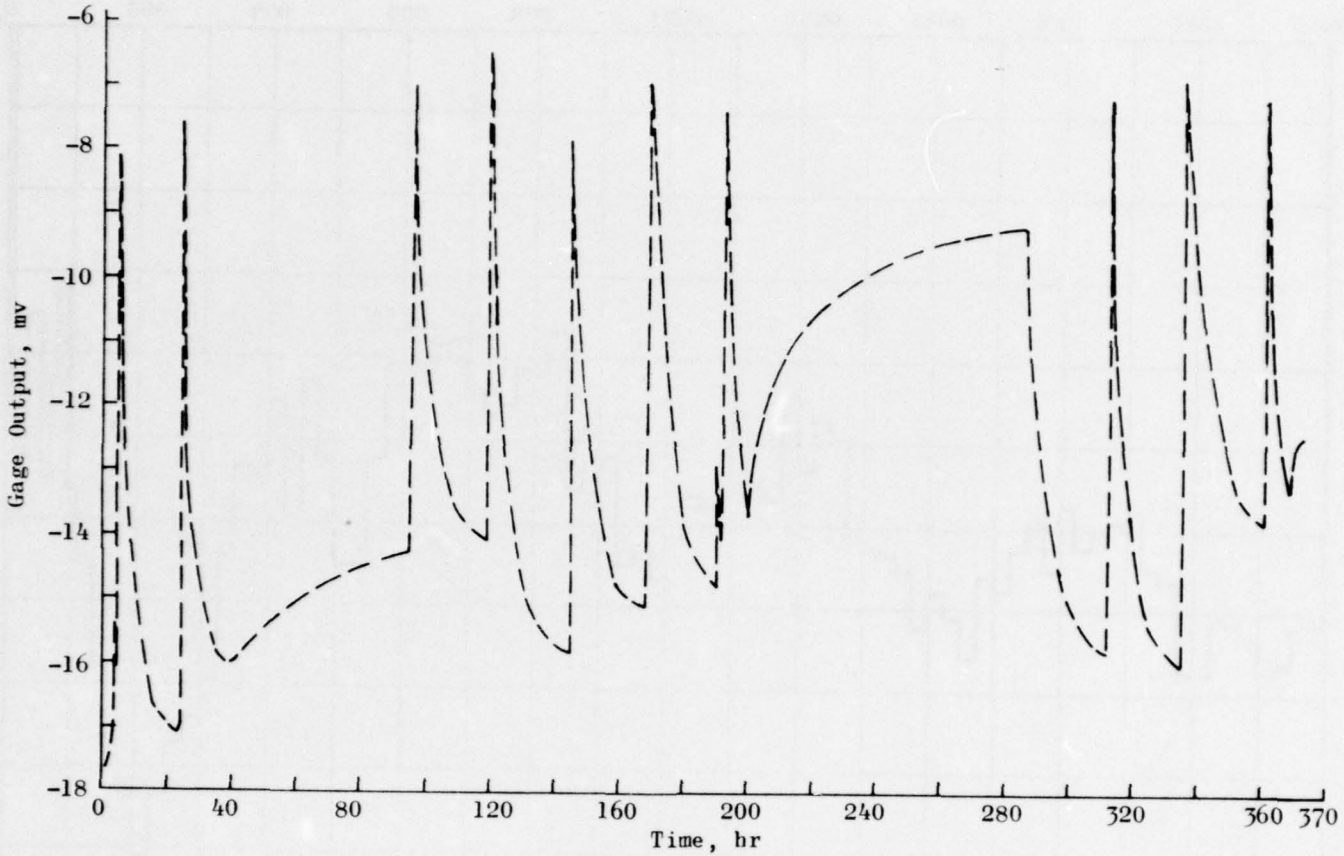

Figure 130. Normal Gage N7-63 Response, Second Captive-Flight Simulation Test

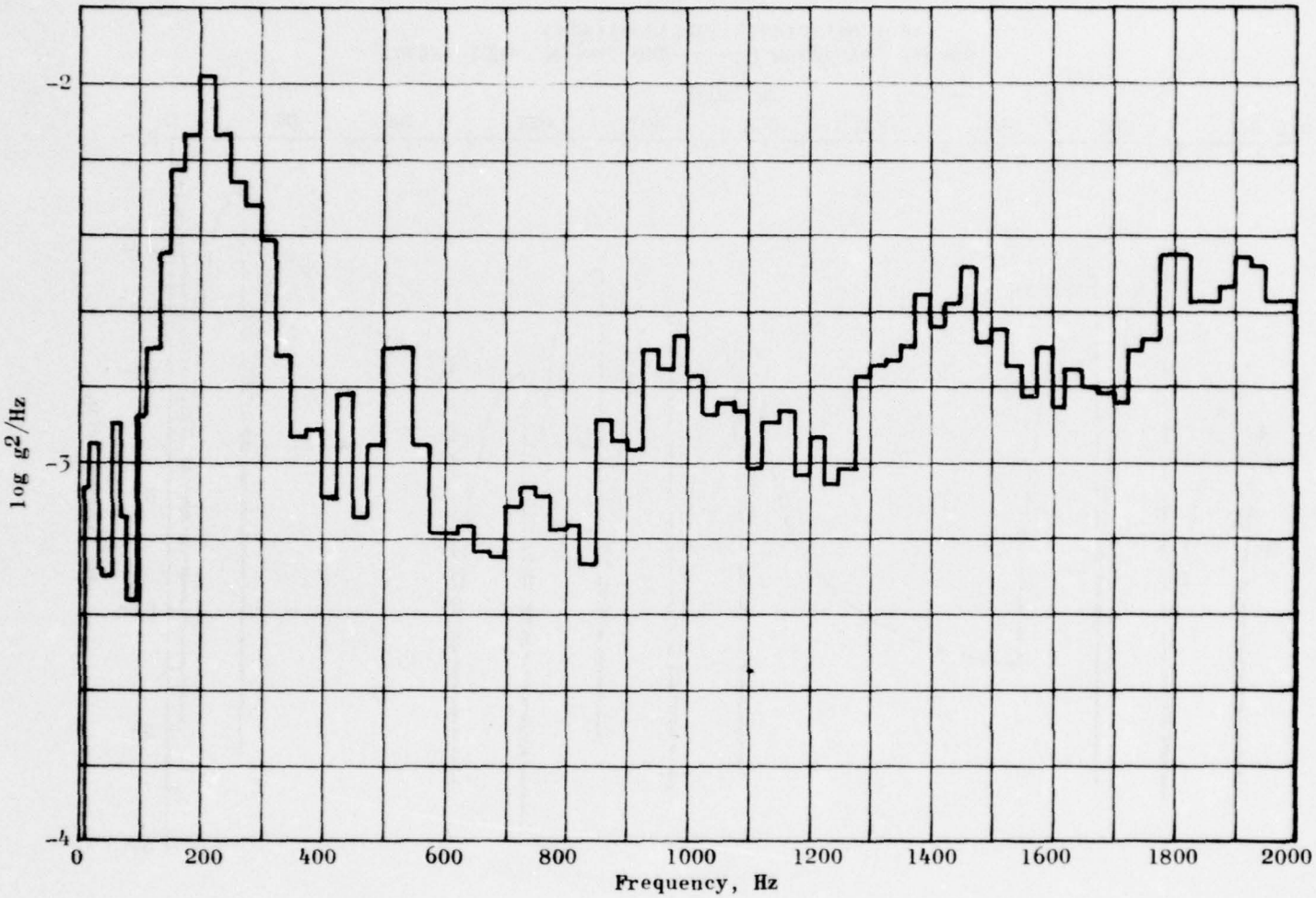

Figure 131. Input Control, Second Series Random Vibration

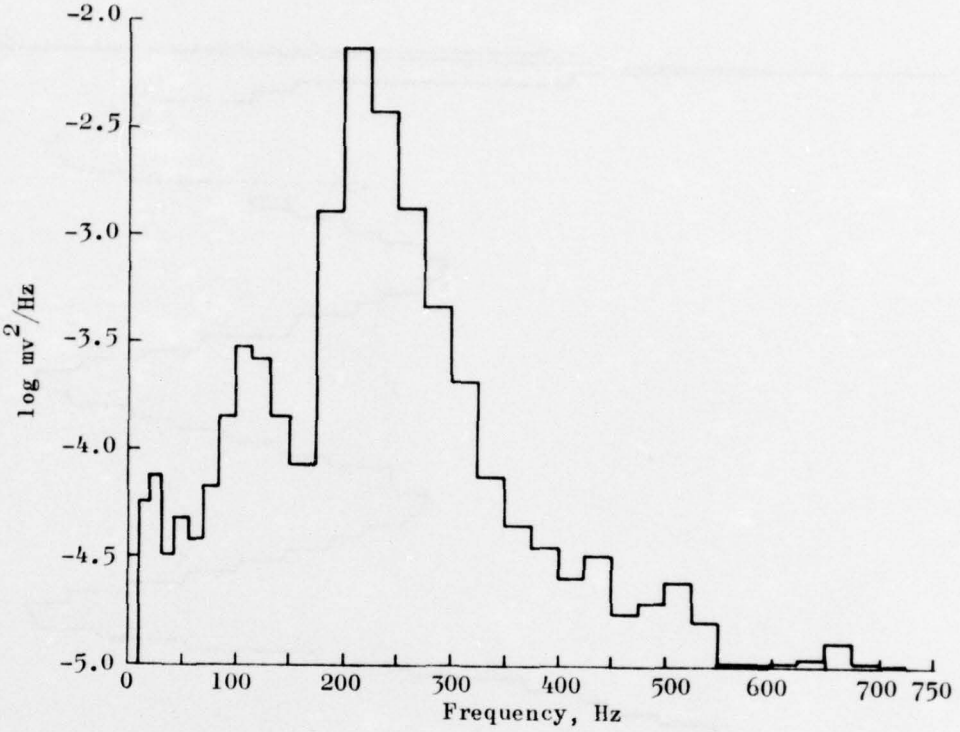

Figure 132. Gage N7-61 Random Vibration Response, Second Series Test

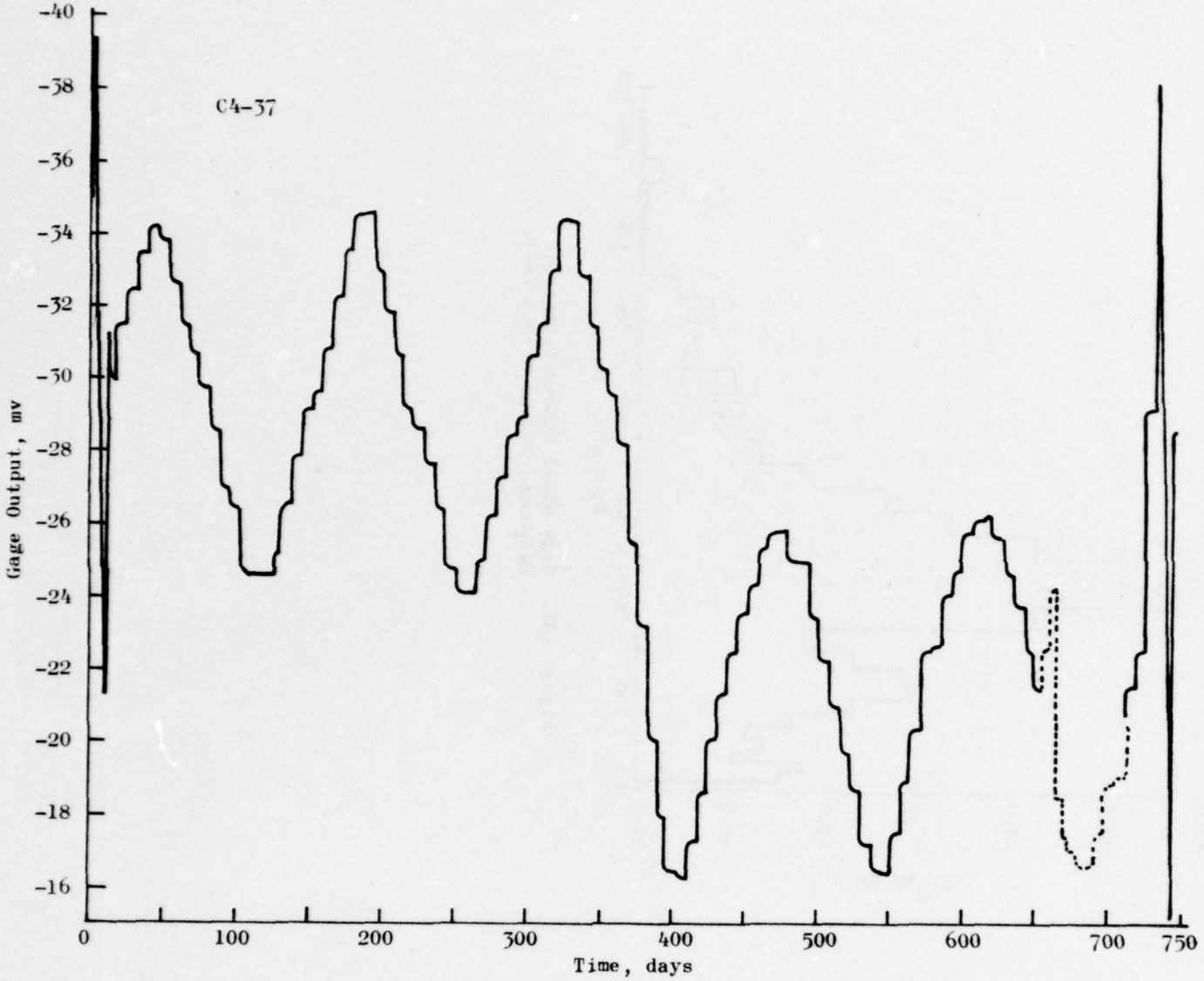

Figure 133. Clip Gage Response During Two-Year Storage Test, Motor 4

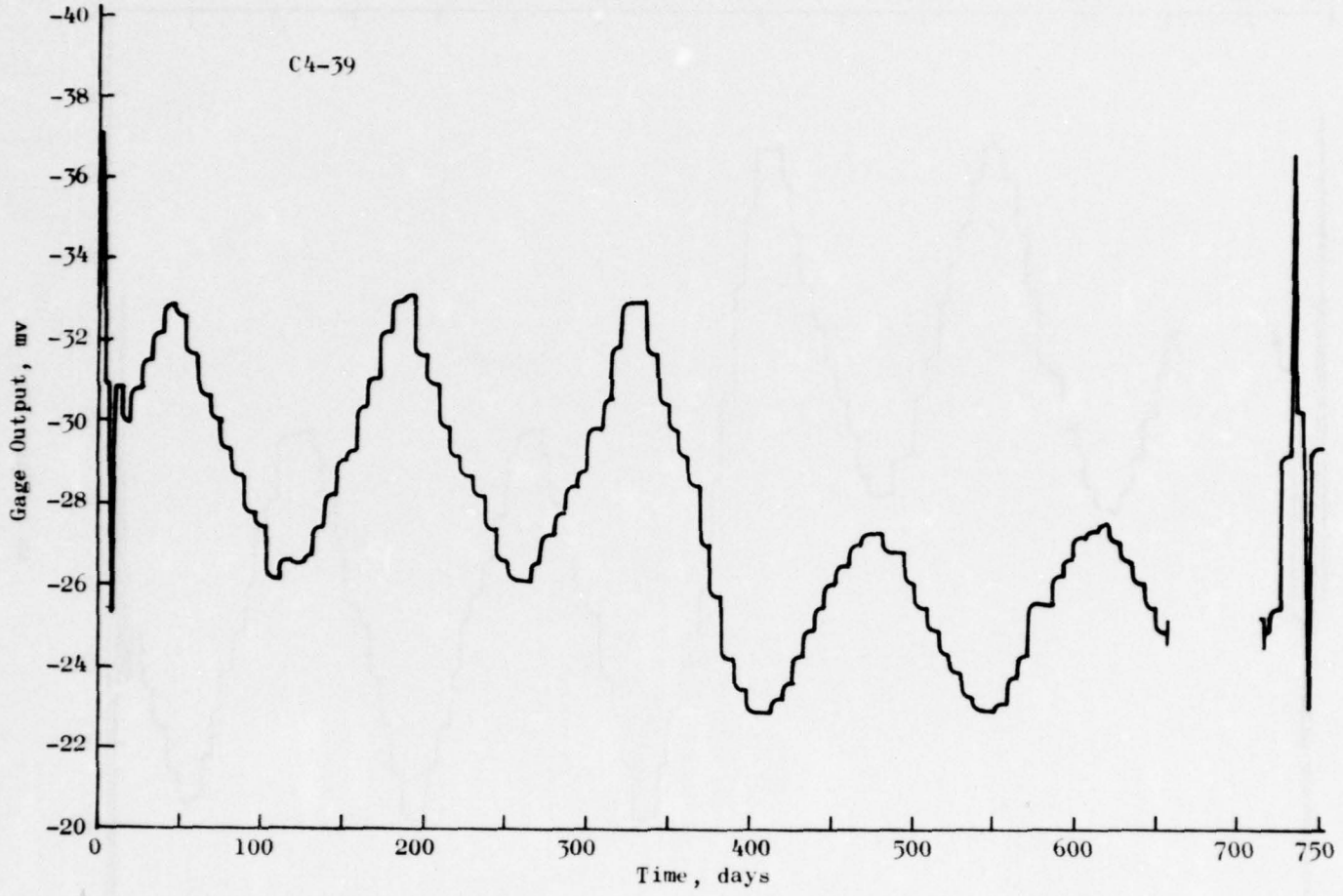

Figure 133. Continued

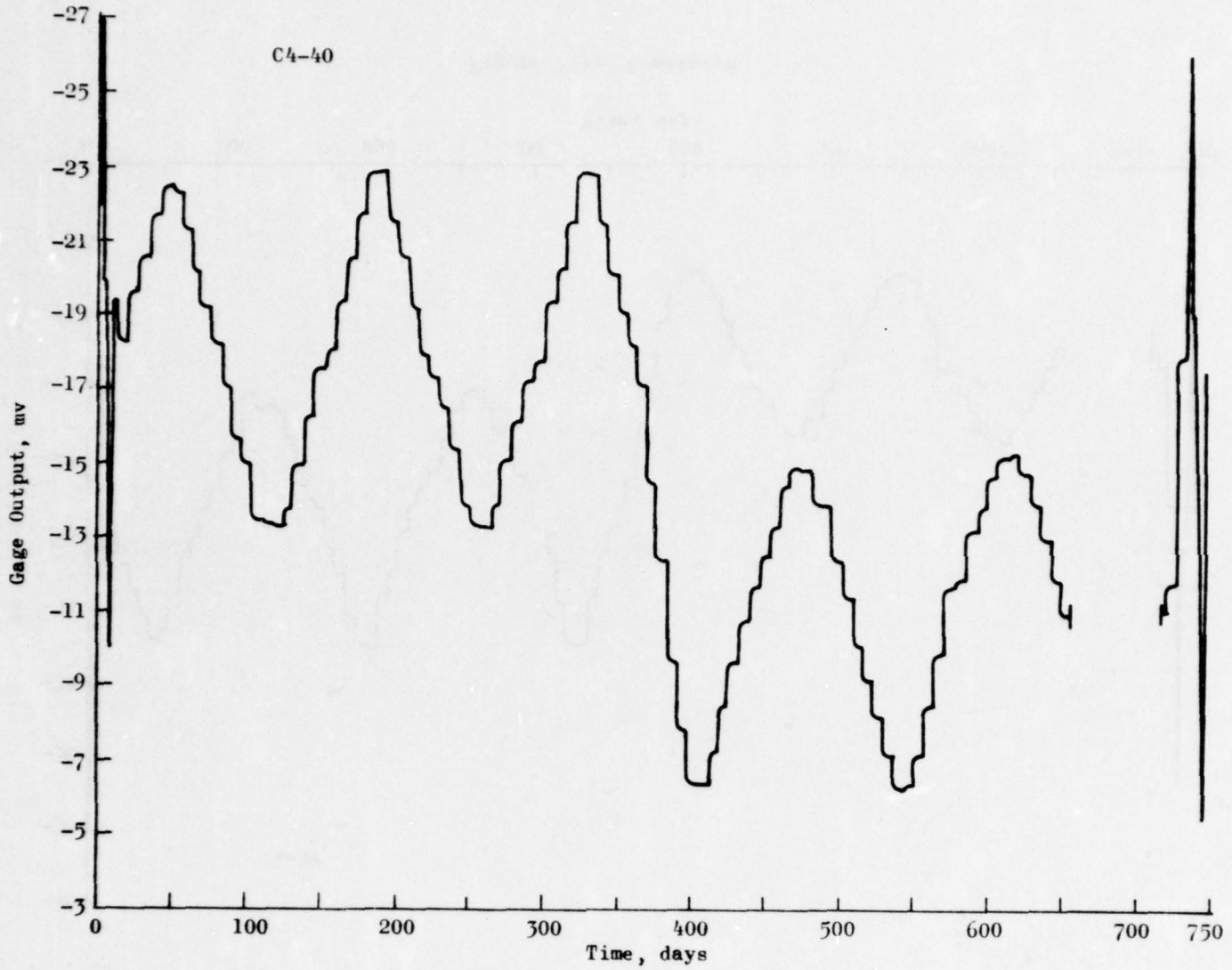

Figure 133. Continued

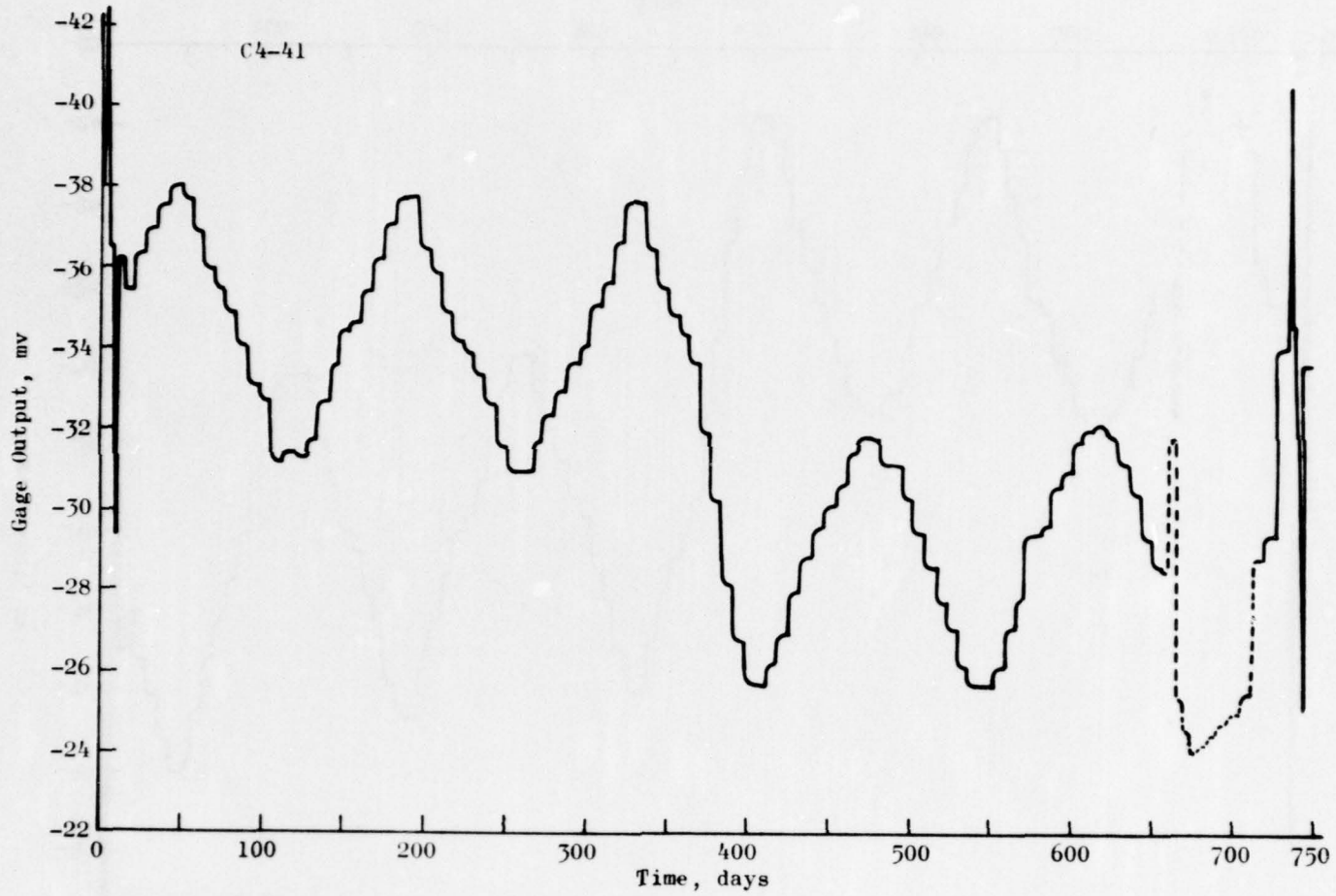

Figure 133. Continued

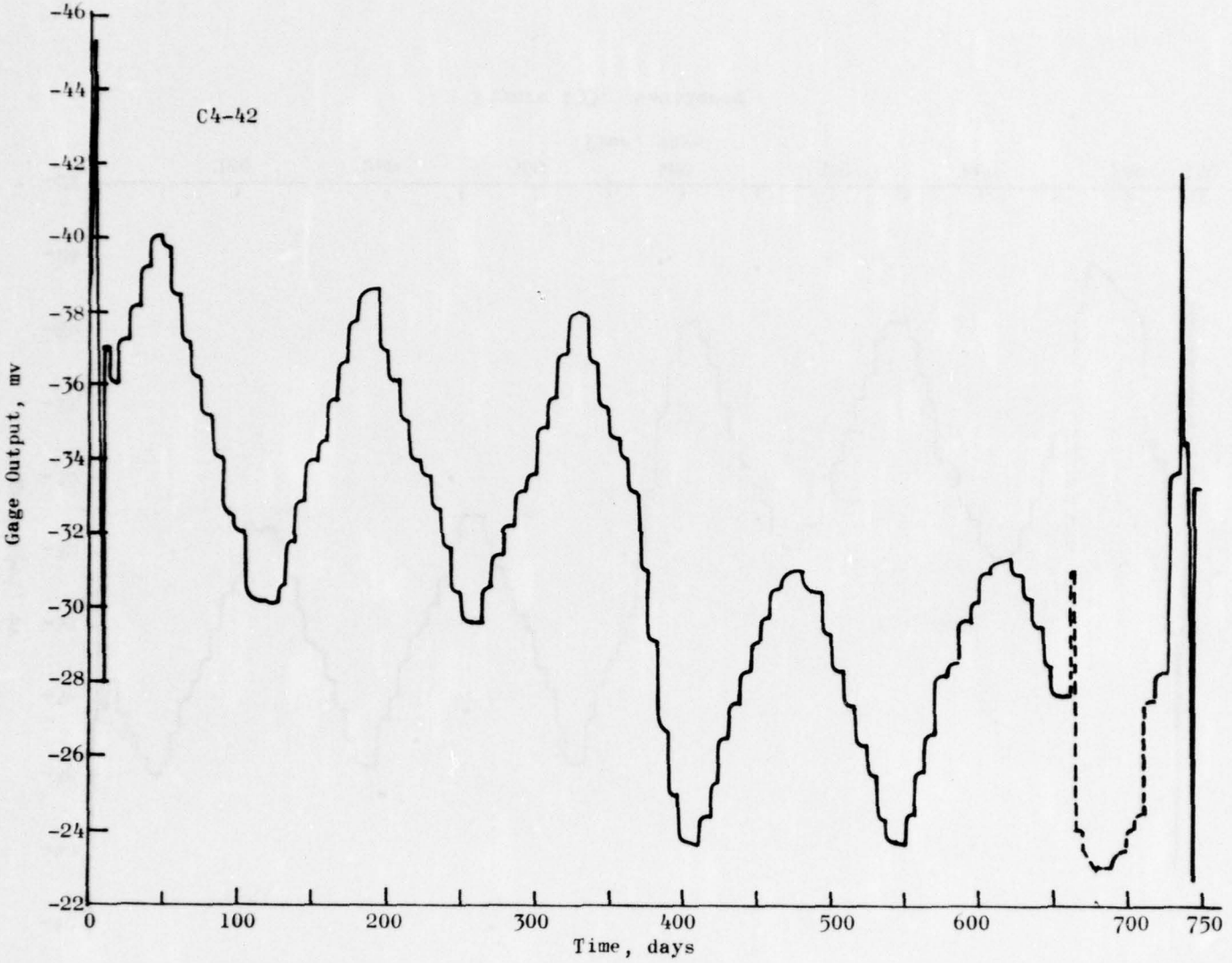

Figure 133. Continued

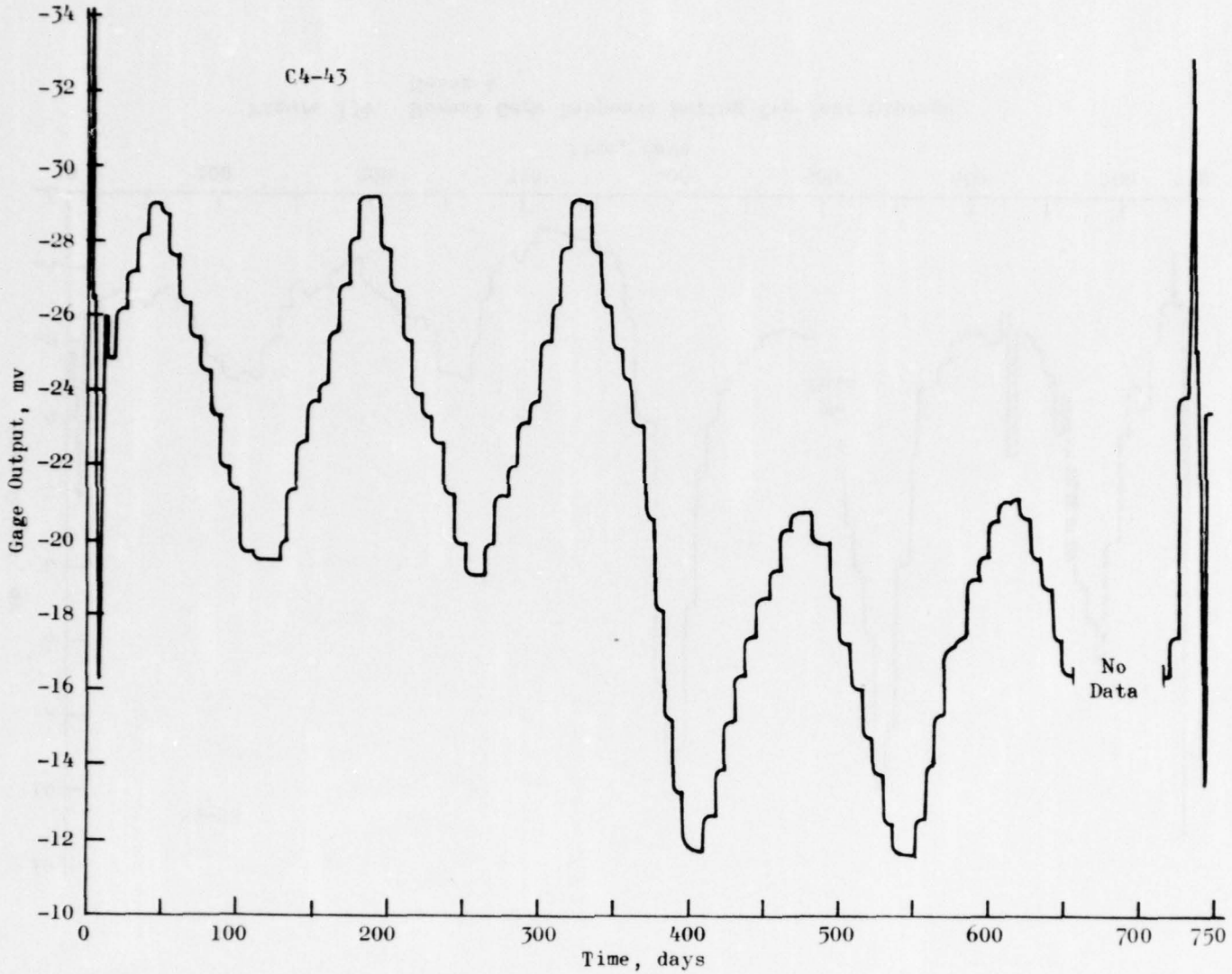

Figure 133. Continued

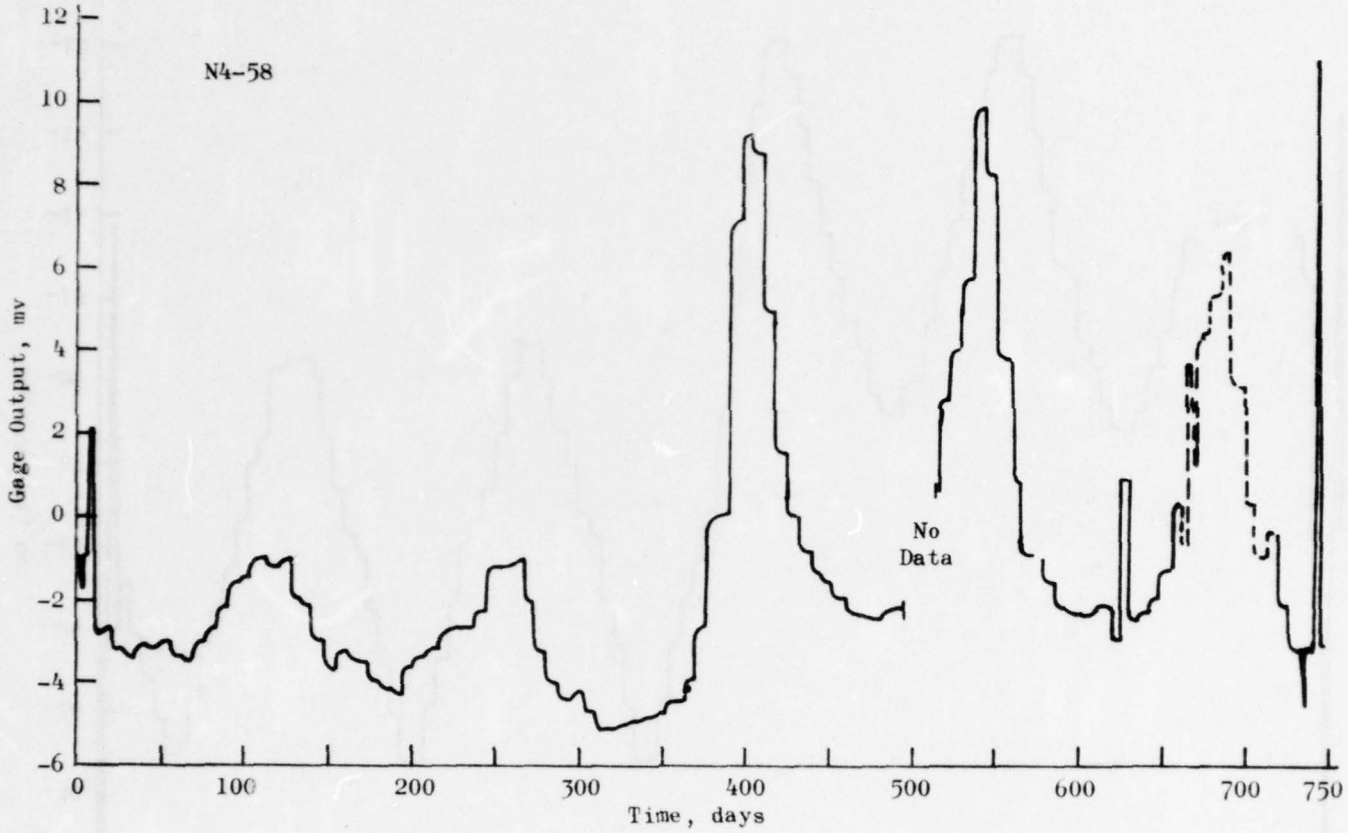

Figure 134. Normal Gage Response During Two-Year Storage, Motor 4

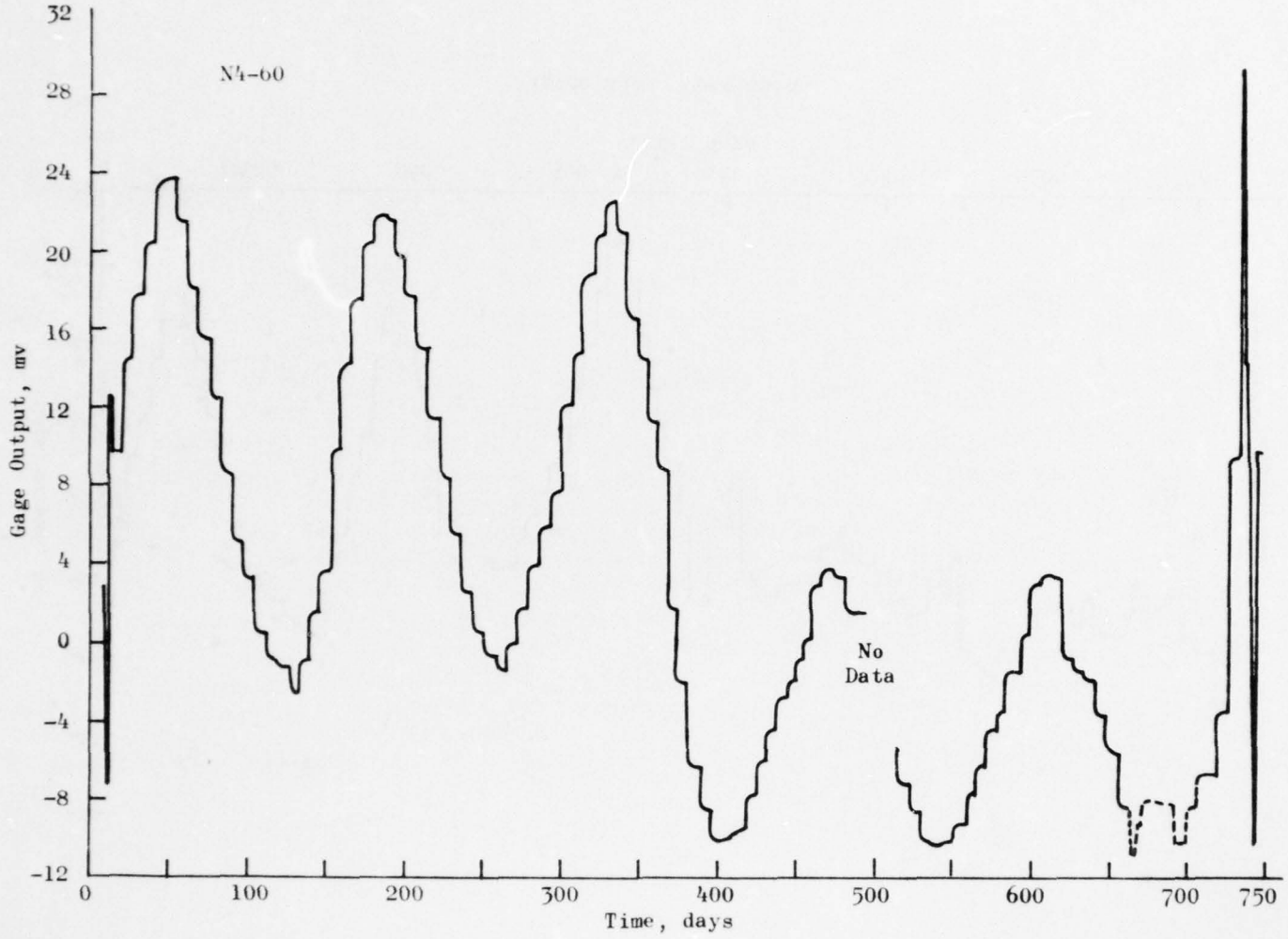

Figure 134. Continued

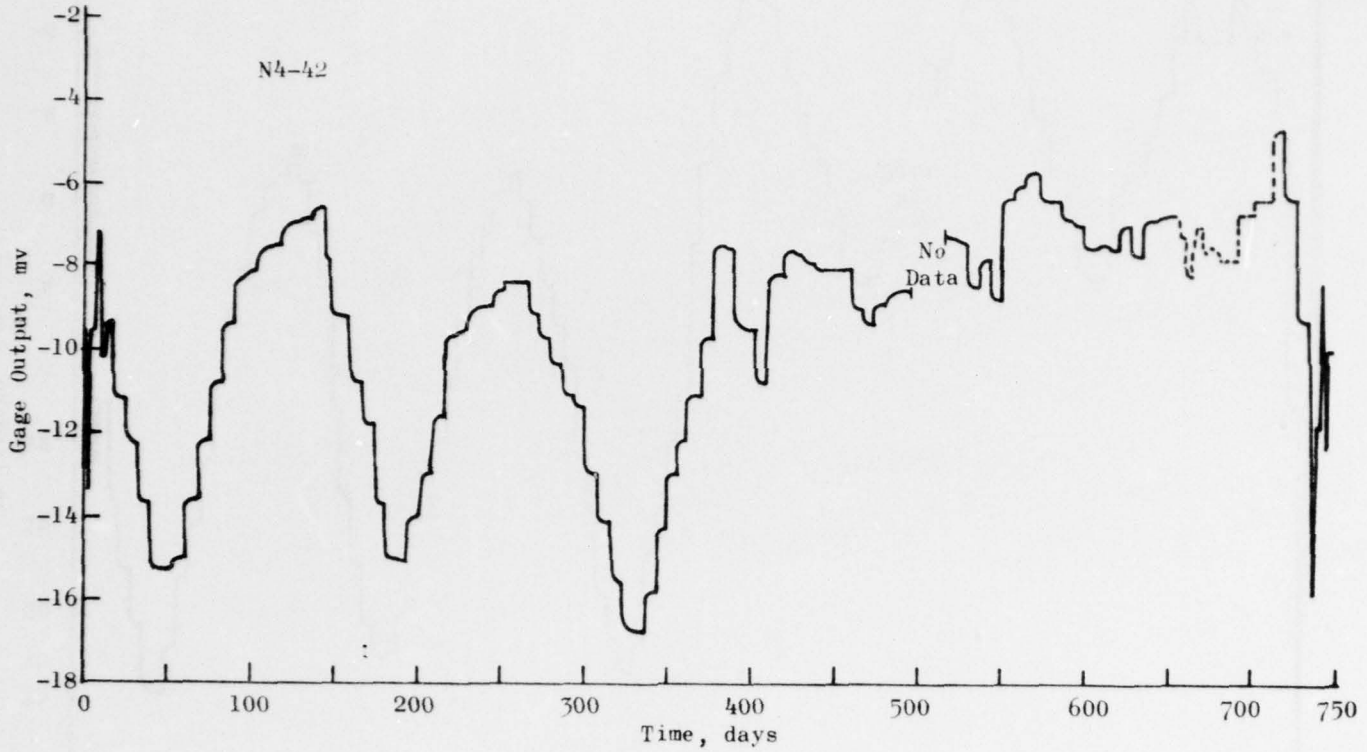

Figure 134. Continued

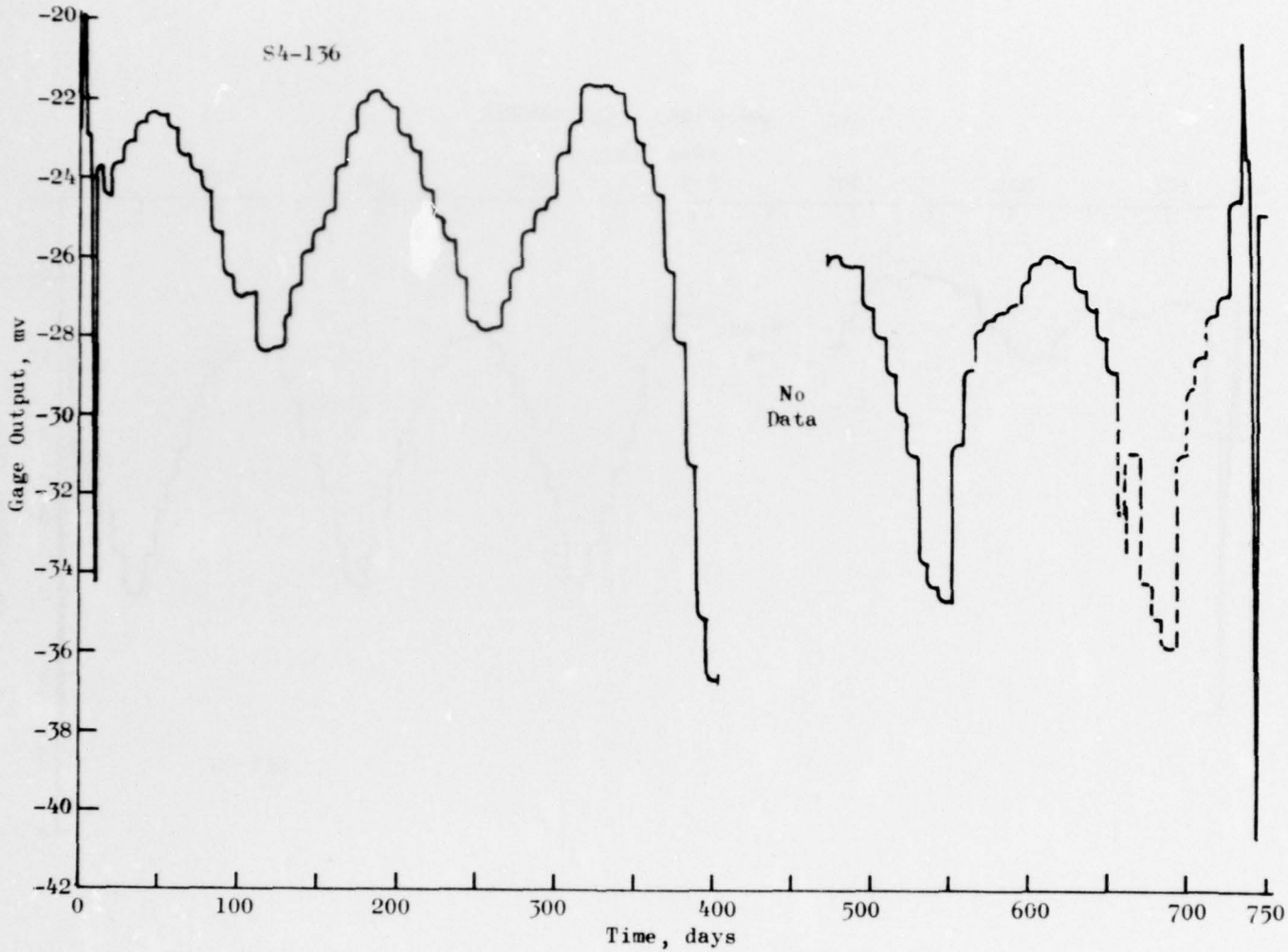

Figure 135. Shear Gage Response During Two-Year Storage Test, Motor 4

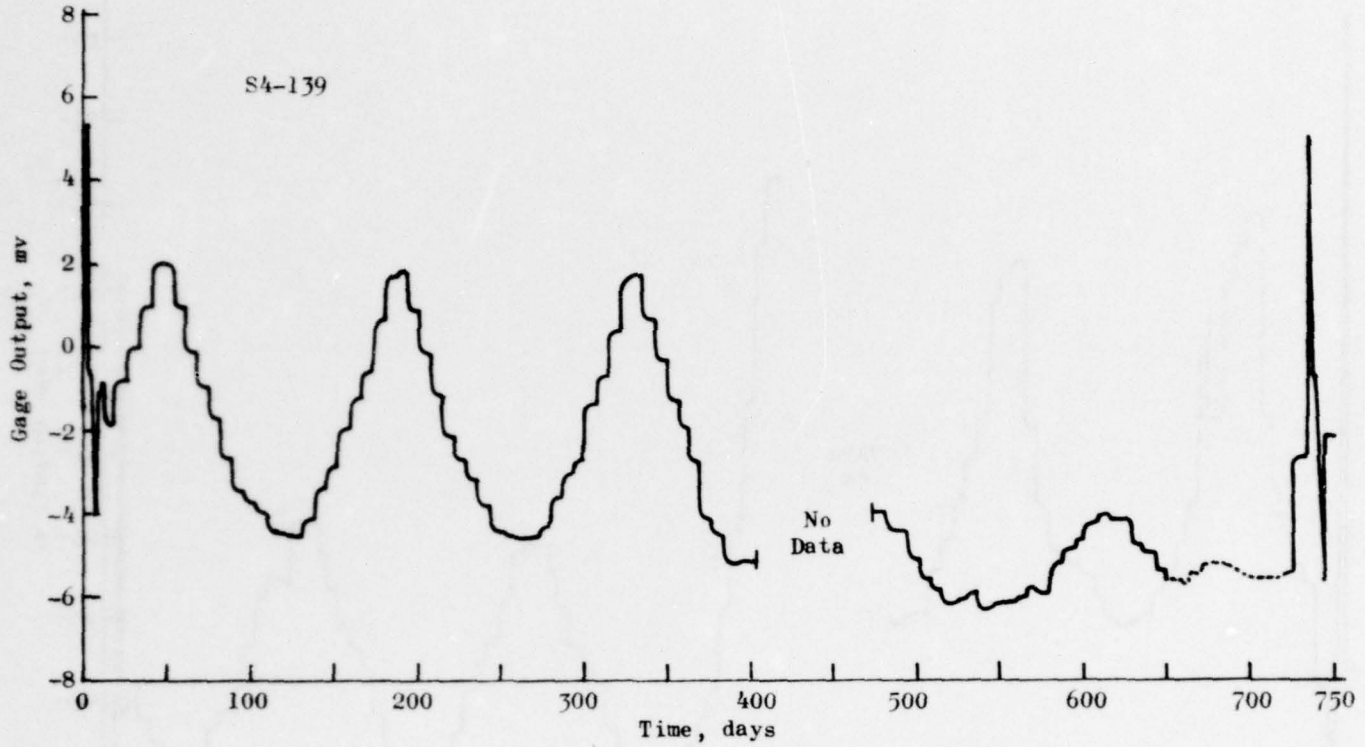

Figure 135. Continued

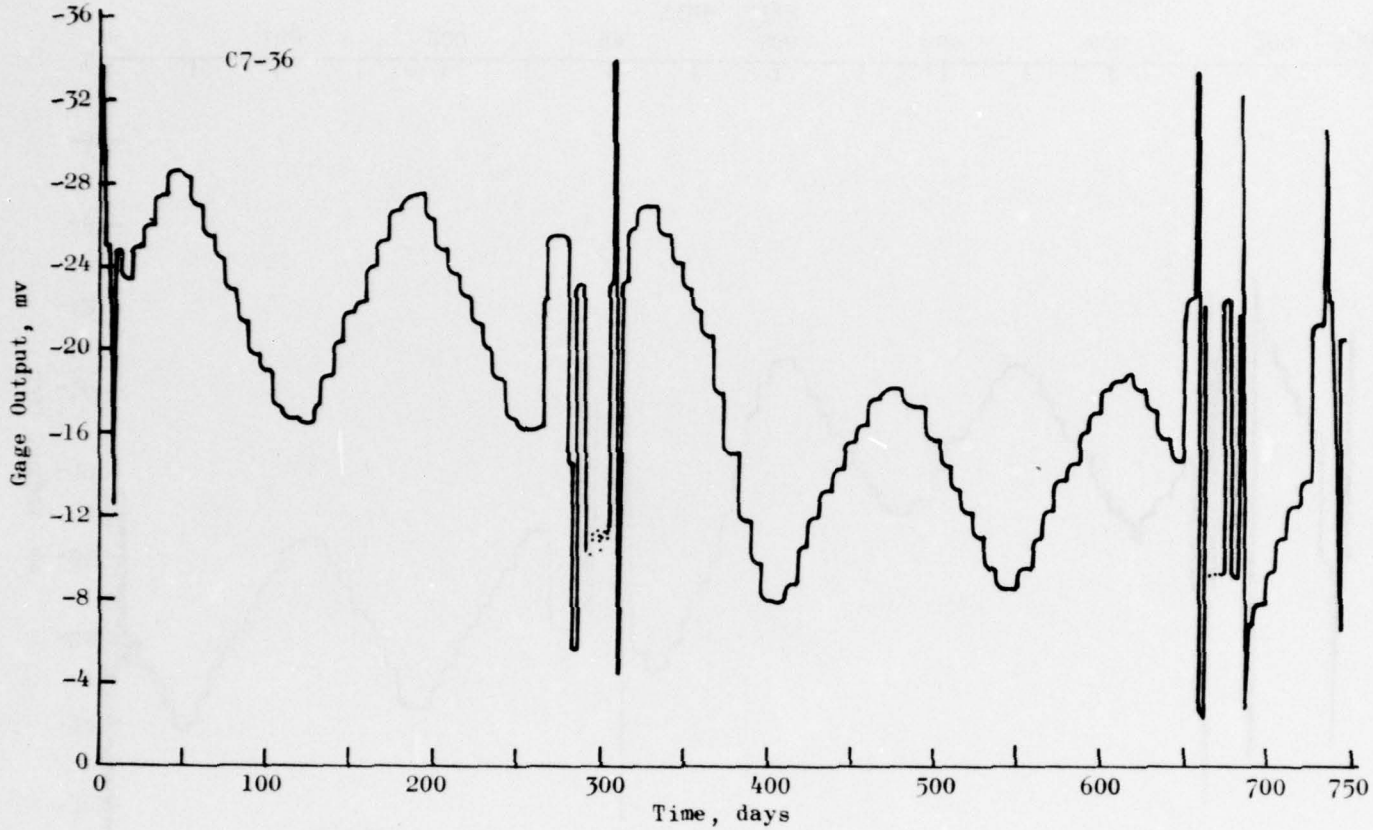

Figure 136. Clip Gage Response During Two-Year Storage Test, Motor 7

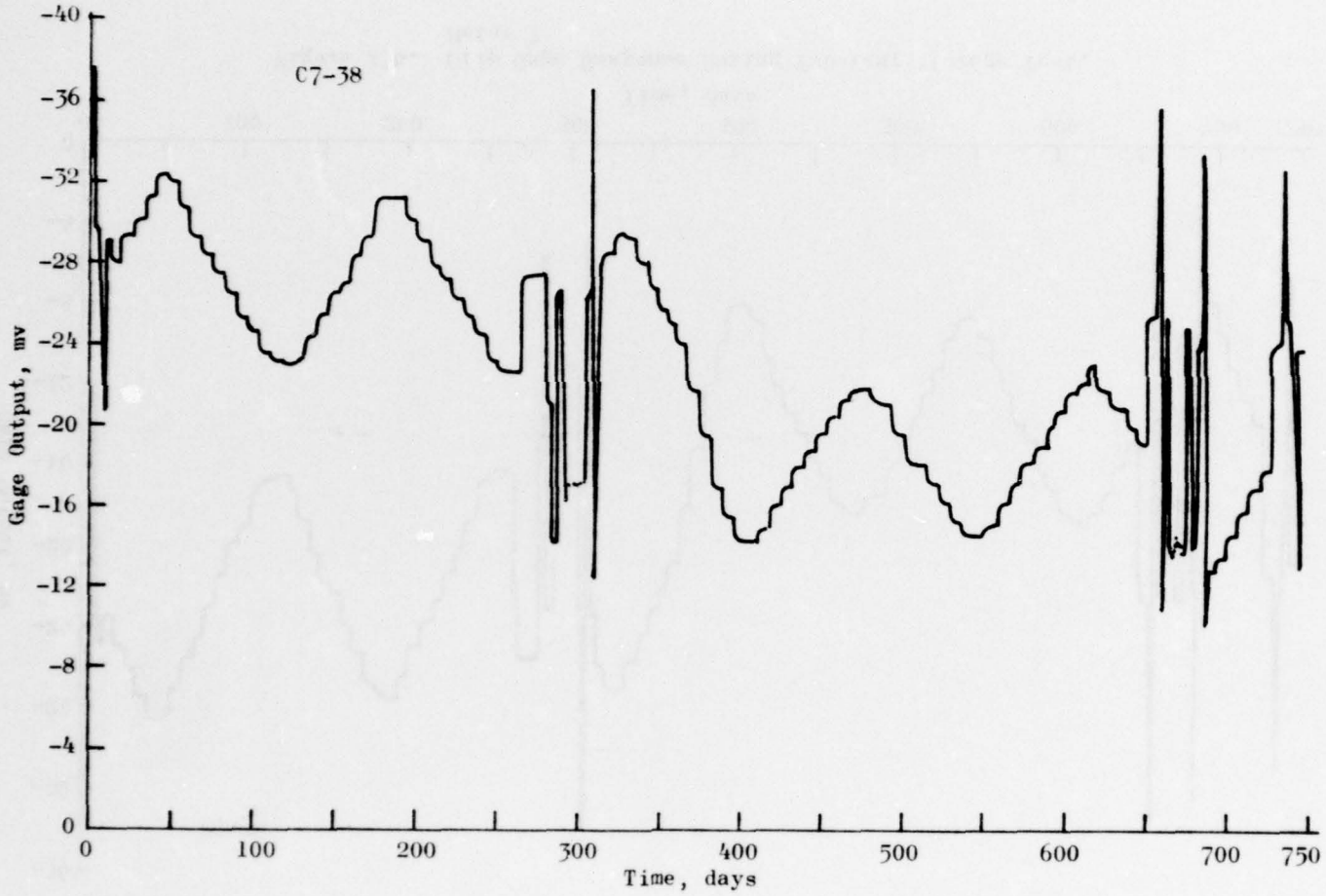

Figure 136. Continued

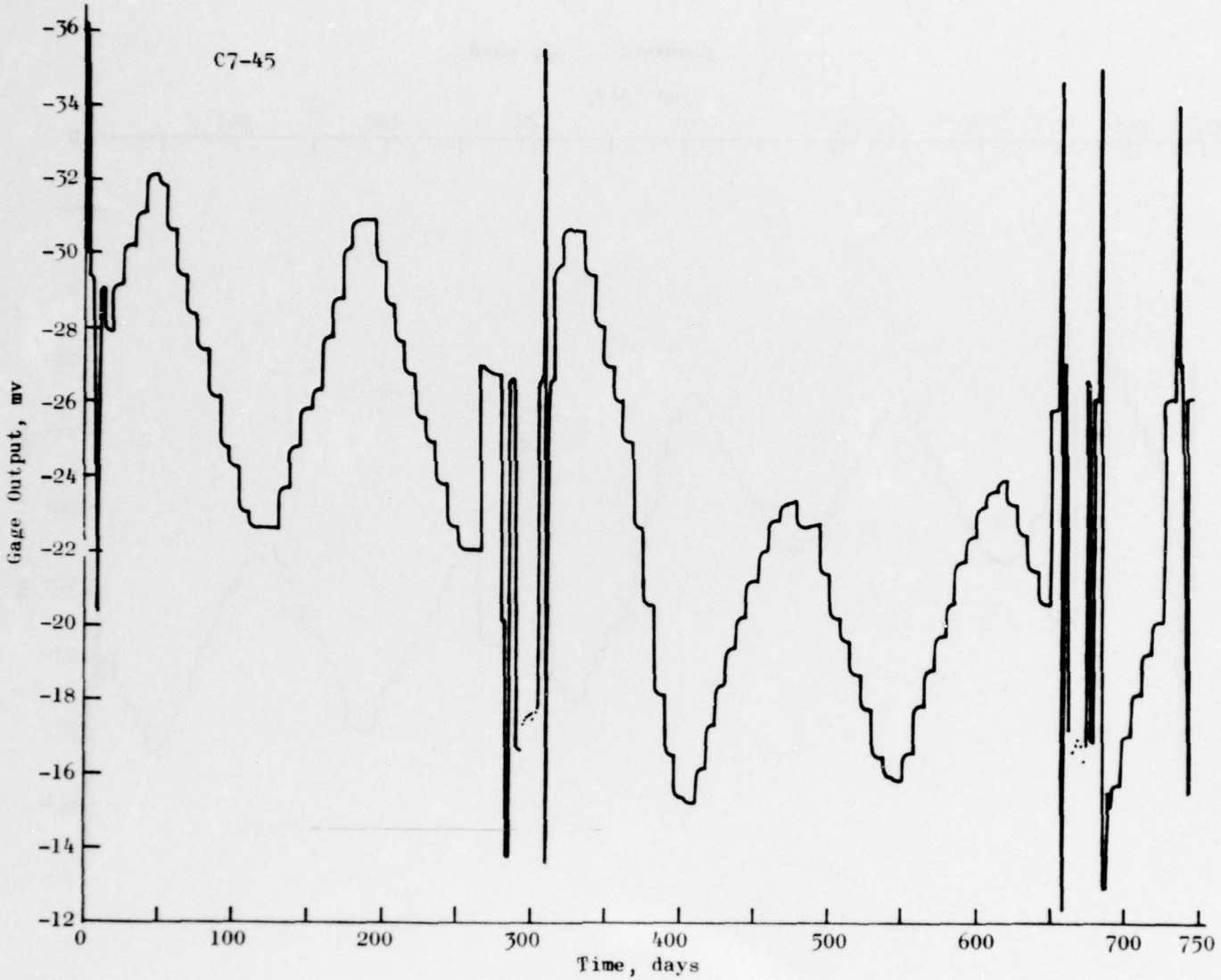

Figure 136. Continued

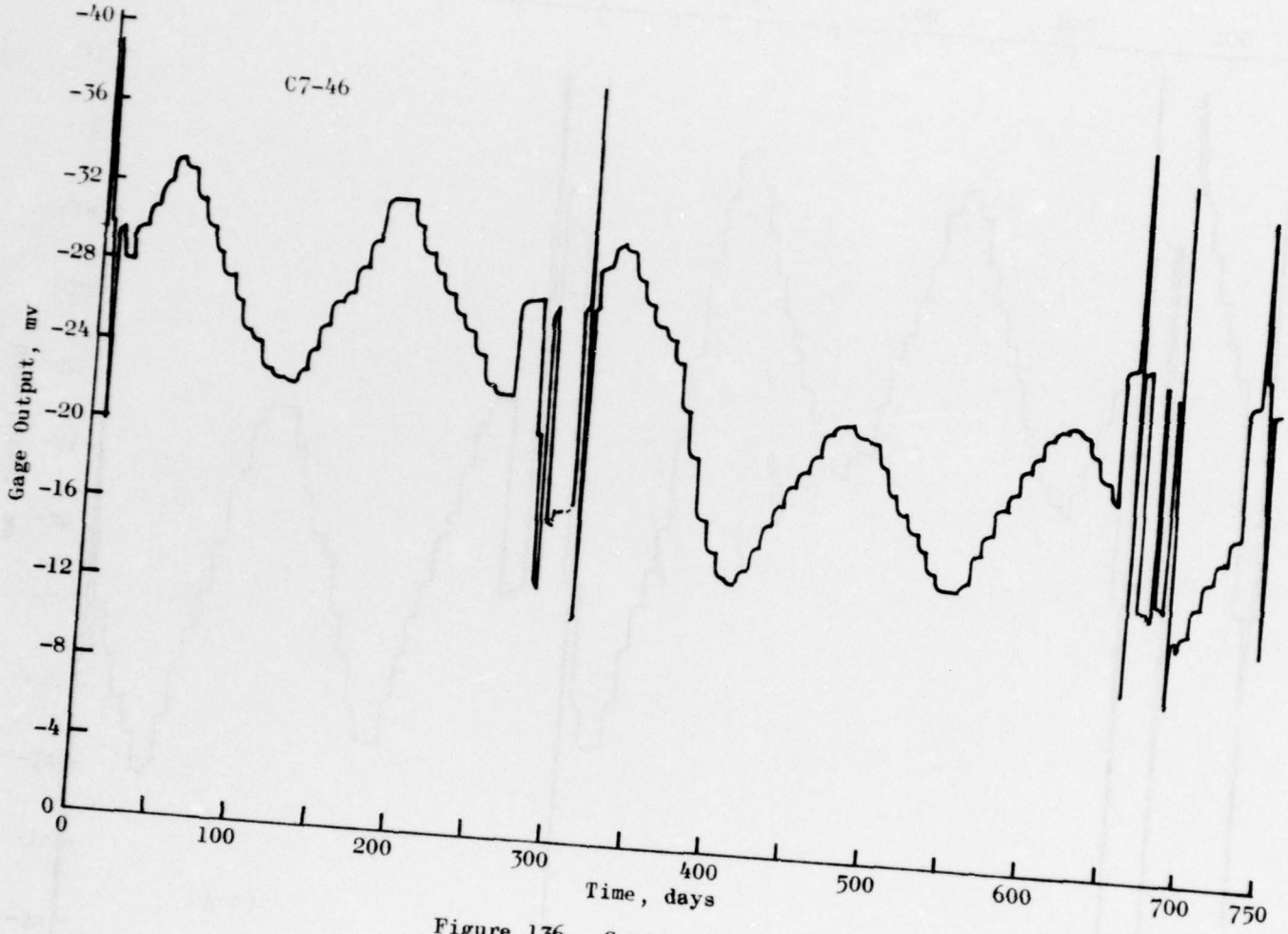

Figure 136. Continued

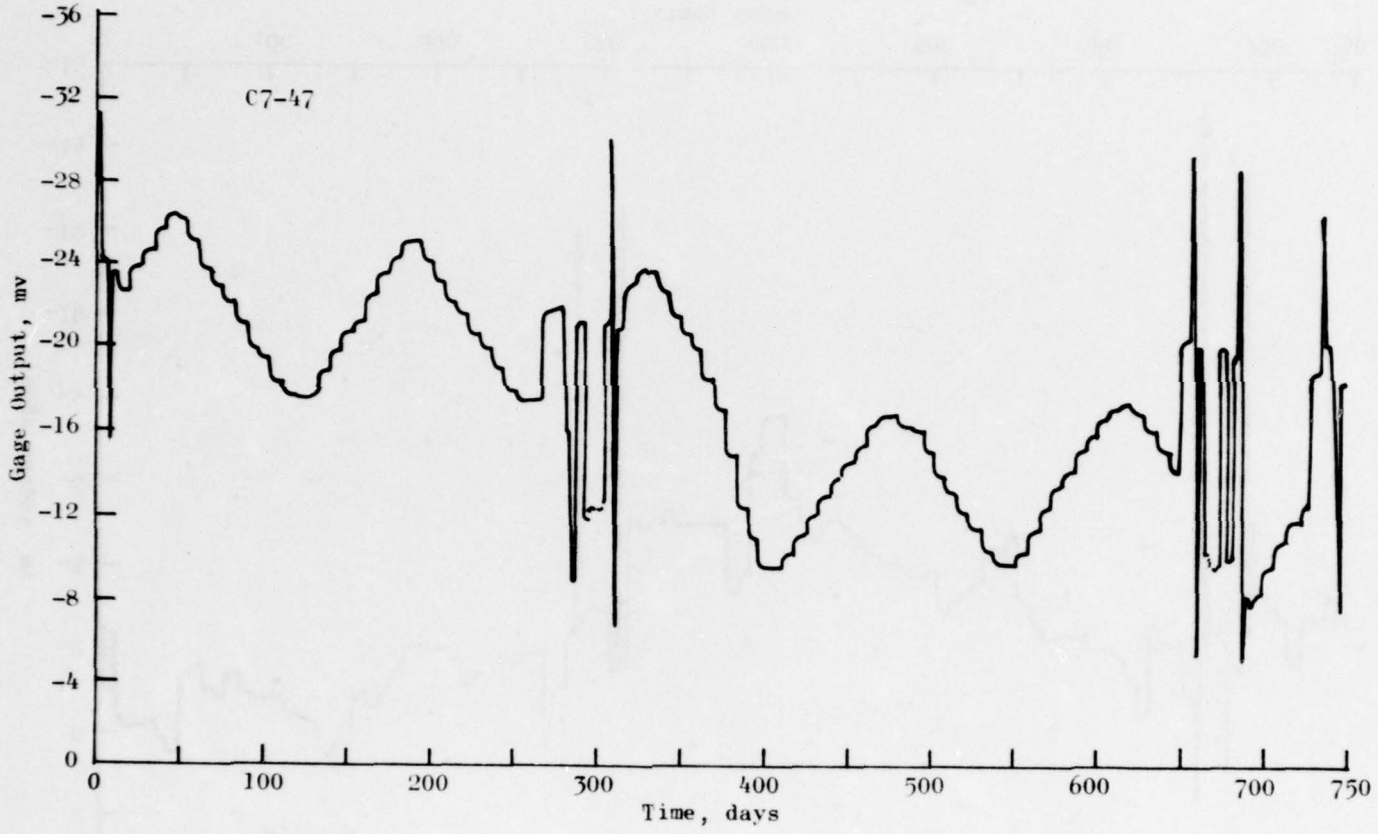

Figure 136. Continued

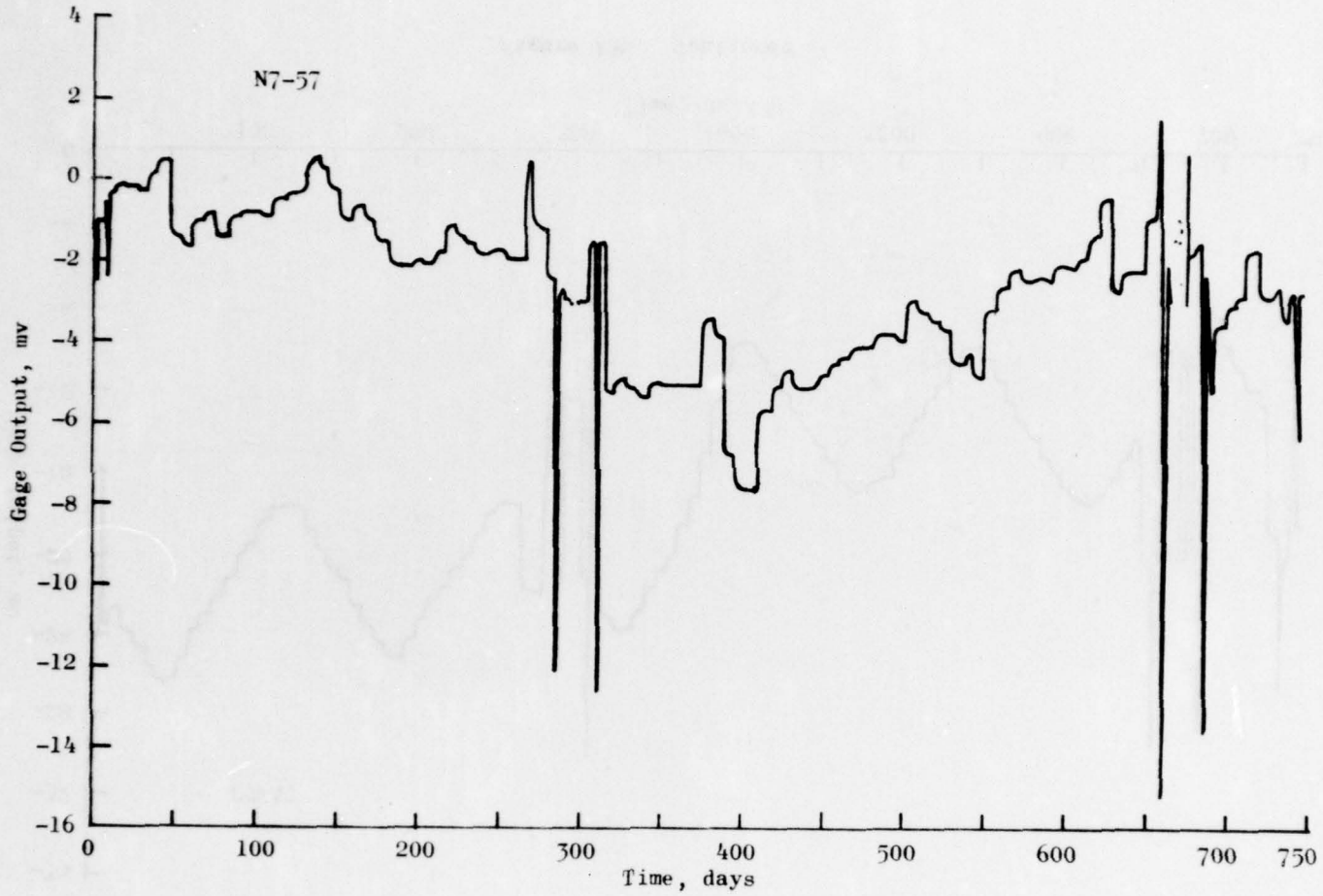

Figure 137. Normal Gage Response During Two-Year Storage Test, Motor 7

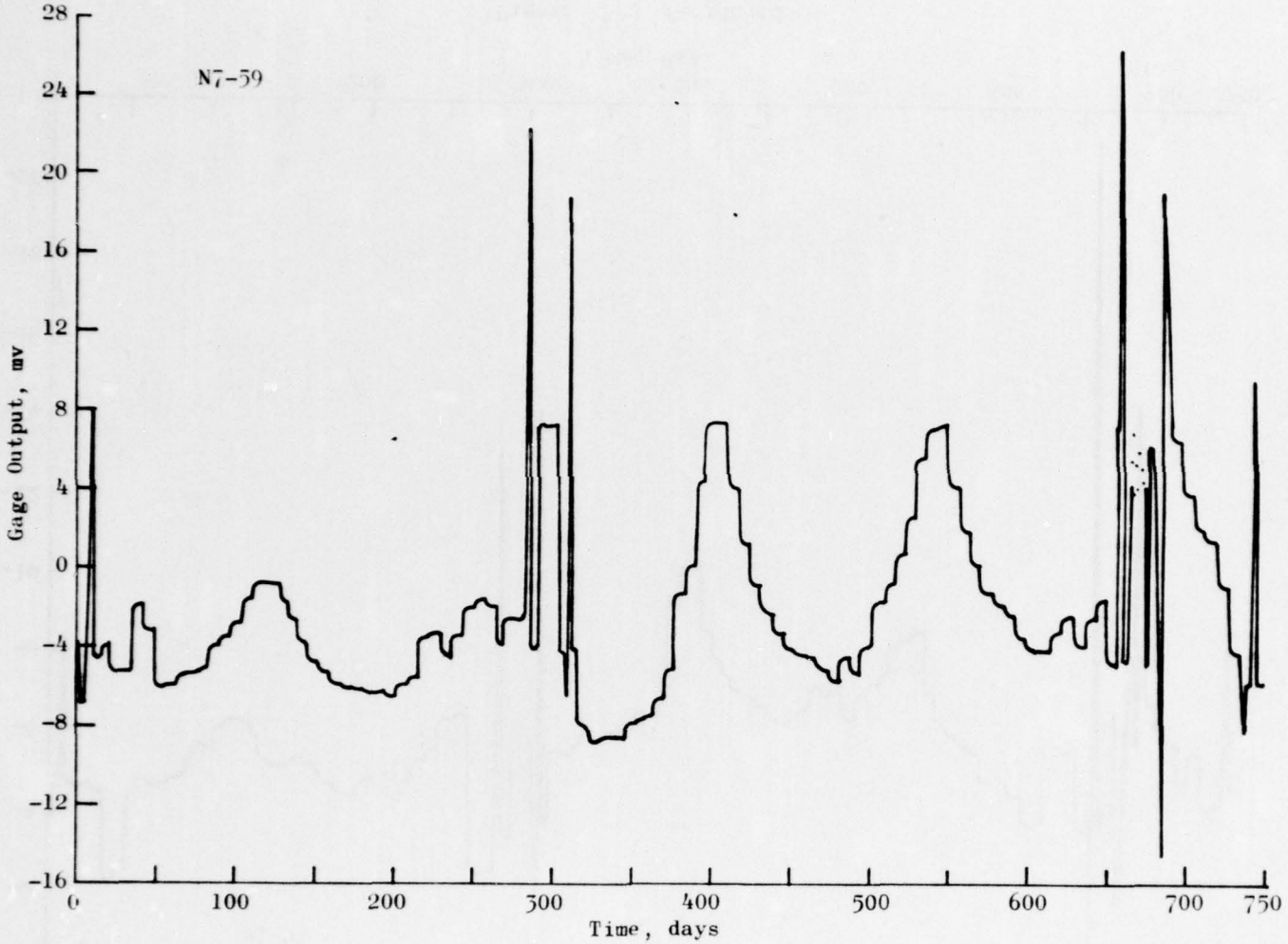

Figure 137. Continued

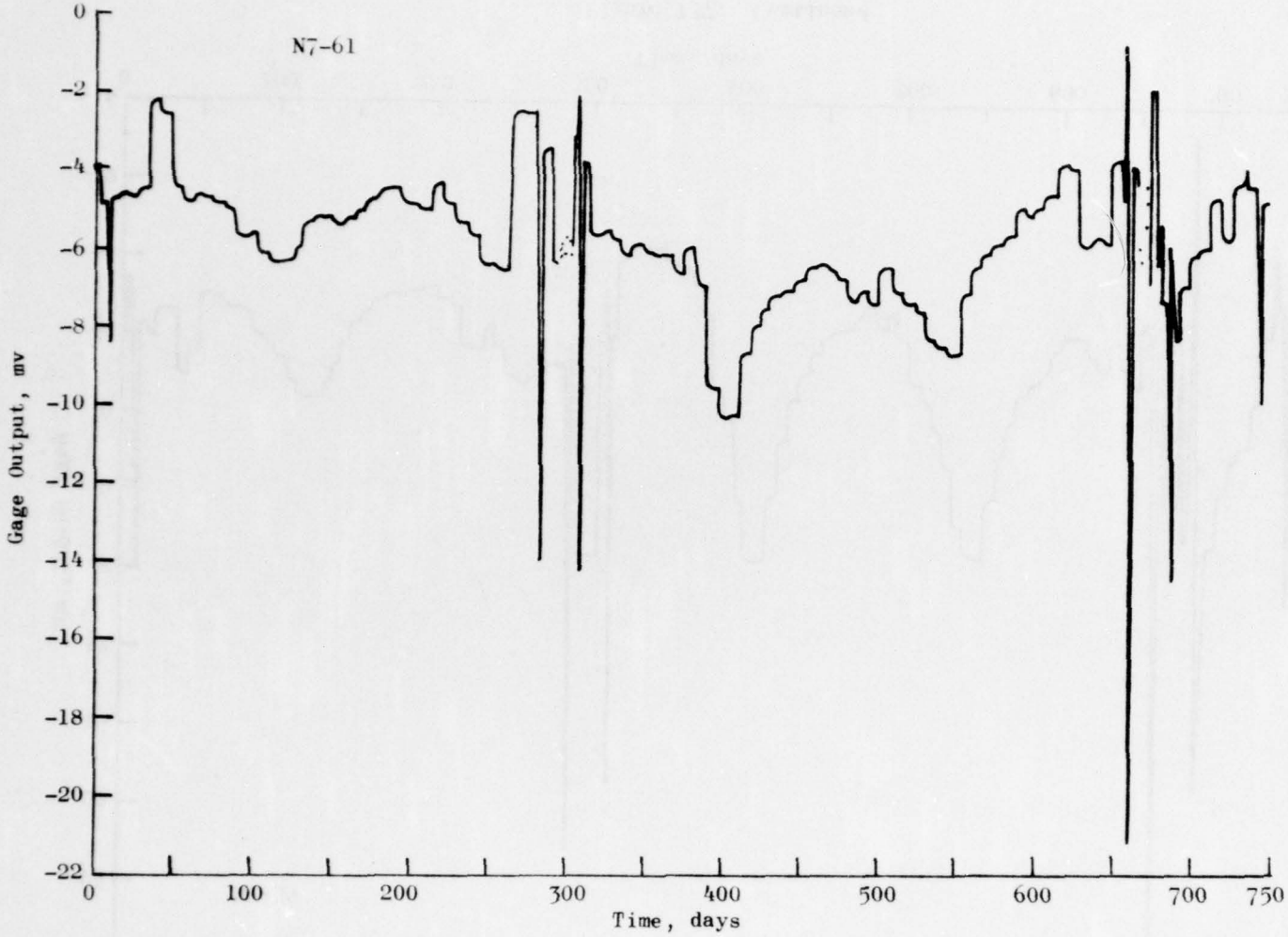

Figure 137. Continued

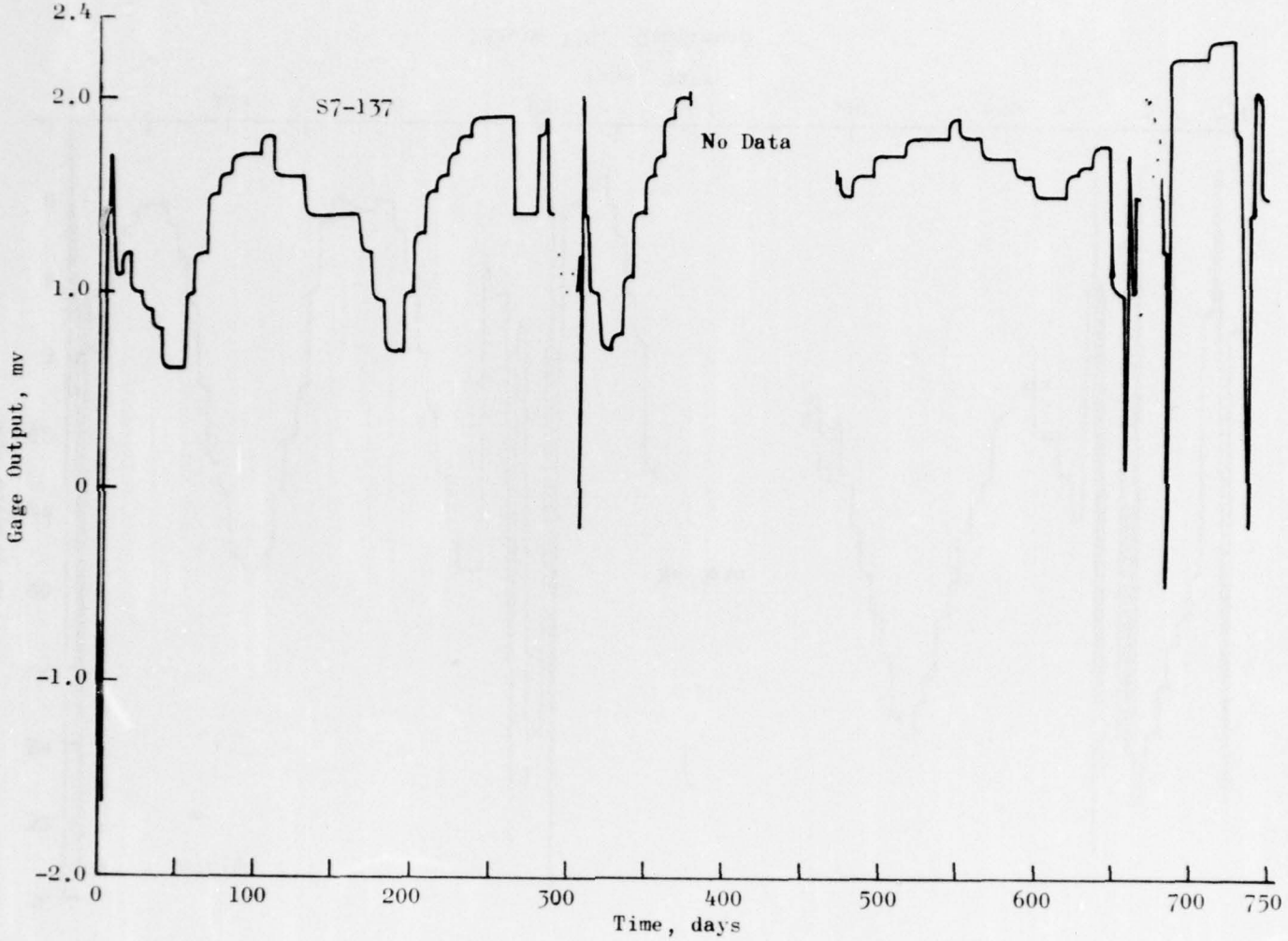

Figure 138. Stress Gage Response During Two-Year Storage Test, Motor 7

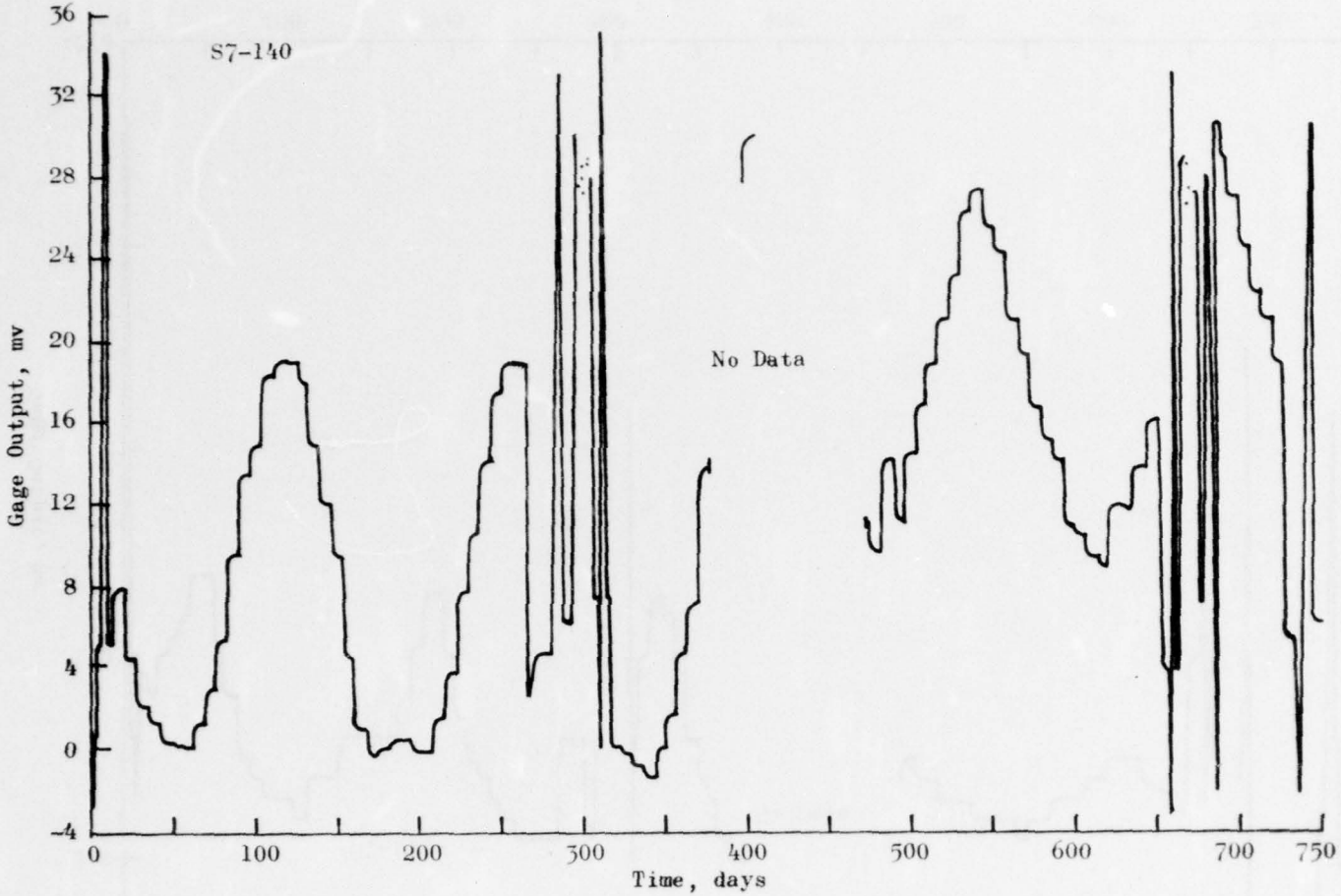

Figure 138. Continued

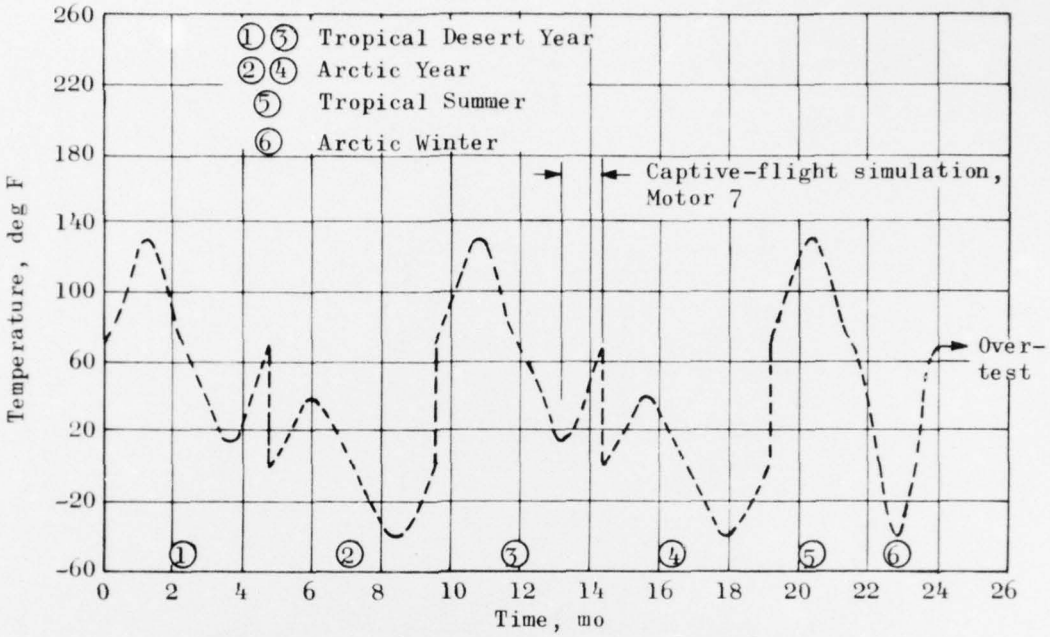

Figure 139. Simulated Storage Environment

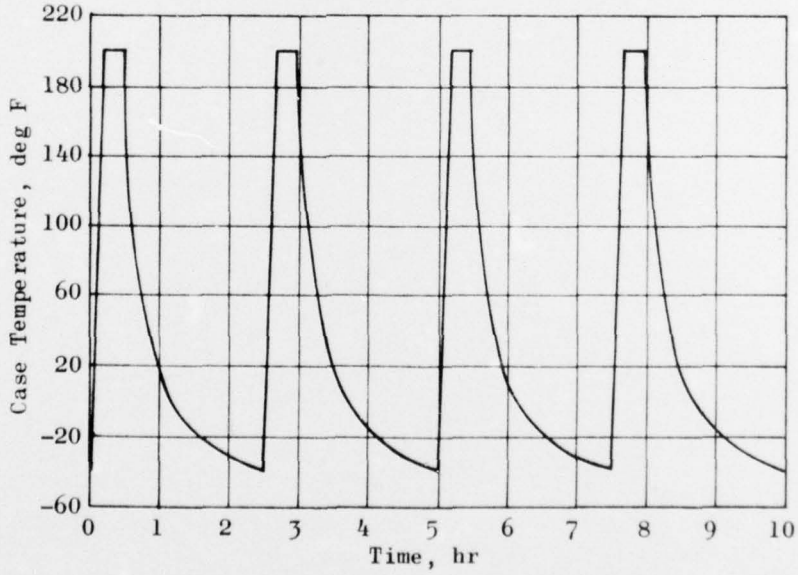

Figure 140. Typical Daily Aeroheat Cycling

Page 222 is blank


FILM
4